Durham E-Theses

Mechanistic studies of leaving group effects on enzymatic catalysis by methylglyoxal synthase

Barry J. Dodd

How to cite:

Use policy

Mechanistic Studies
of Leaving Group Effects on Enzymatic Catalysis by
Methylglyoxal
Synthase

By

Barry J. Dodd

BSc., Chemistry (2004)

University College Dublin

Submitted to the Department of Chemistry

In Partial Fullfilment of the Requirements for the

Degree of Doctor of Philosophy

at

Durham University

1 8 DEC 2008

Durham
University

2008

To my parents

Abstract

This thesis describes the investigations of leaving group effects on enzymatic catalysis by *Methylglyoxal synthase* (MGS). MGS is a glycolytic enzyme involved in bacterial metabolism which catalyzes the irreversible elimination of dihydroxyacetone phosphate (DHAP). In order to probe the effect of various leaving groups to MGS catalysis, a range of 'mutant' substrates have been synthesised where the phosphate group of natural substrate DHAP has been replaced by sulfate, thiosulfate and bromo groups yielding the substrates dihydroxyacetone sulfate (DHAS), dihydroxyacetone thiosulfate (DHATS) and bromohydroxyacetone (BHA). To quantify an overall enzymatic rate acceleration detailed kinetic analysis of the solution, non-enzymatic reactions of these substrates have been made. Rates for elimination and enolization via C-1 and C-3 deprotonation respectively have been quantified for each substrate using high resolution ^{1}H NMR spectroscopy for a range of pD values. From the second order rate constants for buffer catalyzed deprotonation, k_B (M^{-1}s^{-1}) comparisons can be made with k_{cat}/K_M (M^{-1}s^{-1}) for the enzymatic reactions at the same pD values.

The non-enzymatic reactions of DHAS were monitored in the pD range of 7.3-9.2 using phosphate and quinuclidinone buffers. Second order rate constants, k_B (M^{-1}s^{-1}) of 5.60 x 10^{-4}, 5.28 x 10^{-3}, 5.82 x 10^{-3} and 7.40 x 10^{-3} M^{-1}s^{-1}for C-1 deprotonation and 1.41 x 10^{-3}, 2.24 x 10^{-3} and 3.30 x 10^{-3} for C-3 deprotonation show that increasing the pD results in an increase in the rate of buffer catalyzed deprotonation (phosphate catalyzed C-3 deprotonation was not observed at this pD). This is indicative of a general base catalyzed deprotonation mechanism. First order rate constants, k_{int} (s^{-1}) for the buffer independent catalyzed deprotonation reactions of 1.39 x 10^{-5}, 1.22 x 10^{-4}, 1.26 x 10^{-4} and 2.04 x 10^{-4} for C-1 deprotonation and 9.66 x 10^{-5}, 1.10 x 10^{-4} and 9.30 x 10^{-5} for C-3 deprotonation show that an increase 0.7 pD units leads to only a 67 % and 12

% respective increase in the rates of deprotonation at the C-1 and C-3 positions. This is reflected

in the relatively level pD rate profile of the reaction. The background, non-enzymatic reactions

of DHATS were carried out in acetic acid buffers and DCl solutions. In DCl solution an average

k_{int} (s^{-1}) value of 1.33 x 10^{-5} s^{-1} was obtained. For the acetate catalyzed C-1 deprotonation

reactions it was found that moving from pD 3.75 to 4.38 leads to an overall 4.5 fold increase in

the value of k_{int} (s^{-1}) for the buffer independent deprotonation reaction of the C-1 protons of the

molecule. Values of 9.03 x 10^{-5}, 1.03 x 10^{-4} and 4.07 x 10^{-4} s^{-1} were obtained for the reactions in

acetate 5, 10 and 20 % f_B respectively. Accordingly, in the same pD range the values for the

average of first order rate constants, k_{av} (s^{-1}) increase by a factor of 4.9 fold. This is believed to

represent a hydroxide dependent reaction. An average k_B $(M^{-1}s^{-1})$ of 5 x 10^{-2} $M^{-1}s^{-1}$ was obtained

for the acetate catalyzed reaction at the C-1 position of the molecule. Reactions of the C-3

protons of this molecule were not quantifiable by ^1H NMR and thus were followed by mass

spectrometry which suggests that a potential dimerisation reaction occurs following

deprotonation at this position. Reactions of the C-3 protons of BHA were monitored in

quinuclidinone buffers with values of $k_B(M^{-1}s^{-1})$ = 3.35 x $10^{-3}M^{-1}s^{-1}$ and k_{int} (s^{-1}) = 9.35 x 10^{-5} s^{-1}

obtained for the buffer catalyzed reaction and buffer-independent reaction respectively. The C-1

deprotonation reactions of BHA were monitored in acetate buffers (70-90 % f_B). An average k_B

$(M^{-1}s^{-1})$ of 9.17 x 10^{-5} $M^{-1}s^{-1}$ was obtained for the buffer catalyzed reaction in this pD range

(5.18-6.09). In the same pD range values of k_{int} (s^{-1}) = 3.7 x 10^{-6}, 4.7 x 10^{-6} and 1.19 x 10^{-5} s^{-1}

were obtained. The reactions of DHA and DHAS were monitored in the presence of MGS (19.6

and 78.4 μg/mL). While no reaction was observable for DHA in the presence of enzyme, DHAS

was found to undergo C-1 and C-3 deprotonation leading to average k_{cat}/K_M values of 56.5 $M^{-1}s^{-1}$

and 43.5 $M^{-1}s^{-1}$ for exchange and elimination respectively. The rate for elimination is

approximately 90,000 fold slower than that observed for natural substrate DHAP, $k_{cat}/K_M = 5.2 \times 10^6 \, M^{-1}s^{-1}$ indicating that the phosphodianion group of DHAP is crucial for optimal catalysis.

Abbreviations

Å	angstrom(s)
aa	amino acid
Ar	aryl
Asn	asparagine
Asp	aspartic acid
BHA	bromohydroxyacetone
b.p.	boiling point
br.	broad (spectral)
Bu	butyl
ca.	circa
cat.	catalyst
°C	degree centigrade
CHARMM	chemistry at Harvard molecular mechanics
cm^{-1}	wavenumbers
^{13}C NMR	carbon 13 nuclear magnetic resonance
CO_2	carbon dioxide
δ	chemical shift
d	doublet
Da	dalton (s)
DCM	dichloromethane
DFTB	density functional tight binding
DHA	dihydroxyacetone
DHAP	dihydroxyacetone phosphate
DHAS	dihydroxyacetone sulfate
DHATP	dihydroxyacetone thiophosphate
DHATS	dihydroxyacetone thiosulfate
DMF	dimethylformamide
DMSO	dimethyl sulfoxide

DNA	deoxyribonucleic acid
D₂O	deuterium oxide
ΔE	energy change
ED	enediolate
ESR	electron spin resonance
Et	ethyl
EtOAc	ethyl acetate
Fig.	Figure
ΔG	Free energy change
g	gram(s)
GA	glyceraldehyde
GAP	glyceraldehyde-3-phosphate
Glx I	glyoxalase I
GSH	glutathione
HCl	hydrochloric acid
His	histidine
¹H NMR	proton nuclear magnetic resonance
HMQC	heteronuclear multi quantum coherence
HOMO	highest occupied molecular orbital
hr	hour(s)
HSQC	heteronuclear single quantum coherence
Hz	hertz
***i*Pr**	isopropyl
IPTG	isopropyl β-D-1-thiogalactopyranoside
IR	infra red
IUPAC	International Union of Pure and Applied Chemistry
J	coupling constant
k	rate constant
K	kelvin
K	equilibrium constant
***K*ₐ**	acidity constant

K_M	Michaelis constant
kcal	kilocalorie(s)
kDa	kilodalton(s)
kJ	kilojoule(s)
λ	wavelength
L	litre(s)
LDA	lithium di-isopropylamide
LFER	linear free energy relationship
lit.	literature
ln	natural logarithm
log	logarithm
LUMO	lowest unoccupied molecular orbital
M	moles/litre (Molar)
m-	*meta*
m	multiplet (spectral)
Me	methyl
MG	methylglyoxal
MGS	methylglyoxal synthase
MM	molecular mechanics
μg	microgram
μL	microlitre
min	minute(s)
mL	millilitre(s)
mm	millimetre(s)
mmol	millimole(s)
mol	mole(s)
m.p.	melting point
ms	millisecond(s)
m/z	mass per unit charge
NAD^+	nicotinamide adenine dinucleotide
o-	*ortho*

p-	*para*
PAGE	polyacrylamide gel electrophoresis
PCR	polymerase chain reaction
PG	phosphoglycolate
PGH	phosphoglycolohydroxamate
Ph	phenyl
pm	picometre(s)
ppm	parts per million
ps	picoseconds
QM	quantum mechanics
Q_{net}	Löwdin net atomic charge
QTOF	quadrupole time of flight
R	alkyl substituent
Rf	retention factor
RNA	ribonucleic acid
ρ	reaction constant
σ	substituent constant
s	second(s)
s	singlet (spectral)
SDS	sodium dodecyl sulfate
SSHB	short strong hydrogen bond
t	triplet (spectral)
THF	tetrahydrofuran
TIM	triosephosphate isomerase
t.l.c	thin layer chromatography
TS	transition state
µL	microlitre(s)
UV	ultraviolet
VIS	visible
wk	week(s)
wt.	Weight

Acknowledgements

Firstly I would like to thank my supervisor Dr. AnnMarie O'Donoghue. Over the past few years I have learned a huge amount of chemistry from Annmarie. All of the work described in this thesis would not have been possible without her continuous help, guidance and support. Thank you for giving me the opportunity to conduct a research project in such an interesting and exciting field.

I would like to thank all the other lab members past and present, Anita, Shelley, Eleanor, Terry, Greg, Paddy, Dara and Dave. It was an absolute pleasure to work with such fun and talented scientists. To all the lads in UCD, particularly Cillian and Podge. Who will ever forget the discussions about distillation and liquor, the 'heated' football matches and the chemsoc events? You guys know what I mean!

To all the guys in Durham; Andrejz, Emma, Kiran, Alan, Blondie, Ed, Ollie, Markus, Vicky, Marie, Khairul, Doncadh, Chris, Graham, Ian, Joe, Andy, Ricky, Helen, Emma, Lucas and Dave who were so welcoming particularly when we needed to borrow a chemical or two in the early days of setting up the new lab! The daunting task of moving to Durham was made so much easier thanks to you all. To all the analytical staff in Durham particularly Dr. Alan Kenwright, Mr. Ian McKeag and Ms Catherine Heffernan. Thank you for providing such an excellent NMR service. To Dr Ian Cummins, Dr David Dixon and Dr Mark Skipsey for all the expert help with the biological procedures.

To Ollie and Laura! What a joy it must be for you guys to finally have a free dinner table! No more notes, laptop or mess! The Nintendo Wii was a welcome distraction when the writing up got tough. To Dawn and Ricky. Thank you for your kindness and hospitality during the early

months of writing up. To Emma, my new sister in law and to my brothers Martin and Peter. You guys are not only great brothers but also great friends.

A special thank you to Dr. Michael Lyons for a huge amount of advice and support throughout this project.

Finally to my parents. All that I have accomplished in my life is a result of your continuous love and support. This thesis is dedicated to you both.

Table of contents

13

15

16

Chapter 1

Introduction

1.0 Proton transfer reactions

Proton transfer is a fundamental process encompassing solution and gas phase chemistry as well as having a central role in biochemical reactions. The heterolytic cleavage of stable carbon-hydrogen bonds through proton transfer is a key step in a range of non-enzymatic and enzymatic processes, including elimination, carboxylation, phosphoryl transfer and Aldol and Claisen condensations [1-7]. Analysis of these processes can provide insights to the many mechanistic pathways of organic reactions. The following chapter will provide an introduction to proton transfer reactions at carbon and enzyme-catalyzed proton transfer reactions. In Sections 1.1 and 1.2 the kinetics of proton transfer reactions will be discussed with emphasis on linear free energy relationships that describe proton transfer processes. An overview of physiologically important enzyme catalyzed proton transfer reactions will be discussed in Section 1.3. The main focus of this introduction will be presented in Section 1.4 where the mechanisms of the non-enzymatic and enzymatic catalyzed proton transfer processes of glycolytically important triose phosphate molecules will be described in detail.

1.1 Catalysis by proton transfer (Bronsted Acid-Base Catalysis)

Acid–base chemistry plays a predominant role in describing the mechanisms of proton transfer reactions in solution. According to the Brønsted-Lowry definition, an acid is a substance that donates a proton (hydrogen ion H^+), and a base is a substance that accepts a proton [8]. The most widespread form of catalysis in aqueous solution is Brønsted acid and base catalysis.

1.1.1 Specific and general acid-base catalysis

The role that such catalysts play can be determined by kinetic techniques from which it is possible to recognise several distinct types of catalysis by acids and bases. The two major types of catalysis are specific and general catalysis. Specific acid catalysis is observed when a reaction proceeds through a protonated intermediate which is in equilibrium with its conjugate base. Since the equilibrium position is a function of the concentration of solvated protons, only a single acid-dependent term appears in the kinetic expression. An example of a reaction which is subject to specific acid catalysis is the acid-catalyzed hydrolysis of an ester [9] (Scheme 1.1).

Scheme 1.1
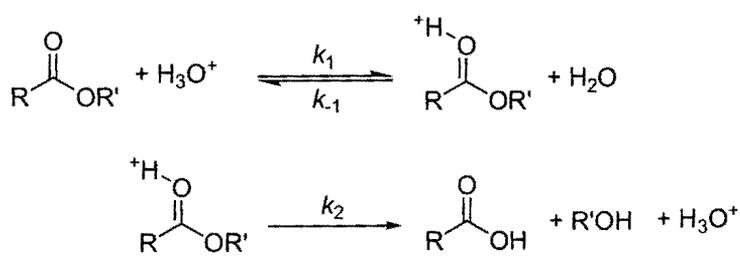
$$\text{Rate} = k_2[\text{EH}^+] = Kk_2[\text{E}][\text{H}_3\text{O}^+]$$

$$= k_{\text{obs}}[\text{H}_3\text{O}^+][\text{E}]$$

$$\text{where } k_{\text{obs}} = Kk_2$$

For the hydrolysis of an ester, the overall rate law will have the form of Equation 1.1 where $k_0[\text{E}]$ represents the uncatalysed hydrolysis of an ester in the presence of solvent.

$$-d[E]/dt = k_0[E] + k_H[H_3O^+] \qquad \textbf{Equation 1.1}$$

$$= k_{obs}[E]$$

$$\text{where } k_{obs} = k_0 + k_H[H_3O^+]$$

The second order rate constant, k_H ($M^{-1}s^{-1}$), may be obtained experimentally as the slope of a plot of pseudo first order rate constant, k_{obs}, against the concentration of hydronium ion. In many cases solvent induced ester hydrolysis is negligible. The observed first order rate constants, k_{obs}, for a specific acid catalyzed reaction are kinetically independent of buffer acid concentration at constant pH. This can be demonstrated experimentally by varying the concentration of the acidic buffer component at constant pH. This is achieved by keeping a constant ratio of the acidic and basic forms of the buffer whilst having different absolute concentrations of both components. If the pseudo first order rate constant, k_{obs}, does not increase as the buffer concentration is increased, then the weak acidic buffer does not catalyse the reaction.

A reaction that is specific base catalyzed involves proton transfer from substrate to hydroxide ion to yield an activated intermediate in a non-rate determining step, e.g. the specific base-catalyzed self condensation of an aldehyde (Scheme 1.2).

Scheme 1.2
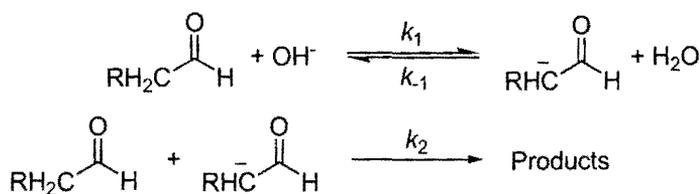
$$\text{Rate} = k_2[A^-][A] = k_2[A]K[A][OH^-]$$

$$= k_{OH}[OH^-][A]^2$$

$$\text{where } k_{OH} = Kk_2$$

21

For the above reaction the overall rate law will have the form of Equation 1.2

$$-d[A]/dt = k_0[A]^2 + k_{OH}[OH^-][A]^2$$

$$= k_{obs}[A]^2$$

Equation 1.2

where $k_{obs} = k_0 + k_{OH}[OH^-]$

Specific base catalysis thus describes a reaction where the reaction rate is kinetically dependent only on the concentration of the conjugate base of the solvent, hydroxide ion in aqueous solution, and is independent of other bases which may be present in solution (e.g. phosphate or carboxylate salts).

From Equation 1.2, a plot of k_{obs} against the concentration of hydroxide ion in a specific-base catalyzed reaction will give a straight line with gradient, k_{OH}, and intercept, k_0. This is analogous to the determination of k_0 and k_H for a specific acid catalyzed reaction. As with the specific acid catalyzed hydrolysis of an ester (where varying the concentration of acid buffer present has no effect on k_{obs}), varying the concentration of the basic form of buffer will have no effect on the pseudo first order rate constant.

In the case of general acid and base catalysis, the nature and concentration of all acids (HA) or bases (A⁻) present in solution affect the rate of the reaction. If the reaction rate increases with increasing buffer concentration at a constant pH, the reaction is seen to be dependent on the concentration of a component of the buffer: [AH] for general acid catalysis and [A⁻] for general base catalysis. The experimental rate law for the reaction (Scheme 1.3) of a compound S catalyzed by H_3O^+ as well as a weak acid A-H will have the form of Equation 1.3.

Scheme 1.3

$$S \xrightarrow[k_{obs}]{H_3O^+, A\text{-}H, H_2O} \text{Products}$$
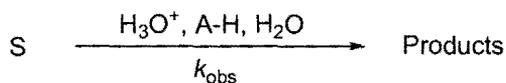
$$-d[S]/dt = k_{obs}[S]$$

Equation 1.3

$$\text{where } k_{obs} = k_0 + k_H[H_3O^+] + k_{HA}[AH]$$

Similarly a general base catalyzed reaction (Scheme 1.4) will have the form of Equation 1.4.

Scheme 1.4

$$S \xrightarrow[k_{obs}]{OH^-, B, H_2O} \text{Products}$$
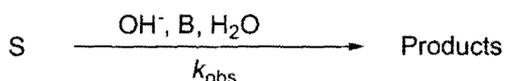
$$-d[S]/dt = k_{obs}[S]$$

Equation 1.4

$$\text{where } k_{obs} = k_0 + k_{OH}[OH^-] + k_B[B]$$

The addition of another weak acid or base to the reaction will result in overall rate constants as shown in Equations 1.5 and 1.6 where each general acid or base present contributes to the reaction.

$$k_{obs} = k_0 + k_H[H_3O^+] + k_{AH}[AH] + k_{BH}[BH]$$

Equation 1.5

$$k_{obs} = k_0 + k_{OH}[OH^-] + k_B[B] + k_A[\bar{A}]$$

Equation 1.6

23

General acid and base catalysis is usually associated with rate determining proton transfer at carbon in contrast to the fast proton transfer to and from oxygen and other heteroatoms (specific catalysis) which are usually diffusion controlled.

1.1.2 Linear free-energy relationships and proton transfer at carbon

Proton transfer reactions at carbon involve most of the important features that characterize polar reactions including the formation and cleavage of bonds, the transfer of charge, delocalization of charge, solvation of products/desolvation of reactants and the effect of potentially unequal progress in the development of these features leading to so-called transition state imbalances [10-12]. Proton transfer from normal acids is usually very fast and diffusion controlled. However proton transfer at carbon is typically much slower having lower intrinsic rate constants or higher intrinsic barriers [13]. These intrinsic barriers are dependent on the structural properties of an acid or a base and the behaviour of an acid or a base on dissociation in solution is intimately related to its behaviour as a general acid or base catalyst. This relation was fully quantified by Brønsted and Pederson in the early 1920's [14].

The Brønsted relationship (Equations 1.7 and 1.8) is one of the earliest examples of a linear free energy relationship [15, 16]. This relationship is between the catalytic constants for a reaction catalyzed by a family of general acids or bases such as carboxylic acids or tertiary amines and the relevant pK_a values for these acid/base catalysts. The Brønsted coefficients α and β, are constants dependant on reaction conditions and independent of the catalyst involved. These coefficients can be determined from a logarithmic plot of the catalytic constants k_{HA} or k_{A^-}

against the pK_a values of the catalytic acids or bases. The magnitude of the Brønsted coefficient is taken as a measure of the extent of proton transfer in the transition state of the general acid/base catalyzed reaction which involves rate-determining proton transfer at the substrate.

$$\text{Log } k_{HA} = \alpha \text{ logK}_{HA} + C = -\alpha \text{ } pK_{HA} + C \quad \textbf{Equation 1.7}$$

$$\text{Log } k_{A^-} = -\beta \text{ logK}_{A^-} + C = -\beta \text{ } pK_{A^-} + C \quad \textbf{Equation 1.8}$$

For a general acid catalyzed reaction if the extent of proton transfer is minimal in the transition state then a poor proton donor will be as effective as a good proton donor resulting in a small value of α. Alternatively if proton transfer at the transition state is almost complete a stronger acid will be a much more effective catalyst and α will have a value close to unity (Figure 1.1) [9].

Figure 1.1: Proton transfer progression at the transition state

$$\left(\text{S---H''A} \right)^{\ddagger} \qquad \left(\text{S--H--A} \right)^{\ddagger} \qquad \left(\text{S''H----A} \right)^{\ddagger}$$

| Little proton transfer at the transition state | Proton half transferred in transition state | Near complete proton transfer at transition state |
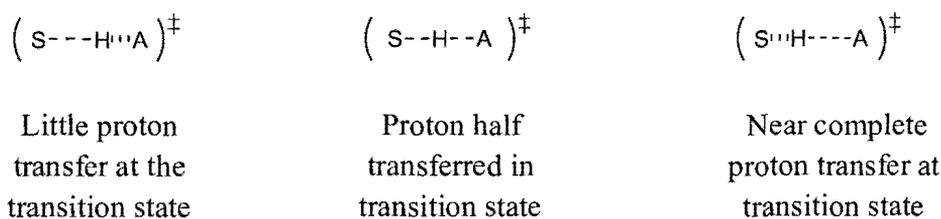
For the general-base catalyzed enolization of dihydroxyacetone phosphate (DHAP) and glyceraldehyde-3-phosphate (GAP) by a series of 3-substituted quinuclidine bases values of β =

0.48 and 0.45 respectively indicate a central transition state with proton approximately half way between substrate and basic acceptor [17].

The β value of 0.48 for buffer catalyzed enolization of DHAP is substantially lower than $\beta = 0.88$ for enolization of acetone by 4-substituted carboxylate anions [18] and the β value of 0.75 for base catalyzed elimination of 4-(4-nitrophenoxy)-2-oxobutane by a series of anionic bases with pK_a's in the range of 4.8 to 10.6 [19]. A possible explanation for the smaller β value for DHAP deprotonation is that electrostatic interactions between buffer and phosphodianionic group of substrate decrease the effective charge of the buffer catalyst in the transition state.

An unusually large value of $\beta = 1.09$ for the deprotonation of ethyl acetate catalysed by a series of 3-substituted quinuclidine bases shows that there is essentially complete proton transfer from ethyl acetate to the tertiary amine base in the rate-limiting transition state for this reaction and hence the rates of these thermodynamically uphill proton transfers are limited by diffusional separation of the intimate ion pair to give free enolate and protonated ammonium ion in solution [20]. This means that reverse protonation is diffusion controlled and also marks the abrupt change from a rate-limiting chemical step to a rate limiting transport step. This is described by Richard *et al* as one of the "reaction clocks" for carbanions.

In situations where ambiguity exists about a mechanistic pathway, such as a hydrolysis reaction where nucleophilic catalysis and mechanistic general base catalysis are possible with the family of bases used, a plot of log k_B against pK_{BH}, giving a β value outside the range of 0 and 1 would be evidence of the presence of nucleophilic catalysis. In the case of nucleophilic catalysis the plot of log k_B against pK_{BH} expresses an empirical relationship between catalytic effectiveness and base strength for the family of nucleophiles, and proton transfer is not involved.

1.1.3 Anomalous α and β values.

The notion that Brønsted exponents measure the transition state structure was questioned when systems were discovered where the exponents lie outside the range 0-1 [21]. These results clearly conflict with the hypothesis that α or β is equal to the degree of proton transfer at the transition state in that negative proton transfer or more than complete proton transfer can have no real meaning. However these results leading to such transition-state imbalances are now well understood and the circumstances in which they occur can now be fairly well predicted. These anomalies most commonly arise with proton transfer from nitroalkanes [22-24] where there is an inverse relationship between the rates of proton abstraction and acidities in the series CH_3NO_2, $CH_3CH_2NO_2$ and $(CH_3)_2CHNO_2$ and the hydroxide ion.

Here there is a progressive decrease in the rates of deprotonation by hydroxide (relative rates 113:18:1), whereas the acidities change in the opposite manner. (relative pK_a's 10.2, 8.5, and 7.7) [25]. Similarly, the logarithmic rates of deprotonation of $ArCHMeNO_2$, and $ArCH_2CHMeNO_2$ by hydroxide ion in 50% v/v aqueous methanol correlate with their pK_a values with a value of α = 1.31 and 1.61 respectively [21]. This means that the coefficients for protonation of the $ArCMeNO_2^-$ and $ArCH_2CMeNO_2^-$ ions by solvent must be −0.31 and −0.61 respectively, since the sum of Brønsted coefficients for the forward and reverse reactions must equal unity.

Scheme 1.5

$$HA + H_2O \underset{k_r}{\overset{k_f}{\rightleftharpoons}} A^- + H_3O^+$$
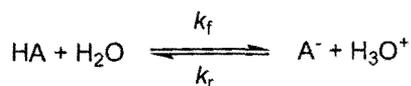
where $K_a = k_f/k_r$ **Equation 1.9**

Restriction of the Brønsted coefficients to values between 0 and 1 arose from the application of the Brønsted relationship predominantly to oxygen or nitrogen acids and bases such as carboxylic acids and carboxylate ions, amines and ammonium ions, pyridinium ions and pyridines. Here the position of the equilibrium (K_a) is more sensitive to structural changes than the microscopic rate constants (k_f and k_r) (see Scheme 1.5). However for carbon acids, which must undergo extensive structural reorganization to form an ion, substituent effects can lead to changes in k_f and k_r in the same manner as delocalization of the charge lags behind deprotonation. This is described by Bernasconi as the principle of non-perfect synchronization [26]. In the series CH_3NO_2, $MeCH_2NO_2$ and Me_2CHNO_2, proton abstraction by hydroxide is retarded by methyl substitution, but proton abstraction by the nitronate ion ($CH_2=NO_2^-$) from the solvent is slowed to an even greater extent. This results in a negative Brønsted coefficient for a plot of $\log k_f$ vs. $\log K_a$ ($\alpha \cong -0.7$) and a coefficient larger than 1 for a plot of $\log k_r$ vs. $\log K_{BH+}$ ($\beta \cong 1.7$).

Scheme 1.6

The strongly electron withdrawing nitro group produces a carbanion in which the negative charge has been almost completely removed from the carbon atom (see Scheme 1.6). This removal of charge from the carbon slows down the rate at which the carbon can pick up a proton to form the conjugate acid. Thus nitroalkanes such as nitromethane have a higher acid strength than is consistent with the rate of ionization because the carbanion is resonance stabilized.

Scheme 1.7

This effect is negated by the addition of π-donor substituents to the nitroalkanes such as 4-MeOPh or 4-Me$_2$NPh, seen in the reaction of piperidine with substituted β-nitrostyrenes, **(A)**, [27]. These substituents lead to resonance stabilization of the olefin **(B)**, (Scheme 1.8) which results in a reduction of the equilibrium constants (K_a) for the nitroalkanes derivatives. This would be expected to also lower the forward reaction rate (k_f), as this resonance not only stabilizes the olefin but pre-organizes the electronic structure to be more product-like, facilitating the delocalization of the negative charge starting to develop in the transition state. The result is more like the structure **(C)** where the transition state is stabilised and the intrinsic barrier to reaction is lowered. Without this pre-organization delocalization of the incipient negative charge into the nitro group lags behind bond formation and would resemble structure **(D)**.

Scheme 1.8

(A)

(B)

(C)

(D)
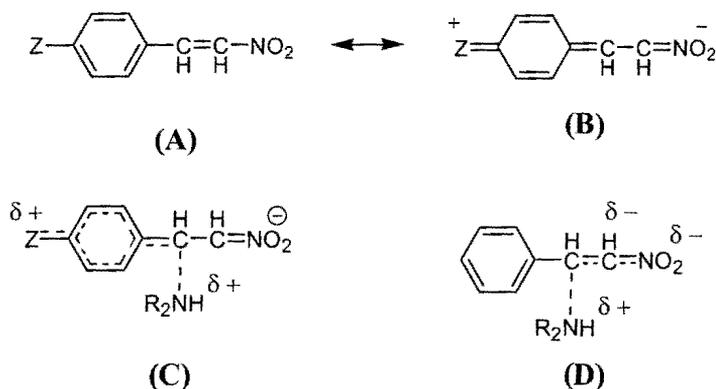
Similar if less pronounced behaviour is expected from carbonyl groups, which are less efficient than nitro groups at removing the negative charge from carbon. Cyano groups and sulfones are less effective still. However halogenated carbonyl compounds such as trifluoropentane-2,4-dione (pK_a 7.0) have an increased efficiency towards removal of the negative charge from carbon in the transition state by comparison with nitroalkanes of similar pK_a values.

As well as negative deviations, positive deviations from the Brønsted relationship for carbon acids are seen for reactions of compounds containing two carbonyl or carbethoxy groups. Cyano and sulfone containing carbon acids give the greatest positive deviation from the correlation for carbon acids. Changing ring size can also create anomalous Brønsted coefficients such as seen in cyclic ketoesters. 5-membered rings ionize similarly to their analogous straight chain, showing a positive deviation, however 6-membered rings ionize much more slowly and are weaker acids.

1.1.4 Proton transfer at electronegative atoms.

The linearity implied by the Brønsted relations (Equations 1.7 and 1.8) will hold only over a certain range and usually only for proton transfers involving carbon acids.

Scheme 1.9

$$AH + B \underset{k_r}{\overset{k_f}{\rightleftharpoons}} A + BH^+$$
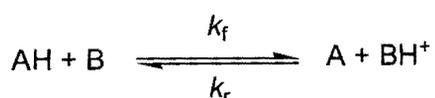
For a proton transfer reaction from an acid to a base (Scheme 1.9), the rate of proton transfer (k_f) cannot increase indefinitely in accordance with the Brønsted relationship. As an acid is made stronger the rate of the reaction will increase until the diffusion limit is met. At this point further

increases in the strength of the acid will have no effect on the rate of reaction. In this case the rate of proton transfer (k_f) will be independent of the acidity constant for HA (K_{AH}) and thus α will be equal to zero, whereas β will equal unity. However, decreasing the strength of the acid AH will lead to an increase in k_r until the diffusion limit is reached for this reverse reaction. Under these conditions β will equal zero with an α value of unity. Based on these assumptions neither Brønsted coefficient can be constant over any wide pK_a range of catalysts as both exponents change regularly between the limits of zero and one. Sharp curves known as Eigen curves (plots) [28] seen in some Brønsted plots occur for proton transfer between electronegative atoms such as oxygen and nitrogen [29]. These proton transfers can be described by the mechanism shown in Scheme 1.10.

Scheme 1.10

$$AH + B \underset{k_{-1}}{\overset{k_1}{\rightleftharpoons}} AH.B \underset{k_{-2}}{\overset{k_2}{\rightleftharpoons}} A^-.HB^+ \underset{k_{-3}}{\overset{k_3}{\rightleftharpoons}} A^- + HB^+$$
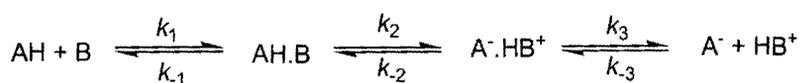
There are three distinct steps: initial diffusion together of the acid and base molecules resulting in the formation of an encounter complex AH.B, intramolecular proton transfer to form the complex $A^-.HB^+$, and dissociation of this complex to form the conjugate acid and base HB^+ and A^- respectively. Mechanistic proposals for this proton transfer reaction where the basic sites A^- and B are nitrogen or oxygen suggest that the second order rate constants, k_1 and k_{-3}, are at the diffusion limit with values approximately 10^{10} $M^{-1}s^{-1}$. For a thermodynamically favourable reaction where $pK_{AH}(AH) \ll pK_{AH}(BH^+)$ the rate of formation of the encounter complex $A^-.HB^+$ will be very fast with a rate constant, k_1. For a thermodynamically unfavourable reaction where $pK_{AH}(AH) \gg pK_{AH}(BH^+)$ diffusion apart of A^- and HB^+ is rate limiting. In the case where pK_{AH}

31

~ pK_{HB+} the proton transfer step is rate-determining. Therefore the slope $\delta(\log k_f)/\delta(\Delta pK) = 0 = \beta$ for the forward reaction occurs where ΔpK is positive (i.e thermodynamically downhill). The slope for the reverse reaction under the same conditions $\delta(\log k_r)/\delta(\Delta pK) = -1 = \beta$ where ΔpK is positive. For a thermodynamically uphill reaction (negative ΔpK) the reverse reaction becomes diffusion controlled and $(\delta \log k_r)/\delta(\Delta pK) = 0 = \beta$, and $(\log k_f)/\delta(\Delta pK) = +1 = \beta$. These values are represented schematically by an Eigen plot (Figure 1.2)

Figure 1.2: Symmetrical charge distribution
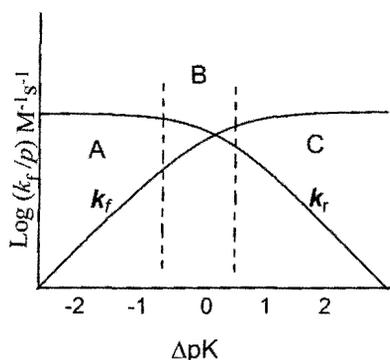
In section B of the plot, where the pK_a of AH and BH^+ are similar ($\Delta pK \sim 0$), the slopes of the forward and reverse reaction change from 0 to 1 and 0 to -1 respectively. For proton transfer reactions where there is a symmetrical balance of charge such as in Figure 1.2, the curves for the forward and reverse reaction should also be symmetrical. There are cases where many proton transfer reactions present an asymmetry of charge (Figure 1.3). One such example is in the α-proton transfer reaction of 2-(1-Hydroxybenzyl oxythiamin).

Figure 1.3: Unsymmetrical charge distribution
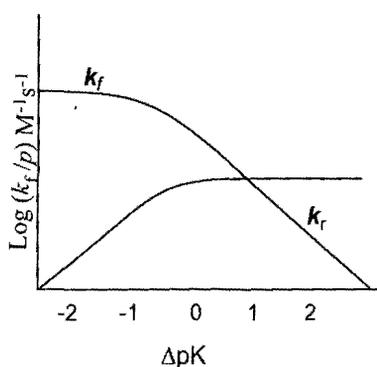
The rate of diffusion controlled proton transfer between neutral molecules is not the same as proton transfer between charged molecules. This results in asymmetry in the Brønsted plot due to differences in the slopes and curvature of the plots.

Sharply curved Brønsted relations have also been observed for some carbon acids. Such Eigen-like behaviour for carbon acids have negated the idea that such curves in the Brønsted plot are a function of the particular atoms between which the proton is being transferred. As for oxygen/nitrogen acids and bases, proton transfer to and from carbon is also intrinsically fast for carbon acids including chloroform, cyanocarbon acids and phenyl acetate. Linear Brønsted plots where $0 < \alpha, \beta < 1$ are a result of slow proton transfer between carbon acids and bases even when the reaction is thermodynamically favourable. Support for a connection between reactivity and Brønsted plot curvature comes from the Marcus theory.

1.1.5 Brønsted coefficients and the Marcus Theory

The Marcus theory [30], originally developed for outer-sphere electron transfer processes in solution, relates the free energy of activation for a proton transfer reaction, $\Delta G^{\ddagger}$, to the standard

free energy of the reaction, ΔG_0 (Equation 1.10). In this equation the $\Delta G_0^{\ddagger}$ term refers to the free energy of activation for a thermoneutral reaction ($\Delta G_0 = 0$) and is usually referred to as the intrinsic barrier.

$$\Delta G^{\ddagger} = (1 + \Delta G_0/4 \Delta G_0^{\ddagger})^2 \Delta G_0^{\ddagger} \qquad \textbf{Equation 1.10}$$

Differentiation of $\Delta G^{\ddagger}$ with respect to ΔG_0 results in an expression for the Brønsted coefficient α (Equation 1.11).

$$\alpha = \delta(\Delta G^{\ddagger})/\delta(\Delta G_0) = (1 + \Delta G^0/4 \Delta G_0^{\ddagger})/2 \qquad \textbf{Equation 1.11}$$

When $\Delta G_0 = 0$, then $\alpha = \frac{1}{2}$, for exothermic reactions $\Delta G_0 < 0$ and thus $\alpha < 1/2$ and for endothermic reactions $\Delta G_0 > 0$ resulting in $\alpha > 1/2$. Curvature of the Brønsted plot can be identified with the rate of change of α with ΔG_0 and thus immediately provides a connection between the degree of curvature and reactivity. This relationship predicts that for intrinsically slow reactions such as proton transfer at carbon, large values of $\Delta G_0^{\ddagger}$ and low values of the second derivative, $\delta(\alpha)/\delta(\Delta G_0)$ will result which will lead to little curvature in the Brønsted plot. On the other hand intrinsically fast reactions such as proton transfer between electronegative atoms will show sharp curvature as a result of small values of $\Delta G_0^{\ddagger}$ and large values of $\delta(\alpha)/\delta(\Delta G_0)$ [28].

1.2 Enolization reactions of carbonyl compounds

Despite the short-lived and transient nature of many enols and enolate intermediates, formation of these species are crucial in a range of chemical and biological proton transfer reactions [31]. A large number of enzymes catalyze the heterolytic abstraction of the α-proton from a carbon acid substrate to initiate 1,1-, 1,2- and 1,3- migrations of protons as well as β-elimination, Aldol and Claisen condensation reactions.

According to the Marcus equation the free energy of activation ($\Delta G^{\ddagger}$) for such a unimolecular reaction may be divided into two parts; i) the intrinsic kinetic barrier (ΔG_{int}) and ii) the thermodynamic barrier (ΔG_0). The enolization of carbonyl compounds involving heterolytic cleavage of α-protons adjacent to carbonyl centres is intrinsically slow. Large pK_a differences between reacting groups as well as the high intrinsic free energy barriers result in the slow formation of such labile enolate intermediates [32].

Thus the solution, non-enzymatic formation of enol or enolate intermediates is generally thermodynamically and kinetically unfavourable (the thermodynamic barrier for the formation of enolates of ketones and carboxylic acid derivatives is known to be high with an unfavourable equilibrium constant for the formation of the corresponding enolates, pK_a >19) [33]. Also, the rate of non-enzymatic proton abstraction of an α-proton of a carbon acid is slower than the rate of abstraction of a proton from a normal acid or a heteroatom of equal acidity. The intrinsic kinetic barrier for proton transfer from a carbon acid is typically greater than that of a normal acid (3 kcal/mol) [34]. This difference is believed to occur as a result of an overall solvent reorganisation process where the development of a negative charge on the carbonyl oxygen results in changes in the orientation of the solvent dipoles.

35

{

An overview of some of the important methods of studying enolization is presented in Section

ε

1.2.1.1 and 1.2.1.2.

}

}

1.2.1.1 Halogen trapping

Historically, the main method of studying enolization processes is in using a scavenger species

which can trap the enol and enolate intermediates [35]. In the majority of cases this species is an

electrophilic halogen [36]. The kinetics of enolization reactions have been made possible by

these reactions in the cases of both acid (Scheme 1.11) and base (Scheme 1.12) catalyzed

reactions.

Scheme 1.11
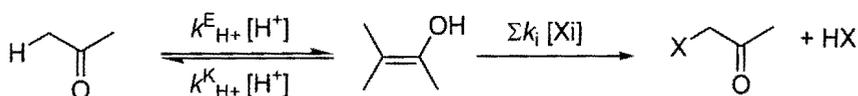
In Scheme 1.11 k^E_{H+} [H$^+$] represents the rate constant for acid catalyzed enolization, $k^K_{H}{}^+$[H$^+$]

represents the rate constant for acid catalyzed ketonisation. Σ k_i [Xi] represents the sum of the

first order rate constants for possible halogenating species in acidic solution; X_2 and $X_3{}^+$.

Scheme 1.12
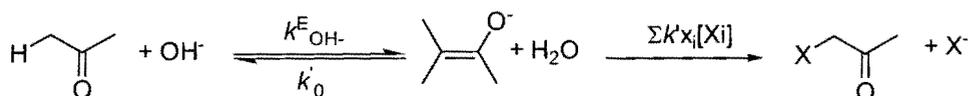
In Scheme 1.12 k^E_{OH-} represents the rate constant for base catalyzed enolization, k'_0

36

represents the rate constant for base catalyzed ketonisation. $\Sigma \, k'x_i \, [X_i]$ represents the sum of the first order rate constants for possible halogenating species in basic solution; X_2 and X_3^-, XOH and XO^-.

In solution formation of the enolate is generally presumed to be rate-determining (with fast halogenation). In the case of the acid catalyzed halogenation reaction (Scheme 1.11) it can be assumed that in dilute acidic solutions halogenation of the enol is much faster than the ketonization reaction. Experimentally this can be confirmed by the observed zero order kinetics for the rate of halogenation and the first order dependence of the reaction on the concentration of acid catalyst, with no apparent saturation at higher concentrations of acid. Increasing the acid concentration may lead to a partially or fully rate-determining halogenation step due to the fact that ketonisation of the enol intermediate is acid catalysed whereas halogenation is not. The iodination of acetophenone has been shown to be dependent on the concentration of iodine in solution containing greater than 50 % H_2SO_4. Alternatively, rate-limiting halogenation has been determined more accurately by using very low concentrations of halogen. This results in a reduction of the rate of halogenation, $k_i \, [X_i]$, to a rate comparable to that of enolization, k^E_{H+} $[H^+]$. From this method it has been demonstrated that the second order rate constants for halogenation of simple enols with Cl_2, Br_2 and I_2 are essentially similar with the rate of halogenation at the diffusion limit $(5 \times 10^9 \, M^{-1} \, s^{-1})$.

In alkaline solution (Scheme 1.12) the assumption that the halogenation of the enolate intermediate is zero order in halogen cannot be made. Based on the chlorination reaction of ketones in alkaline solution, it was observed that the reaction has a term in the rate law which is first order in the hypochlorite species ClO^-. Results from the halogenation of acetone in dilute NaOH have shown that the reaction rate is sensitive to the concentration of all halogen species

37

present in solution. Rate-limiting enolate formation can only be made possible on use of a large concentration of halogen species. Furthermore enolization of the molecule pinacolone in dilute alkaline solution results in a rate law which shows second order dependence on the concentration of halogen (hypobromite species in this case). Based on these experimental observations it is clear that obtaining the rates for base catalyzed halogenation (and thus enolization) are more difficult than the corresponding acid catalysed reaction.

Following the first halogenation of a carbonyl compound, it is likely that successive halogenations will occur. In the situation of base catalyzed reaction successive α-halo substitution results in an increase in the rate of halogenation and thus enolization. Monohalogenated products are commonly observed in the case of acid-catalyzed halogenation as acid-catalyzed enolization (halogenation) is retarded by α-halo substitution. On this basis, acid catalyzed halogenations of simple aldehydes and ketones are often so slow that initial rate methods (zero-order kinetics) are employed to study these reactions. Conversely, base-catalyzed halogenation reactions are generally fast enough to be studied under first-order conditions.

1.2.1.2 Isotopic hydrogen exchange

Enolization processes result in intermediate species which are generally unstable and short-lived. Therefore direct observation of such species is difficult. However, in the situations where the enol or enolate species can be made to constitute a significant fraction of the equilibrium mixture it is possible to observe enol-enolate formation directly. For example in the case of β-dicarbonyl compounds the enolate formed is resonance stabilised and thus is sufficiently stable in alkaline solution to make up a significant proportion of the equilibrium. In these cases the enol-content can be enhanced by using solvents such as DMSO which are less polar than water.

38

The exchange of a proton for deuterium or tritium at the α-carbon of a carbonyl compound [37] is an important method in directly monitoring the formation of unstable enols and enolates particularly with improvements in analytical methods such as NMR spectroscopy and mass spectrometry.

Modern high resolution ^{1}H NMR spectroscopy has proven particularly useful in monitoring the mechanisms of enolization of a range of organic reactions. The background enolization reactions of triose phosphate molecules such as dihydroxyacetone, dihydroxyacetone phosphate and glyceraldehyde-3-phosphate (these are discussed in the next section) [38] are particularly relevant as these molecules play a vital role in enzyme catalyzed biological processes such as glycolysis . The second order rates for general base catalyzed enolization, when combined with k_{cat}/K_M for the corresponding enzymatic reaction quantify fully the overall enzymatic rate acceleration. Incorporation of the isotope at the α-carbonyl carbon is good evidence for the formation of an enolate intermediate (Scheme 1.13).

Scheme 1.13
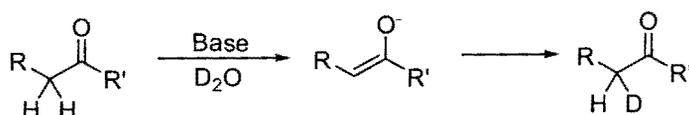
Furthermore the rate-limiting step in the exchange reaction is enolate formation. Thus determination of rate constants for exchange provides access to rate constants for enolization.

1.3 Enzymatic catalysis of enolization and proton transfer at carbon

As with reactions in solution which are catalyzed by acids or bases, many enzymes contain active groups which promote acid or base catalysis.

The catalytic efficiency and overall specificity of enzymes makes them the paragons of catalysis in solution particularly at near to neutral pH values. Changes in pH often lead to loss of catalytic activity due to enzyme denaturation and for this reason the majority of enzymes operate in a narrow pH range, each having an optimal pH value.

Enzyme reactions occuring near neutrality in biological systems rely largely on general catalysis as the concentrations of hydroxide and hydronium ions at these pH values are low. Covalent bond formation between enzyme and substrate is quite limited due to the inert nature of the enzyme peptide chain. However, a selective few ionizable groups such as carboxylic acids, amines, phenols and alcohols are nucleophilic enough to react with electrophilic centres of the substrates in the enzyme active site. More frequently the ionisable amino acid groups of the enzyme can act as either a proton acceptor or donor exhibiting acidic or basic properties respectively e.g. the active site residues of the glycolytic enzyme *triosephosphate isomerase* include a glutamate residue which functions as a general base catalyst and a histidine residue functioning as an electrophilic catalyst in the isomerisation reaction of dihydroxyacetone phosphate (DHAP) **(1)** (Scheme 1.14 A) [39]. Similarly *methylglyoxal synthase* catalyzes the elimination of phosphate from DHAP using an aspartate general base and a local electrophilic catalyst (Scheme 1.14 B) [40]. These reactions are discussed in more detail in Section 1.4.

Scheme 1.14

(A)　　　　　　　　　　(B)

(1)　　　　　　　Asp 71

$^{2-}O_3PO$ ... OH ... H

His 98

$^{2-}O_3PO$ ... OH ... H　　Glu 165

Electrophile O
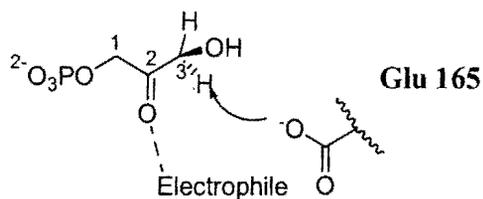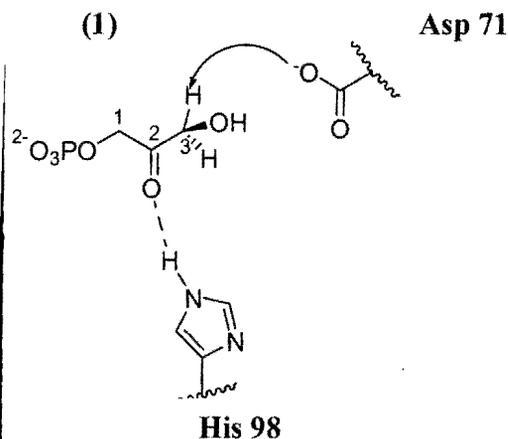
In the following sections an overview of enzyme catalyzed proton transfer reactions will be presented.

1.3.1 Keto-enol tautomerisation and enzymatic proton transfer

For enzyme-catalyzed enolization, the problems posed by high intrinsic kinetic and thermodynamic barriers can be avoided as a result of several processes. Firstly, the thermodynamic barrier to the formation of an enolate intermediate can be reduced by H-bonding and electrostatic interactions at the enzyme active site [41-44]. The intrinsic kinetic barrier may be reduced by concerted general acid-base catalysis as well as appropriate placement of active site electrophilic and nucleophilic catalysts adjacent to the carbonyl oxygen. This stabilizes the developing charge on the carbonyl oxygen and ultimately reduces the kinetic barrier to enolate formation. This section will provide an overview of some of the enolization reactions occurring

41

in biological systems and how the individual enzymes involved avoid the problems associated with the equivalent non-enzymatic catalyzed enolization reactions.

1.3.1.1 Ketosteroid isomerase catalyzed proton transfer

Isomerisation reactions are common in biological systems and particularly in cellular processes. Enzymes which catalyze isomerisation reactions via carbon acid deprotonation include the glycolytic enzyme *triosephosphate isomerase*, glyoxalase I and the enolase family of enzymes such as mandelate racemase [45-48]. The 3-oxo-Δ^5-steroid isomerase enzymes (ketosteroid isomerases) are involved in microbial steroid metabolism [49]. One well studied member of this family of enzymes catalyze the isomerisation of the Δ^5-3-ketosteroid, 5-androstene 3,17 –dione (2), and the Δ^4-3-ketosteroid, 4-androstene 3,17-dione (4) (Scheme 1.15) at a near diffusion-controlled rate; $k_{cat}/K_m = 4 \times 10^8$ M^{-1}s^{-1} [50, 51]. In contrast, the non-enzymatic acetate ion catalyzed enolization reaction is thermoneutral, with rates of 6.1 x 10^{-4}s^{-1} and 1.3 x 10^{-8}s^{-1} for formation of the enolate intermediate from substrate and product respectively. Such slow rates can be understood from the high energy nature of the conjugate anionic intermediates of transient species resulting from α-proton abstraction as well as high intrinsic barriers. Computational studies have shown that these enzymes reduce the barrier to formation of the enolate from both product and substrate by 10 kcal/mol and 9 kcal/mol respectively via a series of H-bonding and electrostatic interactions at the active site. In the forward reaction the β-proton at the sp^3 hybridised C-4 carbon of substrate 5-androstene-3,17-dione (2) (pK_a ~ 12) is abstracted by an active site base (Asp 40). Reketonization occurs at the sp^2 hybridised C-6 of the enolate intermediate to yield the isomerisation product 4-androstene-3,17-dione (4) (pK_a ~16). As well as

containing a general acid/base residue the mainly hydrophobic active site pocket contains polar Tyr16 and Asp140 groups. All three residues are essential to catalysis where the latter two are believed to be involved in the stabilization of the developing negative charge on O-3 of substrate via hydrogen bonding. Development of such hydrogen bonds at the active site has been proposed as a major reason for such high catalytic efficiency of the ketosteroid isomerase enzyme.

Scheme 1.15
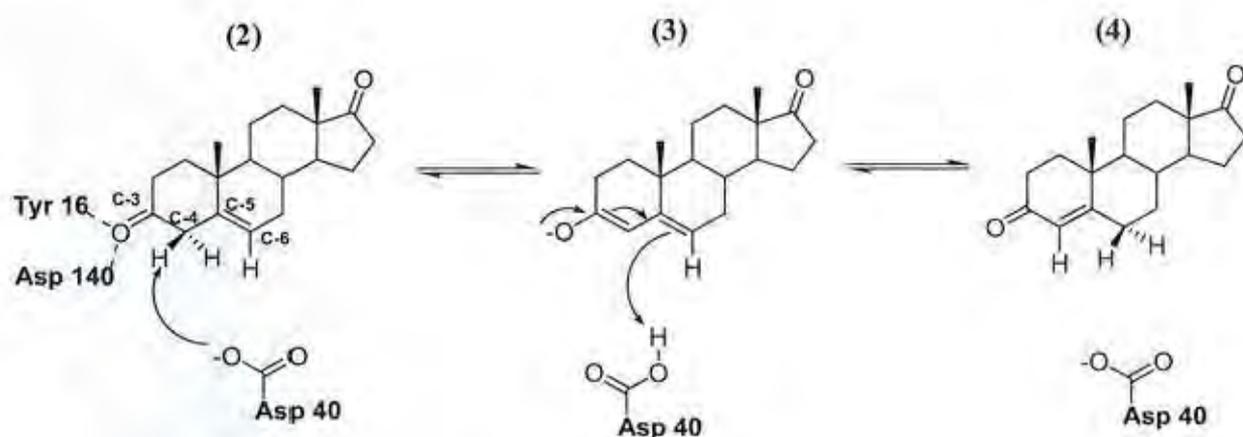
1.3.1.2 Mandelate racemase

The enolase superfamily includes the enzymes mandelate racemase, enolase and muconate-lactonizing enzyme [52]. Each member of the superfamily, while catalysing a distinct overall reaction, shares a common step in the abstraction of the α-proton of a carboxylic acid. Mandelate racemase isolated from *pseudomonas putida* catalyzes the Mg^{2+} dependent interconversion of the two stereoisomers of mandelic acid [53, 54]. The mechanism of the reaction involves two proton transfer reactions; the α-proton of substrate (*R*)-mandelate is abstracted by His 297, and the α-proton of product (*S*)-mandelate is derived from solvent via an active site general acid catalyst. This 'two-base' mechanism is shown in Scheme 1.16.

43

Scheme 1.16
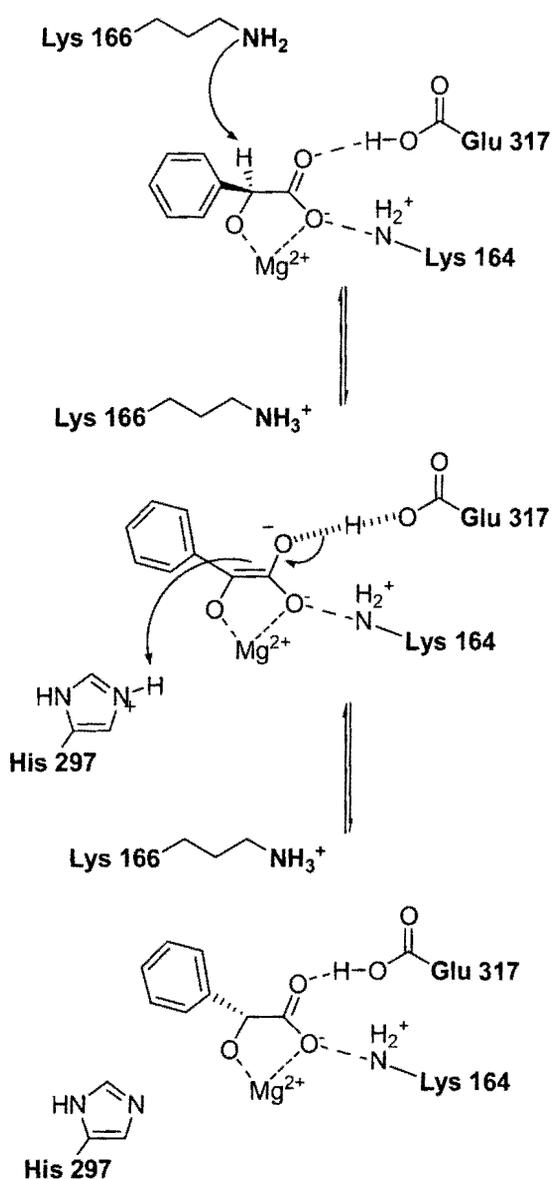
The catalytic involvement of His 297 and Lys 166 in the reaction has been demonstrated using combined NMR exchange studies/X-ray crystallography. Deuterium exchange studies used to isolate the rate constant for enzymatic racemization show that the first order rate constants for racemization of mandelate in H_2O and D_2O, at pH 7.5 and pD 7.5 respectively are equal (within experimental error) suggesting that there is no solvent isotope effect. These rate constants were

44

also equal, within experimental error to the first order rate constant for deuterium incorporation into mandelate in D_2O at pD 7.5. Therefore racemization occurs with a first order rate constant equivalent to that of deuterium exchange at the same pD. Non-enzymatic racemization of mandelic acid is extremely slow being observed only at elevated temperatures and in the presence of concentrated acid. Determination of the rate of racemization in the absence of enzyme (k_{non}) shows that at 25 °C the free energy of activation for racemization is 34.6 ± 0.9kcal/mol. This corresponds to a non-enzymatic rate constant equal to ~ 3 x 10^{-13} s^{-1}. Comparison of k_{non} with the turnover number, k_{cat} = 500s^{-1}, indicates a rate enhancement of 1.7 x 10^{15} at pH 7.5 and 25 °C. The rate acceleration provided by mandelate racemase surpasses the levels achieved by most enzymes.

1.3.1.3 Fructose 1,6-bis phosphate aldolase

One of the best studied aldolases is fructose-1,6-bisphosphate aldolase which is a key enzyme in glycolysis [55, 56]. This enzyme catalyzes the reversible conversion of fructose-1,6-bisphosphate (5) to dihydroxyacetone phosphate (1) and glyceraldehyde-3-phosphate (6) [57]. The mechanism of the aldolase reaction requires the ring opened ketose whose carbonyl oxygen is either polarized by a metal ion as in the case of class II aldolases or reacts with an active site lysine residue to form a Schiff base intermediate as seen in class I aldolase catalyzed reactions (Scheme 1.17).

Scheme 1.17

(5) (6) (1)
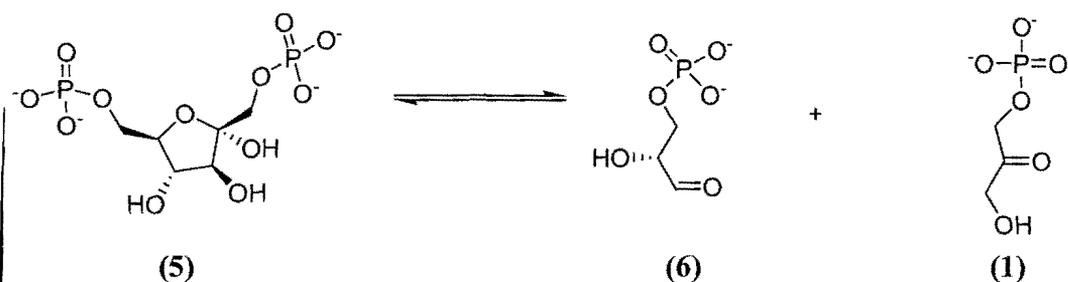
1.4 Enzymatic reactions of triose sugars

As the turnover of the triosephosphates DHAP **(1)** and GAP **(6)** by TIM and DHAP by MGS are directly relevant to this thesis, the following section will be devoted to the reactions involving these and related substrates. Section 1.4.1 will provide a brief overview of the reactions catalyzed by MGS and TIM. The solution reactions of these substrates in the absence of enzyme will be discussed in Section 1.4.2. Section 1.4.3 will deal with the overall tertiary, quaternary and active site arrangement of each enzyme and the intricate kinetic experiments carried out to identify the individual catalytic residues of MGS. Finally, a comparison between the catalytic residues, mechanism of catalysis and origins of the product outcome of the two enzymes will be discussed in Section 1.4.4.

1.4.1 MGS and TIM: A mechanistic overview

The importance of triose phosphates such as DHAP **(1)** and GAP **(6)** in biological reactions can be ascertained by their centrality in processes such as glycolysis and the Calvin cycle [39] . The

interconversion of DHAP **(1)** and GAP **(6)** is catalyzed by the enzyme *triosephosphate isomerase* (TIM) [58, 59] (Scheme 1.18).

Scheme 1.18

Triosephosphate Isomerase

In this reaction, stereospecific abstraction of the C-3 (*pro-R*) proton of DHAP **(1)** by an active site base (Glu 165), leads to the formation of an enediolate intermediate **(1a)** [60, 61]. This intermediate is then reprotonated at the C-2 position (His 95) to give the isomerisation product, D-glyceraldehyde 3-phosphate **(6)**. A value of $k_{cat}/K_m = 9.25 \times 10^5 \, M^{-1}s^{-1}$ is observed for the TIM catalyzed isomerisation of DHAP **(1)** to GAP **(6)**. The thermodynamically downhill isomerisation of GAP **(6)** to DHAP **(1)** is also catalyzed by TIM, with k_{cat}/K_m near the diffusion limit [62]. The isomerisation reaction from DHAP **(1)** to GAP **(6)** is kinetically limited only by the rate of diffusion of substrate onto and off of the enzyme surface and for this reason TIM is said to have evolved to catalytic perfection.

Studies on the mechanisms and pathways of bacterial glycolysis have revealed that the enzyme *methylglyoxal synthase* (MGS) provides bacteria with an alternative to the TIM reaction in metabolizing DHAP **(1)** [40, 63-65]. MGS catalyzes the stereospecific abstraction of a C-3 (*pro-S*) proton by an active site base (Asp 71) from DHAP **(1)** to form the enediolate intermediate **(1a)** [66]. However, unlike TIM, MGS catalyzes the collapse of this intermediate to

47

$$\Theta = \frac{[L]^n}{K_d + [L]^n}$$ **Equation 1.12**

Where θ = number of binding sites filled, [L] = ligand concentration, k_d = dissociation constant and n = Hill coefficient which describes cooperativity.

$$v = \frac{V_{max}[S]}{K_M + [S]}$$ **Equation 1.13**

Where K_M = Michaelis constant, [S] = substrate concentration, v = initial rate of production of product and V_{max} = maximum initial rate of production of product.

The toxic nature of MG indicates that an appropriate balance of detoxification and production is crucial for cell viability. The electrophilicity of this compound means that its formation interferes with nucleic acid and protein synthesis, ultimately leading to cell death. However, cells have developed a number of methods of detoxifying and metabolising MG **(8)**. One of the main methods of MG detoxification involves the glyoxalase I/glyoxalase II system which catalyses the glutathione-dependent conversion of MG to D-lactoylglutathione **(9)** [46, 72, 73] (Scheme 1.20).

Scheme 1.20

Methylglyoxal Synthase

(1)   **(8)**   **(9)**

GSH =

(10)
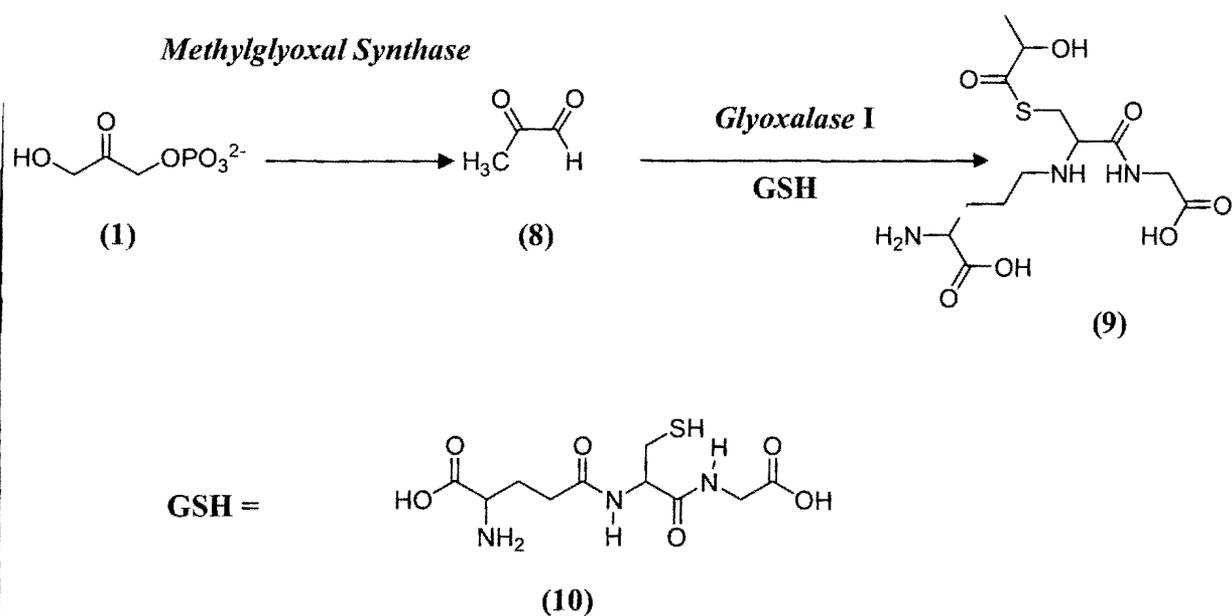
D-lactoylglutathione **(9)** is also cytotoxic in millimolar quantities, interfering with the formation of intermediate filaments. In this case the enzyme glyoxalase II converts D-lactoylglutathione to harmless D-lactate **(11)** (Scheme 1.21) which can be used in cell-wall biosynthesis in gram-negative bacteria.

Scheme 1.21

(9)   **(11)**

50
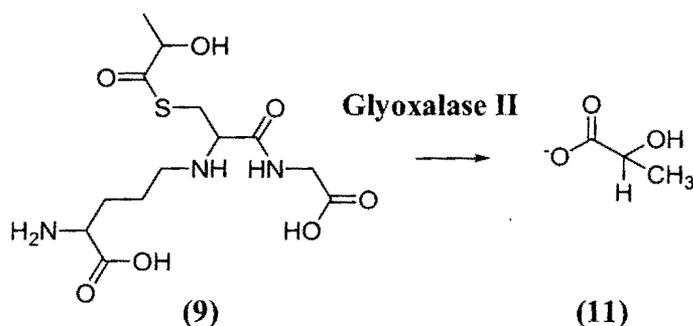
1.4.1.1 Stereospecificity in the MGS reaction

MGS has been shown to abstract the pro-*S* proton at the C-3 position of DHAP (1) stereospecifically while reprotonation at the C-3 position of elimination product, MG, occurs non-stereospecifically. Verification of these mechanistic observations came from isotopic labelling experiments. (3R)-[3-^{3}H] DHAP (1') was reacted with MGS to form isotopically labelled MG (8') [66](Scheme 1.22).

Scheme 1.22
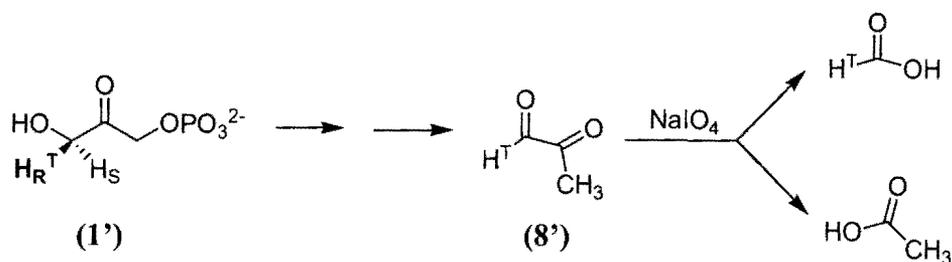
Cleavage of MG using sodium tetraiodate (NaIO$_4$) resulted in the formation of acetic acid and formic acid. No counts of radioactivity were observed for acetic acid molecule indicating that intramolecular transfer of the pro-*R* proton of DHAP (1') had not occurred to the C-3 methyl group of MG (8'). Also, the level of radioactivity of formic acid was found to be similar to that of free MG prior to cleavage, suggesting that MGS catalyzed deprotonation is specific for the pro-*S* proton of DHAP. Further experiments were carried out where the MG (8') product of DHAP (1') was reacted further to 2,4-dinitrophenylhydrazine. The product, dinitrophenylhydrazone, was extracted into ethyl acetate and the counts of radioactivity of the organic phase were compared to counts in the aqueous phase. It was found that > 95 % of the

radioactivity was EtOAc extractable becoming so at the same rate as product formation. This suggested the absence of a secondary isotope effect and also the irreversible nature of the MGS catalyzed elimination reaction. Analogously, for the MGS catalyzed elimination reaction of (3S)-[3-^{3}H] DHAP, the radioactive counts in the aqueous phase were far greater than those extracted into ethylacetate. This provided further support for the stereospecific abstraction of the C-3 proton of DHAP (1) by MGS. To investigate the presumed non-stereospecificity of reprotonation at the C-3 position of MG, two separate experiments were carried out; 1) Inhibition studies of the enzyme with MG (8'). The ability of MG to act as an inhibitor was tested with concentrations > 100 mM. However it was found that rate of elimination was unaffected by the presence of MG. Therefore this implied that the non-stereospecific protonation of the enolaldehyde at the C-3 position occurs non-enzymatically in solution resulting in formation of MG (8).

1.4.2 The reactions of triose phosphates in solution

It is generally presumed that the mechanisms employed by enzymes to achieve catalysis are similar to those for the corresponding solution reactions. Energetically it is unfavourable that the two mechanisms should differ as before any net catalysis from transition state stabilisation can be achieved the enzyme must first lower the barrier to the observed solution reaction.

It has been proposed that the solution elimination and isomerisation reactions of DHAP (1) and L-GAP (6) proceed through an enediolate intermediate thus mirroring the corresponding enzymatic mechanisms. Verification of enediolate intermediate formation came from experimental observations that the general base catalyzed solution isomerisation and elimination

52

reactions of L-GAP were completely blocked in the presence of $K_3Fe(CN)_6$, a known oxidant of enediols [74]. The rate constants for the elimination and isomerisation reactions of DHAP (1) and GAP (6) from these early studies were determined for single sets of reaction conditions. However more recently, in a detailed study by Richard *et al*, the rates for the uncatalyzed, hydroxide catalyzed and buffer catalyzed solution reactions of these triose phosphates have been obtained over the entire pH range. In solution, the elimination and isomerisation reactions of DHAP (1) and GAP (6) occur via rate-limiting substrate deprotonation followed by partitioning of the enediolate intermediate between elimination, k_e and isomerisation, k_2, k_{-1} (Scheme 1.23).

Scheme 1.23
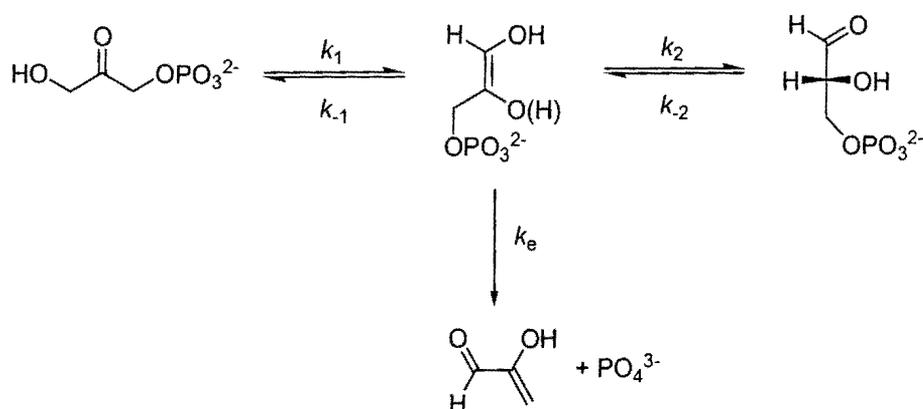
The elimination reactions of $[^{32}P]$ DHAP and $[^{32}P]$ GAP were monitored by Richard *et al* using a radiolabelled assay method [17]. Reactions were initiated on addition of buffer or KOH (pH 7-14). At specific time intervals aliquots of the solution were withdrawn followed by the addition of sodium molybdate. The phosphate-molybdate complex was then extracted into isobutyl alcohol and the unreacted radiolabelled DHAP (1) or L-GAP (6) was determined as the radioactive counts remaining in the water layer. The values of the pseudo first order rate constants, k_{obs} (s^{-1}) for elimination were determined from the slope of the plots of 6-10 values of

ln (C_t-C_∞) against time where C_t is the counts of radioactivity remaining in the water layer at a given time and C_∞ represents the counts of radioactivity in the water layer at infinite time. The second order rate constant, k_B, for the general base catalysed elimination reaction were determined from the slope of the plots of k_{obs} against the concentration of buffer at constant pH.

1.4.2.1 Elimination reaction of DHAP and L-GAP in solution

The mechanism of DHAP (1) and GAP (6) elimination is believed to be an E1cb-type which proceeds through an enediolate intermediate. As discussed by Richard, experimental evidence for enediolate formation and an E1cb-type elimination comes from the following observations:

1) The similar second order rate constants for the hydroxide–catalyzed elimination reactions of DHAP (0.56 $M^{-1}s^{-1}$) and hydroxide catalyzed deprotonation of acetone (0.25 $M^{-1}s^{-1}$) [75] under similar conditions of temperature and ionic strength suggest that deprotonation at the C-3 position of DHAP is the rate-limiting step for elimination which proceeds via an enediolate intermediate.

2) Elimination by an E1 mechanism cannot occur as such a reaction would lead to the formation of an α-carbonyl carbocation, a species much too unstable to have a finite lifetime in solution. Moreover, the deoxy analogue of DHAP, lacking the carbonyl group is stable for 10 hours at room temperature in 0.1M NaOH , conditions which would rapidly degrade DHAP with a half-time of 2 minutes.

3) The solvent isotope effects observed for the elimination of L-GAP in quinuclidinone buffers, $(k_B)H_2O/(k_B)D_2O = 1.1$ and on the quinuclidinonium-catalyzed isomerisation of L-GAP $(k_{BH}/k_e)H_2O/(k_{BD}/k_e)D_2O = 3.2$ are consistent with a two step mechanism involving rate determining deprotonation of substrate followed by rapid elimination and slower isomerisation of the enediolate intermediate to form DHAP (1).

4) The buffer catalysis plots for the 3-quinuclidinone and 3-quinuclidinol catalyzed elimination of DHAP are shown below in Figure 1.4 and Figure 1.5 respectively

Figure 1.4: Effect of the concentration of quinuclidinone free base on the observed first order rate constant, k_{obsd} (s^{-1}), for elimination of DHAP at pH 8*
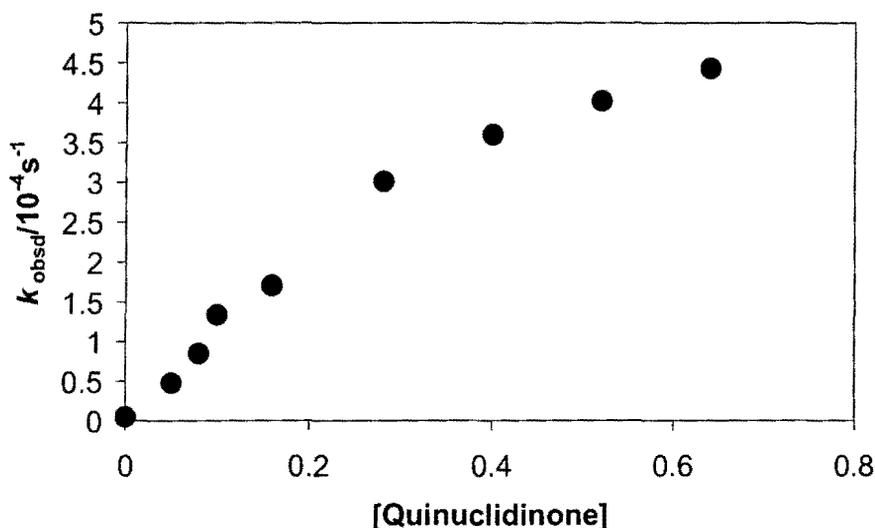
- Replotted from Richard *et al*, JACS, 1984, 106 pg 4928

Figure 1.5: Effect of the concentration of quinuclidinol free base on the observed first order rate constant, k_{obsd} (s^{-1}), for elimination of DHAP at pH 10*
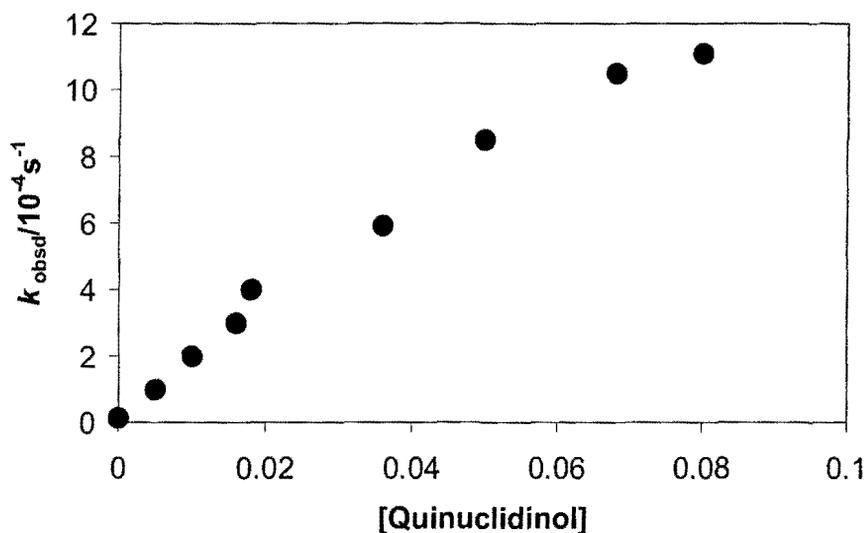
* Replotted from Richard *et al*, JACS, 1984, 106 pg 4928

At high buffer concentrations there is visible levelling off of the pseudo first order rate constants for elimination, k_{obsd} (s^{-1}). Richard attributed this to a change in the rate-determining step in going from low buffer concentrations, where the observed rate constant for elimination is the same as substrate deprotonation, to higher buffer concentrations where the increased amount of 3-quinuclidinonium or 3-quinuclidinolium cations results in an increase in the rate of protonation, k_2, of the enediolate intermediate to form the isomerisation product L-GAP. At these concentrations of buffer, the expulsion of leaving group, k_e, becomes the rate determining step.

Shown in Figure 1.6 are the Brønsted plots for the general base catalyzed elimination reactions

of LGAP (closed symbols) and DHAP (open symbols).

Figure 1.6: Brønsted plots for the elimination of DHAP (diamonds) and L-GAP (circles) by

3-substituted quinuclidines*. Triangle and squares represent the values

obtained for carbonate and hydroxide respectively.
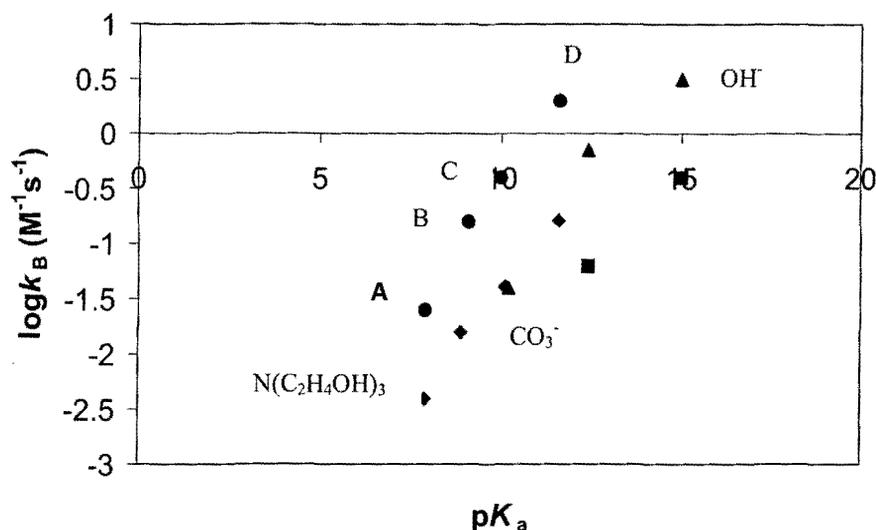
*Replotted from Richard *et al*, JACS, 1984, 106 pg 4932 where A= Quinuclidinone, B =

Chloroquinuclidine, C = Quinuclidinol, D = Quinuclidine. The anomalous OH⁻, CO₃⁻ and

triethanolamine values are explained in the text.

The slopes of the Brønsted plots for the elimination of DHAP **(1)** and L-GAP **(6)** by 3-

substituted quinuclidines are 0.48 and 0.45 respectively. Deviations from the 3-substituted

quinuclidine Brønsted plots defined line are seen for hydroxide, carbonate, and triethanolamine

bases. A large desolvation energy can explain the lower reactivity of the hydroxide ion for its

pK_a. The 13 fold greater k_B value for quinuclidinol catalyzed elimination compared to carbonate catalysis has been attributed to better transition state stabilisation by the former base. On reaction of an array of the 3-substituted quinuclidine bases with DHAP (1), the transition state is stabilised due to electrostatic interactions between the negatively charged phosphodianion group of substrate and the partially positively charged amine catalyst. Such a degree of stabilisation for carbonate induced elimination will not be observed due to destabilising transition state interactions between the negatively charged group of the phosphodianion substrate and the negatively charged carbonate base. The deviation from the line for triethanolamine may be a result of steric hinderance as triethanolamine has greater conformational flexibility than quinuclidine.

The β value of 0.48 for DHAP (1) elimination is considerably smaller than β = 0.88 for the deprotonation of acetone by 4-substituted carboxylate anions and the β = 0.75 for the E1cb irreversible elimination reaction of 4-(4-nitrophenoxy)-2-oxobutane by ten anionic bases with pK_a's from 4.8 to 10.6. Electrostatic interactions in the transition state between the phosphodianion group of DHAP (1) and buffer may lead to a decrease in the effective charge available to the buffer for catalysis. This will lead to a lower observed β value for DHAP (1) deprotonation.

Shown below in Figure 1.7 are the pH rate profiles for the elimination of DHAP (1) (lower curve) and L-GAP (6) (upper curve). Each point on the rate profiles were obtained by extrapolation of the relevant buffer data to zero buffer concentration.

Figure 1.7: pH-rate profiles for the elimination of DHAP and L-GAP*
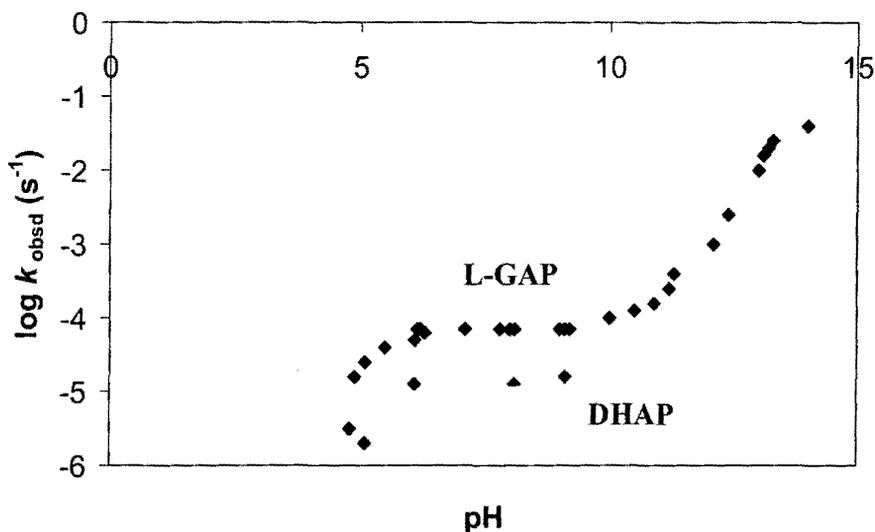
Key: Data obtained in solution, pH < 5 refers to acetate buffers, pH 6-10 refers to imidazole, triethanolamine and triethylamine buffers, pH > 10 refers to carbonate buffers and OH⁻ solution.

As discussed by Richard *et al* the pH rate profile can be divided into three distinct regions:

1) Above pH 10 the positive slope of the pH rate profile indicates specific catalysis by hydroxide. At very high pH there is a levelling off in the pH rate profile for the elimination of L-GAP. L-GAP is predominantly hydrated in solution (~ 95 %). Thus the downward break in the pH rate profile of L-GAP at ~ pH 13 can be partially attributed to a decrease in the active aldehyde form caused by ionisation of the C-3 hydroxyl of the aldehyde hydrate. Although the hydrate forms of both DHAP **(1)** and L-GAP **(6)** are unreactive to elimination, the rates are obtained by correction of k_{obs}, i.e. dividing k_{obs} by the fraction of carbonyl substrate. The

59

corrected rate constants for L-GAP (6) are larger than those of DHAP (1) given the more acidic α-aldehydic position compared to the α-ketone. This is apparent from the pH rate profile. A similar levelling is seen for the DHAP (1) pH-rate profile.

2) Between pH 7 and 10 the rate of elimination of DHAP and L-GAP are pH independent. There are two suggestions for the origin of this pH independent region based on transition state structures of L-GAP and DHAP phosphodianions; water catalyzed deprotonation (12) and intramolecular deprotonation by the phosphate dianion (13) (Figure 1.8)

Figure 1.8: Transition structures of DHAP and LGAP
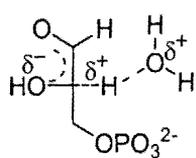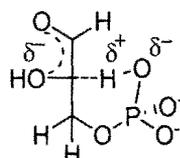
(12)   (13)

The conclusion that the pH independent region and k_0 are a result of transition state (13) was made on the basis of several experimental observations. Intramolecular deprotonation has been reported for the elimination reaction of 4-(4-nitrophenoxy)-2-oxobutane-1-phosphate and the intramolecular carboxylate and amine deprotonation has been reported for the reactions of a series of ω-carboxy-substituted 2-ketones and ω-amino-substituted 2-ketones respectively. DHAP (1) and acetone are deprotonated at the C-3 position by hydroxide at similar rates. However the rate constant for the pH independent reaction of DHAP (1) is 10^5 larger than the rate constant for deprotonation of acetone by water. In contrast the second order rate constants

60

for the hydroxide ion catalyzed deprotonation of DHAP (1) and acetone are very similar. This indicates that the phosphodianion acts to accelerate the pH-independent C-3 deprotonation. Furthermore, if water is behaving as a base, then the deprotonation of DHAP phosphate monoanion by water must be slower than the deprotonation of the dianion in order to account for the downward break in the pH rate profile. However, 3-quinuclidinone catalyzed deprotonation of DHAP phosphate monoanion is 3-fold faster than deprotonation of the DHAP phosphodianion, suggesting that the role of water is negligible. Therefore the pH-independent, uncatalyzed elimination mechanism of DHAP (1) is believed to occur by intramolecular deprotonation at the C-3 position by the phosphodianion group.

3) Below pH 6 there is a downward break in the pH rate profiles for DHAP (1) and L-GAP (6) elimination. This suggests that the rates of elimination are reduced due to protonation of the phosphodianion to form the monoanionic substrate. The downward break for the DHAP (1) reaction occurs at a slightly lower pH than for the L-GAP (6) elimination reaction as the pK_a of DHAP is 0.3 units smaller than that for L-GAP.

1.4.2.2 Isomerisation of DHAP and L-GAP in solution

In solution, the isomerisation of DHAP (1) is much slower than the elimination reaction with 1 % of all solution products formed being attributed to the isomerisation product GAP (6). Once the enediolate intermediate is formed, partitioning occurs between enediolate protonation to form the isomerisation product, and elimination product (Scheme 1.24). Partitioning of the enediolate intermediate greatly favours elimination ($k_{elim} >> k_{isom}$) however as discussed previously, at high concentrations of buffer it has been suggested that there is a partial change in the rate-

determining step from buffer catalyzed, rate-limiting deprotonation of substrate at low buffer concentrations to uncatalyzed rate-limiting leaving group expulsion (k_e) at higher buffer concentrations (see Scheme 1.24).

For the reaction of L-GAP (6) in solution the rate constant ratio k_{iso}/k_{elim} has been reported where the individual components, k_{iso} and k_{elim} refer to the rate constants for isomerisation and elimination respectively under the same conditions. The first order rate constant of isomerisation of L-GAP, k_{iso}, shows a second order dependence on the total buffer concentration (Figure 1.9).

Figure 1.9: Effect of the concentration of total quinuclidinol concentration on the observed first order rate constant, k_{iso} (s^{-1}), for the isomerisation of L-GAP at pH 9, 8.5 and 8.1*
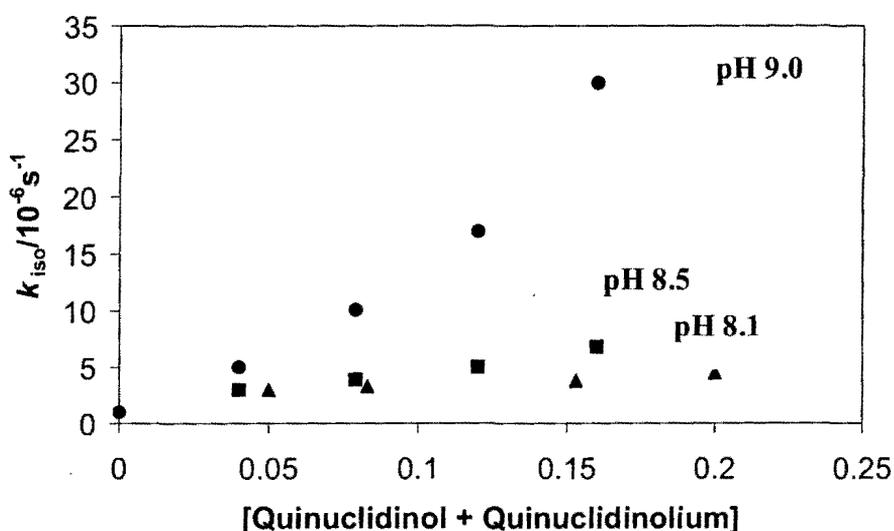
* Replotted from Richard *et al*, JACS, 1984, 106 pg 4928

As discussed by Richard *et al*, this second order dependence can be attributed to the combined first order rate constant for deprotonation of substrate by buffer base and first order catalysis of enediolate protonation by buffer acid which increases the fraction of enediolate progressing to DHAP (1). Dividing by the first order rate constant for elimination, k_{elim} (s^{-1}), linearizes the second order plots and removes the contribution of buffer base to the isomerisation reaction (Figure 1.10)

Figure 1.10: Ratio of rate constants for L-GAP isomerisation and elimination, k_{iso}/k_{elim} against the concentration of 3-quinuclidinol cation ion for reaction at pH 9, 8.5 and 8.1*
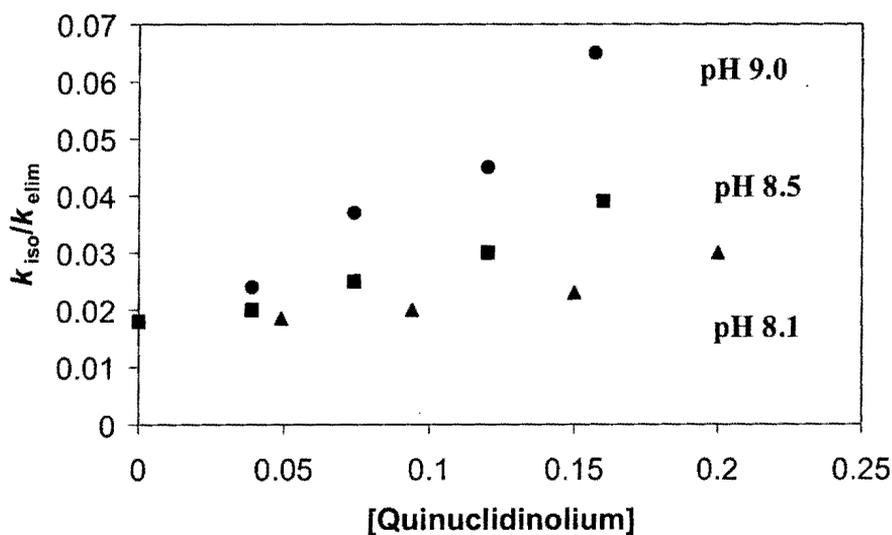
* Replotted from Richard *et al*, JACS, 1984, 106 pg 4928

Unlike the buffer catalysis plots for the elimination of DHAP, there is no observed downward curvature at high buffer concentrations for the isomerisation reaction of L-GAP. This implies that general acid catalysis of leaving group expulsion from the enediolate intermediate is minimal.

The pH rate profiles of the rate constant ratios for partitioning of the enediolate intermediate between elimination and isomerisation are shown below in Figure 1.11

Figure 1.11: pH-rate profiles for the partitioning of the enediolate intermediate between elimination and isomerisation*
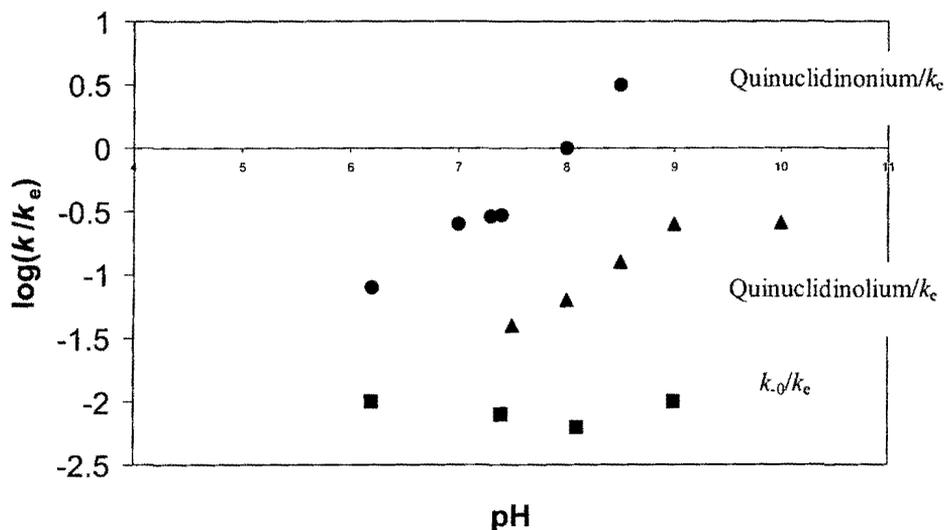
* Replotted from Richard *et al*, JACS, 1984, 106 pg 4934

In solution the enediolate intermediate exists as a mixture of cis and trans isomers, the O-1 and O-2 oxyanions, and the phosphomonoanion and phosphodianion. At low pH where the phosphate group of substrate is predominantly in its monoanionic form, the limiting value k_{BH}/k_e for

quinuclidinonium induced protonation is equal to the rate constant for partitioning of the phosphomonoanion, k_{BH}'/k_e (Scheme 1.24)

Scheme 1.24

$$\text{Enediolate-PO}_3\text{H}^- \xrightarrow{k_e' + k_{-0}' + k_{BH}'[BH]} \text{Products}$$

$$\Updownarrow$$

$$\text{Enediolate-PO}_3{}^{2-} \xrightarrow{k_e + k_{BH}[BH]} \text{Products}$$
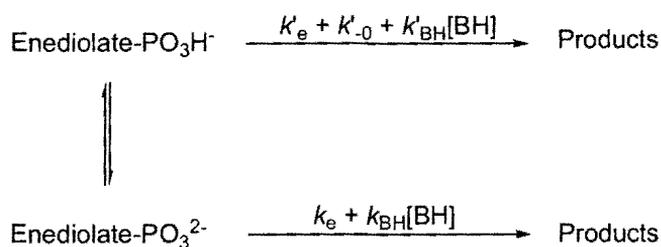
Similarly, at higher pH values where the substrate is predominantly in its phosphodianionic form the limiting observed k_{BH}/k_e is equal to the rate constant ratio for partitioning of the phosphodianion, k_{BH}/k_e. There is a large increase in k_{BH}/ke in moving to higher pH which also results in the partitioning to the phosphodianionic form of L-GAP (**6**). An increase in the basicity of the phosphate moiety results in a decrease in the rate of elimination, k_e, thus an increase in the rate of isomerisation/elimination. The uncatalyzed rate for enediolate reprotonation, k_{-0} mirrors the uncatalyzed rate for substrate deprotonation seen for the corresponding elimination reaction, k_0. In the range of pH 6-10, the observed k_{-0}/k_e ratio is pH independent as both isomerisation and elimination and protonation occur through the same intermediate.

The Brønsted plot for partitioning of the L-GAP enediolate between protonation and elimination is shown in Figure 1.12

Figure 1.12: Brønsted plot for partitioning of the L-GAP enediolate between protonation and elimination*
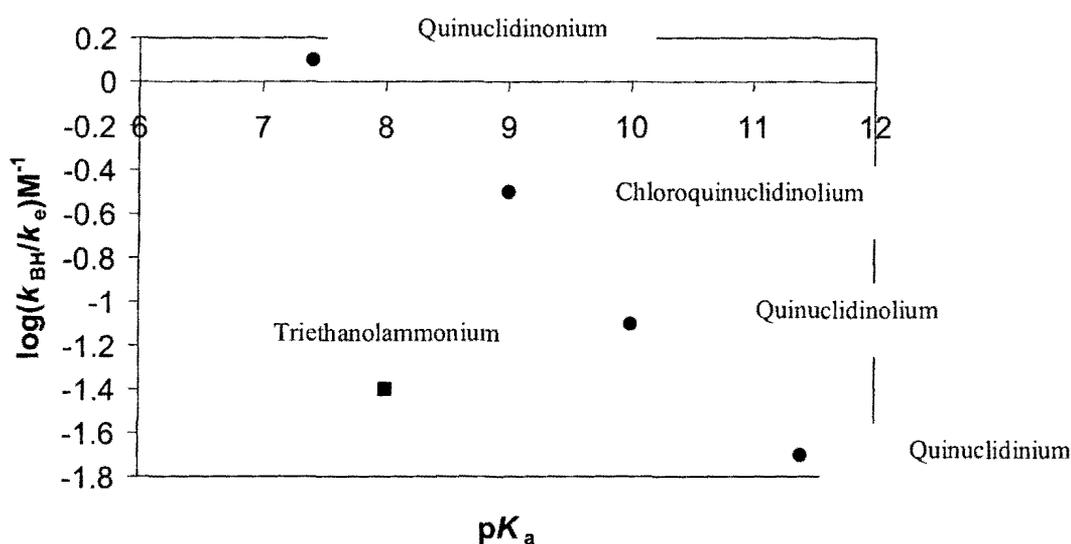
* Replotted from Richard *et al*, JACS, 1984, 106 pg 4934

The log k_{BH}/k_e values for catalysis by a series of 3-substituted quinuclidines at pH 8.1 are plotted against the buffer pK_a. The slope of the Brønsted plot is 0.47 which is equal to the Brønsted α-value for enediolate protonation at C-1. The sum of the Brønsted coefficients $(\alpha + \beta)$ from the plots for the elimination reaction of L-GAP and DHAP (Figure 1.6) and the plot for general acid protonation of the enediolate intermediate (Figure 1.12) equals 0.95. This is within experimental error of the required thermodynamic value of 1. Also the deviation of the rate constant for general base catalysis by triethanolamine (Figure 1.12) ~ 1.16 log units is within experimental error of the deviation of the triethanolammonium cation from the Brønsted plot defined by the 3-substituted quinuclidinium cations, ~ 1.14 log units, for general acid catalysed protonation.

1.4.3 Overall structural properties of MGS and TIM

Structurally, TIM is a dimeric protein of two identical subunits each approximately 27 kDa [76, 77]. The tertiary structure of each subunit is made up of 8 parallel β-strands on the inside and 8 α-helices on the outside. This commonly observed structural motif is called an α,β barrel where the enzyme active site is at the centre of the barrel (Figure 1.13)

Figure 1.13: X-Ray crystal structure of *triosephosphate isomerase* (TIM)*
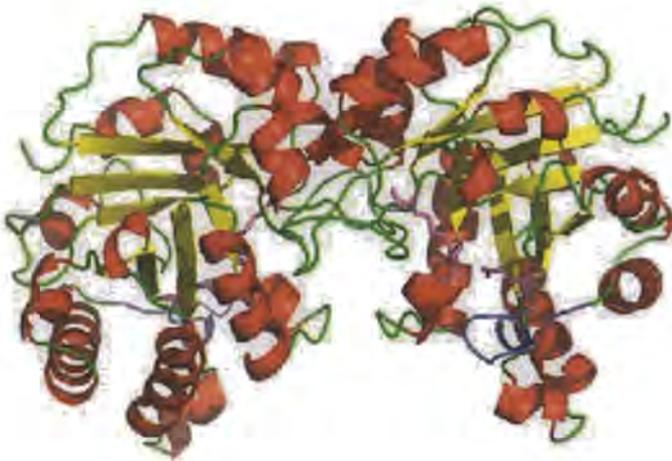
* Taken from the EMBL-EBI (European bioinformatics institute)

The reversible interconversions of DHAP (1) and GAP (6) catalyzed by TIM rely on the specific properties of an active site loop which operates with 'lid-like' movement [78-81]. Loop 6 in TIM, located between β-strand 6 and α-helix 6 is a highly conserved structural motif consisting of 11 amino acid residues. Two conformations have been observed for the loop; The 'open' (Figure 1.14) and 'closed' (Figure 1.14a) forms which are crucial in enabling TIM to achieve

67

catalysis at levels near the diffusion limit as well as preventing hydrophobic aggregation at the active site.

Figure 1.14: 'Open' conformation of TIM*　　　**Figure 1.14a: 'Closed' conformation**
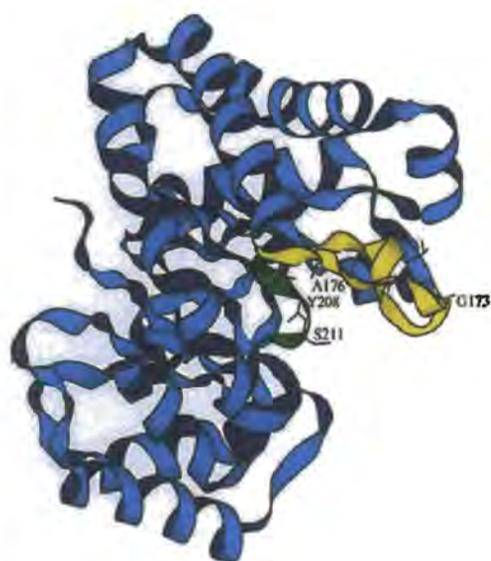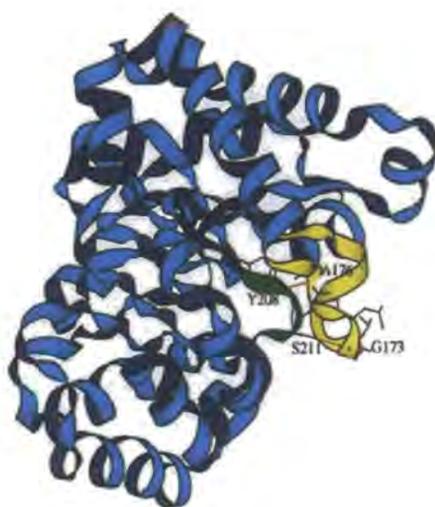
of TIM

Figures 1.14 and 1.14a illustrate the ribbon diagrams of the open and closed forms of TIM monomer. The surface residues of the loop shown in yellow operate with hinge-like movement to open or close.

In the open conformation, the active site of TIM is exposed to solvent thereby allowing substrate binding or product release. The closed position of the loop induces the alignment of the glutamate catalytic base (E165) into a position where deprotonation of substrate DHAP **(1)** can occur. Loop closure also results in the ideal orientation of an active site histidine residue (His 95) to polarise the carbonyl oxygen of substrate. As discussed, in solution, the enediolate

intermediate formed by deprotonation of (1) at the C-3 position, collapses to form methylglyoxal and inorganic phosphate 100 times faster than reprotonation at the same intermediate. The reaction of DHAP 'catalyzed' by a loop deletion mutant of yeast TIM (removal of loop 6) has a similar fate. Deletion of the loop results in a decrease in the steady state concentration of (*enzyme-bound*) intermediate therefore leading to an increase in the formation of elimination product due mainly to elimination in solution. Thus the impaired enzyme no longer has the capability to catalyze substrate deprotonation or intermediate reprotonation to the same extent as the wild type enzyme. Loop-deletion mutant catalysis of GAP (6) results in partitioning of the endiolate intermediate in a ratio of 5.5:1 to favour the elimination products [82]. On this basis one of the main functions of the loop is to sequester the intermediate at the active site and shield it from bulk solvation. Once the substrate is bound, a hydrogen bond between the phosphate oxygen of DHAP (1) and an amide group of G171 in the centre of loop 6 is the only substrate-loop interaction which occurs when the loop is in the closed position. In the absence of substrate, stabilization of the closed form of the loop is achieved through numerous hydrogen bonded interactions with the neighbouring loop 7. Stabilization of the closed form of loop 6 by these interactions is crucial for catalysis as quantified by further mutagenic studies on yeast TIM. Removal of the A176 H-bonded interaction between loop 6 and loop7 due to mutation results in k_{cat} and k_{cat}/K_M values 1000 and 2400 fold respectively lower than the corresponding values of wild type TIM. Thus while the role of the loop itself is crucial for catalysis, hydrogen bonded interactions of the loop with a neighbouring loop structure are also vital for optimal turnover of DHAP (1). Catalytic loops such as that found in TIM are also quite common in a range of other enzymes including ribulose bisphosphate [83], enolase [84] and glyoxalase I [85]. The loops in these enzymes have similar functions to those in TIM where intermediate decomposition is

prevented and transition state stabilisation is achieved. The functionally analogous flexible peptide loop in glyoxalase I provides evidence that TIM and glyoxalase I are related by structure and function and perhaps have converged on the same evolutionary path.

X-ray crystallography has shown that MGS has a homohexameric structure consisting of interacting five-stranded β/α proteins unlike the α/β barrel structure of TIM (Figure 1.15) [69]. While having no loops or other structural moieties outside of the active site which are considered crucial for catalysis, the thermostability of MGS is notably high with wild-type enzyme stable up to temperatures of 90 °C [86]. This physical attribute of the enzyme is believed to be a function of the high numbers of conserved and non-conserved proline residues (approximately 6 % of the 150 amino acid sequence).

Figure 1.15: X-ray crystal structure of *methylglyoxal synthase* (MGS)*
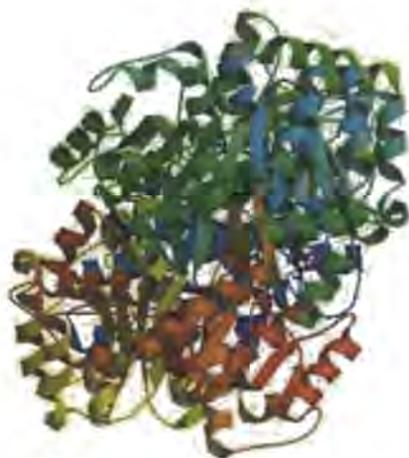
* Taken from RCSB, PDB

1.4.4 Mechanistic comparisons of MGS and TIM

Despite sharing neither structural nor sequence similarities, both TIM and MGS bind the same substrate and catalyze their respective reactions near the diffusion limit with remarkable similarities in specificity and kinetics. The values of k_{cat}, K_M and k_{cat}/K_M for the turnover of DHAP by MGS and TIM are shown below in Table 1.1

Table 1.1: Comparison of k_{cat}, K_M, k_{cat}/K_M for MGS and TIM.

k_{cat}, K_M, k_{cat}/K_M	MGS	TIM
k_{cat}	$220\ s^{-1}$	$600\ s^{-1}$
K_M	0.2 mM	0.65 mM
k_{cat}/K_M	$1.1 \times 10^6\ M^{-1}s^{-1*}$	$9.2 \times 10^5\ M^{-1}s^{-1}$

* Correction for the hydrate form of DHAP leads to a value of $5.2 \times 10^6\ M^{-1}s^{-1}$

The fact that TIM and MGS are on parallel metabolic pathways, and utilize the same substrate, sharing a common intermediate, led to early suggestions that the two enzymes are related by divergent evolution. Evidence supporting the divergent pathway comes from the loop deletion mutant of TIM, discussed earlier. This loop-deletion mutant confers *methylglyoxal synthase*-like activity upon the mutant enzyme. However, it is more likely that the two enzymes are related convergently. Evidence for this evolutionary pathway comes from the fact that despite mutation, TIM retains its ability to dephosphorylate GAP (**6**) to methylglyoxal and inorganic phosphate whereas MGS is highly specific for DHAP (**1**) and is unable to abstract a C-2 proton from GAP

(6). This suggests that while the active site residues may be similar, the different product outcomes could be a result of subtle differences in the arrangement of the catalytic residues.

1.4.4.1 The active site arrangements of MGS and TIM

While much is known about the catalytic mechanisms employed by TIM, the precise mechanistic pathways involved in MGS induced catalysis as well as the origin of the catalytic specificity of the two enzymes has remained elusive until recently. The active site arrangements of the catalytic residues of TIM are well documented. However, in order to make comparisons of these catalytic residues with those of MGS and the overall mechanism of catalysis, X-ray crystallography experiments of MGS and TIM binding the competitive inhibitors and substrate analogues 2PG (phosphoglycolate (14) and PGH (phosphoglycolohydroxamate) (15) (Figure 1.16) were carried out.

Figure 1.16: Competitive inhibitors phosphoglycolate (2PG) and

   phosphoglycolohydroxymate (PGH)
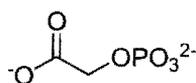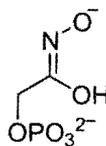
(14)   (15)

As discussed above, the initial deprotonation at the C-3 position of DHAP (1) is achieved by TIM and MGS using Glu 165 and Asp 71 active site residues respectively. However the deprotonation is stereospecific with a pro-S proton of DHAP abstracted by Asp 71 and a pro-R proton of DHAP abstracted by glutamate 165. The X-ray crystal structures of MGS-bound with

2PG show that the Asp 71 catalytic base is located on the opposite face of the 2PG carboxylate plane from the Glu 165 base of TIM (Figure 1.17). The positioning of catalytic bases on opposite sides of the substrate is also observed from binding studies with PGH (15). This is consistent with the opposite sterospecificites seen for MGS and TIM.

Figure 1.17: Stereodiagram of the superimposition of MGS complexed to competitive inhibitor PGH (Dark blue and light blue) and TIM binding PGH (Yellow and orange)*
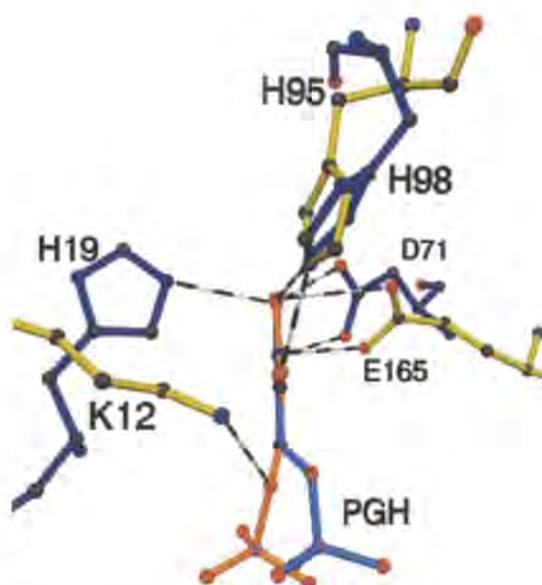
* Taken from Harrison *et al*, Biochemistry, 2001, 40, 6805-6815

Shown above is a stereodiagram of the superimposition of MGS complexed to competitive inhibitor PGH (Dark blue and light blue) and TIM binding PGH (Yellow and orange). The distances to Asp 71 and Glu 165 to the hydroxamic acids are similar but the angles of approach for deprotonation are different. The catalytic base residues of both MGS and TIM are located and

surrounded largely by hydrophobic groups. As a result of their environments, the pK_a of the carboxylate groups of Glu 165 and Asp 71 are analogously increased relative to the pK_a of the C-3 protons of substrate resulting in elevated rates of deprotonation at this position. Asp 71 of MGS is also located in close proximity to Asp 101 (~ 5 Å). Asp 101 forms a salt bridge with an arginine residue of a neighbouring subunit and therefore is likely to be negatively charged. This will further decrease the stability of Asp 71 and increase the pK_a of the residue. A higher pK_a value for Asp 71 may result in faster substrate deprotonation and ultimately lead to an alternative rate limiting step. This may explain the lack of a primary substrate kinetic isotope effect for the MGS reaction . Such an effect is not seen in the TIM catalyzed reaction. The role of the histidine residues at the active sites of MGS (His 98) and TIM (His 95) was originally believed to reduce the pK_a of the bound enediolate intermediate by polarization of the carbonyl group. Evidence for this in the TIM catalysed reaction of DHAP (1) comes from the fact that DHAP bound at the active site of TIM is approximately 8 times more susceptible to reduction by sodium borohydride than free DHAP . It is thus likely that His 95 functions as an electrophilic catalyst at the active site of TIM however the function of the analogous residue in MGS is believed to be different. The results of mutagenesis studies on the His 98 residue of MGS suggest that the main functional role of this residue is to promote equilibration between the active and inactive conformers of MGS. However it is also probable that the residue has an electrophilic role in reactions at the active site. This will be discussed in more detail in the next section. The function of lysine 12 at the active site of TIM is mainly as an electrophilic catalyst. This residue stabilizes the charge on the His 95 residue and also has the role of attracting the charged phosphate group of DHAP and GAP. The closest equivalent residue in MGS is the His 19 residue. However, the resulting X-ray crystal structures of MGS complexed with 2PG show that His 19 is not within H-bonding

74

distance of the carboxylate of 2PG. Also, His 19 is not near the phosphate moiety of 2PG unlike Lys 12 in TIM with DHAP (1) and GAP (6) suggesting that an alternative function may exist for this residue in the active site of MGS.

Both TIM and MGS have evolved to bind DHAP (1) however the inability of MGS to abstract a C-2 proton from GAP (6) is a functional requirement for the enzyme. If the reverse reaction were possible, deprotonation of the pro-S proton of DHAP (1) would lead to isomerisation product S-GAP. S-GAP has known inhibitory properties, causing the inactivation of fructose bisphosphate 1,6 aldolase and sn-glycerol 3-phosphate acetyltransferase The fact that MGS does not abstract a proton from the C-2 position of R-GAP is not surprising as Asp 71 residue is located on the opposite side of the molecule. The inability of MGS to abstract a proton from the C-2 position of S-GAP can be explained based on the rigidity of Asp 71 compared to Glu 165 of TIM. The X-ray crystal structure of MGS binding 2PG overlapped with the mirror image of the TIM active site binding the same molecule show that overlap between the His 98 and His 95 residues occurs. However the carboxylate groups of Asp 71 and Glu 165 do not overlap. Changes in the torsional angle for Glu 165 allow this catalytic residue to make a closer approach to the C-2 carbon of 2PG than Asp 71. Similar changes made to the torsional angle of His 98 and His95 result in a closer approach of the latter to the bound 2PG molecule. (Figure 1.18)

Figure 1.18: Stereodiagrams obtained following the superimposition of MGS and the
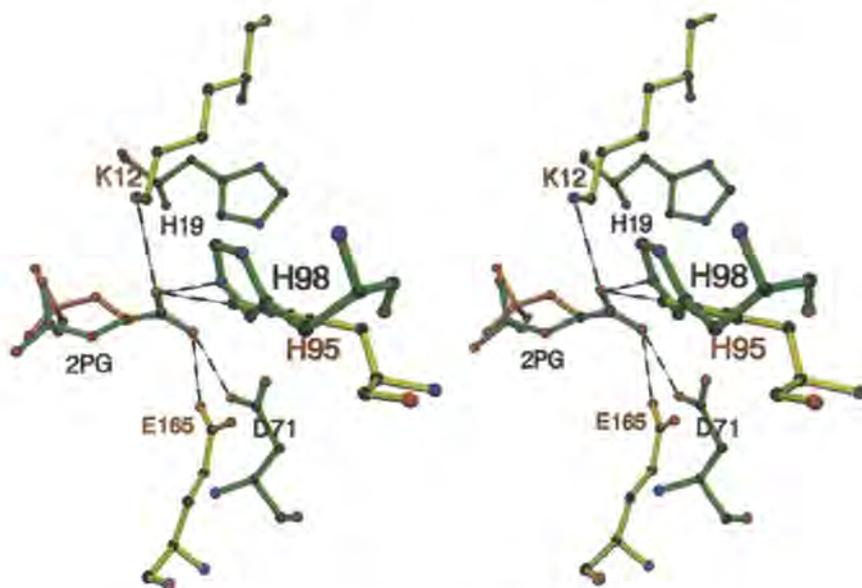
mirror image of TIM using the acetyl moiety of bound 2PG*

Shown above in Figure 1.18 are the stereodiagrams obtained following the superimposition of MGS and the mirror image of TIM using the acetyl moiety of bound 2PG.

From these modelling studies the distance of the carboxylate group of Asp 71 to the C-2 proton of GAP (6) is too far for realistic deprotonation to occur even if the carboxylate residue was on the correct side. Also, the N-1 nitrogen of the His 98 residue is too far from the C-1 carbonyl oxygen of GAP (6) for efficient electrophilic catalysis to occur. Further modelling studies of GAP (6) bound to the active site of MGS show that the C-1 position of GAP (6) is approximately 2.8, 3.7 and 3.4 Å from the conserved residues of His 19, Phe 88 and Val 17 respectively. These conserved hydrophobic residues form a well-defined cavity which would prevent phosphorylated

2-keto sugars from participating in elimination as the distances of the residues to the C-1 position of GAP (6) indicate that binding to the active site of MGS would be sterically hindered.

In solution, TIM suppresses the background elimination reaction so effectively that a product specificity of 10 towards isomerisation is observed. TIM is believed to favour binding of the dianionic substrate (no binding of monoanionic dihydroxyacetone sulfate is observed) and to prevent elimination by binding the dianionic form of substrate and not the monoanion. This comes from the fact that no observed binding of monoanionic dihydroxyacetone sulfate (DHAS) is observed. Electrostatic interactions to substrate in the active site of TIM are quite sparse with only two H-bonds from the mobile loop to one of the C-1 phosphoryl oxygens. In contrast to the TIM active site, the active site of MGS contains 11 charged and uncharged H-bond donors and acceptors surrounding all four phosphoryl oxygens. The contribution of all eleven H-bonded interactions are thought to have the effect of lowering the pK_a of the phosphate group and thus make it more favourable to eliminate DHAP (1). Conformationally, the active site of MGS does not change. This means that the the H-bond donors and acceptors are still in position to bind the expelled phosphotrianion following elimination. However given the high background rate for elimination of PO_4^{3-} from the enediolate, $k_e \sim 10^6$ s^{-1}, this suggests that the specific role of the H-bond donors and acceptors is possibly to position DHAP (1) at the active site.

1.4.4.2 Identification of the catalytic residues of MGS

Sequence analysis of the wild-type MGS shows that while no glutamic acid residues are conserved, there are four conserved aspartic acid residues at the active site (Asp 20, Asp 91, Asp 71 and Asp 101) [40]. The conclusion that Asp 71 is the catalytic base involved in the

deprotonation of DHAP has been made based on results obtained from the mutations of each residue.

Mutations were made to either an asparagine (an isostere of aspartate, lacking the negative charge) or a glutamate residue (where the negative charge is conserved but displaced by one methylene residue). The resulting mutations provided mutant proteins with the same CD-spectra and gel filtration mobility as wild type MGS and with the secondary and quaternary structures largely unchanged. The melting temperature, T_m, of the mutant proteins was also relatively unchanged ($\pm$ 5 °C). On this basis it was presumed that protein stability was not a contributing factor to the kinetic results.

Mutations of either D20 or D91 to asparagine or glutamate resulted in a relatively small 50 fold reduction of the value of k_{cat}. Based on these findings it was presumed that one of these residues is involved in the conformationl stabilisation of the enzyme, i.e. controlling the equilibrium between active (taut) and inactive (relaxed) states.

As discussed in the previous section, binding of inorganic phosphate inhibits the enzyme conformationally (as observed by sigmoidal kinetics) rendering the enzyme inactive, however the reaction with competitive inhibitors (and substrate analogues) such as phosphoglycolohydroxamate (PGH) or phosphoglycolate (2PG) results in formation of the more active, taut state and increases the activity of the enzyme towards binding of more of these inhibitors. Both the D20N and D91N mutants showed unusual results with time-dependent substrate inhibition observed. Addition of high concentrations of inorganic phosphate (> 1mM) led to a restoration of the enzyme activity. The corresponding D20E and D91E mutants showed no such behaviour. It was thus proposed that the significance of two negatively charged

78

carboxylate active site aspartates is to increase the pK_a of active site Lys 23 thus stabilising its conjugate acid form. Without these negatively charged residues the Lys 23 residue at the active site would likely form a Schiff base **(16)** with the keto oxygen of DHAP (Scheme 1.25)

Scheme 1.25
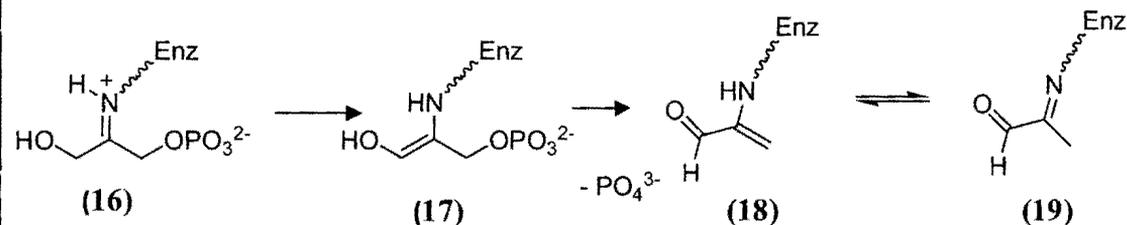
The final product of this reaction is the imine **(19)**, which would be expected to hydrolize slowly and inhibit the enzyme. Therefore the inhibition observed for the D20N and D91N in the presence of DHAP **(1)** can possibly be attributed to the formation of this product. Based on these kinetic findings it was deemed unlikely that Asp 20 or Asp 91 were involved in the catalytic turnover of DHAP **(1)**.

In contrast, mutations of Asp 71 and Asp 101 led to large effects on k_{cat} indicating that one of these residues likely controls the catalytic ability of MGS. The values of k_{cat} for wild type MGS and each mutant investigated are shown below in Table 1.2 (Data taken from Harrison *et al.*Biochemistry 1998, 37 (28) p 10079.

Table 1.2: Comparison of k_{cat} (s^{-1}) for wild-type MGS and mutated MGS in the absence and presence of inorganic phosphate.

MGS	k_{cat} (s^{-1})[a]	k_{cat} (s^{-1})[b]
Wild type MGS	220 ± 10	203 ± 39
D71E mutant	0.24 ± 0.01	0.22 ± 0.01
D71N mutant	0.09 ± 0.04	0.07 ± 0.03
D101E mutant	0.06 ± 0.03	0.05 ± 0.00
D101N mutant	0.04 ± 0.00	0.02 ± 0.00

a. k_{cat} (s^{-1}) determined in the presence of 0 mM Pi (inorganic phosphate). b. k_{cat} (s^{-1}) determined in the presence of 0.3 mM Pi.

Results from the catalytic binding of inhibitor 2-phosphoglycolate (2PG) **(14)** provided further evidence of the identity of the active site base involved in deprotonation of DHAP. Glutamate and asparagine mutants of aspartate 71 and 101 were inhibited by 2PG **(14)** competitively and uncompetitively respectively. Unusually the D71E mutant showed initial activation upon the addition of inhibitor in the *absence* of phosphate. However, from ~ 0-5 µM 2PG there is an initial activation stage for the reaction.

Unlike wild-type MGS these mutants did not show co-operativity in the absence or presence of phosphate although by analogy with the 2PG **(14)** activated, phosphate inhibited wild-type enzyme, the mutants are in the activated, 'taut' conformation. The activation of the D71E mutant

in the absence of phosphate may be explained by the displaced negative charge of the glutamate

residue. This may have the same role as phosphate in wild-type MGS, activating the enzyme into

the 'taut' state. Lineweaver-Burke plots of the activity of each mutant in the presence of 2PG

(14) suggest that activation of the D101E by 2PG is 10 fold greater than for the D71E mutant.

This implies that this mutant is in an even greater "taut" state than the latter indicating that

binding of 2PG (and therefore enediolate intermediate) should be greater for Asp 101. However

the final binding constants, K_i, suggested otherwise. Similarities in the K_i values for 2PG **(14)** at

the active site of the D71E and D71N mutants with wild-type MGS indicate tighter binding of

the competitive inhibitor to the active sites. The values obtained for the D101N and D101E

mutants are considerably higher than for wild-type enzyme (Table 1.3).

Table 1.3: K_i inhibition values (µM) for wild-type MGS and mutated MGS

MGS	K_i (2PG) (µM)
WT	5.6 ± 1.4
D71N	4.1± 0.7
D71E	3.7 ±4.9
D101N	66 ±7[a]
D101E	760 ±350

The tighter binding of 2PG (14) to the active site of the D71E mutant compared to the D101E mutant implies that the actual enediolate intermediate of DHAP will bind tighter to Asp71 at the active site.

The fact that the D101N mutant is inhibited uncompetitively suggests that 2PG binds at a position other than the active site of the enzyme thus not competing with substrate DHAP. Therefore it is likely that mutation to Asp 101 induces distortion of the active site. This rules out the role of Asp 101 as a catalytic base in deprotonating DHAP at the C-3 position. In MGS the activity of the D71E and D71 N mutants is 100 fold less than wild type enzyme. At the same time, the inhibition constant K_i is approximately the same. For TIM, mutation of the active site base glutamate 165 to an aspartate residue results in a 500 fold loss in activity when compared to wild type. Interestingly the inhibition constant, K_i, remains similar for both mutant and wild-type enzyme. On this basis it was proposed that Asp 71 in MGS and Glu 165 have similar catalytic roles i.e deprotonation of DHAP at the C-3 position. Mechanistic proposals for MGS catalysis suggest that deprotonation of DHAP (1) at the C-3 position is catalyzed by Asp 71. Following this, the role of Asp 101 is likely to increase the pK_a of Asp 71 in a largely hydrophobic active site environment.

1.4.4.3 Mechanistic ambiguity in MGS catalysis

The similarities in structure and function of the catalytic residues of both MGS and TIM binding 2PG suggests that the mechanism of MGS enediolate formation has converged with that of TIM.

However, the exact mechanism of enediolate formation catalyzed by MGS was made based on two different proposals. X-ray crystal structures of the MGS and TIM active sites bound with the competitive inhibitor PGH have suggested that the elimination and isomerisation mechanisms of the respective enzymes may depend more on short strong hydrogen bonds (SSHB) and other strong electrostatic interactions than originally anticipated. SSHB are recognisable from NMR and X-ray crystallography by their shorter bond length than normal hydrogen bonds (usually 2.2-2.7 Å) and their presence is usually indicative of the specific mechanism employed by the enzyme. PGH is isostructural to the enediolate of DHAP and resembles the intermediate more closely than 2PG. The arrangement of Asp 71 and Glu165 carboxylate groups and the imidazole ring of His 98 and His 95 are similar in MGS and TIM. High resolution NMR spectroscopy and X-ray crystallography were used in determining the role of the SSHB observed from each of these residues to PGH at the active site. Similarities in positioning and structure of the active site residues of MGS and TIM led to initial presumptions that the mechanism of MGS catalyzed enediolate formation followed a route similar to that of TIM catalyzed enediolate formation via a series of SSHB (Scheme 1.26)

Scheme1.26
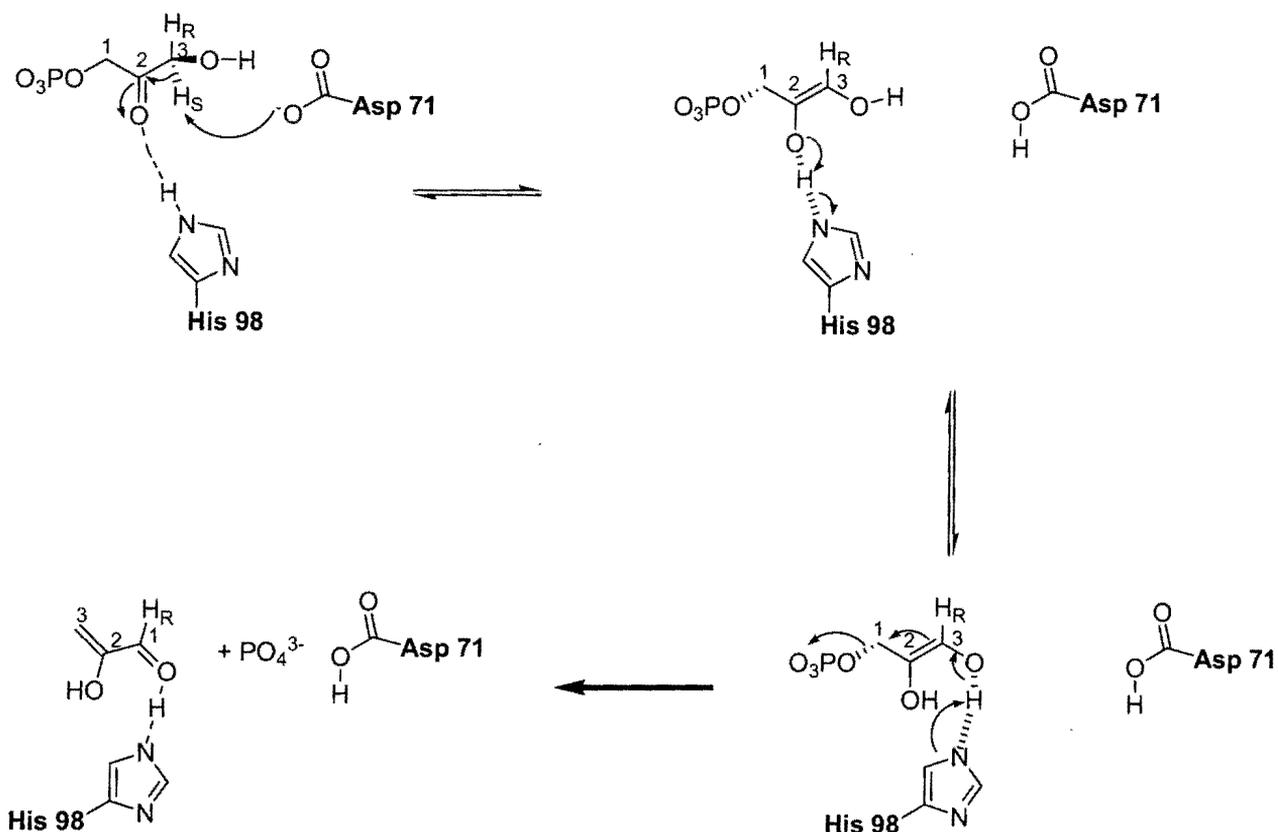
In this 'TIM-like' mechanism a C-3 proton from DHAP (1) is abstracted by the active site Asp 71 residue to form an enediolate intermediate. Stabilization of this intermediate is achieved through a SSHB between the O-2 and His 98 (much like His 95 stabilisation of the enediolate in TIM). The O-2 anion then abstracts the His 98 proton resulting in the formation of a rare imdazolate anion. This anion forms a SSHB with the O-3 hydroxyl group and abstracts the hydroxyl proton. The enediolate then collapses with the 1,4 elimination of the phospho-trianion, forming the enol of methylglyoxal. The simplistic nature of this route and the fact that proton transfer between groups with similar pK_a values is permitted make this a thermodynamically favourable mechanism for catalysis by MGS.

Despite this, the 'TIM-like' mechanism proposed fails to explain the 10^2 fold difference in binding constant for MGS binding the competitive inhibitor PGH ($K_i = 38$ nM) compared to that of TIM binding PGH (7.6 μM). The binding of 2PG to MGS and TIM are in the same order as the latter and similar in value to the binding constant of 2PGH to the D101N mutant of MGS. Also, mutation of the Asp101 residue (which does not appear in the mechanistic proposal) to Asn results in a 10^4 fold drop in k_{cat} when compared to wild-type MGS. The proposed 'TIM-like' mechanism cannot explain this loss in activity. On this basis an alternative mechanism was suggested based on the binding studies of PGH (15) at the active site. These proposals led to an alternative mechanistic route for MGS catalysis (Scheme 1.27).

Scheme 1.27

85
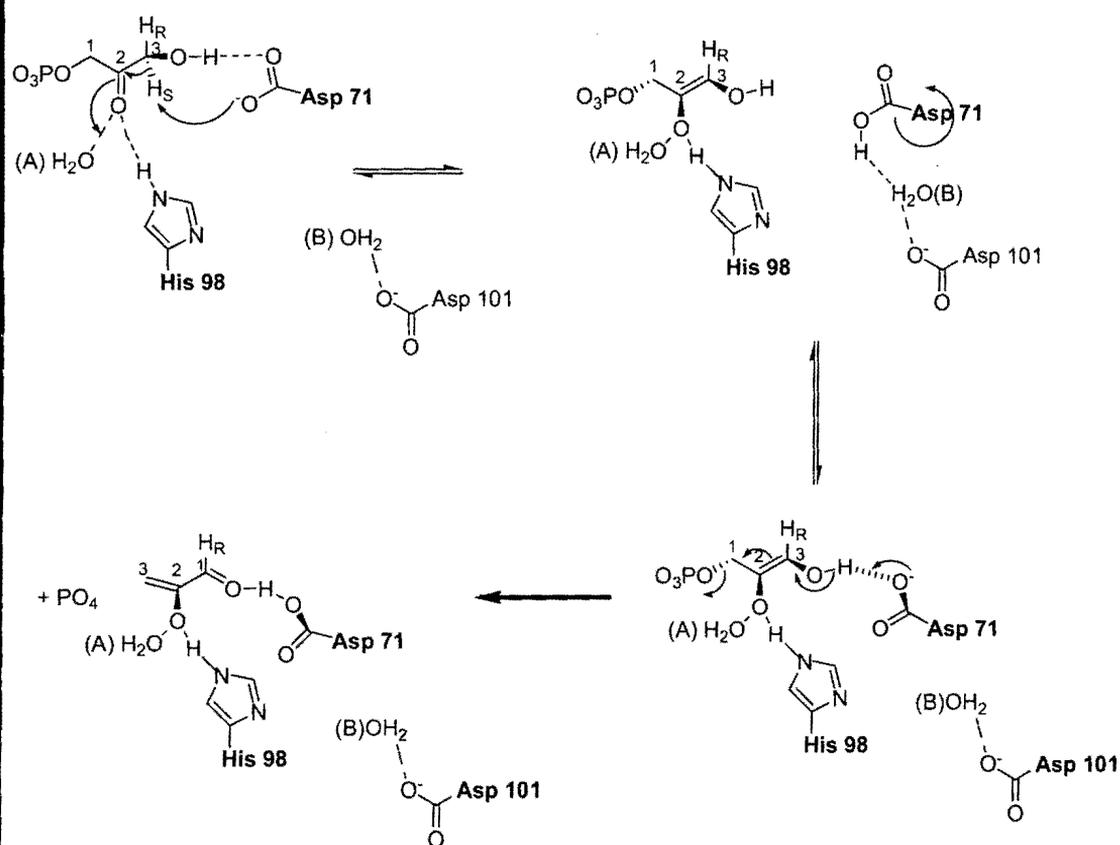
Initial binding of DHAP (1) to the enzyme active site is enhanced by a H-bond interaction between the O3 hydroxyl of DHAP (1) and the NεH of His 98. The negatively charged O-2 formed following substrate deprotonation is stabilised by H-bonded interactions with His 98 and the water molecule (A) from the surrounding bulk solvent. Asp 71 undergoes a conformational change to shuttle its proton via water molecule (B) to Asp 101. The now negatively charged Asp 71 undergoes another conformational change and approaches the hydroxyl group at the C-3 position of enediolate forming a SSHB. This conformational switch is required as approach of Asp 71 from the *Re* face results in the positioning of the phosphate group out of the enediolic plane on the same *Re* face. Based on this mechanistic proposal, elimination of phosphate occurs via a suprafacial 1,4 reaction following deprotonation of the C-3 hydroxyl group of the enediolate intermediate. The role of the water molecules and Asp 101 seem to be significant. This is reflected in the 10^4 fold loss in activity of MGS on mutation of the Asp101 residue to asparagine.

To further probe the 'TIM-like' mechanism the His 98 residue of wild type MGS was mutated to either asparagine or glutamine by Harrison and co-workers. Both these moieties have similar H-bonding capacities as the Nε1 or C-5 protons of Histidine 98. The loss in catalytic activity on mutating His 98 suggests that the residue is not critical for catalysis (k_{cat}/K_M ~10 fold lower in the mutants than wild-type MGS). However, considerable inhibition-like effects were seen on mutation. The H98N mutant showed similar cooperative binding patterns as wild type MGS in the presence of phosphate and competitive inhibition was observed on addition of PGH (15). However the H98Q mutant displayed competitive inhibition as opposed to conformational

inhibition in the presence of submillimolar concentrations of phosphate. Shown below in Figure 1.19 and 1.19a are a comparison of the kinetic profiles for the H98N and H98Q mutants of MGS.

Figure 1.19: H98N mutant*　　　　　　　　　　**Figure 1.19a: H98Q mutant**
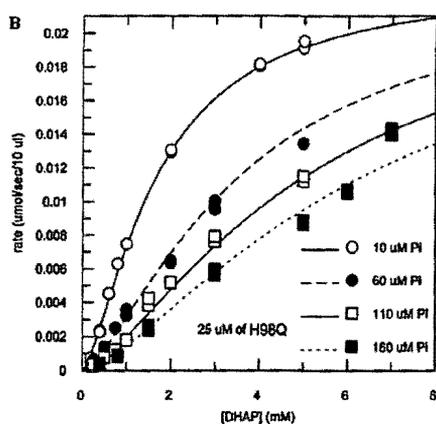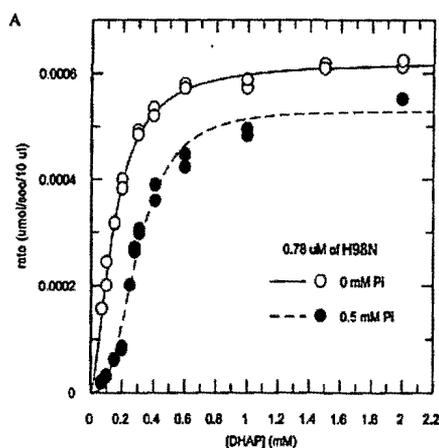
* Taken from Harisson *et al*, Biochemistry, 2004, 42, 3802-3813

It can be seen that the H98Q mutant is competitively inhibited in the presence of small concentrations of inorganic phosphate while the H98N mutant displays conformational (allosteric) inhibition in the presence of inorganic phosphate.

This suggests that the main function of His 98 is establishing an equilibrium between the active 'taut' states of the enzyme and inactive 'relaxed' state. On the basis of these mutations it is likely that a combination of the 'TIM-like' mechanism and the PGH based mechanism are required for complete operation of MGS. While the results obtained above do confirm the importance of the PGH-based mechanism, the 'TIM-like' mechanism cannot be excluded completely. Mutation of the active site residues to asparagine and glutamine result in relatively small reductions in k_{cat}/K_M

when compared to the activity of wild-type MGS. These can be explained by slight changes in the substrate conformations in going from PGH **(15)** to DHAP **(1)**. Also, the above results do not exclude the 'TIM-like' mechanism operating in wild-type MGS. Therefore energetically, there is no difference between the 'TIM-like' mechanism and the PGH-based mechanism for elimination.

1.4.4.4 Origins of the product outcomes of MGS and TIM

The reactions catalyzed by MGS and TIM form a remarkable pair of examples for catalytic efficiency and specificity with both enzymes catalyzing their respective reactions near the diffusion limit. While great efforts have been made to understand the specific mechanistic details for each reaction, the factors controlling the specificities and product formation are less well established. Until recently it was generally accepted that the reason behind the different product outcomes of the two enzymes was a stereoelectronic effect [87, 88]. Binding studies of 2PG **(14)** and PGH **(15)** suggested that the specific conformational arrangements of the substrates at the active sites of each enzyme were different. For elimination of phosphate to occur there must be sufficient overlap between the orbitals of the C-1, C-2 π system of the double bond formed and the leaving phosphate group. In MGS, it was found that the torsional angle (ø) around the C-1, C-2 bond of 2PG brings the phosphate group out of the plane by ~ 55° (Figure 1.20).

Figure 1.20: Conformation of 2PG at the active site of MGS

88

The model shows that the C-1 σ orbital has a significant component parallel to the π orbitals of the C2-C3 double bond in the enediolate of DHAP **(1)** (Figure 1.21).

Figure 1.21: Conformation of the enediolate of DHAP at the active site of MGS
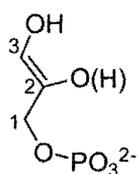
This alignment is believed to be necessary for the elimination of phosphate from DHAP **(1)** (Scheme 1.28). In this conformation, the bridging phosphoryl oxygen sits below the plane of the enediolate intermediate. The sp^3 hybridised C^1 is orientated for optimal overlap with the π-system of the enediolate system

Scheme 1.28: The enediolate orbital orientation at the active site of MGS
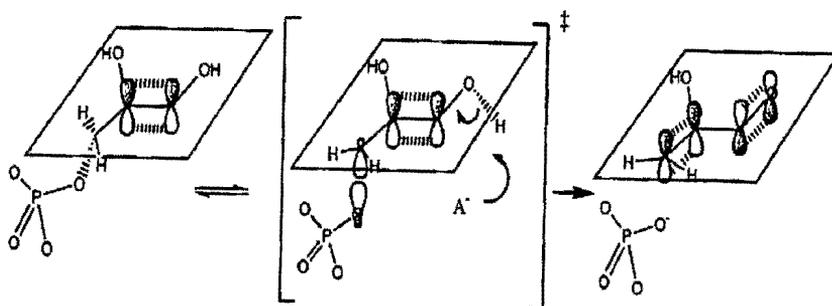
For TIM binding 2PG, the bridging oxygen of C^1 is almost co-planar with the C^2 with ø = 5 ° (Figure 1.22).

Figure 1.22: Conformation of 2PG at the active site of TIM

Therefore from this model no component of the phosphoryl oxygen, C^1 bond is sufficiently parallel with the π orbitals of the C^2-C^3 double bond of DHAP for sufficient elimination to occur (Scheme 1.29).

Scheme 1.29: The enediolate orbital orientation at the active site of TIM
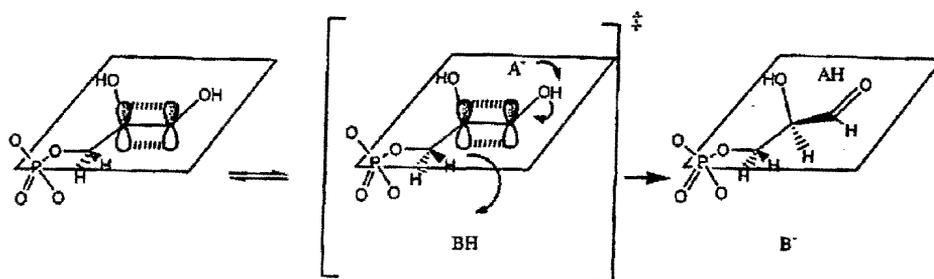
In Scheme 1.29 shown above, the phosphoryl bridging oxygen is in the plane of the enediolate. The conformation minimizes the overlap between the sp^3 orbital of C^1 and the π enediolate system. For this reason it was proposed that elimination is less favoured in the TIM catalyzed reaction due to poorer orbital overlap between breaking the C^3-O^3 bond and the π-enediolate system. Similar behaviour was observed for MGS and TIM binding PGH with the torsional angles along the O^2-C^2-C^3-O^3 were found to be ~ 45 ° in MGS and ~ 15 ° in TIM. The slight differences in torsional angle may be due to structural differences between the two substrate analogues.

90

Despite the *physical* validity of elimination being favoured by MGS catalysis as opposed to TIM as a result of orbital overlap, there are other factors which may contribute significantly to explaining the product outcomes. As discussed in the previous section there are a variety of mechanistic possibilities for the initial part of MGS catalysis based on mutations and inhibition studies. Shown below in Scheme 1.30 is collection of the possible pathways.

Scheme 1.30* The possible mechanistic pathways of TIM and MGS throught common enediolate intermediates
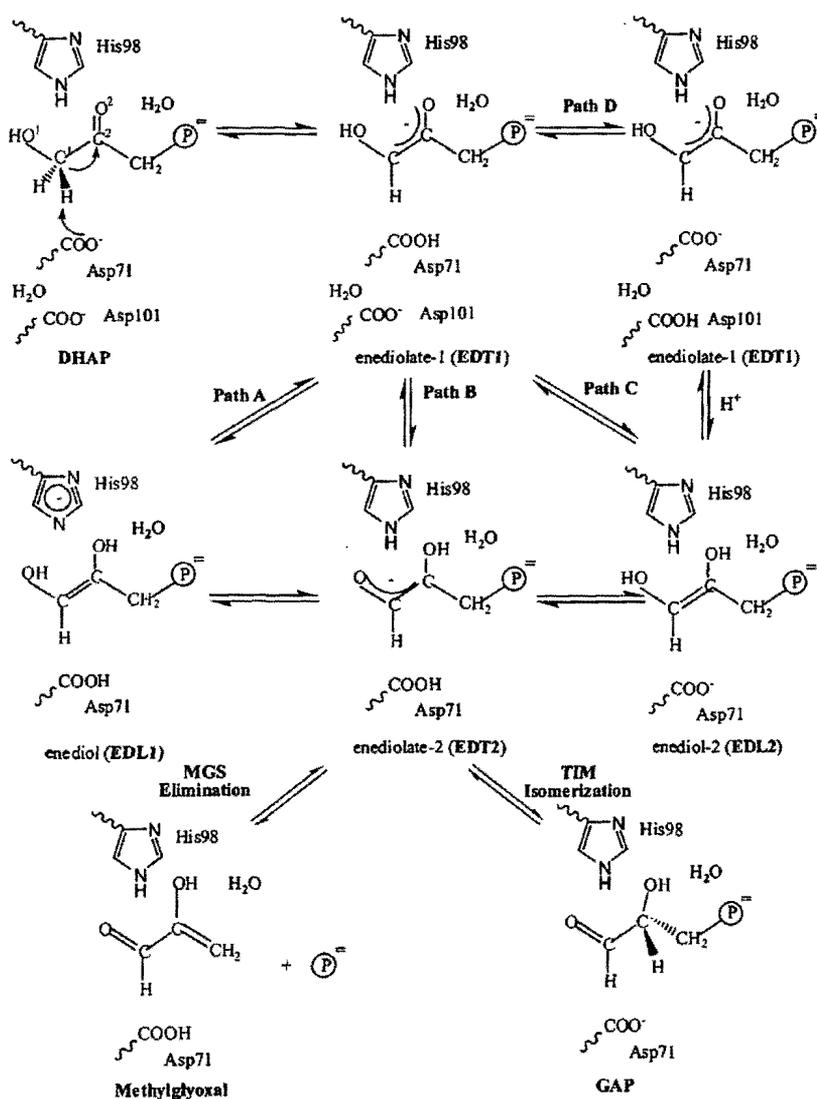
The energy barrier heights of each pathway have been determined by Harrison and co-workers and combined with those of TIM. The reaction pathway for the TIM reaction is well known and all the energy barrier heights have been determined experimentally previously by Knowles and Albery. The barrier heights for these experiments were determined by DFTB/CHARMM. While CHARMM was used to establish the enzymatic barrier heights, SCC-DFTB was used to look at the effect in the gas phase of varying the O^2-C^2-C^3-O^3 torsional angles. Shown below in Figure 1.22 are the free energy surfaces for the isomerisation (solid line) and phosphate elimination reactions (dashed line) in MGS (red) and TIM (blue).

Figure 1.22: Free energy surfaces for the isomerisation of TIM and elimination of MGS*
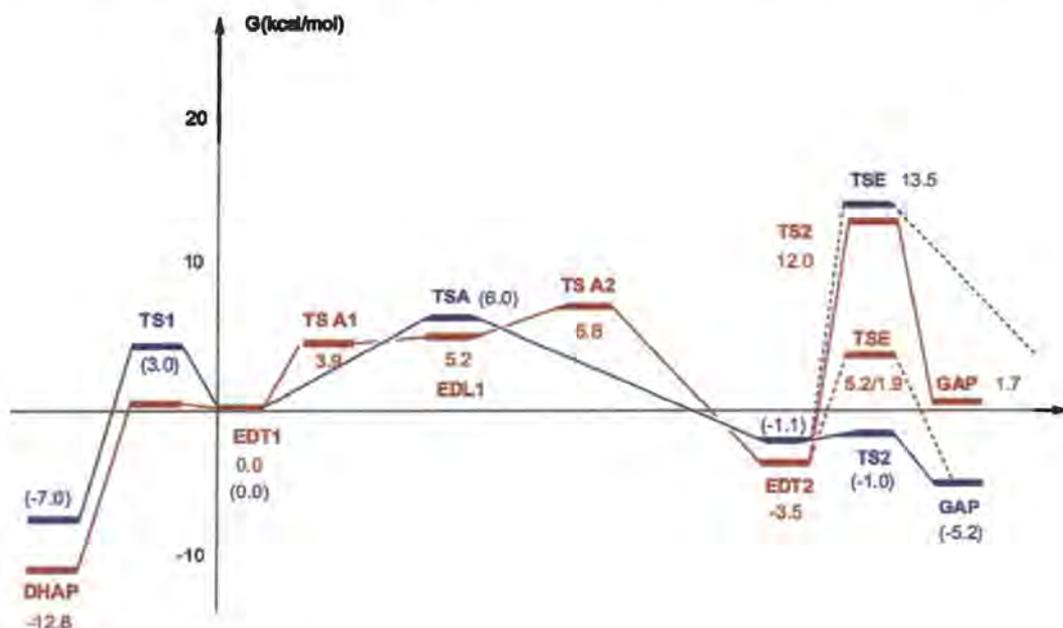
The energy levels obtained at each intermediate and transition state are similar in MGS and TIM up to the enediolate species EDT2. The barrier from EDT2 to TS1 and TS2 represents the last step of the isomerisation reaction i.e. protonation of the substrate by the conjugate acid forms of Glu 165 in TIM and Asp 71 in MGS. The MGS-EDT2 – TS2 (~16 kcal/mol) is considerably larger than the TIM-EDT2 - TS2 (~ 0.1 kcal/mol). These results are consistent with the fact that while TIM catalyzed isomerisation from DHAP (1) to GAP (6) is practically diffusion controlled, MGS catalyzed isomerisation is not observed. Furthermore, it has been found that concentrations of *R,S* GAP up to 3 mM do not allosterically inhibit MGS thus GAP (6) does not serve as a DHAP (1) analogue (unlike 2PG and PGH) in overcoming phosphate inhibition. Therefore these energy barriers are also consistent with the observation that GAP is not an allosteric inhibitor of MGS.

Perturbation analysis calculations suggest that the high barrier for GAP formation from MGS is due to the distance between protonated Asp 71 and the negatively charged C-2 in EDT2 (~ 3.4 Å). The distance between protonated Glu 165 in TIM and the charged C-2 of EDT2 is considerably less (1.9 Å) (Figure 1.23).

Figure 1.23: Comparisons of distance between protonated Glu 165 in TIM and charged C-2

of EDT2 *

EDT2 in MGS   EDT2 in TIM
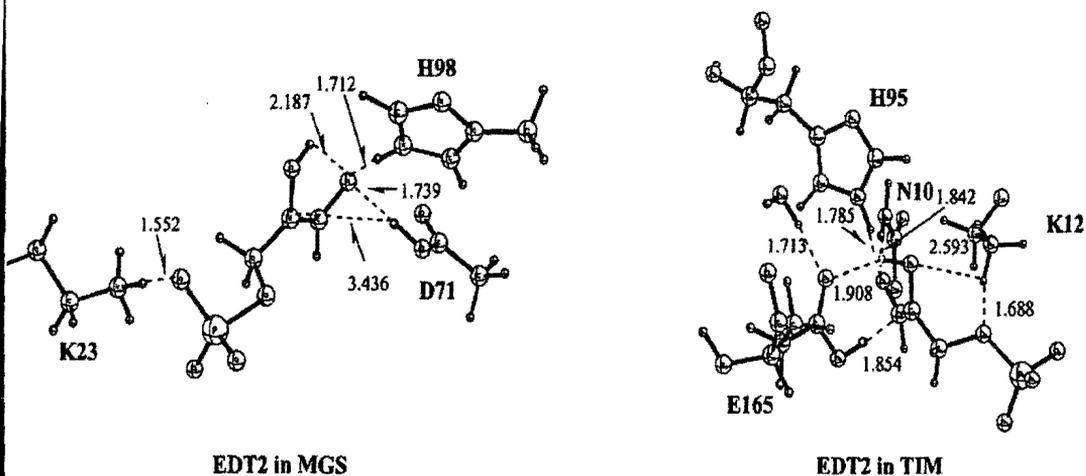
* Taken from Harrison *et al*, JACS, 2002, 124, 14871-14878

The QM/MM studies show that the barrier to elimination for TIM (EDT2 – TSE) is ~ 15 kcal/mol. The barrier to elimination for MGS (EDT2 – TSE) is ~ 9 kcal/mol. The barrier to elimination is the only one where two values are given which correspond to the energy differences between the protonated and non-protonated forms of the leaving phosphate group. For MGS, the protonated and non-protonated forms of the phosphodianion group are represented by the values +1.9 and 5.2 kcal/mol respectively. Similarly for TIM the value for the barrier to elimination of the protonated phosphodianion group is 13.5 kcal/mol and that for the non-protonated from of the phosphodianion is 14.6 kcal/mol. Therefore there is ~ 6 kcal/mol difference in the barrier to elimination for MGS and TIM.

The basis for the stereoelectronic theory was made due to differences in the O^2-C^2-C^3-O^3 torsional angles of PGH and PGA at the active sites of TIM and MGS. However varying this torsional angle between 0 and 60 ° has an effect of only 4 kcal/mol on the barrier to elimination in EDT2 at the C-O distance of 2 Å (Figure 1.24).

Figure 1.24 * The results of changing the protonation state of the phosphodianionic group

of DHAP on the overall barrier to elimination
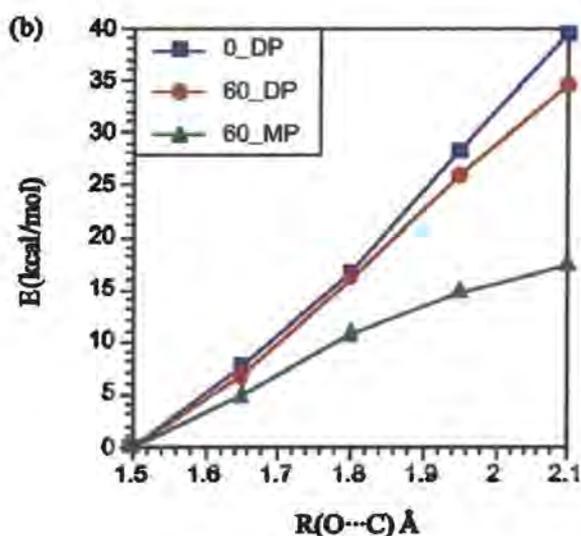
* Taken from Harrison et al, JACS, 2002, 124, 14871-14878

However changing the protonation state of the phosphodianion group hugely decreases the barrier to elimination by ~13 kcal/mol. Despite the TIM-PGH, TIM-PGA and MGS-PGH and MGS-PGA compexes having different torsional angles the calculated EDT2-MGS (18°) and EDT2-TIM (21°) torsional angles are similar. Based on these findings it is unlikely that the stereoelectronic theory plays a dominant role in determining the product outcomes of the two enzymes. It was thus proposed to be more likely that the functional specificites of MGS and TIM

is mainly due to differences in the electrostatic binding of the phosphate groups in the two enzyme active site pockets. As discussed, the X-ray crystal structures TIM-PGH complex shows only two hydrogen bond interactions to the phosphate group whereas in the MGS-PGH structure there are approximately 11. In addition the arrangement of water molecules around the phosphate group in both structures is significantly different. However, an experimental quantification of the relative contributions of the phosphate group to the reactions of DHAP (1) catalyzed by MGS and TIM has to date not been made.

1.4.5 Further investigations of the catalytic role of the phosphodianion of DHAP

A remarkable feat of the MGS/TIM pair is the ability to catalyse their respective reactions near the diffusion limit without an active site metal ion. Similar behaviour has been observed for sugar phosphate isomerases. These enzymes catalyze the isomerisation of sugars with k_{cat}/K_M $\sim 10^8 M^{-1}s^{-1}$, a rate much greater than the closely related sugar isomerases which catalyze the metal ion dependent hydride transfer isomerisation of sugars lacking a charged phosphate group ($k_{cat}/K_M \sim 10^3 M^{-1}s^{-1}$) [89]. The measure of the contribution of the phosphate group to the TIM (GAP-DHAP) enzymatic reaction has been achieved by comparing the TIM-catalyzed isomerisation reaction of natural substrate R-GAP with that of mutant substrate R-glyceraldehyde (R-GA) (Scheme 1.30)

Scheme 1.30
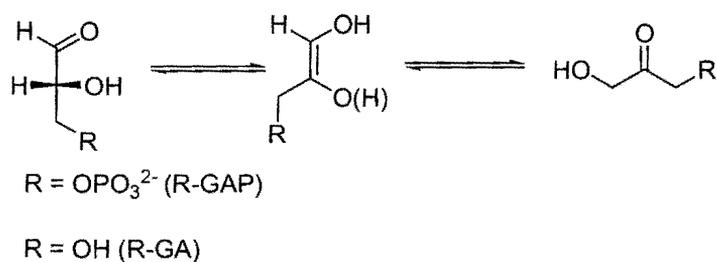
R = OPO$_3$$^{2-}$ (R-GAP)

R = OH (R-GA)

The activity of TIM towards isomerisation of GA to give dihydroxyacetone (DHA) was monitored by high resolution ^{1}H NMR spectroscopy. Corrections were made for the non-specific protein catalyzed degradation of GA by repeating the reaction in the presence of active site inhibitor 2PG (14). The second order rate constant for the deprotonation of GA at the active site by TIM in D$_2$O and at pD 7 was estimated to be $k_{cat}/K_M = 0.34$ M^{-1}s^{-1} [38].This result may be compared with the value of $k_{cat}/K_M = 2.4$ x 10^8 M^{-1}s^{-1} for deprotonation of GAP by TIM. The second order rate constant for the non-enzymatic deprotonation of the C-2 proton of GAP (6) by 3-quinuclidinone, k_B, was found to be 6.5 x 10^{-3} M^{-1} s^{-1}. Shown below in Figure 1.25 is the free energy reaction coordinate profile for the TIM-catalyzed and 3-quinuclidinone catalyzed enolization reactions of R-GA overlayed with the free energy profile created for R-GAP by Knowles and co-workers [90].

Figure 1.25: Free energy profiles for the TIM –catalyzed and 3-quinuclidinone catalyzed enolization reactions of R-GA overlayed with the free energy profile created for R-GAP by Knowles et al*

From the free energy profile it can be seen that the difference in free energies of binding of R-GA and R-GAP to the active site of TIM, $\Delta\Delta G_b < 4.2$ kcal/mol. The total intrinsic binding energy of the phosphodianion of GAP to TIM in the transition state for C-2 deprotonation (eneolization), $\Delta\Delta G^{\ddagger} = 16.4$ kcal/mol. From the free energy profile the intrinsic binding energy (IBE) for GAP (TIM) = 20.4 kcal and IBE for GA (TIM) = 2.3 kcal/mol. Thus Δ IBE = 14.1 kcal/mol. From the free energy profile it can be seen that approximately 80 % of the rate acceleration of TIM-catalyzed reaction of GAP **(6)** can be directly attributed to utilization of the intrinsic binding energy of the small substrate phosphodianion group which is remote from the site of chemical transformation. Interestingly, such a large contribution of the phosphodianion

group interactions to the TIM-catalyzed GAP **(6)** reaction seems to contradict the proposed phosphate interaction explanation for the different product outcomes of TIM and MGS as discussed in the previous section. However, the contribution of the phosphodianion intrinsic binding energy of substrate DHAP **(1)** (the relevant substrate for the MGS reaction) to the TIM catalyzed reaction could be different to that found for GAP **(6)**.

1.5 Project aims

QM/MM studies of MGS and TIM binding substrate analogues and competitive inhibitors 2PG and PGH, have suggested that the differences in the product outcomes were mainly due to differences in the protonation state of the phosphodianion group of susbtrate DHAP. X-ray crystallography implied that at the active site of TIM, there were only two hydrogen-bonded interactions to the phosphodianion group of substrate whereas at the active site of MGS there were eleven. Changes in the protonation state of substrate was found to have an effect of up to 14 kcal/mol on the overall barrier to elimination suggesting the importance of these interactions at the active site pockets. However in order to probe the importance of these phosphodianionic interactions experimental quantification was needed.

Thus the major aim of this work was to determine the role of the phosphodianion group of DHAP in catalysis by MGS. To determine the importance of this remote group a range of substrate analogues have been synthesized where the dianionic phosphate group of natural substrate has been replaced by other groups. In this work dihydroxyacetone, hydroxyacetone, dihydroxyacetone sulfate, dihydroxyacetone thiosulfate, dihydroxyacetone thiophosphate and bromohydroxyacetone have been investigated. Apart from hydroxyacetone and

dihydroxyacetone which were commercially available, the substrates were synthesized following established literature methods or using adaptations of such protocols.

Prior to monitoring the turnover of these substrates by MGS it was necessary to fully characterize the background, non-enzymatic enolization and elimination reactions of each molecule. In order to quantify any overall enzymatic rate acceleration a comparison between k_{cat}/K_M for the second order enzyme catalyzed rate was made with the second order rate, k_B for the buffer catalyzed reactions at the same pD.

From the data gathered for the reactions of substrate in the presence and absence of MGS comparisons could be made to the effect of substrate mutations on the TIM catalyzed reaction of GAP and GA thus providing insights into the mechanisms employed by each enzyme when substrates other than natural DHAP are employed.

Chapter 2

Results

2.0 Foreword

The following chapter describes the results obtained during these studies. In Section 2.1 an overview of the various synthetic aspects of the work is presented. Section 2.2 deals with the kinetic studies on the substrates in aqueous solution in the absence of enzyme. In Sections 2.3 and 2.4 the reactions and kinetics of these substrates in the presence of MGS are discussed in detail.

2.1 Synthesis

In order to quantify the importance of the different interactions between the phosphodianion group of natural substrate DHAP (1) and *methylglyoxal synthase*, a range of substrate analogues have been synthesised.

The synthesis of bromohydroxyacetone (BHA) (22) was achieved in a one step reaction from 2-chloro-2-propen-1-ol (20) and N-bromosuccinimide (NBS) (Scheme 2.1), which likely occurs via an intermediate chloroepoxide (21)[91].

Scheme 2.1

(20)   (21)   (22)

Recrystallisation of the product from dichloromethane resulted in the formation of a mixture of a monomeric BHA (22) and a dimeric species as confirmed by mass spectrometry. Druekhammer *et al* suggest that crystallisation from DCM results in the formation of the dimeric species (23)

102

(Scheme 2.2). In our case, irrespective of the solvent and temperature used for recrystallisation, a mixture of monomeric and dimeric BHA was formed in varying ratios. Although the extent of the proposed dimer present could be slightly decreased by slower recrystallisation, it was always present in large excess over the monomer. For the purpose of kinetic studies regeneration of the monomer was achieved by dissolving the dimer in DCl (1M) at 25 °C. Complete formation of the monomer took approximately 48 hours. This will be discussed further in Section 2.2.

Scheme 2.2

(22)   (23)

Crystalline BHA (mixture of monomer and dimer) was further reacted to form two more substrates. Reaction with excess sodium thiophosphate in H_2O with the pH maintained at 8.1 (by the addition of 2M KOH) resulted in the formation of dihydroxyacetone thiophosphate (DHATP) (24) (Scheme 2.3). The reaction was complete in 10 minutes as a result of rapid cleavage at the C-1 position of the molecule, with the departure of the bromide anion [91].

Scheme 2.3

(22)   (24)

An analogous synthetic method was used for the formation of dihydroxyacetone thiosulfate (DHATS) (25) (Scheme 2.4). In this case BHA (22) was reacted with excess sodium thiosulfate in H_2O and EtOH. As with the previous reaction, direct cleavage at the C-1 position of BHA (22) was believed to occur. However, the reaction time in this case for the displacement of the bromide anion was considerably longer than for the formation of DHATP (24) (approximately 3 hours as opposed to 10 minutes).

Scheme 2.4

(22)   pH 7   (25)

The synthesis of dihydroxyacetone sulfate (DHAS) (27) was achieved in one step from the reaction of dihydroxyacetone (DHA) (26) and sulfur trioxide-triethylamine complex (Scheme 2.5) [92].

Scheme 2.5

(26)   (27)

An adaptation of the literature was used in the purification of DHAS (27). Following ion exchange chromatography, a methanol precipitation step was used to isolate the sulfate product.

4-Ethoxy-1-hydroxybutan-2-one (**29**) was synthesised in a one step mercuric oxide catalyzed

hydration reaction from the addition of mercuric oxide catalyst, to a solution of butynediol (**28**)

in EtOH (Scheme 2.6) [93]. Addition of the alkyne (over a period of 5 hours) was regulated to

maintain a temperature of 35-40 °C. This material was prepared prior to use without further

purification.

Scheme 2.6

(28)   (29)

The resulting butanone (**29**) was dissolved in dry ether and cooled to 0 °C. Following the

addition of triethylamine to induce deprotonation of the alcohol group at the C-4 position,

pivaloyl chloride was added dropwise over a period of 25 minutes. This resulted in the formation

of 4-ethoxy-2-oxobutyl ester (**30**) (Scheme 2.7). Purification of this compound was achieved by

column chromatography [94].

Scheme 2.7

(29)   (30)

The pivaloyl protected ether (**30**) was reacted with dry sodium iodide in dry dichloromethane

which was flushed with dry argon. Freshly distilled chlorotrimethylsilane was added dropwise at

0 ° C over a period of 15 minutes with gentle stirring. This led to the formation of 4-iodo-2-oxobutyl ester (31) (Scheme 2.8).

Scheme 2.8

(30)   NaI, Me₃SiCl / DCM   (31)

It was found that dry sodium iodide and freshly distilled chlorotrimethylsilane were crucial for the reaction to proceed successfully. Due to the labile nature of the iodide (31), it was prepared immediately prior to use in the next stage of the synthesis.

The synthesis of the 3-oxo-4-(2,2-dimethylpropionyl)oxobutylphosphonic acid diisopropyl ester (32) was achieved by reacting the iodide (31) with distilled triisopropyl phosphite in an Arbuzov displacement reaction (Scheme 2.9).

Scheme 2.9

(31)   P(O^{i}Pr)₃   (32)

Distillation of triisopropyl phosphite was of vital importance for the reaction to proceed. Excess solvent was removed under reduced pressure and the phosphodiester product (32) was purified by column chromatography.

In the final step of the reaction, the phosphodiester (32) was refluxed in conc. HCl and H_2O for 3-8 hours with the aim of forming the final 'phosphonate' product (33) (Scheme 2.10). The literature procedure suggests that hydrolysis of both the pivaloyl ester and phosphate ester groups occur after 4 hours. While hydrolysis was found to occur rapidly at the C-6 position, hydrolysis was not observed at the phosphate ester end of the molecule. Changing the literature reaction conditions such as increasing the acid concentration, temperature and reaction times led to decomposition of the molecule.

Scheme 2.10

(32)   (33)

The attempted hydrolysis reactions of (32) are discussed in Section 2.2.

2.2 Analysis of the solution reactions of DHAP analogues in the absence of MGS using ^{1}H NMR spectroscopy

Literature proposals suggest that the background elimination reaction of DHAP (1) proceeds through an enediolate intermediate [17]. For DHAP (1) in solution, the rate-determining step for elimination is enolization, thus a measure of the rate constant for enolization provides an overall rate for elimination. High resolution ^{1}H NMR spectroscopy has proved to be a convenient tool for monitoring the enolization reactions of α-carbonyl substrates by monitoring low levels of deuterium incorporation at the α-carbonyl carbon [1, 37, 38, 89, 95]. Similar methods were

employed to follow the solution, non-enzyme catalyzed reactions of DHAS (27), DHATS (25) and BHA (22).

For each substrate in buffered D_2O solutions, there are different sites of the molecule where buffer or deuteroxide anion (DO⁻) may react. Deprotonation at the C-3 position of general mutant substrate (34) leads to the formation of the enediolate intermediate (35). The intermediate could then react with the conjugate acid of the buffer (or with D_2O) leading to the incorporation of a deuterium atom at the C-3 position (36). Further deprotonation and re-deuteration at this position could lead to complete deuterium incorporation at the C-3 position (37) (Scheme 2.11).

Proton transfer between the two enediol oxygens of enediolate intermediate (35) results in the formation of (38). This switch facilitates the elimination of the leaving group (Br⁻, SSO_3^{2-}, or OSO_3^{2-}) to form enol (39). Tautomerisation of the enol (39) leads to the elimination product MG (40). Alternatively, following this proton switch reprotonation of the enolate (38) could occur at the C-2 position rather than at C-3, leading to the isomerisation product (41). In the case of DHAP (1), no deuterium exchange at the C-3 position could be detected in competition with elimination in buffered D_2O solutions at pD 6-8. Furthermore, isotopic labelling experiments have revealed that a maximum of 1 % isomerisation could be detected relative to elimination from pD 6-12 as mentioned in Chapter 1. As Br⁻, SSO_3^{2-} and OSO_3^{2-} are similar or better leaving groups than OPO_3^{3-}, it is expected that elimination will also out compete C3-H/D exchange and isomerisation in these cases.

Finally, deprotonation at the C-1 position of (34) to yield enediolate intermediate (42) followed by reprotonation at C-1 by BD^+ or D_2O would yield the exchange product (43) and ultimately

108

(44). In this case elimination or isomerisation cannot occur as the group 'X' is not a hydroxyl group.

Scheme 2.11

X = Br, SSO₃⁻, OSO₃⁻

$X = Br, SSO_3^-, OSO_3^-$

2.2.1 Dihydroxyacetone Sulfate (DHAS) (27)

The solution non-enzyme catalyzed reactions of DHAS (27) were studied by 400 and 500 MHz ^{1}H NMR spectroscopy. In buffered D_2O solutions the carbonyl group of DHAS (27) is extensively hydrated and thus an equilibrium exists between the free ketone and hydrate form (27h) of the substrate (Scheme 2.12). Furthermore, the sulfate group is expected to be in the monoanionic form at all the pD's used for kinetic measurement (pD ≥ 7), as typical pK_a values for alkylsulfuric acids are in the 1-3 range [96, 97].

Scheme 2.12

(27)   (27h)

The equilibrium constant, K_{hyd}, can be represented by Equation 2.1

$$K_{hyd} = [27h]/[27]$$

Equation 2.1

Interconversion of the free ketone and hydrate of DHAS is relatively slow on an NMR timescale. Therefore separate ^{1}H NMR peaks will be seen due to both the hydrated and free keto forms of the molecule.

Shown below (Figure 2.1) is a representative partial ^{1}H NMR spectrum of DHAS (27) (10 mM) in DCl (1M) and 25 °C at zero reaction time. Also present is imidazole (5 mM) as an internal standard. This spectrum in Figure 2.1 has been used as the zero timepoint for all reactions

studied as the initial substrate and internal standard concentration was identical under all reaction conditions. For the zero time point it is likely that the substrate is mostly protonated (Scheme 2.13).

Scheme 2.13

(27')   (27'h)

This leads to subtle changes in the peak positions when compared to the corresponding peaks of the ^1H NMR spectra for the buffered reactions of substrate. The reactant peak areas remained constant with respect to internal standard in the case of this 1M DCl substrate sample over a period of weeks.

Figure 2.1 Representative ^{1}H NMR spectrum at 500 MHz of DHAS (20) (10 mM), obtained at zero reaction time in DCl (1M) at 25 °C (I = 1.0). Imidazole (5mM) is present as internal standard.

The broad singlets at 7.25 and 8.15 ppm are due respectively to the two C-4 and C-5 protons, and the C-2 proton, of the imidazolium cation internal standard. The singlet at 7.25 ppm was used as the reference peak for integration as the C-4 and C-5 protons of the imidazolium cation are significantly less susceptible to deuterium exchange than the C-2 protons [98]. Two singlets, **A** and **B** are observed at 4.75 ppm and 4.48 ppm which integrate 1:1 with respect to each other. Two further singlets, **C** and **D** are observed at 3.55 ppm and 4.0 ppm which also integrate 1:1 with respect to each other. The more downfield set of two singlets (4.48, 4.75 ppm) are due to the two CH$_2$ groups of free keto form of substrate DHAS **(27)** whereas the more upfield set of singlets (3.55, 4.0 ppm) are due to the two CH$_2$ groups of the hydrate form of substrate **(27h)**. Peaks due to the protons of a hydrated carbonyl compound are typically located at lower field

than peaks due to analogous hydrogens of the free keto form. The ratio of the sum of the areas of the two singlets due to the hydrate (27h) to that of the two singlets due to the keto form (27) yielded a value for the equilibrium constant, K_{hyd} = 1.2 in these conditions.

In order to further assign the singlets due to hydrate and keto forms to either the CH_2OD or $CH_2OSO_3^-$ groups, HMQC and HSQC cross correlation ^1H NMR experiments were attempted. However despite several attempts, varying the concentration and degassing the solutions these experiments were not successful. In the case of DHAP (1) at pD 8, the $CH_2OPO_3^{2-}$ protons yield peaks which are at lower field than the CH_2OD protons in the free keto form but at higher field for the hydrate form. Evidence for this comes from coupling to ^{31}P. However in buffers of lower pD (such as acetic acid) the peak positions of the keto CH_2 peaks switch as a result of protonation of the phosphodianion of DHAP (see Section 2.4). Thus it was unclear as to what to expect for peaks due to analogous protons on the keto and hydrate forms of DHAS (27).

The reactions of DHAS (10mM) were monitored in quinuclidinone (40-100 mM, 70-90 % f_B, pD 8.52-9.35) and phosphate buffers (60-100 mM, 70 % f_B, pD 7.89-8.04) at 25 °C (I =1.0, KCl). Reactions were initiated by direct addition of the required amount of buffer and internal standard to the solid substrate. For experiments carried out at 500 MHz the sample remained in the NMR probe throughout the reaction time course with spectra taken over varying time periods. Experiments on the lower field instruments were prepared on a larger scale and incubated at 25 °C. The reactions were initiated in the same way (i.e addition of buffer to neat substrate) however were quenched over certain time periods. Shown below (Figure 2.2) are representative

partial ^{1}H NMR spectra taken during the reaction of DHAS (10 mM) in 40 mM quinuclidinone buffer, 70 % f_B, pD 8.52. The zero timepoint ^{1}H NMR spectrum is for a 1M DCl solution of substrate at the same concentration.

Figure 2.2 **Representative ^{1}H NMR spectra at 500 MHz of DHAS (27) (10 mM, pD 8.52), obtained during the reaction in quinuclidinone buffer 70 % f_B, 40 mM (pD 8.52) in D$_2$O at 25 °C (I = 1.0, KCl). The timepoint is indicated above each spectrum in minutes.**

Each NMR spectrum was recorded over a period of 40 minutes (128 transients) with the reaction time t calculated from the time at the midpoint of these analyses. The reaction was followed in the probe of the spectrometer. The ratio of the areas of singlets **D:B** at pD 8.52 yields a value of K_{Hyd} = 1.17. Thus deprotonation of the sulfate group does nothing to the distribution of the hydrate and keto forms at equilibrium.

The changes in the ^{1}H NMR spectra over time are indicative of the pathways by which DHAS (**27**) reacts under the experimental conditions mentioned above. A decrease in the singlet at 4.79 ppm, **A**, due to one of the CH_2 groups of the keto form of DHAS (**27**), is accompanied by the simultaneous appearance of a small broad upfield triplet ($^2J_{HD}$ = 3 Hz) at 4.75 ppm **H**. This triplet is assigned to the $CHDOSO_3^-$ group of the keto form of DHAS (**27a**) labelled with deuterium at the C-1 position (Scheme 2.14). As mentioned earlier it is not expected that C3 H/D exchange will compete with the elimination of OSO_3^{2-}. On this basis peak **A** is assigned to the $CH_2OSO_3^-$ group of the keto form of DHAS (**27**).

Scheme 2.14

(27)   (27a)   (27b)

Analogously, a decrease in the singlet at 3.91 ppm **C**, due to the $CH_2OSO_3^-$ group of DHAS hydrate, is accompanied by an increase in a broad upfield singlet at 3.85 ppm **G**. This singlet is due to the $CHDOSO_3^-$ group of DHAS hydrate which is a result of deuterium incorporation at the C-1 position of DHAS keto form. The interconversion of the keto and hydrate forms is faster than the deuterium exchange process.

As the reaction proceeds, two further new singlets are observed at 4.81 ppm, **F**, and 5.25 ppm, **E**. These are due to the C-1 protons of the bishydrate (**40h**) and the monohydrate (**41mh**) forms of methylglyoxal respectively (Figure 2.3). Methylglyoxal is extensively hydrated in aqueous solution and exists as a mixture of 60 % monohydrate and 40 % bishydrate*.

Figure 2.3

(40h)   (40mh)

The ratio of the areas of the two singlets remains constant over time at a fixed value of 3:2 for the 5.25: 4.81 ppm singlets. It was not expected that signals due to the methyl peaks of the elimination product would be observed as the C-1 position DHAS **(27)** will be deuterated to a large extent prior to elimination (Scheme 2.15). Also, this region of the spectrum is obscured by peaks due to buffer.

* This peak assignment was confirmed by the preparation of a buffered D_2O solution (I = 1.0, KCl) of commercial methylglyoxal (40 wt % in H_2O)

Scheme 2.15

Analysis of the spectra indicates that there are no new peaks formed which could be assigned to isomerisation product 2-deuterio-glyceraldehyde-3-sulfate **(45)** (Figure 2.4).

116

Figure 2.4

(45)   (45h)

In solution both glyceraldehydes (46) and glyceraldehyde-3-phosphate (6) are approximately 95

% hydrated [45]. The C-1 proton of both of these hydrates appears as a doublet with very similar

chemical shifts at 4.91 and 4.89 ppm respectively in a D_2O solution at pD 8 and ionic strength, I

= 1.0 (KCl). In both cases deuterium exchange at the C-2 position of both aldehydes (46) and (6)

results in a decrease of the doublets due to the C1-Hs and the appearance of broad singlets

slightly upfield of the midpoint of the doublets. This is because vicinal coupling to deuterium has

a less than 2Hz coupling constant. A small doublet also appears at ~ 9.59 ppm corresponding to

the aldehydic protons of the free keto forms of the molecules. Similarly for the product of a

potential isomerisation reaction of DHAS (27), 2-deuterio-glyceraldehyde-3-sulfate (45) should

also be present predominantly as hydrate (45h). The C1-H of hydrate (45h) would be expected to

yield a singlet at approximately 4.9 ppm however the only peak in this region can be clearly

assigned to the bishydrate of methylglyoxal (See Figure 2.2).

Therefore the decrease in the singlets at 3.91 and 4.79 ppm is due to both exchange and

elimination reactions of the substrate. The C1-H/D exchange reaction is significantly faster than

elimination. There is also a decrease in the singlets at 3.56 ppm and 4.56 ppm (D and B) due to

117

the CH_2OD protons (hydrate and keto forms). In this latter case the decrease is due to elimination only as no C3-H/D exchange is observed.

The progress of the reaction at the C-1 side of substrate due to both exchange and elimination was monitored by determining the sum of the integrated peak areas of the singlets at 3.91 ppm and 4.79 ppm (due to the $CH_2OSO_3^-$ group of the keto and hydrate froms of DHAS respectively) over time, t, relative to the sum of the same peak areas at zero reaction time. The fraction of substrate remaining, $f(s)$, was determined from Equation 2.2

$$f(s) = \frac{(A_{C1\text{-}CH2(Keto)})t + (A_{C1\text{-}CH2(Hyd)})t}{(A_{C1\text{-}CH2(Keto)})t_0 + (A_{C1\text{-}CH2(Hyd)})t_0}$$ **Equation 2.2**

The disappearance of the two singlets at 3.56 ppm and 4.48 ppm due to the CH_2OD group of the hydrate and keto forms of DHAS (**27**) was also followed by ^1H NMR spectroscopy. This disappearance is due to an elimination reaction only. In this case the fraction of substrate remaining, $f(s)'$, was calculated using Equation 2.3.

$$f(s)' = \frac{(A_{C3\text{-}CH2(Keto)})t + (A_{C3\text{-}CH2(Hyd)})t}{(A_{C3\text{-}CH2(Keto)})t_0 + (A_{C3\text{-}CH2\text{-}(Hyd)})t_0}$$ **Equation 2.3**

The observed pseudo first order rate constants for the disappearance of substrate could be determined as the slope of the semi-logarithmic plots of either $f(s)$ or $f(s)'$ against time (Equations 2.4 and 2.5)

$$\ln f(s) = -k_{obs}{}^T t \qquad\qquad \textbf{Equation 2.4}$$

$$\ln f(s)' = -k_{obs}{}^E t \qquad\qquad \textbf{Equation 2.5}$$

The pseudo first order rate constant $k_{obs}{}^T$ (s^{-1}) is for the total disappearance of substrate due to both C1-H/D exchange and elimination. The pseudo first order rate constant $k_{obs}{}^E$ (s^{-1}) is for elimination only. The observed experimental first order rate constants $k_{obs}{}^T$ and $k_{obs}{}^E$ could potentially be the sum of the contributions of all the catalytic species to the rate of exchange and/or elimination including the solvent, deuteroxide and buffer base contributions (Equation 2.6).

$$k_{obs} = k_0 + k_{DO}[DO^-] + k_B[B] \qquad\qquad \textbf{Equation 2.6}$$

The term k_0 refers to the rate constant for a potential uncatalyzed, pH independent elimination or exchange reaction in solution. The background pH independent elimination reaction of DHAP (1) is believed to be catalyzed by the remote phosphodianion group of substrate acting as an intramolecular base as discussed in Chapter 1. We predict that this would be significantly less likely for DHAS (27) as the sulfate anion is much less basic than the phosphodianion (pK_a

RSO$_3$H ~ 2-3, pK_a ROPO$_3$H$^-$ ~6.6 [17]). Therefore we initially would predict that this term may not contribute significantly unless an intermolecular reaction with water is competitive with the other two terms. The term $k_{DO}[DO^-]$ refers to a deuteroxide catalyzed elimination or exchange reaction in solution where k_{DO} is the second order rate constant for the DO$^-$ catalyzed reaction. The term k_B is the second order rate rate constant for general base catalysis. General acid catalysis of exchange or elimination is not expected as it in not significant in the cases of DHAP (1).

To determine the contribution of buffer species to exchange and elimination, reactions were run at a fixed pD and at constant buffer ratio while varying the total concentration of buffer. Under these conditions increases in the pseudo first order rate constant (k_{obs}) with increasing buffer concentration are indicative of buffer catalysis.

Reaction data and the experimental first order rate constants (k_{obs}^T, s^{-1}), due to both exchange and elimination are shown below in Tables 2.1-2.4. Table 2.1 shows data for the disappearance of the C1-H singlets at 3.91 ppm and 4.79 ppm (due to the CH$_2$OSO$_3^-$ group of the keto and hydrate forms of DHAS respectively) in quinuclidinone buffer 90 % f_B, pD 9.21, at 25 °C (I = 1.0, KCl). The values of k_{obs}^T (s^{-1}) shown in Table 2.1 were obtained from the slopes of the semi-logarithmic plots (Figure 2.5) of the fraction of substrate remaining, f(s), against time.

Table 2.1: First order rate constants for the disappearance of the C1 protons of DHAS (27) in quinuclidinone buffers 90% f_B in D_2O at 25 °C (I=1.0, KCl).

[Buffer] (M)	[DO⁻][a] (M)	Time (s)	$f(s)$[b]	Ln $f(s)$	k_{obs}[c] (s⁻¹)
		0	1	0	
		150	0.863	-0.143	
0.060	2.91 x 10⁻⁶	390	0.652	-0.432	8.74 x 10⁻⁴
	(pD 9.21)	660	0.564	-0.571	
		840	0.481	-0.733	
		1020	0.393	-0.933	
		0	1	0	
		510	0.587	-0.543	
0.080	3.35 x 10⁻⁶	900	0.426	-0.862	9.74 x 10⁻⁴
	(pD 9.27)	1230	0.331	-1.091	
		1590	0.204	-1.571	
		1740	0.174	-1.743	
		0	1	0	
		360	0.594	-0.513	
		720	0.363	-1.012	
0.100	4.03 x 10⁻⁶	1080	0.233	-1.441	1.24 x 10⁻³
	(pD 9.35)	1410	0.161	-1.823	

(a) Measurements were made in quinuclidinone buffers, 90 % f_B (60, 80, 100 mM, total buffer concentration) in the

pD 9.21– 9.35 range. [DO⁻] was calculated using [DO⁻] = $(10^{pD-pK_w})/\gamma_{OD}$ with pK_w = 14.87, where γ_{OD} = 0.75 is the

activity coefficient of deuteroxide ion under our experimental conditions. (b) The fraction of substrate remaining

f(s), was calculated according to Equation 2.2. Measurements were made at an initial substrate concentration of 10

mM. (c) The value of the first-order rate constant (k_{obs}^{T}) was obtained from the slope of the plot of ln f(s) against

time.

Figure 2.5: Semi-logarithmic plot of the fraction of remaining C1 hydrogens against time

for the reaction of DHAS (27) in quinuclidinone buffer 90% f_B, at 25 °C (I =

1.0 ,KCl) (● 60 mM, ■ 80 mM, ▲100mM).

Time (sec)

Figure 2.6: **Effect of the concentration of quinuclidinone on the first order rate constants for both exchange and elimination at pD 9.21, I =1.0 (KCl).**

The second order rate constant for buffer catalysis k_B ($M^{-1}s^{-1}$) is determined as 1.07×10^{-2} $M^{-1}s^{-1}$ from the slope of the plot of pseudo first order rate constants, k_{obs}^T, against the concentration of basic buffer form of quinuclidinone (Figure 2.6). The level of buffer catalysis observed is relatively small. A 1.67-fold increase in the total buffer concentration leads only to a 42 % increase in the observed first order rate constant, k_{obs}^T (s^{-1}). The y-axis intercept of the plot shown above is the value of k_{int}^T for the buffer independent reaction of DHAS (**27**). The y-axis intercept is obtained as $k_{int}^T = 2.97 \times 10^{-4}$ s^{-1} at pD 9.2. The intercept potentially has contributions from both pH-independent and DO^- catalyzed exchange and elimination as described by Equation 2.7.

$$k_{int}^T = k_0 + k_{DO}[DO^-]$$ **Equation 2.7**

Table 2.2 shows the data for the disappearance of the C1-H singlets at 3.91 ppm and 4.79 ppm in quinuclidinone buffer 80 % f_B, pD 8.90, at 25 °C (I =1.0, KCl). The values of k_{obs}^T (s^{-1}) shown in Table 2.2 were obtained from the slopes of the semi-logarithmic plots (Figure 2.7) of the fraction of substrate remaining, f(s), against time.

Table 2.2: **First order rate constants for disappearance of the C1 protons of DHAS (27) in quinuclidinone buffers 80% f_B in D$_2$O at 25 °C (I=1.0, KCl).**

[Buffer] (M)	[DO$^-$]^a (M)	Time (s)	f(s)^b	Ln f(s)	$k_{obs}^{T\,c}$ (s^{-1})
		0	1	0	
		900	0.614	-0.487	
		1560	0.456	-0.783	
0.040	1.42 x 10^{-6}	2280	0.335	-1.093	4.77 x 10^{-4}
	(pD 8.90)	2640	0.272	-1.301	
		3000	0.232	-1.457	
		3330	0.204	-1.586	
		0	1	0	
		510	0.781	-0.246	
0.060	1.68 x 10^{-6}	900	0.579	-0.545	6.12 x 10^{-4}
	(pD 8.97)	1590	0.398	-0.921	
		2280	0.249	-1.389	

124

		0	I	0	
		900	0.527	-0.638	
		1260	0.392	-0.935	
0.080	1.88×10^{-6}	1620	0.333	-1.098	7.22×10^{-4}
	(pD 9.02)	1920	0.233	-1.456	
		2340	0.188	-1.667	

(a) Measurements were made in quinuclidinone buffers, 80 % f_B (40, 60, 80 mM, total buffer concentration) in the pD 8.90– 9.02 range. [DO⁻] was calculated using $[DO^-] = (10^{pD-pKw})/\gamma_{OD}$ with $pK_w = 14.87$, where $\gamma_{OD} = 0.75$ is the activity coefficient of deuteroxide ion under our experimental conditions. (b) The fraction of substrate remaining $f(s)$, was calculated according to Equation 2.2. Measurements were made at an initial substrate concentration of 10 mM. (c) The value of the first-order rate constant (k_{obs}^T) was obtained from the slope of the plot of ln $f(s)$ against time.

Figure 2.7: Semi-logarithmic plot of the fraction of remaining C1 protons against time for the reaction of DHAS (27) in quinuclidinone buffer 80% f_B, at 25 °C (I = 1.0, KCl) (● 40 mM, ■ 60 mM, ▲ 80 mM).

Figure 2.8: Effect of the concentration of quinuclidinone on the first order rate constants for both exchange and elimination at pD 8.9, I =1.0 (KCl).

The second order rate constant for buffer catalysis k_B ($M^{-1}s^{-1}$) is determined as 8.06×10^{-3} $M^{-1}s^{-1}$ from the slope of the plot of pseudo first order rate constants, k_{obs}^T, against the concentration of basic buffer form of quinuclidinone (Figure 2.8). A 2-fold increase in the total buffer concentration leads only to a 51 % increase in the observed first order rate constant, k_{obs}^T (s^{-1}). The y-axis intercept of the plot shown above is the value of k_{int}^T for the buffer independent reaction of DHAS (27). The y-axis intercept is obtained as $k_{int}^T = 2.36 \times 10^{-4}$ s^{-1} at pD 8.9.

Table 2.3 shows the data for the disappearance of the C1-H singlets at 3.91 ppm and 4.79 ppm (due to the $CH_2OSO_3^-$ group of the keto and hydrate forms of DHAS respectively) in quinuclidinone buffer 70 % f_B, pD 8.52, at 25 °C (I =1.0, KCl). The values of k_{obs}^T (s^{-1}) shown in

Table 2.3 were obtained from the slopes of the semi-logarithmic plots (Figure 2.9) of the fraction

of substrate remaining, $f(s)$, against time.

Table 2.3: **First order rate constants for the disappearance of the C1 protons of DHAS**
(27) in quinuclidinone buffers 70% f_B in D_2O at 25 °C (I=1.0, KCl).

[Buffer] (M)	[DO⁻]ᵃ (M)	Time (s)	$f(s)$ᵇ	Ln $f(s)$	k_{obs}ᵀ ᶜ (s⁻¹)
		0	1	0	
		480	0.800	-0.222	
		840	0.672	-0.396	
0.040	6.38 x 10⁻⁷	1170	0.628	-0.465	3.87 x 10⁻⁴
	(pD 8.52)	1350	0.586	-0.534	
		1530	0.544	-0.608	
		0	1	0	
		540	0.785	-0.277	
		1230	0.585	-0.500	
		1920	0.368	-0.999	
0.080	7.33 x 10⁻⁷	2640	0.274	-1.451	6.05 x 10⁻⁴
	(pD 8.61)	3300	0.143	-1.941	
		3990	0.694	-2.361	
		4680	0.664	-2.745	

		0	1	0	
		840	0.589	-0.529	
		1200	0.376	-0.886	
0.100	1.13×10^{-7}	1590	0.258	-1.010	6.44×10^{-4}
	(pD 8.69)	1920	0.216	-1.330	
		2220	0.177	-1.410	
		3630	0.063	-2.441	
		5010	0.041	-3.200	

(a) Measurements were made in quinuclidinone buffers, 70 % f_B (40, 80, 100 mM, total buffer concentration) in the pD 8.52– 8.69 range. [DO⁻] was calculated using [DO⁻] = $(10^{pD-pK_w})/\gamma_{OD}$ with pK_w = 14.87, where γ_{OD} = 0.75 is the activity coefficient of deuteroxide ion under our experimental conditions. (b) The fraction of substrate remaining $f(s)$, was calculated according to Equation 2.2. Measurements were made at an initial substrate concentration of 10 mM. (c) The value of the first-order rate constant (k_{obs}^T) was obtained from the slope of the plot of ln $f(s)$ against time.

Figure 2.9: Semi-logarithmic plot of the fraction of remaining C1 hydrogens against time for the reaction of DHAS (27) in quinuclidinone buffers 70% f_B, at 25 °C (I = 1.0, KCl) (● 40 mM, ■ 80 mM, ▲ 100mM).
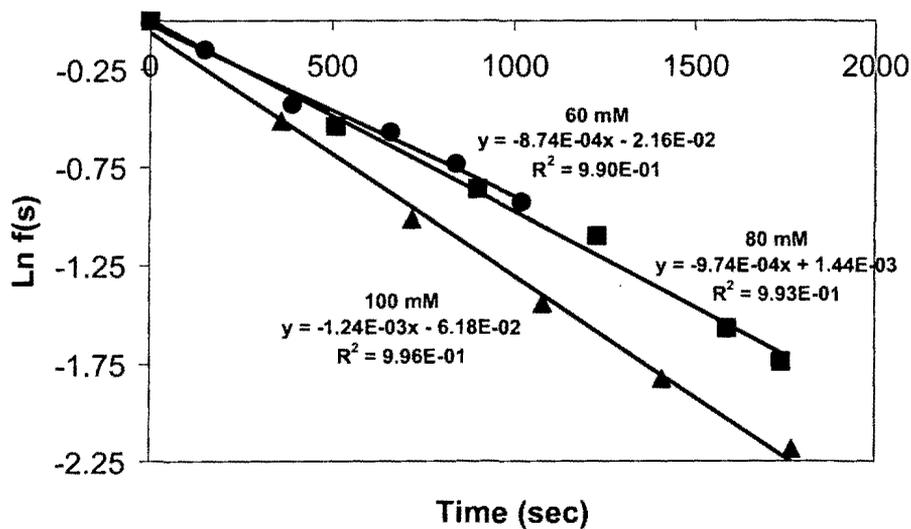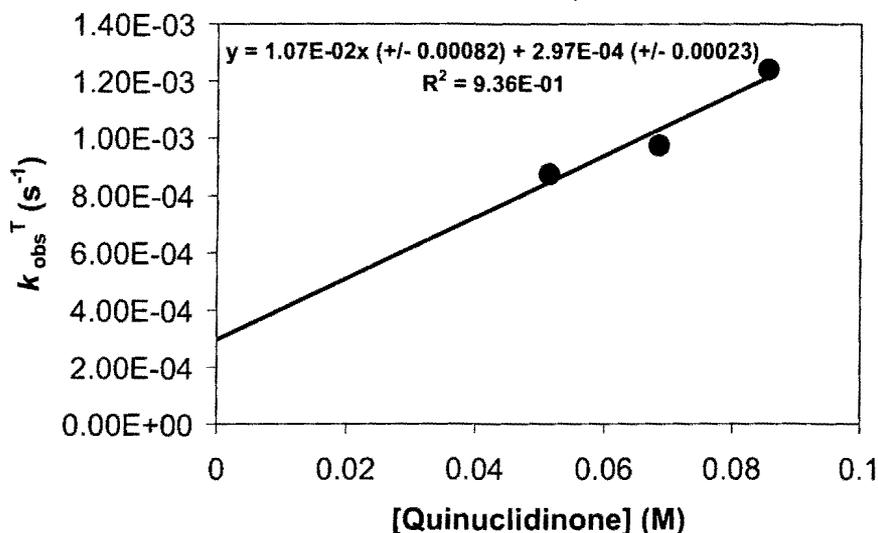

Figure 2.10: Effect of the concentration of quinuclidinone on the first order rate constants for both exchange and elimination at pD 8.5, I =1.0 (KCl).

The second order rate constant for buffer catalysis k_B ($M^{-1}s^{-1}$) is determined as 6.69×10^{-3} $M^{-1}s^{-1}$ from the slope of the plot of pseudo first order rate constants, k_{obs}^{T}, against the concentration of basic buffer form of quinuclidinone (Figure 2.10). A 2.5-fold increase in the total buffer concentration leads to a 66 % increase in the observed first order rate constant, k_{obs}^{T} (s^{-1}). The y-axis intercept of the plot shown above is the value of k_{int}^{T} for the buffer independent reaction of DHAS (27). The y-axis intercept is obtained as $k_{int}^{T} = 2.19 \times 10^{-4}$ s^{-1} at pD 8.52.

Table 2.4 shows the data for the disappearance of the C1-H singlets at 3.91 ppm and 4.79 ppm (due to the $CH_2OSO_3^{-}$ group of the keto and hydrate froms of DHAS respectively) in phosphate buffer 70 % f_B, pD 7.45, at 25 °C (I =1.0, KCl). The values of k_{obs}^{T} (s^{-1}) shown in Table 2.4 were obtained from the slopes of the semi-logarithmic plots (Figure 2.11) of the fraction of substrate remaining, $f(s)$, against time.

Table 2.4: **First order rate constants for the disappearance of the C1 hydrogens of DHAS (27) in phosphate buffers 70% f_B in D_2O at 25 °C (I=1.0 KCl).**

[Buffer] (M)	[DO⁻]ᵃ (M)	Time (s)	$f(s)$ᵇ	Ln $f(s)$	$k_{obs}^{T\,c}$ (s^{-1})
		0	1	0	
		7200	0.732	-0.304	
0.060	3.67×10^{-8}	13440	0.669	-0.400	3.62×10^{-5}

	(pD 7.31)	19680	0.534	-0.627	
		25920	0.341	-1.074	
		36720	0.276	-1.286	
		0	1	0	
		1320	0.931	-0.071	
0.080	4.21×10^{-8}	10020	0.692	-0.360	4.37×10^{-5}
	(pD 7.37)	17700	0.486	-0.719	
		26040	0.311	-1.167	
		0	1	0	
		540	0.946	-0.057	
		1260	0.928	-0.072	
0.100	5.06×10^{-8}	2640	0.874	-0.134	5.11×10^{-5}
	(pD 7.45)	4350	0.811	-0.209	
		6420	0.721	-0.327	
		7980	0.649	-0.432	

(a) Measurements were made in phosphate buffers, 70 % f_B (60, 80, 100 mM, total buffer concentration) in the pD 7.31– 7.45 range. [DO⁻] was calculated using $[DO^-] = (10^{pD-pK_w})/\gamma_{OD}$ with $pK_w = 14.87$, where $\gamma_{OD} = 0.75$ is the activity coefficient of deuteroxide ion under our experimental conditions. (b) The fraction of substrate remaining $f(s)$, was calculated according to Equation 2.2. Measurements were made at an initial substrate concentration of 10 mM. (c) The value of the first-order rate constant (k_{obs}^T) was obtained from the slope of the plot of $\ln f(s)$ against time.

Figure 2.11: Semi-logarithmic plot of the fraction of remaining C1 hydrogens against time for the reaction of DHAS (27) in phosphate 70% f_B, I = 1.0 (KCl) at 25 °C (● 60 mM, ■ 80 mM, ▲ 100 mM).

100 mM
y = -5.11E-05x - 6.61E-03
R^2 = 9.91E-01

60 mM
y = -3.62E-05x + 6.36E-03
R^2 = 9.69E-01

80 mM
y = -4.37E-05x + 1.51E-02
R^2 = 9.93E-01

Ln f(s)

Time (sec)

Figure 2.12: Effect of the concentration of phosphate on the first order rate constants for both exchange and elimination at pD 7.31, I =1.0 (KCl).

y = 5.60E-04x (+/- 4.20E-05)+ 1.39E-05 (+/- 3.48E-06)
R^2 = 1.00E+00

$k_{obs}^T (s^{-1})$

$[DPO_4^{2-}]$ (M)

132

The second order rate constant for buffer catalysis k_B ($M^{-1}s^{-1}$) is determined as $5.60 \times 10^{-4}\ M^{-1}s^{-1}$ from the slope of the plot of pseudo first order rate constants, k_{obs}^T, against the concentration of basic buffer form of phosphate (Figure 2.12). A 1.67-fold increase in the total buffer concentration leads only to a 41 % increase in the observed first order rate constant, k_{obs}^T (s^{-1}). The y-axis intercept of the plot shown above is the value of k_{int}^T for the buffer independent reaction of DHAS (27). The y-axis intercept is obtained as $k_{int}^T = 1.39 \times 10^{-5}\ s^{-1}$ at pD 7.31.

As mentioned previously, the C3 protons of DHAS (keto and hydrate forms) decrease over time due to elimination only. Competing C3-H/D exchange or isomerisation reactions are not observed by ^{1}H NMR spectroscopy over time. Reaction data and the experimental first order rate constants for elimination (k_{obs}^E, s^{-1}) for disappearance of the C3 hydrogens of DHAS due to an elimination reaction are shown below in Tables 2.5-2.7. Table 2.5 show the data for the elimination in quinuclidinone buffers, 90 % f_B at 25 °C (I= 1.0 KCl). The values of k_{obs}^E (s^{-1}) shown in Table 2.5 were obtained from the slopes of the semi-logarithmic plots (Figure 2.13) of the fraction of substrate remaining, $f(s)'$, against time.

Table 2.5: First order rate constants for disappearance of the C3 hydrogens of DHAS (27) in quinuclidinone buffers 90% f_B in D_2O at 25 °C (I =1.0, KCl)

[Buffer] (M)	[DO⁻]ᵃ (M)	Time (s)	$f(s)$[,b]	Ln $f(s)$'	k_{obs}[E,c] (s⁻¹)
		0	1	0	
		150	0.947	-0.053	
		390	0.900	-0.104	
0.060	2.91 x 10⁻⁶	660	0.851	-0.161	2.74 x 10⁻⁴
	(pD 9.21)	840	0.789	-0.236	
		1020	0.748	-0.290	
		0	1	0	
		510	0.845	-0.167	
0.080	3.35 x 10⁻⁶	900	0.744	-0.294	3.01 x 10⁻⁴
	(pD 9.27)	1230	0.706	-0.347	
		1590	0.617	-0.483	
		1740	0.588	-0.539	
		0	1	0	
		360	0.866	-0.144	
		720	0.733	-0.310	
0.100	4.03 x 10⁻⁶	1080	0.631	-0.461	3.88 x 10⁻⁴
	(pD 9.35)	1410	0.557	-0.584	

(a) Measurements were made in quinuclidinone buffers, 90 % f_B (60, 80, 100 mM, total buffer concentration) in the pD 9.21– 9.35 range. [DO⁻] was calculated using [DO⁻] = $(10^{pD-pK_w})/\gamma_{OD}$ with pK_w = 14.87, where γ_{OD} = 0.75 is the activity coefficient of deuteroxide ion under our experimental conditions. (b) The fraction of substrate remaining $f(s)'$, was calculated according to Equation 2.3. Measurements were made at an initial substrate concentration of 10 mM. (c) The value of the first-order rate constant (k_{obs}^E) was obtained from the slope of the plot of $\ln f(s)'$ against time.

Figure 2.13: **Semi-logarithmic plot of the fraction of remaining C3 hydrogens against time for the reaction of DHAS (27) in quinucldinone buffers 90% f_B, in D_2O at 25 °C (I = 1.0, KCl) (● 60 mM, ■ 80 mM, ▲ 100 mM).**

Time (sec)

Figure 2.14: Effect of the concentration of quinuclidinone on the first order rate constants for elimination at pD 9.2, I =1.0 (KCl).

The second order rate constant for buffer catalysis k_B ($M^{-1}s^{-1}$) is determined as 3.33×10^{-3} $M^{-1}s^{-1}$ from the slope of the plot of pseudo first order rate constants, k_{obs}^E, against the concentration of basic buffer form of quinuclidinone (Figure 2.14). A 1.67-fold increase in the total buffer concentration leads only to a 42 % increase in the observed first order rate constant, k_{obs}^E (s^{-1}). The y-axis intercept of the plot shown above is the value of k_{int}^E for the buffer independent reaction of DHAS (27). The y-axis intercept is obtained as $k_{int}^E = 9.30 \times 10^{-5}$ s^{-1} at pD 9.2.

Table 2.6 show the data for the elimination in quinuclidinone buffers, 80 % f_B at 25 °C (I= 1.0 KCl). The values of k_{obs}^E (s^{-1}) shown in Table 2.1 were obtained from the slopes of the semi-logarithmic plots (Figure 2.15) of the fraction of substrate remaining, $f(s)$', against time.

Table 2.6: First order rate constants for disappearance of the C3 hydrogens of DHAS (27) in quinuclidinone buffers 80% f_B in D_2O at 25 °C (I=1.0, KCl).

[Buffer] (M)	[DO$^-$]^a (M)	Time (s)	$f(s)$'^{b}	Ln $f(s)$'	k_{obs}^{Ec} (s^{-1})
		0	1	0	
		900	0.862	-0.148	
		1560	0.750	-0.287	
0.040	1.47 x 10^{-6}	2280	0.671	-0.398	1.82 x 10^{-4}
	(pD 8.90)	2640	0.595	-0.518	
		3000	0.577	-0.550	
		3330	0.560	-0.579	
		0	1	0	
		510	0.898	-0.167	
0.060	1.68 x 10^{-6}	900	0.826	-0.190	2.05 x 10^{-4}
	(pD 8.97)	1590	0.739	-0.301	
		2280	0.602	-0.506	
		2910	0.525	-0.643	
		3540	0.484	-0.725	
		0	1	0	
		900	0.815	-0.203	
		1260	0.706	-0.347	
0.080	1.88 x 10^{-6}	1620	0.600	-0.510	2.50 x 10^{-4}

(pD 9.02)	1920	0.574	-0.554
	2340	0.562	-0.576
	3000	0.469	-0.736
	3660	0.390	-0.941
	5100	0.274	-1.293

(a) Measurements were made in quinuclidinone buffers, 80 % f_B (40, 60, 80 mM, total buffer concentration) in the pD 8.90– 9.02 range. [DO⁻] was calculated using [DO⁻] = $(10^{pD-pKw})/\gamma_{OD}$ with pK_w = 14.87, where γ_{OD} = 0.75 is the activity coefficient of deuteroxide ion under our experimental conditions. (b) The fraction of substrate remaining $f(s)'$, was calculated according to Equation 2.3. Measurements were made at an initial substrate concentration of 10 mM. (c) The value of the first-order rate constant (k_{obs}^{E}) was obtained from the slope of the plot of $\ln f(s)'$ against time.

Figure 2.15: **Semi-logarithmic plot of the fraction of remaining C3 hydrogens against time for the reaction of DHAS (27) in quinuclidinone 80% f_B, in D_2O at 25 °C (I = 1.0, KCl) (● 40 mM, ■ 60 mM, ▲ 80 mM).**

40 mM
y = -1.82E-04x + 3.06E-03
R2 = 9.90E-01

60 mM
y = -2.05E-04x + 3.00E-03
R^2 = 9.93E-01

80 mM
y = -2.50E-04x - 2.41E-02
R^2 = 9.89E-01

Time (sec)

Figure 2.16: **Effect of the concentration of quinuclidinone on the first order rate constants for elimination at pD 8.9, I =1.0 (KCl).**

The second order rate constant for buffer catalysis k_B ($M^{-1}s^{-1}$) is determined as 2.24×10^{-3} $M^{-1}s^{-1}$ from the slope of the plot of pseudo first order rate constants, k_{obs}^E, against the concentration of basic buffer form of quinuclidinone (Figure 2.16). A 2-fold increase in the total buffer concentration leads only to a 37 % increase in the observed first order rate constant, k_{obs}^E (s^{-1}). The y-axis intercept of the plot shown above is the value of k_{int}^E for the buffer independent reaction of DHAS **(27)**. The y-axis intercept is obtained as $k_{int}^E = 1.10 \times 10^{-4}$ s^{-1} at pD 8.9.

Table 2.7 show the data for the elimination in quinuclidinone buffers, 70 % f_B at 25 °C (I= 1.0 KCl). The values of k_{obs}^E (s^{-1}) shown in Table 2.7 were obtained from the slopes of the semi-logarithmic plots (Figure 2.17) of the fraction of substrate remaining, $f(s)$', against time.

Table 2.7: First order rate constants for disappearance of the C3 hydrogens of DHAS (27) in quinuclidinone buffers 70% f_B in D_2O at 25 °C (I=1.0, KCl).

[Buffer] (M)	[DO⁻][a] (M)	Time (s)	$f(s)$'[b]	Ln $f(s)$'	k_{obs}[Ec] (s⁻¹)
		0	1	0	
		480	0.862	-0.050	
		840	0.750	-0.110	
0.040	1.32 x 10⁻⁶	1170	0.671	-0.167	1.36 x 10⁻⁴
	(pD 8.52)	1530	0.595	-0.197	
		0	1	0	
		540	0.944	-0.056	
0.080	8.70 x 10⁻⁷	1230	0.847	-0.165	1.66 x 10⁻⁴
	(pD 8.61)	1920	0.762	-0.271	
		2640	0.660	-0.415	
		3300	0.591	-0.525	
		3990	0.546	-0.623	
		4680	0.465	-0.765	
		0	1	0	
		840	0.838	-0.176	
		1200	0.807	-0.289	
0.100	8.88 x 10⁻⁷	1590	0.693	-0.365	1.94 x 10⁻⁴

(pD 8.69)	1920	0.711	-0.339
	2220	0.666	-0.406
	3630	0.478	-0.736
	5010	0.374	-0.982
	6360	0.287	-1.246

(a) Measurements were made in quinuclidinone buffers, 70 % f_B (40, 80, 100 mM, total buffer concentration) in the

pD 8.52– 8.69 range. [DO⁻] was calculated using [DO⁻] = $(10^{pD-pKw})/\gamma_{OD}$ with pK_w = 14.87, where γ_{OD} = 0.75 is the

activity coefficient of deuteroxide ion under our experimental conditions. (b) The fraction of substrate remaining

$f(s)'$, was calculated according to Equation 2.3. Measurements were made at an initial substrate concentration of 10

mM. (c)The value of the first-order rate constant (k_{obs}^E) was obtained from the slope of the plot of ln $f(s)'$ against

time.

Figure 2.17: **Semi-logarithmic plot of the fraction of remaining C3 hydrogens against time**

for the reaction of DHAS (27) in quinuclidinone 70% f_B, in D_2O at 25 °C (I =

1.0, KCl) (● 40 mM, ■ 80 mM, ▲100 mM).

Figure 2.18: Effect of the concentration of quinuclidinone on the first order rate constants for elimination at pD 8.5, I =1.0 (KCl).

The graph plots k_{obs}^E (s^{-1}) on the y-axis against [Quinuclidinone] (M) on the x-axis with the fitted line:

$$y = 1.41E\text{-}03x\ (+/-\ 1.06E\text{-}04) + 9.67E\text{-}05\ (+/-\ 2.42E\text{-}06)$$
$$R^2 = 9.71E\text{-}01$$

The second order rate constant for buffer catalysis k_B $(M^{-1}s^{-1})$ is determined as $1.41 \times 10^{-3}\ M^{-1}s^{-1}$ from the slope of the plot of pseudo first order rate constants, k_{obs}^E, against the concentration of basic buffer form of quinuclidinone (Figure 2.18). A 2.5-fold increase in the total buffer concentration leads only to a 43 % increase in the observed first order rate constant, k_{obs}^E (s^{-1}). The y-axis intercept of the plot shown above is the value of k_{int}^E for the buffer independent reaction of DHAS (**27**). The y-axis intercept is obtained as $k_{int}^E = 9.67 \times 10^{-5}\ s^{-1}$ at pD 8.69.

For all of the above reactions the pD values were checked at the end of each reaction. It was found that these values remained unchanged. Further attempts to monitor the reactions at the C-1 and C-3 positions of DHAS (**27**) were made using acetic acid (100 mM, 90 % f_B), quinuclidinol (100 mM, 50 % f_B) and quinuclidine buffers (100 mM, 10 % f_B). It was found that the reactions

142

in acetic acid buffers were too slow to monitor conveniently. Conversely the reactions carried out in quinuclidinol and quinuclidine were much too fast to monitor by ^{1}H NMR and thus accurate kinetic data was not obtained under these conditions.

Shown below in Table 2.8 is the combined rate data obtained for DHAS (27). Also shown are the second order rate constants, k_B for buffer catalysis at each pD. No elimination of DHAS was detected in phosphate buffers at the pDs analyzed. The value of k_{int}^{Ex} was obtained by subtracting k_{obs}^E from k_{obs}^T at the relevant pD.

Table 2.8 Combined rate data for the exchange and elimination reactions of DHAS (27).

pD	k_{obs}^T (s^{-1})	k_{obs}^E (s^{-1})	k_{int}^T (s^{-1})	k_{int}^E (k_{int}^{Ex}) (s^{-1})	k_B^T (M^{-1}s^{-1})	k_B^E k_B^{Ex} (M^{-1}s^{-1})
7.31	3.62 x 10^{-5}	n/e		-		-
7.37	4.37 x 10^{-5}	n/e	(1.39 x 10^{-5})	(1.39 x 10^{-5})	5.60 x 10^{-4}	(5.60 x 10^{-4})
7.45	5.11 x 10^{-5}	n/e				
8.52	3.87 x 10^{-4}	1.36 x 10^{-4}		9.67 x 10^{-5}		1.41 x 10^{-3}
8.61	6.05 x 10^{-4}	1.66 x 10^{-4}	(2.19 x 10^{-4})	(1.22 x 10^{-4})	6.69 x 10^{-3}	(5.28 x 10^{-3})

8.69	6.44×10^{-4}	1.94×10^{-4}				
8.90	4.77×10^{-4}	1.82×10^{-4}				
				1.10×10^{-4}		2.24×10^{-3}
8.97	6.12×10^{-4}	2.05×10^{-4}	(2.36×10^{-4})	(1.26×10^{-4})	8.06×10^{-3}	(5.82×10^{-3})
9.02	7.22×10^{-4}	2.50×10^{-4}				
9.21	8.74×10^{-4}	2.74×10^{-4}				
				9.30×10^{-5}		3.33×10^{-3}
9.27	9.74×10^{-4}	3.01×10^{-4}	(2.97×10^{-4})	(2.04×10^{-4})	1.07×10^{-2}	(7.37×10^{-3})
9.35	1.24×10^{-3}	3.88×10^{-4}				

The observed amount of buffer catalysis as indicated by the magnitude of the k_B values, although small, increases with increasing pD. This is consistent with general base catalysis and the absence of general acid catalysis. The pD rate profiles for the elimination and exchange reactions of DHAS (27) are shown below in Figure 2.19. From the values obtained for the k_{int}^E and k_{int}^{Ex} the reactions appear to be pD independent in the 8.5-9.2 range with a decrease in rate occurring at pD ~8. This data will be discussed further in Chapter 3.

Figure 2.19: pD rate profiles for the elimination reactions and exchange reactions of DHAS (27).

$\Delta = k_{int}^E$

$o = k_{int}^{Ex}$

2.2.2 Dihydroxyacetone thiosulfate (DHATS)

The solution non-enzyme catalyzed reactions of DHATS **(25)** were monitored by 400 and 500 MHz ^{1}H NMR spectroscopy. Typical pK_a values for alkyl thiosulfates are in the 1-2 range. It was observed that the C1-H/D exchange reactions of this substrate were too fast to monitor by ^{1}H NMR in buffered D_2O solutions of pD > 5. Therefore kinetic measurements of the exchange at the C-1 position of the molecule were made in acetic acid buffers (pD 3-5) and DCl solutions (1-12 mM). At the lower pD values the thiosulfate anion is likely protonated.

A representative partial ^{1}H NMR spectrum of DHATS (10 mM) **(25)** is shown below in Figure 2.20. The zero reaction time spectrum of DHATS was recorded in DCl (1M) and 25 °C (I =1.0). Also present is imidazole (5 mM) as an internal standard.

145

Figure 2.20: Representative ^{1}H NMR spectra at 500 MHz of DHATS (25) (10 mM, pD 1.4), obtained at zero reaction time in DCl at 25 °C (I = 1.0). Methanol (5mM) is present as internal standard.

As with DHAS (27), in buffered D_2O solutions the carbonyl group of DHATS (25') is hydrated although only to a small extent (Scheme 2.16).

Scheme 2.16

The equilibrium constant, K_{hyd}, can be represented by Equation 2.8

$$K_{hyd} = [25'h]/[25]$$ **Equation 2.8**

146

In the NMR spectrum above the singlet at 3.31 ppm corresponds to the methyl hydrogens of methanol internal standard. The singlets **A** and **B**, which are observed at 4.45 and 3.99 ppm integrate 1:1 with respect to each other. These peaks are due to the C-3 and C-1 protons of the keto form of DHATS (**25'**). The two small upfield peaks at 3.6 and 3.4 ppm, **C** and **D**, which also integrate 1:1 with respect to each other correspond to the C-3 and C-1 hydrate peaks of DHATS (**25'h**). The ratio of the sum of the areas of the two singlets (**C** and **D**) to that of singlets, **A** and **B**, yields a value of $K_{hyd} = 0.05$ in 1M DCl. Further assignment of each of the peaks was attempted by cross-correlation NMR experiments but the same problems were encountered as previously mentioned for DHAS (**27**). Therefore assignment of the singlets to either C1 or C3 hydrogens was based upon the mode of reactivity.

The reactions of DHATS (10mM) were monitored in acetic acid buffers (60-100 mM, 5-20 % f_B, pD 3.88-4.53), phosphate buffers (60-100 mM, 70 % f_B, pD 7.35-7.65), quinuclidinone buffers (60-100 mM, 90 % f_B pD 9.23) and DCl solutions (1-12 mM, pD) at 25 °C (I =1.0, KCl). The reactions were initiated on the addition of buffer or DCl solution to solid substrate.

Shown below (Figure 2.21) are representative partial ^{1}H NMR spectra of the remaining substrate and products during the reaction of DHATS (10 mM) in acetic acid buffer (100 mM, 20 % f_B, pD 4.51).

Figure 2.21: Representative ^{1}H NMR spectra at 500 MHz of DHATS (25) (10 mM, pD 4.51), obtained during the reaction in acetic acid buffer 20 % f_B 100 mM (pD 4.51) in D$_2$O at 25 °C (I = 1.0, KCl). The timepoint is indicated above each spectrum in minutes.

Each NMR spectrum was recorded over a period of 5 minutes (16 transients) with the reaction time t calculated from the time at the midpoint of these analyses. The changes in the ^{1}H NMR spectra over time relative to the time zero spectrum in 1M DCl are indicative of the pathways by which DHATS (25) at this pD. The effect of a change in pD from 1 M DCl to acetic acid buffer has no effect within experimental error on the extent of hydration of DHATS (25).Over time, a decrease in the singlet at 3.98 ppm, **B**, is accompanied by the simultaneous appearance of a small broad upfield triplet **E** ($^2J_{HD}$ = 2 Hz), at 3.96 ppm. This triplet is assigned to the CHDSSO$_3^-$ group of the keto form of DHATS labelled with deuterium at the C-1 position (25a) (Scheme 2.17).

148

Scheme 2.17

(25)   (25a)   (25b)

Like the reaction of DHAS (**27**), deuterium incorporation at this position implies that peak **B** is due to the $CH_2SSO_3^-$ protons. Deuterium exchange would not be expected to compete with elimination on the CH_2OD side of DHATS (**25**) given the low basicity of the thiosulfate leaving group. Analogously, a decrease in the small singlet at 3.40 ppm **D**, due to the $CH_2SSO_3^-$ group of DHAS hydrate, is accompanied by an increase in a broad upfield singlet at 3.39 ppm **F**. This singlet is due to the $CHDOSO_3^-$ group of DHATS hydrate. For DHAS (**27**), reactions at the C-1 and C-3 positions of the molecule inducing exchange and elimination respectively occur at similar pD values. This is not the case for DHATS (**25**). It was found that in acetic acid buffers and DCl solutions, no reaction was observed at the C-3 position and no methylglyoxal formation was observed.

The progress of the exchange reaction at the C-1 position of DHATS (**25**) was monitored by comparing the integrated area of singlet **B** (due to the $CH_2SSO_3^-$ of DHATS keto form) to the integrated area of singlet **A** (due to the CH_2OD of DHATS keto form) over time. The area of singlet **A** remains constant relative to internal standard under these experimental conditions. The fraction of substrate remaining, $f(s)$, was determined from Equation 2.9.

$$f(s) = \frac{(A_{C1\text{-}CH2Keto})^t}{(A_{C3\text{-}CH2Keto})^t} \qquad \textbf{Equation 2.9}$$

As the area of the peaks due to the hydrate form were only ~ 5 % of those due to the keto form it was decided that inclusion of these small peak areas in an equation for $f(s)$ would introduce error into the measurements, thus the former areas were ommited.

The observed pseudo first order rate constants for the disappearance of substrate could be determined as the slope of the semi-logarithmic plot of $f(s)$ against time (Equation 2.10)

$$\ln f(s) = -k_{obs}t^{Ex}$$ **Equation 2.10**

These plots were linear for the half lives examined with 5-8 data points. The observed first order rate constant, k_{obs}^{Ex}, is the sum of the contributions of all the potential catalytic species to the rate of exchange as described by Equation 2.6 in Section 2.2.

To determine the contribution of the buffer to exchange at the C-1 position, reactions were run at a fixed pD and at constant buffer ratio while varying the total concentration of buffer. Thus the concentration of deuteroxide is fixed while the concentration of buffer base is varied. Increases in the pseudo first order rate constants (k_{obs}) with increasing buffer concentration are indicative of buffer catalysis. As was observed for DHAS (**27**), it is expected that the main form of buffer catalysis is general base and not general acid catalysis.

Reaction data and the experimental first order rate constants for the disappearance of the substrate due to exchange, k_{obs}^{Ex} (s^{-1}) are shown below in Tables 2.9-2.12. Table 2.9 shows the data for disappearance of the peak due to the C-1 hydrogens in acetic acid buffers, 20% f_B, at 25 °C (I =1.0, KCl). The values of k_{obs}^{Ex} (s^{-1}) shown in Table 2.9 were obtained from the slopes of the semi-logarithmic plots (Figure 2.22) of the fraction of substrate remaining, $f(s)$, against time.

150

Table 2.9: First order rate constants for the disappearance of the C1 protons of DHATS (25) in acetic acid buffers 20% f_B in D_2O at 25 °C (I=1.0, KCl).

[Buffer] (M)	$[DO^-]^a$ (M)	Time (s)	$f(s)^b$	Ln $f(s)$	$k_{obs}^{Ex\ c}$ (s^{-1})
		0	0.994	-0.005	
		270	0.793	-0.230	
		420	0.702	-0.353	
		570	0.555	-0.588	
0.060	4.31×10^{-11}	720	0.519	-0.654	8.96×10^{-4}
	(pD 4.38)	870	0.455	-0.788	
		1020	0.374	-0.983	
		1170	0.362	-1.015	
		0	0.994	-0.005	
		240	0.774	-0.255	
		390	0.623	-0.472	
		540	0.533	-0.627	
0.080	4.95×10^{-11}	690	0.459	-0.778	1.20×10^{-3}
	(pD 4.44)	840	0.364	-1.008	
		1020	0.318	-1.144	
		1170	0.242	-1.417	
		1320	0.203	-1.592	
		0	0.994	-0.005	

		420	0.691	-0.370	
		810	0.468	-0.759	
0.100	5.95×10^{-11}	1020	0.289	-1.239	1.25×10^{-3}
	(pD 4.52)	1200	0.254	-1.371	
		1380	0.197	-1.625	
		1560	0.145	-1.930	

(a) Measurements were made in acetic acid buffers, 20 % f_B (60, 80, 100 mM, total buffer concentration) in the pD 4.38-4.52 range. [DO⁻] was calculated using $[DO^-] = (10^{pD-pK_w})/\gamma_{OD}$ with $pK_w = 14.87$, where $\gamma_{OD} = 0.75$ is the activity coefficient of deuteroxide ion under our experimental conditions. (b) The fraction of unexchanged substrate remaining $f(s)$, was calculated according to Equation 2.9. Measurements were made at an initial substrate concentration of 10 mM. (c) The value of the first-order rate constant (k_{obs}^{Ex}) was obtained from the slope of the plot of $\ln f(s)$ against time.

Figure 2.22: Semi-logarithmic plot of the fraction of remaining C1-H against time for the reaction of DHATS (25) in acetic acid buffers 20% f_B, at 25 °C (I = 1.0, KCl) (● 60 mM, ■ 80 mM, ▲ 100 mM).

60 mM
y = -8.96E-04x - 1.03E-02
R^2 = 9.90E-01

80 mM
y = -1.20E-03x + 1.63E-02
R^2 = 9.96E-01

100 mM
y = -1.25E-03x + 9.70E-02
R^2 = 9.83E-01

Time (sec)

Figure 2.23: **Effect of the concentration of the acetate anion on the C1-H/D exchange reaction of DHATS (25) in acetic acid buffer 20 % f_B, I = 1.0 (KCl)**

The second order rate constant for buffer catalysis k_B ($M^{-1}s^{-1}$) is determined as 4.66×10^{-2} $M^{-1}s^{-1}$ from the slope of the plot of pseudo first order rate constants, k_{obs}^{Ex}, against the concentration of the acetate form of the buffer (Figure 2.23). A 1.67-fold increase in the total buffer concentration leads only to a 40 % increase in the observed first order rate constant, k_{obs}^{Ex} (s^{-1}). The y-axis intercept of the plot shown above is the value of k_{int}^{Ex} for the buffer independent reaction of DHATS (25). The y-axis intercept is obtained as $k_{int}^{Ex} = 4.07 \times 10^{-4}$ s^{-1} at pD 4.38.

Table 2.10 shows the data for disappearance of the peak due to the C-1 protons in acetic acid buffers, 10% f_B at 25 °C (I =1.0, KCl). The values of k_{obs}^{Ex} (s^{-1}) shown in Table 2.10 were obtained from the slopes of the semi-logarithmic plots (Figure 2.24) of the fraction of substrate remaining, f(s), against time.

Table 2.10: First order rate constants for the disappearance of the C1 protons of DHATS (25) in acetic acid buffers 10% f_B in D_2O at 25 °C (I=1.0 KCl).

[Buffer] (M)	[DO⁻]ᵃ (M)	Time (s)	$f(s)^b$	Ln $f(s)$	$k_{obs}^{Ex\ c}$ (s⁻¹)
		0	0.994	-0.005	
		480	0.867	-0.142	
		840	0.721	-0.321	
		1200	0.628	-0.464	
0.050	2.21 x 10⁻¹¹	1530	0.530	-0.634	4.05 x 10⁻⁴
	(pD 4.09)	2220	0.430	-0.843	
		2910	0.317	-1.145	
		3600	0.236	-1.442	
		4320	0.174	-1.745	
		0	0.994	-0.006	
		480	0.794	-0.230	
		960	0.631	-0.459	
		1320	0.510	-0.662	
0.065	2.59 x 10⁻¹¹	1680	0.420	-0.866	5.59 x 10⁻⁴
	(pD 4.16)	2040	0.351	-1.045	
		2400	0.277	-1.281	
		2760	0.221	-1.506	
		3120	0.187	-1.674	
		3480	0.140	-1.959	

		0	0.994	-0.004	
		480	0.761	-0.358	
		960	0.613	-0.590	
0.080	3.19×10^{-11}	1320	0.447	-0.853	5.98×10^{-4}
	(pD 4.25)	1680	0.363	-1.012	
		2040	0.286	-1.248	
		2400	0.226	-1.486	
		2760	0.182	-1.670	

(a) Measurements were made in acetic acid buffers, 10 % f_B (50-80 mM, total buffer concentration) in the pD 4.09-4.25 range. [DO⁻] was calculated using $[DO^-] = (10^{pD-pK_w})/\gamma_{OD}$ with $pK_w = 14.87$, where $\gamma_{OD} = 0.75$ is the activity coefficient of deuteroxide ion under our experimental conditions. (b) The fraction of unexchanged substrate remaining $f(s)$, was calculated according to Equation 2.9. Measurements were made at an initial substrate concentration of 10 mM. (c) The value of the first-order rate constant (k_{obs}^{Ex}) was obtained from the slope of the plot of $\ln f(s)$ against time.

Figure 2.24: Semi-logarithmic plot of the fraction of remaining C1-H against time for the reaction of DHATS (25) in acetic acid buffers 10% f_B, at 25 °C ($I = 1.0$ KCl) (● 50 mM, ■ 65 mM, ▲ 80 mM).

Plot with Y-axis "Ln f(s)" from 0 to -2, X-axis "Time (sec)" from 0 to 4000.

50 mM
y = -4.05E-04x + 1.68E-02
R^2 = 9.98E-01

80 mM
y = -5.98E-04x - 3.25E-02
R^2 = 9.98E-01
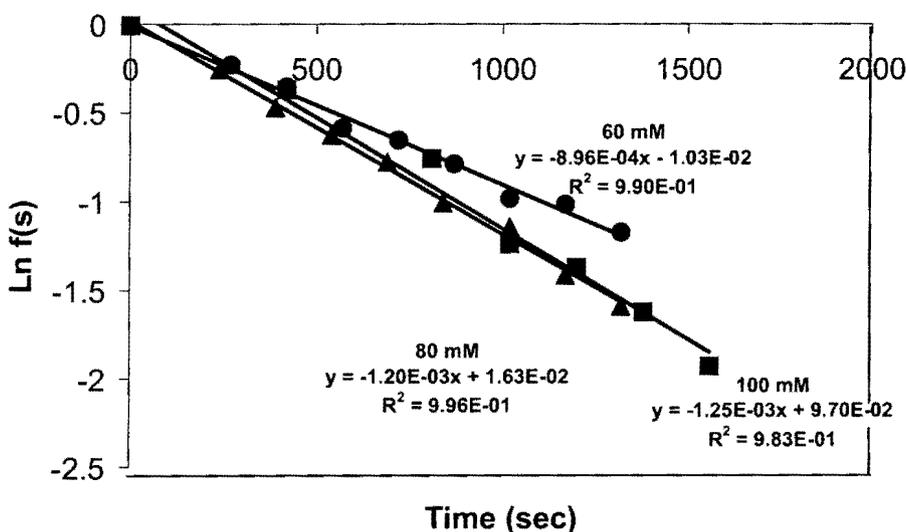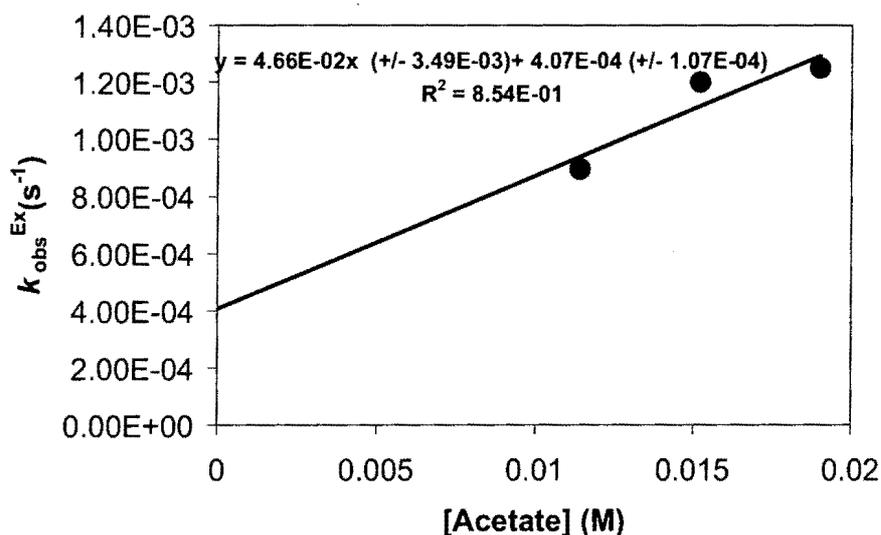
65 mM
y = -5.59E-04x + 3.34E-02
R^2 = 9.97E-01

Figure 2.25: Effect of the concentration of the acetate anion on the C1-H/D exchange reaction of DHATS (25) in acetic acid buffer 10 % f_B, $I = 1.0$ (KCl).

Plot with Y-axis "k_{obs}^{Ex} (s^{-1})" from 0.00E+00 to 7.00E-04, X-axis "[Acetate] (M)" from 0 to 0.008.

y = 6.77E-02x (+/- 5.07E-03) + 1.03E-04 (+/- 2.57E-05)
R^2 = 8.93E-01

The second order rate constant for buffer catalysis k_B ($M^{-1}s^{-1}$) is determined as 6.77 x 10^{-2} $M^{-1}s^{-1}$ from the slope of the plot of pseudo first order rate constants, k_{obs}^{Ex}, against the concentration of basic acetate form (Figure 2.25). A 1.6-fold increase in the total buffer concentration leads only to a 48 % increase in the observed first order rate constant, k_{obs}^{Ex} (s^{-1}). The y-axis intercept of the plot shown above is the value of k_{int}^{Ex} for the buffer independent reaction of DHATS (25). The y-axis intercept is obtained as k_{int}^{Ex} = 1.02 x 10^{-4} s^{-1} at pD 4.09.

Table 2.11 shows the data for disappearance of the peak due to the C-1 protons in acetic acid buffers, 5% f_B at 25 °C (I =1.0, KCl). The values of k_{obs}^{Ex} (s^{-1}) shown in Table 2.11 were obtained from the slopes of the semi-logarithmic plots (Figure 2.26) of the fraction of substrate remaining, $f(s)$, against time.

Table 2.11: **First order rate constants for the disappearance of the C1-H of DHATS (25) in acetic acid buffers 5% f_B in D_2O at 25 °C I=1.0 (KCl).**

[Buffer] (M)	[DO⁻][a] (M)	Time (s)	$f(s)$[b]	Ln $f(s)$	k_{obs}^{Ex}[c] (s^{-1})
		0	0.963	-0.036	
		660	0.847	-0.165	
		1380	0.764	-0.269	
		2070	0.642	-0.441	
0.060	1.01 x 10^{-11}	2760	0.577	-0.548	1.93 x 10^{-4}
	(pD 3.75)	3450	0.522	-0.649	

		4320	0.446	-0.806	
		5010	0.366	-1.002	
		5700	0.314	-1.158	
		6390	0.284	-1.256	
		0	0.938	-0.063	
		840	0.809	-0.211	
		1530	0.735	-0.307	
		2220	0.590	-0.527	
0.080	1.18×10^{-11}	2910	0.501	-0.689	2.25×10^{-4}
	(pD 3.82)	3600	0.433	-0.831	
		4290	0.365	-1.005	
		0	0.995	-0.004	
		2130	0.865	-0.389	
		3510	0.677	-0.917	
0.100	1.42×10^{-11}	4200	0.587	-1.160	2.61×10^{-4}
	(pD 3.90)	4890	0.399	-1.225	
		5580	0.313	-1.431	
		6270	0.293	-1.543	
		6960	0.238	-1.800	

(a) Measurements were made in acetic acid buffers, 5 % f_B (60-100 mM, total buffer concentration) in the pD 3.75-3.90 range. [DO⁻] was calculated using $[DO^-] = (10^{pD-pK_w})/\gamma_{OD}$ with $pK_w = 14.87$, where $\gamma_{OD} = 0.75$ is the activity coefficient of deuteroxide ion under our experimental conditions. (b) The fraction of unexchanged substrate remaining $f(s)$, was calculated according to Equation 2.9. Measurements were made at an initial substrate

158

concentration of 10 mM. (c) The value of the first-order rate constant ($k_{obs}{}^{Ex}$) was obtained from the slope of the plot of ln f(s) against time.

Figure 2.26: Semi-logarithmic plot of the fraction of remaining C1-H against time for the reaction of DHATS (25) in acetic acid buffer 5% f_B, at 25 °C (I = 1.0, KCl) (● 60 mM, ▪ 80 mM, ▲ 100 mM).
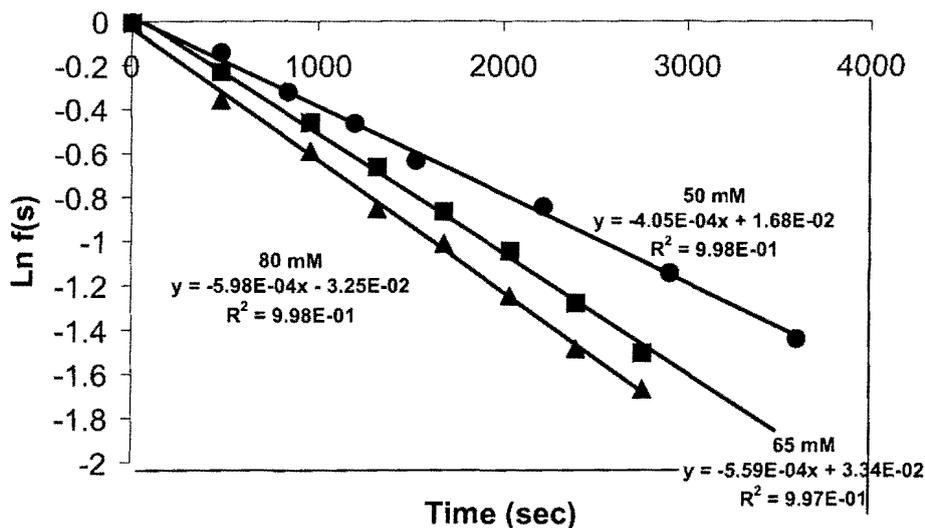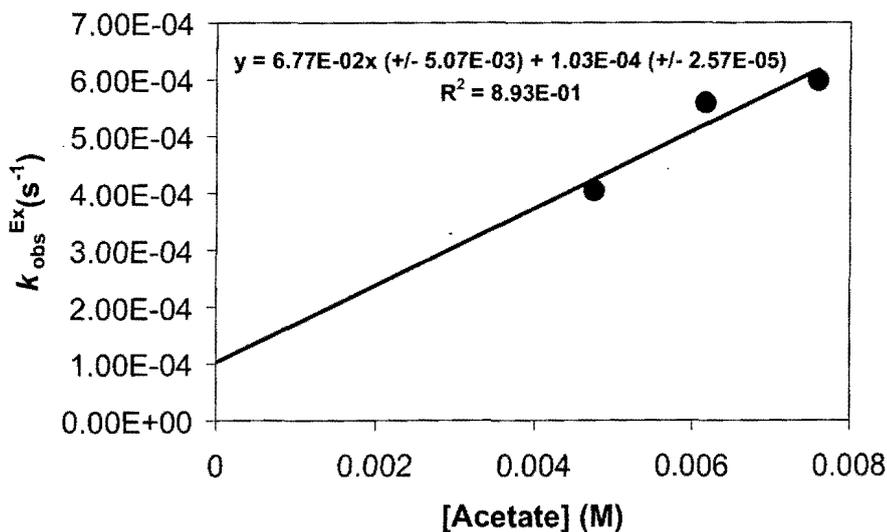
Figure 2.27: Effect of the concentration of the acetate anion on the C1-H/D exchange reaction of DHATS (25) in acetic acid buffer 5 % f_B, I = 1.0 (KCl).

The second order rate constant for buffer catalysis k_B ($M^{-1}s^{-1}$) is determined as 3.58×10^{-2} $M^{-1}s^{-1}$ from the slope of the plot of pseudo first order rate constants, k_{obs}^{Ex}, against the concentration of basic acetic acid buffer form (Figure 2.27). A 2-fold increase in the total buffer concentration leads only to a 35 % increase in the observed first order rate constant, k_{obs}^{Ex} (s^{-1}). The y-axis intercept of the plot shown above is the value of k_{int}^{Ex} for the buffer independent reaction of DHATS (25). The y-axis intercept is obtained as $k_{int}^{Ex} = 9.03 \times 10^{-5}$ s^{-1} at pD 3.75.

Further exchange reactions at the C1-H position of DHATS (25) were monitored in DCl solutions. Table 2.12 shows the data for disappearance of the C-1H peak in DCl solutions, at 25 °C (I =1.0, KCl). The values of k_{obs}^{Ex} (s^{-1}) shown in Table 2.12 were obtained from the slopes of the semi-logarithmic plots (Figure 2.28) of the fraction of substrate remaining, $f(s)$, against time.

Table 2.12: First order rate constants for the disappearance of the C1-H of DHATS (25) in DCl at 25 °C (I=1.0, KCl).

[DCl] (M)	[DO⁻]ᵃ (M)	Time (s)	$f(s)^b$	Ln $f(s)$	k_{obs}^{Exc} (s⁻¹)
		0	0.992	-0.007	
		2580	0.942	-0.058	
		6240	0.881	-0.126	
0.001	3.75×10^{-12}	9900	0.787	-0.238	2.44×10^{-5}
	(pD 3.32)	13980	0.715	-0.335	
		19020	0.629	-0.463	
		0	0.991	-0.001	
		2820	0.947	-0.050	
0.003	1.60×10^{-12}	5820	0.899	-0.106	1.49×10^{-5}
	(pD 2.95)	11160	0.807	-0.213	
		14160	0.782	-0.244	
		16860	0.776	-0.253	
		20100	0.745	-0.294	
		0	0.985	-0.014	
		10560	0.882	-0.124	
0.005	1.01×10^{-12}	18600	0.778	-0.250	9.44×10^{-6}
	(pD 2.75)	28800	0.738	-0.303	
		35400	0.709	-0.342	

		39900	0.665	-0.408	
		0	0.987	-0.012	
		13560	0.826	-0.190	
0.007	6.09×10^{-13}	27960	0.715	-0.335	9.79×10^{-6}
	(pD 2.53)	42240	0.682	-0.381	
		55560	0.536	-0.623	
		79620	0.447	-0.803	
		0	0.986	-0.013	
		11220	0.869	-0.139	
0.009	5.18×10^{-13}	29220	0.736	-0.306	9.61×10^{-6}
	(pD 2.46)	39420	0.657	-0.420	
		49080	0.605	-0.501	
	.	81780	0.448	-0.802	
		0	0.981	-0.018	
		9960	0.918	-0.085	
0.012	3.43×10^{-13}	32040	0.667	-0.404	1.17×10^{-5}
	(pD 2.28)	76980	0.417	-0.874	
		79680	0.385	-0.954	

(a) Measurements were made in DCl in the pD 2.28-3.32 range. [DO⁻] was calculated using $[DO^-] = (10^{pD-pK_w})/\gamma_{OD}$

with $pK_w = 14.87$, where $\gamma_{OD} = 0.75$ is the activity coefficient of deuteroxide ion under our experimental conditions.

(b) The fraction of unexchanged substrate remaining $f(s)$, was calculated according to Equation 2.9. Measurements

were made at an initial substrate concentration of 10 mM. (c) The value of the first-order rate constant (k_{obs}^{Ex}) was obtained from the slope of the plot of ln f(s) against time.

Figure 2.28: **Semi-logarithmic plot of the fraction of remaining C1-H against time for the reaction of DHATS (25) in DCl, I = 1.0 (KCl) at 25 °C (▲ 1mM, ■ 3mM, ● 5mM, △ 7 mM, □ 9mM, ○ 12 mM).**

Summarised below in Table 2.13 are the first order rate constants (k_{int}^{Ex}) obtained for the buffer independent exchange reaction at the C-1 position of DHATS **(25)** at the individual pD values. In the case of reactions in acetic acid buffers, k_{int}^{Ex} values were obtained as the y-axis intercepts of the buffer catalysis plots as mentioned above. However in the case of the reactions in DCl no buffer catalysis can occur thus values for k_{int}^{Ex} can be directly equated with the slopes of the semilogarithmic plots in Figure 2.28 (k_{obs}^{Ex}, s^{-1}).

Table 2.13: Combined rate data for the exchange reactions of DHATS (25).

pD	k_{int}^{Ex} (s^{-1})	Log k_{int}^{Ex}
4.38	4.07×10^{-4}	-3.39
4.09	1.03×10^{-4}	-3.99
3.75	9.03×10^{-5}	-4.04
3.32	2.43×10^{-5}	-4.61
2.95	1.49×10^{-5}	-4.83
2.75	9.61×10^{-6}	-5.01
2.53	2.43×10^{-5}	-4.61
2.46	1.49×10^{-5}	-4.83
2.21	9.41×10^{-6}	-5.03

The pD rate profile for corresponding to the data above is shown in Figure 2.29. This will be discussed further in Chapter 3.

Figure 2.29: pD rate profile for the exchange reaction at the C-1 position of DHATS (25)

To monitor the elimination reaction of DHATS **(25)** it was assumed that buffers in the higher pD range would be required. Elimination reactions were monitored in quinuclidinone and phosphate buffers, and KOD solution. As mentioned previously deprotonation at the C-3 position of DHAS **(27)** should lead to the elimination product methylglyoxal. Therefore it was expected that the analogous reaction at the C-3 position of DHATS **(25)** should proceed by a similar mechanistic pathway ultimately leading to methylglyoxal. In monitoring the reactions, it was observed that while elimination did appear to occur, the overall amount of methylglyoxal formed was almost too small to quantify by ^{1}H NMR. Shown below in Figure 2.30 are representative partial ^{1}H NMR spectra for the reaction of DHATS **(25)** in quinuclidinone buffer 50 % f_B, at 25 ° C (I = 1.0, KCl).

Figure 2.30 Representative ^{1}H NMR spectra at 500 MHz of DHATS (25) (10 mM, pD 7.9), obtained during the reaction in quinuclidinone buffer 50 % f_B 100 mM (pD 7.9) in D_2O at 25 °C and I = 1.0 (KCl). The timepoint is indicated above each spectrum in minutes.

In the spectrum shown above the imidazole internal standard peaks are as described for DHAS (27). The singlets **A** and **B** correspond to the free keto and hydrate protons respectively of the CH_2OD group of DHATS (25). Under these conditions the C1 hydrogens of DHATS (25) had fully exchanged in the time taken to acquire the first timepoint.

It can be seen that over time the singlets corresponding to the CH_2OD keto and hydrate protons of DHATS (25) decrease. A small amount of methylglyoxal, peak **C**, is observed forming presumably due to elimination however the area essentially remains constant after the second

timepoint of the reaction. The fact that the singlets due CH_2OD keto and hydrate protons decrease over a time period of 90 minutes with no significant corresponding increase in peaks due to methylglyoxal or any other peaks was surprising. The reaction of DHATS (25) was also followed in phosphate buffer and KOD. In all cases the same behaviour was observed i.e. the area of the peaks due to the CH_2OD hydrogens decreased over time to zero and there were no new product peaks that could account for this loss of substrate. Although quinuclidinone buffer peaks could have obscured potential new product peaks in Figure 2.33, this could not be the case in phosphate buffer. Figure 2.31 contains representative ^1H NMR spectra for the reaction of DHATS (25) in phosphate buffer 70 % f_B at pD 7.55 (I = 1.0, KCl).

Figure 2.31 Representative ^{1}H NMR spectra at 500 MHz of DHATS (25) (10 mM, pD 7.55), obtained during the reaction in phosphate buffer 70 % f_B 100 mM (pD 7.55) in D_2O at 25 °C (I = 1.0, KCl). The timepoint is indicated above each spectrum in minutes.

In Figure 2.31 above, over the timecourse of the decrease of the two CH_2OD singlets (A and B), other than the small myriad of peaks at ~ 1ppm (whose areas remain constant throughout the reaction) and the small peak C due to methylglyoxal, no other new peaks are observed. It was observed that the colour of the reaction solution turned yellow over the timecourse of the reaction. This could potentially be due to a competing oxidation reaction. To probe this further,

the D_2O buffers were degassed under argon and the reactions repeated. However the same behaviour was observed.

To further probe the fate of the substrate under these conditions, mass spectral analysis of the reaction of DHATS (25) in quinuclidinone buffer was carried out. The initial experiments did not prove conclusive as to the reaction pathway followed by the molecule in 100 mM (90 % f_B) as the buffer species dominated ionization in the mass spectral analysis. This was the case even at relatively low buffer concentrations. Further mass spectrometric experiments were carried out using ammonium bicarbonate buffer at pH 8. Reactions of substrate (1mM) in buffer (1M, I = 1.0) at 4 °C were followed over a period of 72 hours. Positive (ES+) electrospray conditions were used in the fragmentation process. Shown below in Figure 2.32 are overlayed mass spectra for the reaction followed. The time of reaction is indicated above each spectrum in hours. There are several mechanistic possibilities to explain the peaks observed. These will be discussed in detail in Chapter 3.

Figure 2.32: (ES+) mass spectrum of DHATS (25) in ammonium bicarbonate buffer (pH 8).

2.2.3 Bromohydroxyacetone (BHA)

The solution reactions of BHA **(22)** were monitored by 400 and 500 MHz ^{1}H NMR spectroscopy. As mentioned in Section 2.1, recrystallisation yields a mixture of monomeric **(22)** and dimeric **(23)** substrates with the fraction of dimer greater than that of monomer. The presence of both was confirmed by mass spectrometry. The proportion of dimer was found to vary depending on the conditions of crystallisation. However conversion of monomer to dimer could be effected in solutions of low pD over time. Shown below in Figure 2.33 are the overlayed ^{1}H NMR spectra for the formation of the monomer **(22)** from postulated dimer **(23)** in DCl (1M) over time.

Figure 2.33: Representative ^{1}H NMR spectra at 400 MHz of the conversion of BHA dimer (10 mM) (23) to BHA monomer (22) over time, obtained in DCl (1M) at 25 °C (I = 1.0).

The singlets **A** (4.42 ppm), **D** (4.12 ppm), **F** (3.56 ppm) and **H** (3.46 ppm) refer to the presumed dimeric protons present at zero reaction time. The singlets **B** (4.38 ppm) and **C** (4.32 ppm) refer to the C-1 and C-3 protons of the free keto form of BHA while **E** (3.56 ppm) and **G** (3.52 ppm) correspond to the C-1 and C-3 protons of the hydrate form.

Formation of the monomer **(22)** was achieved by dissolving the recrystallised substrate in DCl (1M) and monitoring the changes over a period of approximately 48 hours. The extent of carbonyl hydration (Scheme 2.18) of BHA **(22)** was found to be approximately 60 % ($K_{hyd} = 1.5$) from the relative areas of signals due to the hydrate and keto forms of the molecule. The equilibrium constant for the equilibrium between the free ketone and hydrate form of monomeric BHA is represented by Equation 2.11.

Scheme 2.18

$$K_{hyd} = [22h]/[22] \qquad \textbf{Equation 2.11}$$

Shown below in Figure 2.34 is a partial ^{1}H NMR spectrum of BHA **(22)** after > 95 % conversion to monomer had occured. The zero reaction time spectrum shown was recorded in DCl (1M) and at 25 °C (I =1.0). Also present is imidazole (5mM) as an internal standard.

172

Figure 2.34: Representative ^{1}H NMR spectrum at 500 MHz of BHA (22) (10 mM), obtained at zero reaction time in DCl at 25 °C (I =1.0, KCl). Imidazole (5 mM) internal standard.

The internal standard peaks are as described for the kinetic studies of DHAS (27) in Section 2.2.1. Based on analysis of the observed deuterium exchange reaction of substrate the singlets **B** and **F** at 4.38 and 3.48 ppm respectively correspond to the C-3 protons of the free keto and hydrate form of BHA (22). The singlets **C** and **E** at 4.29 and 3.51 ppm are assigned to the C-1 protons of free keto and hydrate forms of substrate respectively (as discussed above).

The reactions of BHA (10 mM) were monitored in quinuclidinone (90 % f_B 60 -100 mM) and acetic acid buffers (70-90 % f_B 60 -100 mM) at 25 °C (I =1.0, KCl). In this case the substrate was dissolved in DCl (1M) due to the necessity for prior conversion of dimer to monomer thus it was necessary to bring the pD of the substrate sample to that of the relevent buffer before

initiation of the reaction. It was found that deuterium exchange reactions at the C-1 position of

the molecule occured too quickly to monitor in quinuclidinone and phosphate buffers thus acetic

acid buffers were used to monitor this reaction. Shown below (Figure 2.35) are representative

partial ^{1}H NMR spectra taken during the reactions of BHA (10 mM) (22) in 60 mM acetic acid

buffer, 90 % f_B, pD 5.92. At this pD there was no observed elimination.

Figure 2.35: Representative ^{1}H NMR spectra at 500 MHz of BHA (22) (10 mM, pD 5.92),

obtained during the reaction in acetic acid buffer 90 % f_B (60 mM, pD 5.92) in

D$_2$O at 25 °C (I = 1.0, KCl). The timepoint is indicated above each spectrum in

For the reactions of BHA (22) in acetic acid buffers each NMR spectra was recorded over a time

period of 5 minutes (16 transients) and reactions were quenched at specific time points. The

reaction time t was thus calculated at the time of quenching. Mechanistically, the reactions at the

Cl position of BHA **(22)** are analogous to the reactions at the same position of DHAS **(27)** and

DHATS **(25)**. A decrease in the singlets **C** and **E** at 4.31 and 3.52 ppm (corresponding to the

CH_2Br protons of the free keto and hydrate respectively) is accompanied by the appearance and

simultaneous increase of a small broad triplet, **G** ($^2J_{HD}$ = 2 Hz) and singlet, **H** slightly upfield of

the respective peaks. This triplet at 4.29 ppm is due to the CHDBr group of the keto form of

BHA **(22a)** labelled with deuterium at the C-1 position (Scheme 2.19).

Scheme 2.19

Over the reaction time course the areas of the singlets **B** and **F** remain constant relative to

internal standard.

The progress of the exchange reaction at the C-1 position of the molecule was monitored by

comparing the sum of the integrated areas of the C-1 keto and hydrate singlets at time, t, to the

sum of the integrated areas of the C-3 keto and hydrate peaks at time t. The fraction of remaining

C1-hydrogens, $f(s)$ is defined by Equation 2.12.

$$f(s) = \frac{(A_{C1\text{-}CH2,\ keto})t + (A_{C1\text{-}CH2,\ hydrate})t}{(A_{C3\text{-}CH2,\ keto})t + (A_{C3\text{-}CH2,\ hydrate})t} \qquad \textbf{Equation 2.12}$$

The observed pseudo first order rate constants for the disappearance of substrate due to exchange at the C1 position could be determined as the slope of the semi-logarithmic plot of $f(s)$ against time (Equation 2.13).

$$\ln f(s) = -k_{obs}{}^{Ex}t \qquad\qquad \textbf{Equation 2.13}$$

These plots were linear for the half lives examined with 5-8 data points. The observed first order rate constant, $k_{obs}{}^{Ex}$, is the sum of the contributions of all the potential catalytic species to the rate of exchange as described by Equation 2.6 in the previous section (2.2.1).

Reaction data and the experimental first order rate constants for the disappearance of substrate $f(s)$, due to exchange ($k_{obs}{}^{Ex}$, s^{-1}) are shown below in Tables 2.14 – 2.16. Table 2.14 shows the data for the disappearance of the peak due to the C-1 protons in acetic acid buffers, 90 % f_B at 25 ° C ($I = 1.0$, KCl). The values of $k_{obs}{}^{Ex}$ (s^{-1}) shown in Table 2.14 were obtained from the slopes of the semi-logarithmic plots (Figure 2.36) of the fraction of substrate remaining, $f(s)$, against time.

Table 2.14: First order rate constants for the disappearance of the C1-H of BHA (22) in acetic acid buffers 90% f_B in D_2O at 25 °C (I=1.0, KCl).

[Buffer] (M)	[DO⁻][a] (M)	Time (s)	$f(s)$[b]	Ln $f(s)$	k_{obs}^{Ex}[c] (s⁻¹)
		0	1	0	
		3255	0.956	-0.045	
0.060	1.49 x 10⁻⁹	10560	0.887	-0.119	1.63 x 10⁻⁵
	(pD 5.92)	18720	0.795	-0.229	
		27960	0.673	-0.396	
		30960	0.579	-0.546	
		0	1	0	
		3135	0.964	-0.036	
		10440	0.883	-0.124	
0.080	1.92 x 10⁻⁹	18600	0.754	-0.282	1.82 x 10⁻⁵
	(pD 6.03)	27840	0.611	-0.492	
		30840	0.577	-0.549	
		0	1	0	
		3195	0.953	-0.0481	
		10500	0.842	-0.1719	
0.100	2.21 x 10⁹	18660	0.758	-0.2770	1.93 x 10⁻⁵
	(pD 6.09)	27900	0.599	-0.5125	

177

30900   0.540   -0.6142

(a) Measurements were made in acetic acid buffers, 90 % f_B (60, 80 and 100 mM, total buffer concentration) in the

pD 5.92-6.09 range. [DO⁻] was calculated using $[DO^-] = (10^{pD-pK_w})/\gamma_{OD}$ with $pK_w = 14.87$, where $\gamma_{OD} = 0.75$ is the

activity coefficient of deuteroxide ion under our experimental conditions. (b) The fraction of unexchanged substrate

remaining $f(s)$, was calculated according to Equation 2.12. Measurements were made at an initial substrate

concentration of 10 mM. (c) The value of the first-order rate constant (k_{obs}^{Ex}) was obtained from the slope of the

plot of $\ln f(s)$ against time.

Figure 2.36: Semi-logarithmic plot of the fraction of remaining C1-H against time for the reaction of BHA (22) in acetic acid buffers 90% f_B, at 25 °C (I = 1.0, KCl) (● 60 mM, ■ 80 mM, ▲ 100 mM).

60 mM
y = -1.63E-05x + 2.52E-02
R² = 9.56E-01

80 mM
y = -1.82E-05x + 2.80E-02
R² = 9.87E-01

100 mM
y = -1.93E-05x + 2.20E-02
R² = 9.81E-01

Time (sec)

Figure 2.37: **Effect of the concentration of the acetate anion on the C1-H/D exchange reaction of BHA (22) in acetic acid buffer 90 % f_B, I = 1.0 (KCl)**

The second order rate constant for buffer catalysis k_B ($M^{-1}s^{-1}$) is determined as 9.80×10^{-5} $M^{-1}s^{-1}$ from the slope of the plot of the pseudo first order rate constants, k_{obs}^{Ex}, against the concentration of the basic buffer form of acetic acid (Figure 2.37). A 1.67 fold increase in the total buffer concentration leads to an 18 % increase in the observed first order rate constant, k_{obs}^{Ex} (s^{-1}). The y-axis intercept of the plot shown above is the value of k_{int}^{Ex} for the buffer independent reaction of BHA (22). The y-axis intercept is obtained as $k_{int}^{Ex} = 1.19 \times 10^{-5}$ s^{-1} at pD 5.92.

Table 2.15 shows the data for the disappearance of the peak due to the C-1 protons in acetic acid buffers, 80 % f_B at 25 ° C (I = 1.0, KCl). The values of k_{obs}^{Ex} (s^{-1}) shown in Table 2.15 were obtained from the slopes of the semi-logarithmic plots (Figure 2.38) of the fraction of substrate remaining, $f(s)$, against time.

Table 2.15: First order rate constants for the disappearance of the C1-H of BHA (22) in acetic acid buffers 80% f_B in D_2O at 25 °C (I=1.0 , KCl).

[Buffer] (M)	[DO⁻][a] (M)	Time (s)	$f(s)$[b]	Ln $f(s)$	$k_{obs}^{Ex\ c}$ (s⁻¹)
		0	1	0	
		6240	0.949	-0.052	
0.060	4.41 x 10⁻¹⁰	12060	0.926	-0.077	8.89 x 10⁻⁶
	(pD 5.39)	20280	0.857	-0.154	
		26640	0.793	-0.231	
		33240	0.744	-0.295	
		0	1	0	
		6420	0.955	-0.046	
		12300	0.909	-0.954	
0.080	5.95 x 10⁻¹⁰	20520	0.841	-0.173	9.88 x 10⁻⁶
	(pD 5.52)	26880	0.756	-0.279	
		33480	0.732	-0.312	
		0	1	0	
		6300	0.959	-0.042	
		12180	0.921	-0.082	
0.100	7.49 x 10⁻¹⁰	20400	0.829	-0.187	1.16 x 10⁻⁵

(pD 5.62)	26760	0.739	-0.302
	33360	0.691	-0.369

(a) Measurements were made in acetic acid buffers, 80 % f_B (60, 80 and 100 mM, total buffer concentration) in the pD 5.39-5.62 range. [DO⁻] was calculated using $[DO^-] = (10^{pD-pK_w})/\gamma_{OD}$ with $pK_w = 14.87$, where $\gamma_{OD} = 0.75$ is the activity coefficient of deuteroxide ion under our experimental conditions. (b) The fraction of unexchanged substrate remaining $f(s)$, was calculated according to Equation 2.12 Measurements were made at an initial substrate concentration of 10 mM. (c) The value of the first-order rate constant (k_{obs}^{Ex}) was obtained from the slope of the plot of $\ln f(s)$ against time.

Figure 2.38: **Semi-logarithmic plot of the fraction of remaining C1-H against time for the reaction of BHA (22) in acetic acid buffers 80% f_B, at 25 °C (I = 1.0, KCl) (● 60 mM, ■ 80 mM, ▲ 100 mM).**
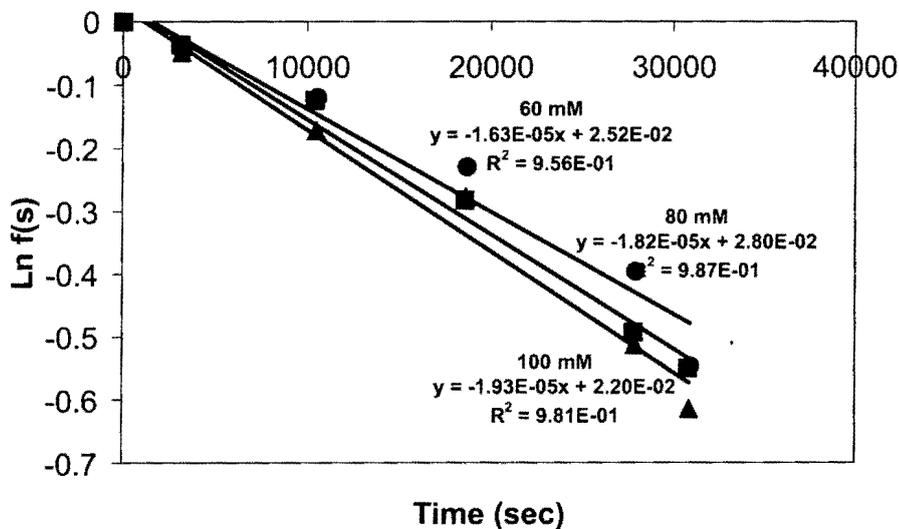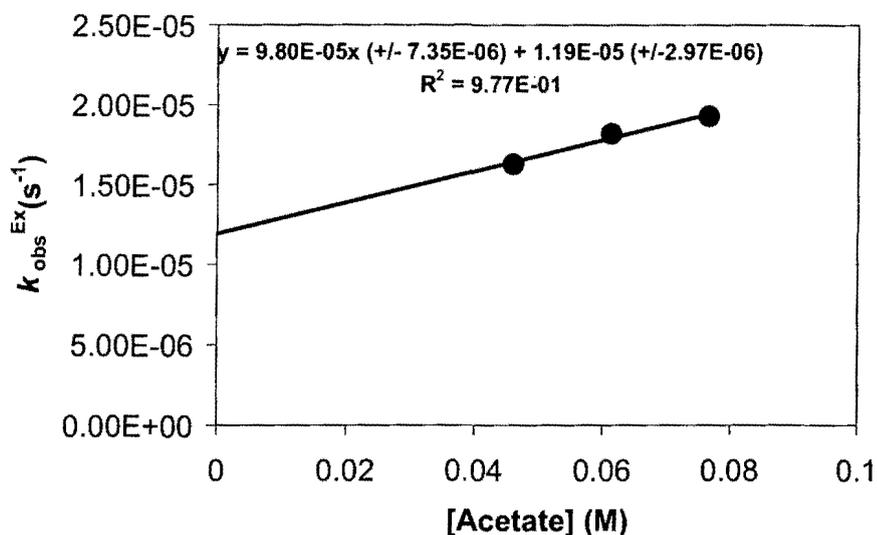

Time (sec)

181

Figure 2.39: **Effect of the concentration of the acetate anion on the C1-H/D exchange reaction of BHA (22) in acetic acid buffers 80 % f_B, I = 1.0 (KCl).**

The second order rate constant for buffer catalysis k_B ($M^{-1}s^{-1}$) is determined as 9.96×10^{-5} $M^{-1}s^{-1}$ from the slope of the plot of the pseudo first order rate constants, k_{obs}^{Ex}, against the concentration of the basic buffer from of acetic acid (Figure 2.39). A 1.6 fold increase in the total buffer concentration leads to a 30 % increase in the observed first order rate constant, k_{obs}^{Ex} (s^{-1}). The y-axis of the plot shown above is the value of k_{int}^{Ex} for the buffer independent reaction of BHA (22). The y-axis intercept is obtained as $k_{int}^{Ex} = 4.70 \times 10^{-6}$ s^{-1} at pD 5.39.

Table 2.16 shows the data for the disappearance of the peak due to the C-1 protons in acetic acid buffers, 70 % f_B at 25 ° C (I = 1.0, KCl). The values of k_{obs}^{Ex} (s^{-1}) shown in Table 2.16 were obtained from the slopes of the semi-logarithmic plots (Figure 2.39) of the fraction of substrate remaining, $f(s)$, against time.

182

Table 2.16: First order rate constants for the disappearance of the C1-H of BHA (22) in acetic acid buffers 70% f_B in D_2O at 25 °C (I=1.0, KCl).

[Buffer] (M)	$[DO^-]^a$ (M)	Time (s)	$f(s)^b$	Ln $f(s)$	$k_{obs}^{Ex\,c}$ (s^{-1})
		0	1	0	
		3960	0.955	-0.048	
0.060	2.72×10^{-10}	8100	0.907	-0.098	6.64×10^{-6}
	(pD 5.18)	16860	0.853	-0.158	
		45520	0.787	-0.239	
		46868	0.713	-0.338	
		0	1	0	
		3780	0.953	-0.048	
		7920	0.893	-0.113	
0.080	3.12×10^{-10}	16680	0.871	-0.138	7.18×10^{-6}
	(pD 5.24)	35340	0.761	-0.273	
		46680	0.701	-0.357	
		0	1	0	
		3660	0.966	-0.035	
		7800	0.891	-0.115	
0.100	3.75×10^{-10}	16560	0.792	-0.233	8.51×10^{-6}
	(pD 5.32)	35280	0.732	-0.312	
		46620	0.660	-0.416	

(a) Measurements were made in acetic acid buffers buffers, 70 % f_B (60, 80 and 100mM, total buffer concentration) in the pD 5.18-5.32 range. [DO⁻] was calculated using $[DO^-] = (10^{pD-pK_w})/\gamma_{OD}$ with $pK_w = 14.87$, where $\gamma_{OD} = 0.75$ is the activity coefficient of deuteroxide ion under our experimental conditions. (b) The fraction of unexchanged substrate remaining f(s), was calculated according to Equation 2.12. Measurements were made at an initial substrate concentration of 10 mM. (c) The value of the first-order rate constant (k_{obs}^{Ex}) was obtained from the slope of the plot of $\ln f$(s) against time.

Figure 2.40: Semi-logarithmic plot of the fraction of remaining C1-H against time for the reaction of BHA (22) in acetic acid 70% f_B, at 25 (I = 1.0, KCl) °C(● 60 mM, ■ 80 mM, ▲100 mM).
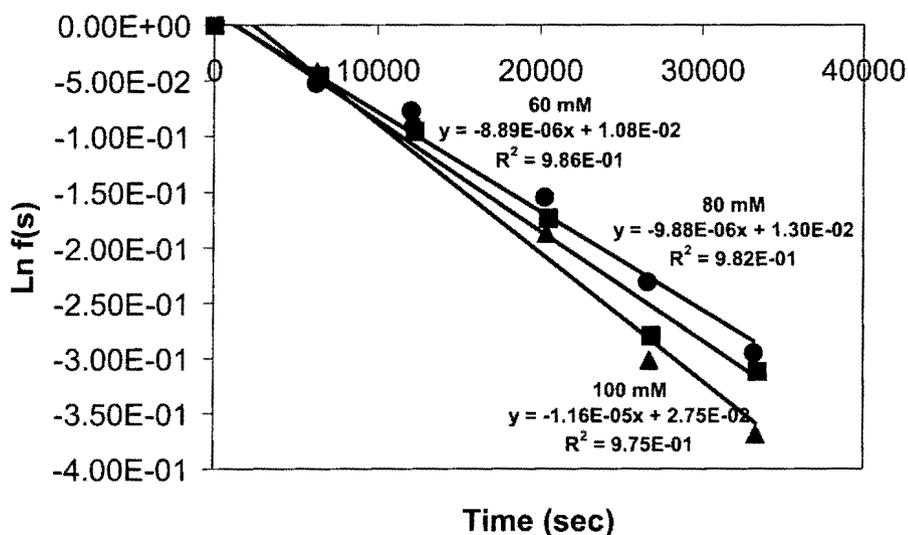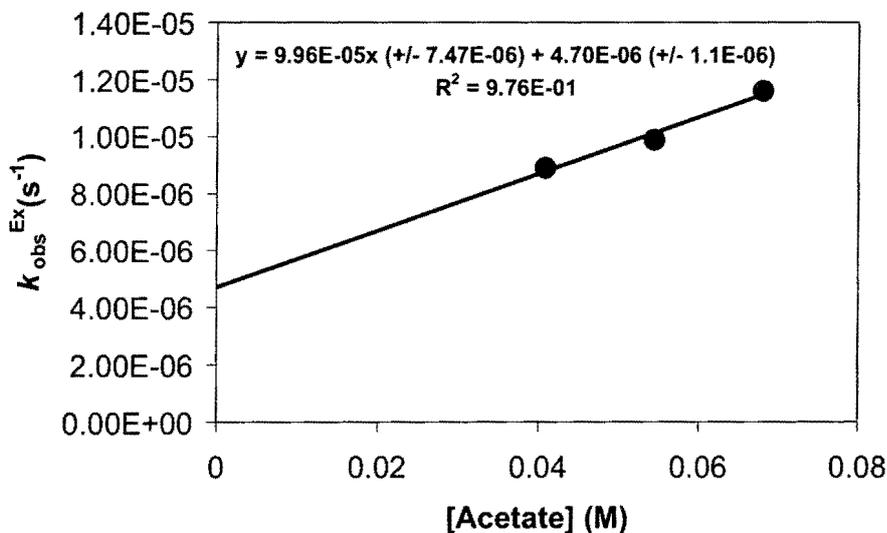
Figure 2.41: Effect of the concentration of the acetate anion on the C1-H/D exchange reaction of BHA (22) in acetic acid buffer 70 % f_B, I = 1.0 (KCl).

The second order rate constant for buffer catalysis k_B ($M^{-1}s^{-1}$) is determined as 7.86×10^{-5} $M^{-1}s^{-1}$ from the slope of the plot of the pseudo first order rate constants, k_{obs}^{Ex}, against the concentration of the basic buffer from of acetate (Figure 2.41). A 1.67 fold increase in the total buffer concentration leads to a 28 % increase in the observed first order rate constant, k_{obs} (s^{-1}). The y-axis of the plot shown above is the value of k_{int}^{Ex} for the buffer independent reaction of BHA (22). The y-axis intercept is obtained as $k_{int}^{Ex} = 3.70 \times 10^{-6}$ s^{-1} at pD 5.18.

The reactions of BHA (10mM) at the C-3 position were monitored in quinuclidinone buffers (60-100 mM, 90 % f_B, pD 9.32) buffers at 25 °C (I =1.0, KCl). Shown below (Figure 2.42) are representative partial ^{1}H NMR spectra of the remaining substrate and products during the reaction of BHA (10 mM) in quinuclidinone buffer (100 mM, 90 % f_B, pD 9.32).

Figure 2.42 Representative ^{1}H NMR spectra at 500 MHz of BHA (22) (10 mM), obtained during the reaction in quinuclidinone 90 % f_B (pD 9.32) in D_2O at 25 °C (I = 1.0, KCl). The timepoint is indicated above each spectrum in minutes.

Under these reaction conditions the peaks due to the C1-hydrogens have almost fully exchanged in the time taken to acquire timepoint 1. As the reaction proceeds, decreases in the areas of singlets B (4.49 ppm) and F (3.6 ppm), which correspond to the CH_2OD free keto and hydrate forms of BHA (22) respectively, are accompanied by the appearance and increase in singlets G (5.24 ppm) and H (4.8 ppm).These singlets which integrate approximately 1.5:1 with respect to internal standard correspond to the C-1 protons of methylglyoxal monohydrate, G and methylglyoxal bishydrate, H. Peaks due to the methyl group of methylglyoxal were not expected to be observed as at the outset of the reaction the C1 position of the molecule is fully deuterated

(see Scheme 2.18). Further analysis of the spectra reveals that a singlet **B***, appears at 4.34 ppm which is not present in the spectrum at zero time.

Over the time period investigated it is also clear that other small peaks appear in the 3.6-4.2 ppm range which do change in area relative to internal standard. These peaks may be due to a competing aldol side reaction.

As other peaks appeared in the spectra for the reaction of BHA **(22)** rates for elimination were estimated by monitoring the appearance of elimination product, methylglyoxal directly. Thus the progress of the elimination reaction was monitored from the ratio of twice the area of the peaks due to the mono and bis-hydrate forms of methylglyoxal to the sum of the areas of singlets **B** and **F** due to the CH_2OD protons of the keto and hydrate forms of BHA **(22)** at time zero (spectrum in 1M DCl afer monomerization). The fraction of elimination product $f(p)^E$, was determined from Equation 2.14.

$$f(p)^E = \frac{2(A_{MG\text{-monohyd}} + A_{MG\text{-bishydrate}})_t}{(A_{CH2OD\ keto} + A_{CH2OD\ hyd})_0} \qquad \textbf{Equation 2.14}$$

The overall fraction of substrate remaining, $f(s)$, after elimination and the other reactions was determined according to Equation 2.15.

$$f(s) = \frac{(A_{CH2OD\ keto} + A_{CH2OD\ hyd})_t}{(A_{CH2OD\ keto} + A_{CH2OD\ hyd})_0} \qquad \textbf{Equation 2.15}$$

The observed pseudo first order rate constants for the total disappearance of substrate, k_{obs}^{T} (s^{-1}), could be determined as the slope of the semilogarithmic plot, $f(s)$ against time (Equation 2.16).

$$Ln\, f(s) = -k_{obs}^{T}$$ **Equation 2.16**

Furthermore, $f(s)'$, the fraction of substrate remaining accounting for reaction due to elimination only, could be determined according to Equation 2.17.

$$f(s)' = 1 - f(p)^{E}$$ **Equation 2.17**

The observed pseudo first order rate constants for the formation of elimination product only could be determined as the slope of the semilogarithmic plot of $f(s)'$ against time (Equation 2.18).

$$Ln\, f(s)' = -k_{obs}^{E}$$ **Equation 2.18**

These plots were linear for the half lives examined with 5-8 data points. The observed first order rate constants, k_{obs}^{T} and k_{obs}^{E} (s^{-1}) are the sum of the contributions of all the potential catalytic species to the rate of exchange as described by Equation 2.6 in section 2.2.1.

Reaction data and the experimental first order rate constants for the disappearance of substrate $f(s)$ due to reaction at the C-3 position are shown below in Tables 2.17 and Table 2.18. The values of k_{obs}^{T} and k_{obs}^{E} (s^{-1}) shown in Table 2.17 were obtained from the slopes of the semi-logarithmic plots (Figure 2.43) of either $f(s)$ or $f(s)'$ against time.

188

Table 2.17: Data for the reaction of BHA (22) in quinuclidinone buffers 90% f_B in D_2O at 25 °C (I=1.0, KCl).

[Buffer] (M)	[DO⁻]ᵃ (M)	Time (s)	$f(p)^{E\ b}$	$f(s)^c$	$f(s)^{,d}$
		0	0	1	1
		480	0.05	0.845	0.95
		810	0.106	0.718	0.894
0.040	2.16 x 10⁻⁶	1200	0.185	0.612	0.815
	(pD 9.08)	1560	0.226	0.543	0.774
		1890	0.281	0.479	0.719
		2250	0.383	0.413	0.617
		0	0	1	1
		990	0.165	0.682	0.835
		1320	0.237	0.531	0.763
0.080	2.59 x 10⁻⁶	1680	0.298	0.434	0.702
	(pD 9.16)	2040	0.375	0.337	0.625
		2370	0.498	0.289	0.502
		0	0	1	1
		510	0.111	0.907	0.889
0.100	2.92 x 10⁻⁶	880	0.217	0.702	0.783
	(pD 9.21)	1240	0.329	0.541	0.671

1660	0.483	0.413	0.517
2520	0.583	0.337	0.417

(a) Measurements were made in quinuclidinone buffers, 90 % f_B (40, 80, 100 mM, total buffer concentration) in the pD 9.08– 9.21 range. [DO⁻] was calculated using $[DO^-] = (10^{pD-pK_w})/\gamma_{OD}$ with $pK_w = 14.87$, where $\gamma_{OD} = 0.75$ is the activity coefficient of deuteroxide ion under our experimental conditions. (b) The fraction of elimination product, $f(p)$ methylglyoxal was calculated according to Equation 2.13. Measurements were made at an initial substrate concentration of 10 mM. (c) The fraction of substrate remaining after to elimination and side reactions, $f(s)$, was calculated according to Equation 2.15. d) The fraction of substrate remaining accounting for reaction to elimination product only was calculated according to Equation 2.17.

Table 2.18: **Data for the reaction of BHA (22) in quinuclidinone buffers 90% f_B in D_2O at 25 °C (I=1.0, KCl)*.**

[Buffer] (M)	[DO⁻][a] (M)	Time (s)	Ln $f(s)$	k_{obs}^{T} (s⁻¹)[b]	Ln $f(s)'$	k_{obs}^{Elim} (s⁻¹)[c]
		0	0		0	
		480	-0.168		-0.05	
		810	-0.331		-0.112	
0.040	2.91 x 10⁻⁶	1200	-0.491	3.94 x 10⁻⁴	-0.205	2.07 x 10⁻⁴
	(pD 9.21)	1560	-0.611		-0.256	
		1890	-0.736		-0.329	
		2250	-0.884		-0.482	

		0	0		1	
		990	-0.383		-0.180	
		1320	-0.633		-0.270	
0.080	3.51×10^{-6}	1680	-0.834	5.39×10^{-4}	-0.353	2.73×10^{-4}
	(pD 9.29)	2040	-1.087		-0.470	
		2370	-1.241		-0.689	
		0	0		0	
		510	-0.097		-0.117	
0.100	4.31×10^{-6}	880	-0.353	5.75×10^{-4}	-0.244	3.70×10^{-4}
	(pD 9.38)	1240	-0.614		-0.398	
		1660	-0.884		-0.659	
		2520	-1.087		-0.874	

(a) Measurements were made in quinuclidinone buffers, 90 % f_B (40, 80, 100 mM, total buffer concentration) in the pD 9.21– 9.38 range. [DO$^-$] was calculated using [DO$^-$] = (10^{pD-pK_w})/γ_{OD} with pK_w = 14.87, where γ_{OD} = 0.75 is the activity coefficient of deuteroxide ion under our experimental conditions. (b) The value of the first-order rate constant (k_{obs}^T) accounting for the total reaction to product was calculated according to Equation 2.16 from the slope of the plot of ln f(s) against time. (c) The value of the first-order rate constant (k_{obs}^{Elim}) accounting for the reaction to elimination product only was calculated according to Equation 2.18. The rate constant was obtained as the slope of the plot of ln f(s)' against time.

*The first timepoint involves loss of 15 % of substrate due to elimination. Peak **B*** at 4.4 ppm is significantly larger than 10 % of the C-1 peak due to the CH_2 protons of the free keto form of BHA (103). Thus it is likely that this peak is adventitious.

Figure 2.43: Semilogarithmic plot of $f(s)$ against time for the reaction of BHA (22) in quinuclidinone 90% f_B, in D_2O at 25 °C (I = 1.0 (KCl) (• 40 mM, ■ 80 mM, ▲ 100 mM).

40 mM
y = -3.94E-04x + 3.76E-04
R^2 = 9.99E-01

100 mM
y = -5.75E-04x + 9.87E-02
R^2 = 9.75E-01

80 mM
y = -5.39E-04x + 5.96E-02
R^2 = 9.86E-01

Time (sec)

Figure 2.44: Semilogarithmic plot of $f(s)'$ against time for the reaction of BHA (22) in quinuclidinone 90% f_B, in D_2O at 25 °C (I = 1.0 (KCl) (• 40 mM, ■ 80 mM, ▲ 100 mM).

40 mM
y = -2.07E-04x + 3.72E-02
R^2 = 9.63E-01

80 mM
y = -2.73E-04x + 5.51E-02
R^2 = 9.35E-01

100 mM
y = -3.70E-04x + 3.85E-02
R^2 = 9.78E-01

Time (sec)

Figure 2.45: Effect of quinuclidinone concentration on the observed first order rate constant for total disappearance of BHA (22) in quinuclidinone buffers 90 % f_B (I = 1.0, KCl).

The second order rate constant for buffer catalysis k_B ($M^{-1}s^{-1}$) is determined as 4.06×10^{-3} ($M^{-1}s^{-1}$) from the slope of the plot of the pseudo first order rate constant, k_{obs}^{T}, against the concentration of the basic buffer from of quinuclidinone (Figure 2.45). A 2.5 fold increase in the total buffer concentration leads to a 45 % increase in the observed first order rate constant, k_{obs}^{T} (s^{-1}). The y-axis of the plot shown above is the value of k_{int}^{T} for the buffer independent reaction of BHA (22). The y-axis intercept is obtained as $k_{int}^{T} = 2.37 \times 10^{-4}$ s^{-1} at pD 9.21.

Figure 2.46: Effect of quinuclidinone concentration on the observed first order rate constant for the elimination reaction of BHA (22) in quinuclidinone buffers 90 % f_B (I = 1.0, KCl).

The second order rate constant for buffer catalysis k_B ($M^{-1}s^{-1}$) is determined as 3.35 x 10^{-3} $M^{-1}s^{-1}$ from the slope of the plot of the pseudo first order rate constants, k_{obs}^{Elim} against the concentration of the basic buffe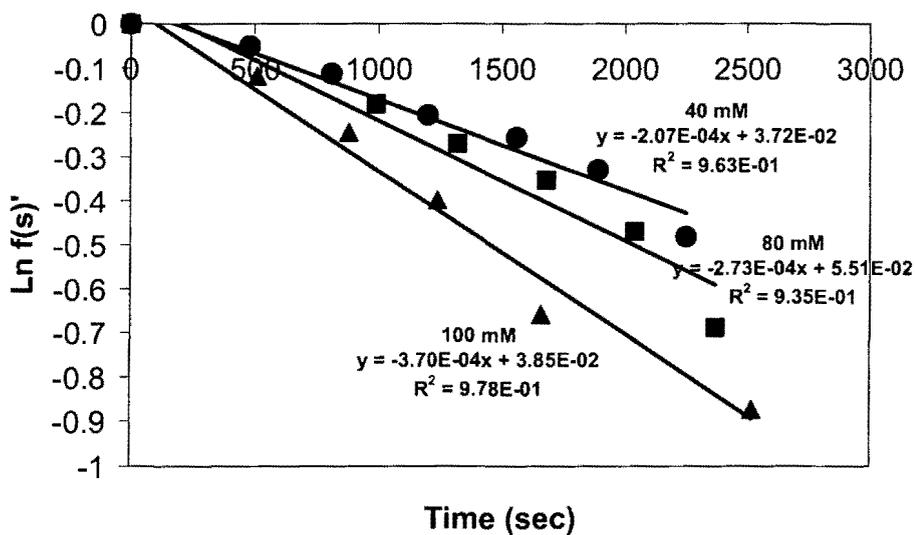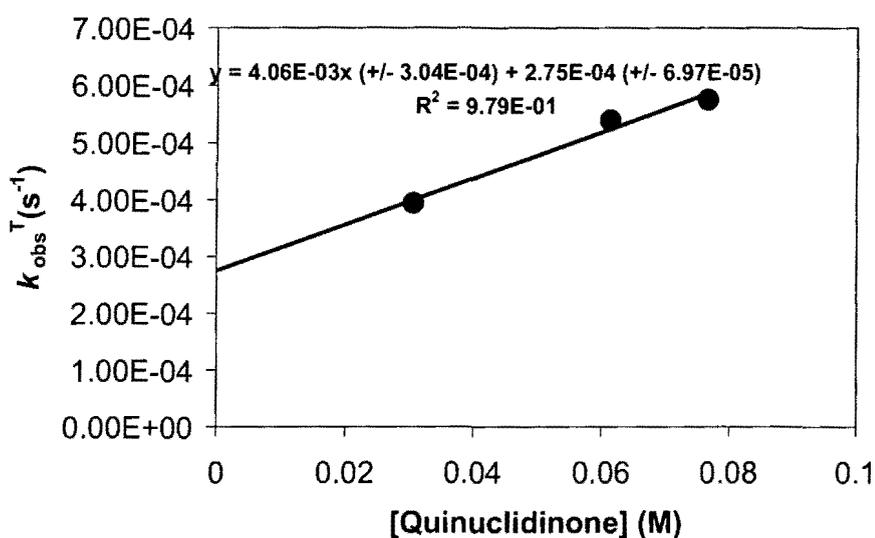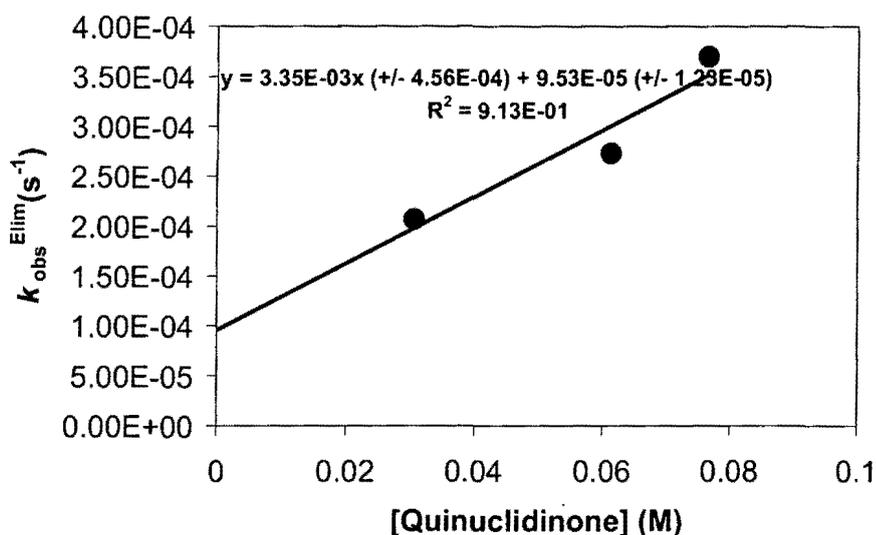r form of quinuclidinone (Figure 2.46). A 1.6 fold increase in the total buffer concentration leads to a 54 % increase in the observed first order rate constant, k_{obs}^{E} (s^{-1}). The y-axis of the plot shown above is the value of k_{int}^{Elim} for the buffer independent reaction of BHA (22). The y-axis intercept is obtained as k_{int}^{Elim} = 9.53 x 10^{-5} s^{-1} at pD 9.21. Data for elimination of the monomeric form of BHA (22) was obtained at only one pD.

As mentioned earlier, BHA was isolated as a mixture of the dimer and monomer with the former present in large excess over the latter. However the exact structure of the dimeric species is unclear. While literature proposals suggest that the dimer formed on recrystallisation is that corresponding to the structure of (23), the results obtained from ^{1}H NMR kinetic experiments are

194

not fully consistent with this. Shown below in Figure 2.47 is a partial ^{1}H NMR spectrum of BHA

dimer/monomer mixture obtained immediately after recrystallisation. The spectrum was recorded

in D_2O at 25 °C (I = 1.0, KCl) with methanol as an internal standard and at 25 °C.

Figure 2.47   **Representative ^{1}H NMR spectrum at 500 MHz of BHA (103) (10 mM), obtained at zero reaction time in D_2O at 25 °C and I =1.0 (KCl). Methanol (5 mM, I =1.0, KCl)) internal standard.**

In the spectrum shown above the singlets **A** (4.44 ppm), **B** (4.12 ppm), **C** (3.56 ppm) and **D** (3.46

ppm) correspond to the protons of dimeric BHA. The singlet at 3.22 ppm corresponds to the CH_3

hydrogens of methanol internal standard. The other smaller peaks are due to monomeric BHA.

The dimeric species **(23)** suggested by Druekhammer *et al* is shown below drawn in the favoured

chair conformation (Figure 2.48).

195

Figure 2.48

(23)

The diastereotopic nature of the methylene protons (C-1, C-3, C-1' and C-3') is consistent with the appearance of the four singlets in the ^1H NMR spectrum shown above.

However observations made on monitoring the reactions of recrystallised sample (dimer/monomer mixture) in phosphate buffer suggest that a dimeric species other than that suggested by Druekhammer *et al* is formed on recrystallisation. Shown in Figure 2.49 are the partial ^1H NMR spectra for the reaction of recrystallised bromohydroxyacetone in phosphate buffer (20 % f_B, I =1.0, pD = 6.56) at 25 ° C. In this case, conversion of dimer to monomer was not attempted prior to the kinetic studies in phosphate buffer.

Figure 2.49: Representative ^{1}H NMR spectra at 400 MHz of the reaction of BHA monomer/dimer mixture in phosphate buffer 20% f_B at 25 °C (I = 1.0, KCl).

The singlet at 3.25 ppm, corresponds to the CH_3 protons of methanol internal standard. Over time, the dimeric peak **B** decreases while a small broad upfield triplet (^2J 2 Hz), **J**, simultaneously appears. The appearance of this triplet is a result of H/D exchange which implies an enolization mechanism. Over the timescale of complete disappearance of peak **B** the other dimer peaks, **A** and **C** remain relatively unchanged. However a parallel decrease in peak **D** is observed and the appearance of a broad upfield singlet, **K**, is also consistent with exchange. Over the timescale of complete disappearance of singlets **B** and **D**, very little monomer formation is observed.

For an exchange reaction to occur, the presence of a carbonyl group with enolizable α-protons is required. As 'monomerisation' is relatively slow compared to the exchange reaction of peaks **B** and **D** it is unlikely that the prior conversion of cyclic dimer **(23)** to monomer can explain this observed exchange reaction. One possible alternative to the species suggested by Druekhammer *et al* is the species **(48)** where peaks **A**, **B**, **C** and **D** correspond to the methylene protons at the C3, C1, C4 and C6 positions of the molecule respectively (Figure 2.50).

Figure 2.50

(48)

It was decided to measure the rate of disappearance of dimer peaks **B** and **D** to see if the data would shed light on the potential structure of the dimeric species. This will be further discussed in Chapter 3.

The reactions of the dimer/monomer mixture were carried out in phosphate and acetic acid buffers. The progress of the exchange at the CH_2 groups corresponding to singlets **B** and **D** was monitored by comparing the integrated areas of singlets **B** and **D** at time, t, relative to the time 'zero' areas of these peaks. The fraction of substrate remaining for each peak, $f(s)$ for peak **B** and $f(s)'$ for peak **D**, is defined by Equation 2.19 and 2.20 respectively.

$$f(s) = \frac{(A_B)_t}{(A_B)_0} \qquad \textbf{Equation 2.19}$$

198

$$f(s)' = \frac{(A_D)_t}{(A_D)_0} \qquad\qquad \textbf{Equation 2.20}$$

The observed pseudo first order rate constants for the disappearance of substrate due to exchange could be determined as the slope of the semi-logarithmic plots of $f(s)$ and $f(s)'$ against time (Equation 2.21 and Equation 2.22).

$$\ln f(s) = -k_{obsB}{}^{Ex}t \qquad\qquad \textbf{Equation 2.21}$$

$$\ln f(s)' = -k_{obsD}{}^{Ex}t \qquad\qquad \textbf{Equation 2.22}$$

These plots were linear for the half lives examined with 5-8 data points. The observed first order rate constants, $k_{obsB}{}^{Ex}t$, and $k_{obsD}{}^{Ex}t$ are the sum of the contributions of all the potential catalytic species to the rate of exchange as described by Equation 2.6 in Section 2.2.1.

Reaction data and the experimental first order rate constants for the disappearance of substrate, due to exchange, are shown below in Table 2.19. Table 2.19 shows the data for the disappearance of peaks **B** and **D** in phosphate buffers, 20 % f_B at 25 ° C (I = 1.0, KCl). The values of $k_{obsB}{}^{Ex}$ and $k_{obsD}{}^{Ex}$ (s^{-1}) shown in the table were obtained from the slopes of the semi-logarithmic plots (Figure 2.51 and 2.52) of the fraction of substrate remaining, $f(s)$ or $f(s)'$, against time.

Table 2.19: First order rate constants for the disappearance of the CH_2 protons of BHA dimer corresponding to peaks B and D in phosphate buffers 20% f_B in D_2O at 25 °C (I=1.0, KCl).

[Buffer] (M)	$[DO^-]^a$ (M)	Time (s)	$f(s)^b$	$Ln f(s)$	k_{obsB}^{Ex} $(s^{-1})^c$	$f(s)'^d$	$Ln f(s)'$	k_{obsD}^{Ex} $(s^{-1})^e$
		0	1	0		1	0	
		300	0.877	-0.108		0.961	-0.039	
0.060	6.53×10^{-9}	600	0.560	-0.578	1.11×10^{-3}	0.563	-0.573	1.19×10^{-3}
	(pD 6.56)	900	0.406	-0.900		0.398	-0.920	
		1200	0.284	-1.258		0.289	-1.124	
		1500	0.213	-1.546		0.216	-1.531	
		1800	0.147	-1.912		0.115	-2.157	
		0	1	0		1	0	
		300	0.766	-0.266		0.869	-0.14	
		450	0.694	-0.365		0.692	-0.367	
		600	0.564	-0.571		0.567	-0.566	
0.080	8.03×10^{-9}	750	0.468	-0.758	1.25×10^{-3}	0.483	-0.727	1.26×10^{-3}
	(pD 6.65)	900	0.379	-0.969		0.383	-0.958	
		1050	0.282	-1.263		0.285	-1.255	
		1200	0.231	-1.463		0.238	-1.431	
		0	1	0		1	0	
		330	0.856	-0.155		0.816	-0.202	

		480	0.573	-0.555		0.544	-0.608	
		630	0.470	-0.755		0.437	-0.826	
0.100	1.06×10^{-8}	780	0.359	-1.024	1.49×10^{-3}	0.344	-1.067	1.39×10^{-3}
(pD 6.77)		930	0.285	-1.255		0.271	-1.303	
		1080	0.218	-1.523		0.213	-1.342	

(a) Measurements were made in phosphate buffers, 20 % f_B (60, 80, 100 mM, total buffer concentration) in the pD 6.56– 6.77 range. [DO⁻] was calculated using $[DO^-] = (10^{pD-pK_w})/\gamma_{OD}$ with $pK_w = 14.87$, where $\gamma_{OD} = 0.75$ is the activity coefficient of deuteroxide ion under our experimental conditions. (b) The fraction of substrate remaining $f(s)$, was calculated according to Equation 2.19. Measurements were made at an initial substrate concentration of 10 mM. (c) The value of the first-order rate constant (k_{obsB}^{Ex}) was obtained from the slope of the plot of ln $f(s)$ against time. (d) The fraction of substrate remaining $f(s)$', was calculated according to Equation 2.20. (e) The value of the first-order rate constant (k_{obsD}^{Ex}) was obtained from the slope of the plot of ln $f(s)$ against time.

Figure 2.51: **Semi-logarithmic plot of the fraction of remaining CH₂ protons, corresponding to peak B, against time for the reaction of BHA in phosphate 20% f_B, at 25 °C (I = 1.0, KCl) (• 60 mM, ■ 80 mM, ▲100 mM).**

Figure 2.52: **Semi-logarithmic plot of the fraction of remaining CH$_2$ protons, corresponding to peak D, against time for the reaction of BHA in phosphate 20% f$_B$, at 25 °C (I = 1.0, KCl) (● 60 mM, ■ 80 mM, ▲100 mM).**

The second order rate constant for buffer catalysis k_B (M^{-1}s^{-1}) is determined as 5.59 x 10^{-2} M^{-1}s^{-1} from the slope of the plot of the pseudo first order rate constants, k_{obsB}^{Ex}, against the concentration of the basic buffer form of phospate (Figure 2.53). A 1.67 fold increase in the total buffer concentration leads to a 44 % increase in the observed first order rate constant, k_{obsB}^{Ex} (s^{-1}). The y-axis of the plot shown above is the value of k_{intB}^{Ex} for the buffer independent reaction of BHA. The y-axis intercept is obtained as k_{intB}^{Ex} = 5.23 x 10^{-4} s^{-1} at pD 6.56.

Figure 2.53: Effect of the concentration of the phosphate anion on the exchange reaction of the CH_2 protons of peak B of BHA monomer/dimer in phosphate buffer 20 % f_B, I = 1.0 (KCl)

The second order rate constant for buffer catalysis k_B ($M^{-1}s^{-1}$) is determined as 2.94×10^{-2} $M^{-1}s^{-1}$ from the slope of the plot of the pseudo first order rate constants, k_{obsD}^{Ex}, against the concentration of the basic buffer form of phosphate (Figure 2.54). A 1.6 fold increase in the total buffer concentration leads to a 54 % increase in the observed first order rate constant, k_{obsD}^{Ex} (s^{-1}). The y-axis of the plot shown above is the value of k_{intD}^{Ex} for the buffer independent reaction of BHA (103). The y-axis intercept is obtained as $k_{intD}^{Ex} = 8.80 \times 10^{-4}$ s^{-1} at pD 6.56.

Figure 2.54: Effect of the concentration of the phosphate anion on the exchange reaction of the CH_2 protons of peak D of BHA monomer/dimer in phosphate buffer 20 % f_B, I = 1.0 (KCl).

2.2.4 Dihydroxyacetone thiophosphate (24)

The dianionic substrate DHATP (24) is isostructural to natural substrate DHAP (1). Similarities in the solution, non-enzymatic elimination and exchange reactions were thus expected. A representative partial ^{1}H NMR spectrum of DHATP (24) (10 mM) is shown below in Figure 2.55. Represented in this spectrum is the first time point (time = 2 minutes) of the reaction after dissolution of this substrate in unbuffered D_2O at 25 °C.

Figure 2.55: Representative ^{1}H NMR spectra at 500 MHz of DHATP (24) (10 mM, pD 5.32), obtained at 'time point one' in D_2O.

As with the other substrates, in buffered D_2O solutions the carbonyl group of DHATP (24) is hydrated (Scheme 2.20).

Scheme 2.20

(24) $\xrightleftharpoons{K_{hyd}}$ (24h)

The equilibrium constant, K_{hyd}, can be represented by Equation 2.23

$$K_{hyd} = [24h]/[24]$$ **Equation 2.23**

For DHATP (24), the extent of carbonyl hydration (Scheme 2.15) was found to be approximately 14 % (K_{hyd} = 0.16). In the above ^{1}H NMR spectrum, the singlet **A** (4.43 ppm) and doublet **B** (3.55 ppm) correspond to the C3 and C1 methylene protons of the free keto form of the molecule respectively. The singlet **C** (3.49 ppm) and doublet **D** (2.89 ppm) correspond respectively to the C3 and C1 hydrate methylene protons of DHATP (24). A trace impurity peak is observed at ~ 3.2 ppm. This is due to a small amount of methanol remaining from the purification procedure. Singlet **A** and doublet **B**, integrate approximately 1:1 with respect to each other. The hydrate peaks, **C** and **D** also integrate approximately 1:1 to each other however DHATP is predominantly in its free keto form under these conditions (keto:hydrate 6:1).

On exposure to air, this substrate proved to be unstable in solid form. Despite being stored at -20 °C and -80 °C post synthesis and purification, the solid substrate decomposed over time (Approximately 10 minutes). Resulting ^{1}H NMR analysis of the decomposed product revealed a

myriad of peaks from which it was not possible to obtain any information as to the structure of 'decomposed' product. However, it was found that on preparation of a D_2O solution of the substrate, decomposition appeared to be delayed to an extent (occurring after a longer period of time, ~ 1 hour). Thus after 2 minutes it was possible to obtain a ^1H NMR and a mass spectrum of the sample for the purposes characterisation. Although kinetic data was not obtained for this substrate, it was observed that after 2 minutes in unbuffered D_2O at pD 5.32 at this pD no reaction had occurred. This is comparable to the lack of reactivity observed for DHAP (1) in unbuffered D_2O solution. For two of the other mutant substrates investigated in this work, DHATS (25) and BHA (22) it was found that in an unbuffered D_2O solution exchange reactions of the C-1 methylene protons generally did occur. Therefore a brief glimpse of the 'lack' of reactivity of DHATP (24) at this pD at the very least provides some crude kinetic information on the substrate which can be compared to its dianionic counterpart, DHAP (1). However further investigations into the origin of the decomposition of the molecule are needed (prior to more detailed kinetic studies).

2.2.5 Hydrolysis of 3-oxo-4-(2,2-dimethylpropionyl)oxobutylphosphonic acid diisopropyl ester (32).

In theory, the kinetic analysis of the background non-enzymatic and enzymatic reactions of the 'phosphonate' analogue (32) of DHAP (1) would have proven interesting due to the isosteric nature of this substrate with natural substrate. However the final hydrolysis step in the synthesis of this molecule proved unsuccessful. Literature proposals for the hydrolysis reaction of 3-oxo-4-(2,2-dimethylpropionyl)oxobutylphosphonic acid diisopropyl ester (32) suggest the conditions

required for hydrolysis consist of stirring for 4 hours at 100 °C in 3M HCl followed by extraction and product isolation. Despite following these conditions stringently the desired 'fully hydrolysed' product was not formed. Varying the conditions to promote a potential quicker hydrolysis reaction (temperature, acid concentration as well as carrying out the reaction in concentrated KOH) had no effect in leading to the desired product. Under the conditions suggested in the literature and the varied conditions mentioned, hydrolysis at the C-4 position of the molecule was observed but not at the phosphate ester end of the molecule. Reaction times were varied from 4 hours (from the original experimental procedure) to 48 hours. Acid concentrations were increased to approximately 10 M. Longer reaction times and higher acid concentrations generally led to decomposition of the product to a volatile black substance which was not identifiable by any analytical method. While it is clear that hydrolysis of phosphate esters is a slow process, under the elevated temperature and acidic conditions the rate should have been increased considerably.

The reaction consisting of 3-oxo-4-(2,2-dimethylpropionyl)oxobutylphosphonic acid diisopropyl ester **(32)** (5mM) was initiated on the addition of quinuclidinone buffer (90 % f_B, 45 mM) and toluene internal standard (10 mM) to the substrate solution at I = 1.0 (KCl) and 25 °C. To solubilise the substrate vigorous shaking was needed. Analysis did suggest that hydrolysis of the *tert*-butyl group had taken place with relative ease (Scheme 2.21).

Scheme 2.21

(32)

Quinuclidinone
⟶
90 % f_B, pD9.0

(32')

(33)

Shown below in Figure 2.56 are the overlayed ^{1}H NMR spectra for the hydrolysis reaction of 3-oxo-4-(2,2-dimethylpropionyl)oxobutylphosphonic acid diisopropyl ester **(32)** monitored in quinuclidinone buffer (45 mM, 90 % f_B) at 25 °C (I = 1.0, KCl).

Figure 2.56: Reaction of 3-oxo-4-(2,2-dimethylpropionyl)oxobutylphosphonic acid diisopropyl ester (32) monitored in quinuclidinone buffer (45 mM, 90% f_B) at 25 °C (I = 1.0, KCl). Toluene (5mM, I = 1.0) internal standard.

As the reaction was carried out in quinuclidinone buffers, the peaks corresponding to the C-1, C-1' and C-4 protons were obscured by buffer peaks, thus the overlayed spectra shows the peaks which correspond to the C-3 protons of 3-oxo-4-(2,2-dimethylpropionyl)oxobutylphosphonic acid diisopropyl ester (32), the C-4 protons of the hydrolysed analogue (32') and the isopropyl methine protons of the molecule which are represented by a multiplet, **B**. While the singlet due to the CH$_3$ protons of toluene internal standard was not obscured, for the sake of clarity this has been omitted from the overlayed spectra. In the above spectrum, singlet **A**, refers to the C-4 methylene protons of the parent 3-oxo-4-(2,2-dimethylpropionyl)oxobutylphosphonic acid diisopropyl ester (32). As mentioned, the multiplet, **B**, at 4.6 ppm corresponds to the isopropyl

methine protons of the molecule. The singlet **C** at 4.28 ppm refers to the hydrolysis product (**32'**) whereas peak **D**, is possibly due to the hydrate methylene protons of hydrolysis product (**32'**). While a hydrolysis reaction clearly occurs in quinuclidinone buffer, a competing exchange reaction at the C-3 position of the parent molecule (**32**) can also be observed as seen by the appearance of broad singlet **E** (4.71 ppm). Complete kinetic analysis of this reaction was not carried out however it was observed relative to an internal standard that over the time frame of the reaction, appriximately 15 % hydrolysis and 30 % exchange had occurred. Further kinetic investigations of the reactions of this substrate are needed to obtain information on the exact nature of the reaction occurring.

2.3 The reactions of DHAP (1), DHA (26) and DHAS (27) in the presence of MGS.

This section has two main parts. Section 2.3.1 provides a brief overview of the molecular biology techniques and methods used to overexpress and purify MGS (all of these techniques are discussed in more detail in Chapter 4) as well as the UV-Vis spectrophotometric assays used to measure the activity, concentration and overall k_{cat} and K_M values of the purified enzyme. In Section 2.3.2 the results obtained from the ^{1}H NMR kinetic experiments used to monitor the reactions of DHAP (**1**), DHA (**26**) and DHAS (**27**) in the presence of MGS are presented.

2.3.1 MGS overexpression and purification

Using the BRENDA database, the genomic coding sequence of MGS from the *E.coli* genome (K12 derivative) was obtained. Three primers were designed to this region;

a) MGS5' Nco CCATgTACACCATggAACTgACgACTCgC

b) MGS3' XhoHis CCCgCgCTCgAgCTTCAgACggTCCgCgAgATAACg

c) MGS3' XhoSTOP CCCgCgCTCgAgTTACTTCAgACggTCCgCg

The MGS His and MGS STOP genomic sequences were amplified by PCR and subcloned into the pET21d expression vector. The above procedures were carried out by Dr. Mark Skipsey. The final plasmid was sequenced and the insert sequence was found to match that of the genomic coding sequence of MGS.

2.3.1.1 MGS STOP

The plasmid containing the MGS STOP gene was transformed into BL21 (DE3) *E.coli* cells lacking the endogenous MGS gene. Following the procedure of Harrisson *et. al* [40], a single ampicillin resistant BL21(DE3) colony was cultured at 37 °C in 1L of LB medium supplemented with ampicillin (100 µg/mL) until the medium optical density reached a value of 0.8 at 600 nm. IPTG was then added to 1mM and the culture was expressed for a further three hours before the cells were harvested via centrifugation. Cells were suspended in imidazole (50 mM)/potassium phosphate (1 mM) buffer and lysed by sonication (5 x 10 second runs with the cells cooled on ice in between runs for 10 seconds). Further centrifugation was carried out resulting in a crude supernatant. Prior to purification, the supernatant was assayed for MGS activity following the procedure of Hopper and Cooper [65] (Scheme 2.22).

Scheme 2.22.

The addition of the supernatant to a solution containing DHAP **(1)** (0.75 mM), imidazole buffer (40 mM, pH 7.1, I = 1.0, KCl), reduced glutathione (1.65 mM) and glyoxalase I (2.2 µg/mL) led to a large increase in absorbance at 240 nm, indicating the presence of assay product D-lactoylglutathione **(9)** and ultimately MGS activity. This was by comparison with a background assay in the absence of supernatant for which no increase in absorbance was observed over the timescale of the assay. In this assay, to ensure that the elimination step was rate-limiting, an excess of glyoxalase I was used. The assay is described in more detail in Section 2.4.1.

The crude lysate was also analysed by SDS-PAGE. Gel analysis confirmed the identity of crude MGS with a strong band at approximately 17 kDa. Under electrophoresis conditions the protein is denatured. Therefore the band at ~ 17 kDa corresponds to monomeric MGS (Figure 2.57).

Figure 2.57: SDS-PAGE (12 %) of Coomasie-blue stained crude supernatant MGS STOP.

a) The sample in lane 3 corresponds to crude MGS monomer with a molecular weight of approximately 16 kDa.

b) The sample run in lane 6 correspond to protein molecular weight standards ranging from 100-6 kDa. SDS-PAGE conditions are described in chapter 4.

c) Lanes 1, 2, 4 and 5 were run with sample buffer containing no MGS. This ensured that no overlap of the proteins in lane 3 and 6 occured.

MGS-STOP was purified by FPLC (DEAE weak anionic resin). Fractions of 1 mL were collected over a total time-period of 60 minutes. Figure 2.58 shows the elution profile of purified

MGS STOP from the DEAE resin (superfine grade) at 280 nm using phosphate/imidazole

loading buffer (1mM/50mM) and phosphate/imidazole (1mM/50mM), NaCl (500mM) eluting

buffer.

Figure 2.58: Ion-exchange elution profile of purified MGS.

Fractions 1-32 were assayed for MGS activity using the Hopper and Cooper assay procedure

described previously. While no apparent activity was observed for fractions 1-12 and fractions

21-32, assaying fractions 13-20 showed an increase in absorbance at 240 nm indicating MGS

activity. This is consistent with the observation of the largest increase in absorbance at 280 nm

for these fractions in the UV elution profile in Figure 2.39. Therefore fractions 13, 17 and 19 were analysed by SDS-PAGE for purity (Figure 2.59).

Figure 2.59: SDS-PAGE (12 %) of coomasie-blue stained purified MGS STOP

a) The samples in lanes 1-3 (fractions 13, 17, 19 respectively) are the purified MGS STOP monomer. Each monomer has a molecular weight of approximately 17 kDa.

b) The sample run in lane 4 is commercially available rabbit muscle *triosephosphate isomerase* (TIM) (monomer MW = 25 kDa). This sample was run as a reference.
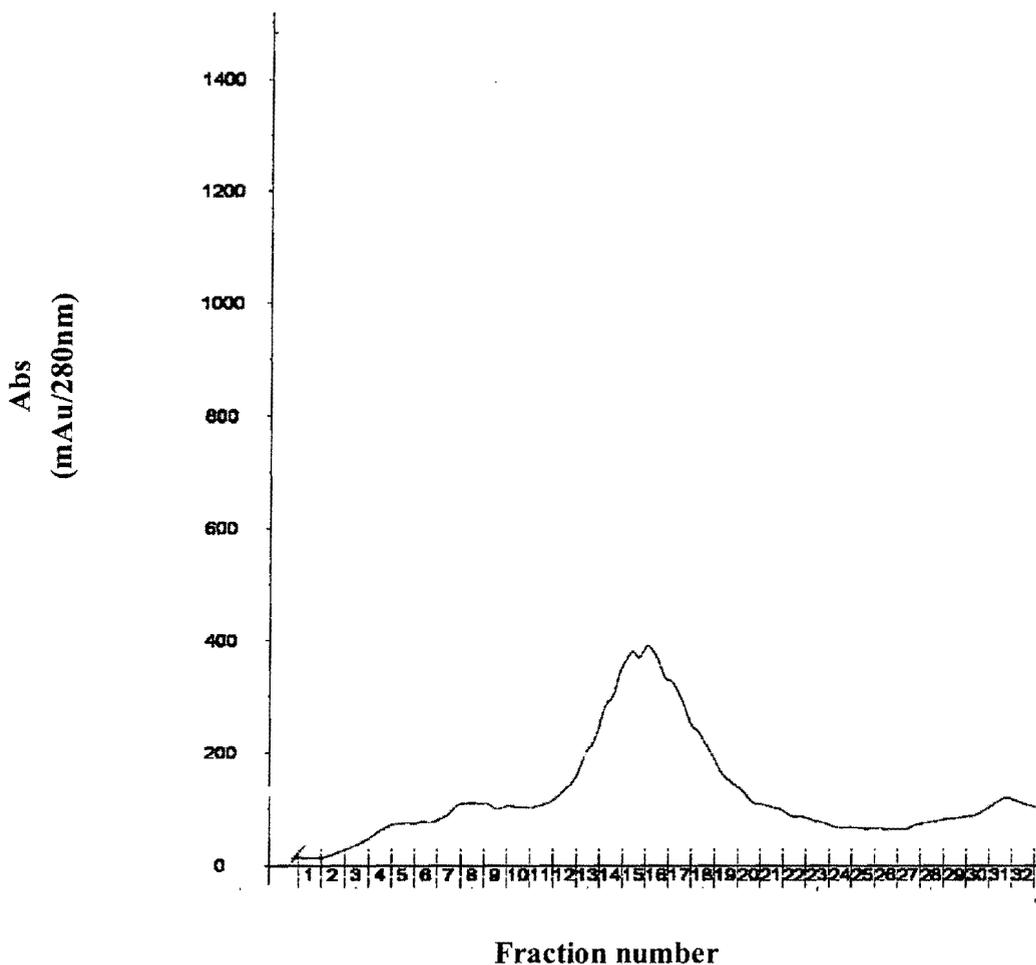
c) The samples run in lane 5 correspond to protein molecular weight standards ranging from 100-6 kDa. SDS-PAGE conditions are described in more detail in Chapter 4.

Fractions 13-19 were combined and concentrated using Millipore ultrafiltration eppendorf tubes with a molecular weight cut-off of 7,000 Da. To confirm the identity and purity of MGS a sample of concentrated enzyme was analyzed by Q- TOF mass spectrometry (Figure 2.60).

216

Figure 2.60: Mass spectrum of purified MGS (Q-TOF)

A molecular weight of 16,918 Da corresponds to the purified monomer of MGS. This is in good

agreement with the reported literature monomer molecular weight of 17,000 Da which was

obtained by two-dimensional gel analysis method.

2.3.1.2 MGS-His

The procedure used in overexpressing MGS His was identical to that described for the

overexpression of MGS STOP in section 2.3.1.1. The His-tagged MGS was purified by a nickel

affinity column (described in Chapter 4). However, it was found that the activity of the purified MGS-His was less than that of crude MGS-STOP and more importantly the purified MGS-His lost activity very rapidly over time. For this reason, all further enzyme kinetic experiments were carried out using purified MGS STOP.

2.3.2 Determination of concentration, k_{cat} and K_M of purified MGS STOP.

Prior to ^{1}H NMR analysis of the reactions of 'mutant' substrates in the presence of MGS, it was necessary to determine the concentration of the purified enzyme as well as reproducing the literature values for k_{cat} and K_M obtained by Harrison *et al*.

The concentration of MGS was determined using the Bradford dye-binding assay (Bio-Rad) with bovine serum albumin as standard. Shown below in Table 2.21 are the dilutions and final concentrations of the protein standard with the corresponding absorbance at 595 nm. The BSA solution was added to the neat dye reagent (800 μL) in a 1mL cuvette. Prior to measuring the absorbance at 595 nm the solution was incubated at room temperature for 5 minutes.

Table 2.21: Changes in absorbance at 595 nm with changing concentration of BSA.

BSA (μL)[a]	H$_2$O (μL)	G250 dye (μL)	[BSA] (μg/mL)[b]	Abs (595nm)
5	195	800	1	0.308
25	175	800	5	0.402
50	150	800	10	0.537
75	125	800	15	0.659

| 100 | 100 | 800 | 20 | 0.728 |

The standard plot obtained from the Bradford assay with the concentration of BSA (µg/ml) is shown in Figure 2.57. The absorbance shift at 595 nm on the y-axis corresponds to binding of the Coomassie brilliant blue (G250) dye reagent to bound arginine and aromatic residues. It was found that at concentrations greater than 20 µg/ml of BSA standard, the plot levelled off (this was found for 25-35 µg/mL concentrations of BSA). These points have been ommited from this graph for the purposes of accuracy. Dilutions of BSA standard (200 µg/mL) were made to give a final concentration range of 1-20 µg/mL.

A volume of 5 µL of concentrated MGS solution was diluted in H_2O (195 µL) and the solution was added to neat dye reagent (800 µL). Following incubation at room temperature the absorbance measured at 595nm was found to be 0.731. Upon repetition of this experiment under identical conditions, the absorbance values of 0.735, 0,730 and 0.729 were obtained. The average value of these absorbances, 0.731, was thus used. From the standard plot for the BSA assay the concentration of purified MGS can be determined based on the absorbance obtained at 595 nm.

Figure: 2.61 Standard Bradford assay plot for BSA concentration.

Extrapolation to the y-axis of the standard plot in Figure 2.61 yields an MGS concentration of 17.7 μg/mL. Taking into account dilution factors this implies that the concentration of MGS from the purification was 3537 μg/mL (3.54 mg/mL). As the final volume of concentrated protein obtained was 1 mL a final yield of 3.54 mg of protein was obtained from a 1L starting culture solution.

As discussed before, one unit of MGS activity is defined as the amount of enzyme required for the formation of 1μL of D-lactoylglutathione/minute under the assay conditions (see Chapter 4). Harrison *et al* determined the specific activity of recombinant wild-type MGS as 1113 units/mg, an apparent K_M for DHAP of 0.20 ± 0.03 mM and a k_{cat} value of $220s^{-1}$. This leads to a k_{cat}/K_M of $1.1 \times 10^6 \, M^{-1}s^{-1}$ (which on correction for the hydrate of DHAP leads to $5.2 \times 10^6 \, M^{-1}s^{-1}$).

Elimination of phosphate over time results in the allosteric inhibition of MGS. However, the amount of phosphate released over 1-10 % of the reaction at substrate concentrations up to 0.6 mM is presumed insufficient to induce inhibition. For this reason initial rate methods were employed to determine the specific values of k_{cat} and K_M for the recombinant MGS produced for this project. It was found that the first 10 % of the reaction of DHAP (0.7 mM) was linear (i.e the plot of [DHAP] against velocity). In this work, to ensure that enough MGS was present to turnover 5-10 % of the concentration of DHAP in a timeframe of approximately 10 minutes, a series of dilutions of the concentrated enzyme were made. A total dilution of 1/500 using imidazole buffer (pH 7.1, I = 0.1) was made from the enzyme resulting in a concentration of 7.08 µg/mL. Changes in absorbance/minute (velocity) determined from the assays were fitted to the Michaelis Menten equation (Equation 2.24) by non-linear least square fitting using Sigma plot to obtain values of k_{cat} and K_M for our purified MGS. For the assays described below Michaelis Menten curves for MGS were constructed using 5 and 10 µL of the diluted enzyme (7.08 µg/mL) resulting in final concentrations of 0.035 µg/mL and 0.071 µg/mL in a total assay volume of 1 mL. DHAP concentrations ranged from 0.05 mM to 1.2 mM. Constant volumes and concentrations of reduced glutathione (15 mM), glyoxalase I (6.6 µg protein/mL), imidazole buffer (50 mM) and KCl (0.1 M) were added for each reaction. Shown below in Tables 2.22 and 2.23 are the changes in absorbances at 240 nm over the first ten minutes (linear range) for the assays carried out with 5 µL and 10 µL of MGS. Reactions were carried out at 25 °C.

.

221

Table 2.22: Observed absorbance change at 240 nm for the assay of MGS activity (0.035 μg/mL final concentration in 1 mL assay volume).

[DHAP][a] (mM)	[GSH][b] (mM)	[MGS][c] (μg/ml)	Glyoxalase I(μg/mL)[d]	[Imidazole][e] (mM)	[KCl][f] (mM)	Δ Abs/min (240nm)[g]
0.05	15	0.035	6.6	50	100	0.0065
0.2	15	0.035	6.6	50	100	0.0226
0.4	15	0.035	6.6	50	100	0.0428
0.6	15	0.035	6.6	50	100	0.0457
1.2	15	0.035	6.6	50	100	0.0442

(a) 1.5, 6, 12, 18 and 36 μL of a DHAP stock solution (33.3 mM, I =0.1, KCl)) were added to give the corresponding final concentrations of 0.05, 0.1, 0.2, 0.4, 0.6 and 1.2 mM. (b) 375 μL of reduced glutathione stock (40 mM) were added to each reaction giving a final concentration of 15 mM. (c) 5μL of MGS (7.08 μg/mL) were added to each reaction. (d) 3 μL of Glyoxalase I (2.2 mg/mL) were added to each reaction giving a final concentration of 6.6 μg/mL. (e) 500 μL of imidazole (100 mM) were added to each reaction giving a final concentration of 50 mM. (f) The volume of KCl (100 mM) added to each reaction varied relative to the volume of DHAP. The volume added brought the total assay volume to 1mL. (g) Absorbance changes were monitored at 240 nm.

Fitting the data to the Michaelis-Menten equation (Equation 2.24) yields the plot shown in Figure 2.62.

$$v = k_{cat}[E][S]/(K_M + [S]) = V_{max}[S]/(K_M + [S]) \qquad \text{Equation 2.24}$$

Figure 2.62: Michaelis-Menten curve for the analysis of the reaction of DHAP in the presence of MGS (final concentration of 0.035 µg/mL).

The Sigma plot fit results in calculated values of $V_{max} = 0.058 \pm 0.0013$ abs/min and $K_M = 0.24 \pm 0.15$ mM. The value obtained for K_M is in fair agreement with the corresponding value determined by Harrison *et al* of 0.2 mM.

Table 2.23: Observed absorbance change at 240 nm for the assay of MGS activity (0.071 μg/mL final concentration in 1 mL assay volume).
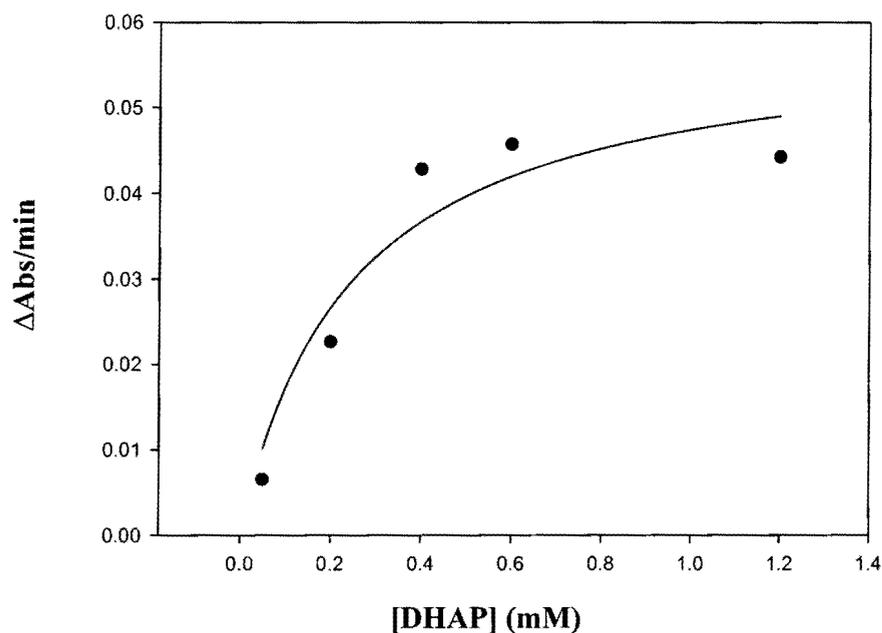
[DHAP][a] (mM)	[GSH][b] (mM)	[MGS][c] (μg/ml)	Glyoxalase[d] I(μg/mL)	[Imidazole][e] (mM)	[KCl][f] (mM)	Δ Abs (240nm)[g]
0.05	15	0.071	6.6	50	100	0.0103
0.2	15	0.071	6.6	50	100	0.0402
0.4	15	0.071	6.6	50	100	0.0711
0.6	15	0.071	6.6	50	100	0.0853
1.2	15	0.071	6.6	50	100	0.0848

(a) 1.5, 6, 12, 18 and 36 μL of a DHAP stock solution (33.3 mM, I = 0.1 (KCl)) were added to give the corresponding concentrations of 0.05, 0.1, 0.2, 0.4, 0.6 and 1.2 mM. (b) 375 μL of reduced glutathione stock (40 mM) were added to each reaction. (c) 10μL of MGS (7.08 μg/mL) were added to each reaction. (d) 3 μL of Glyoxalase I (2.2 mg/mL) were added to each reaction giving a final concentration of 6.6 μg/mL. (e) 500 μL of imidazole (100 mM) were added to each reaction. (f) The volume of KCl (100 mM) added to each reaction varied relative to the volume of DHAP. The volume added brought the total assay volume to 1mL. (g) Absorbance changes were monitored at 240 nm.

Fitting the data to the Michaelis-Menten equation (Equation 2.24) yields the plot shown in Figure 2.63.

Figure 2.63: Michaelis-Menten curve for the analysis of the reaction of DHAP in the presence of MGS (final concentration 0.071 µg/mL).

For this concentration of MGS the Sigma plot fit results in calculated values of $V_{max} = 0.115 \pm 0.0018$ abs/min and $K_M = 0.3 \pm 0.13$ mM. The value obtained for K_M is higher than that obtained by Harrison et al. However the first experiments on determining the activity of MGS isolated directly from E.coli without overexpression (Hopper and Cooper) have determined K_M as 0.5 mM in imidazole buffer, in the absence of phosphate. This value is much higher than that obtained in our work or the value of K_M obtained by Harrison *et al*. This indicates that the value of K_M may vary depending on assay conditions.

From the values obtained for V_{max} and K_M it was possible to determine the value of k_{cat} (s^{-1}) as well as the specific activity (µmoles/mL/minute/mg) for the enzyme.

A value of V_{max} = 0.058 abs min^{-1} was determined for the reaction catalyzed by MGS (0.035μg/mL). This corresponds to a value of V_{max} = 9.7 x 10^{-4} abs sec^{-1}. The extinction coefficient of D-lactoylglutathione is 3.4 mM^{-1} cm^{-1} and thus a value of V_{max} = 2.84 x 10^{-4} mM/sec can be obtained. For the data in Figure 2.43, the enzyme concentration used was 0.035 μg/mL. Correcting to a concentration using the molecular weight of the enzyme[†] (101,508 Da - assuming the hexameric nature of the enzyme) results in a final enzyme concentration of 3.54 x 10^{-7} mM. Thus from $V_{max} = k_{cat}$ [E] = 2.8 x 10^{-4} mM/sec and [E] = 3.54 x 10^{-7} mM, a value of k_{cat} =803 s^{-1}.

This differs 4-fold from that of 200 s^{-1} determined by Harisson *et al* although these authors assumed that MGS was tetrameric rather than hexameric.

The specific activity of the enzyme refers to μmoles/mL/minute per mg of protein. Therefore 3.5 x 10^{-5} mg of protein corresponds to 2.8 x 10^{-4} mM/sec (0.017 mM/min) thus 1mg corresponds to 490 μmoles/mL/min/mg.

For MGS (0.071μg/mL) a value of k_{cat} = 806 s^{-1} was determined using the same methods described above. A specific activity of this concentration of MGS was calculated to be 480 μmoles/mL/min.

[†] Early studies on the structure of MGS have suggested that the enzyme was a tetrameric protein. Data which supported the structure was obtained from gel-filtration chromatography which for MGS indicated a MW of 76,000 Da. This was also consistent with the kinetic Hill coefficient determined in the presence of phosphate. However it is known that many proteins behave anomolously on gel-filtration columns because of either irregularities in shape or general affinity to the gel matrix. The shape of MGS is quite irregular, consisting of three small knobs which protrude from the main body of the protein and thus could result in the protein being retained by the gel-filtration matrix. While the kinetic Hill coefficient is consistent with a

homohexamer of a homotetramer, this can only be used as an approximate estimate of the oligomeric state of the protein. For this reason crystallographic structural analysis best represent the solution oligomeric state of the protein. In these more recent studies MGS was found to be made up of 6 monomeric subunits. For this reason, in the work presented here, the strucutre of MGS is assumed to be the homohexmeric structure suggested in the literature from 2000 onwards. Q TOF mass spectrometry shows unequivocally a monomeric molecular weight of 16,918 Da. Thus the overall molecular weight of the protein was assumed to 101,508 Da.

2.4 UV-Vis spectrophotometric assay of the background elimination of substrates.

In this section the results obtained from the UV-vis spectrophotometric background elimination assays of DHAP (1) and the mutant substrates HA (49), DHA (26), DHAS (27), BHA (22) and DHATS (25) are presented. Elimination assays were carried out based on an adaptation of the assay developed by Hopper and Cooper [65] to determine the activity of MGS.

2.4.1 MGS assay

The MGS activity assay is an exploitation of the detoxification mechanism used by the cell to remove harmful methylglyoxal (see Chapter 1). In this method developed by Hopper and Cooper, spectrophotometric measurement of the activity of MGS is achieved via a coupled assay in which the reaction of MG (8) with glutathione results in the formation of a thiohemiacetal. Excess glyoxalase I subsequently converts this product to D-lactoylglutathione (λ_{max} = 240 nm). From this assay one unit of MGS activity is defined as the amount of enzyme required for the

formation of 1 μmol of MG or D-lactoylglutathione/minute with 1 μL of D-lactoylglutathione reported as having an extinction coefficient (ε) of 3.4 mM^{-1} cm^{-1}.

Attempts to obtain the background rates for elimination of each of the 'mutant' substrates as well as commercially available dihydroxyacetone (DHA) and hydroxyacetone (HA) were made using an adaptation of this assay. However rather than using MGS to induce elimination, the formation of methylglyoxal would be carried out using a series of buffers in the pH 7-11 range (Scheme 2.23).

Scheme 2.23: Formation of D-lactoylglutathione

B = Buffer base or HO⁻

$X = OPO_3^{2-}, SSO_3^-, OSO_3^-, OH$

Glyoxalase I   Reduced Glutathione

D-lactoylglutathione

The formation of methylglyoxal is common to all of the potential elimination reactions of mutant substrates. Therefore it was believed that the assay would provide an alternative method for following the overall elimination reactions of mutant substrates.

2.4.1.1 Reproduction of the extinction coefficient (ε) of D-lactoylglutathione (9)

Before 'applying' the mutant substrates to the UV-vis spectroscopic assay, the literature extinction coefficient, ε of D-lactoylglutathione was reproduced in three separate experiments: 1) directly from commercially available D-lactoylglutathione (9), 2) from the reaction of commercially available methylglyoxal (40 wt % H_2O) with reduced glutathione and glyoxalase I (Scheme 2.24) and 3) from the reaction of natural substrate DHAP (1) in imidazole buffer, followed by the addition of reduced glutathione and *glyoxalase I* (Scheme 2.25). The literature extinction coefficient determined by Hopper and Cooper was obtained via method 3) using MGS to convert DHAP (1) to methylglyoxal (8). Reproduction of the extinction coefficient for D-lactoylglutathione from each of these experiments provides a value that can be used in the quantification of the progress of elimination for each of the 'mutant' substrates.

For method 1), a series of dilutions of a stock solution of commercially available D-lactoylglutathione were made and the absorbance for each concentration was measured in imidazole buffer at pH 7.1, I = 0.1 (KCl) and at 37 °C. The extinction coefficient, ε, was thus taken as the slope of the plot of absorbance (240 nm) against concentration (mM) of D-lactoylglutathione.
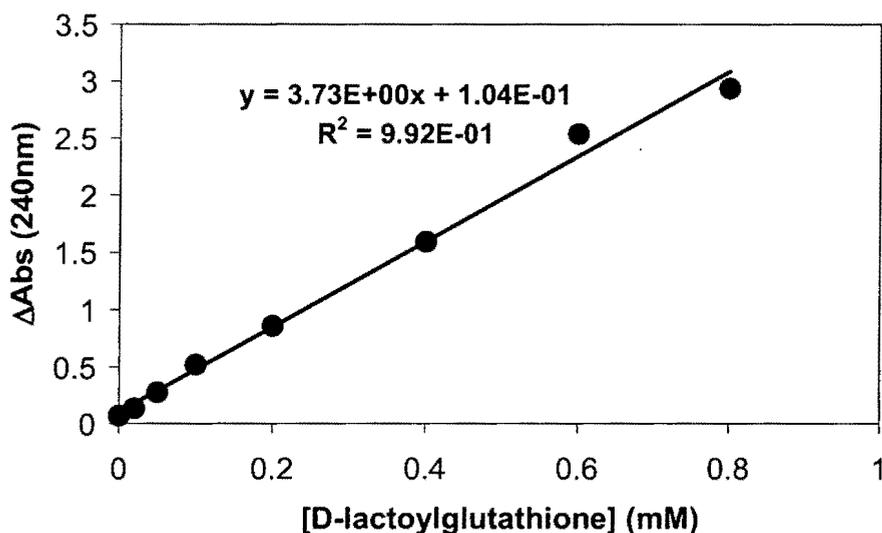
Shown below in Table 2.24 are the absorbance changes relative to concentration of D-lactoylglutathione. Each solution (total volume 1mL) contained D-lactoylglutathione (0-0.8 mM), imidazole buffer (40 mM) and KCl (0.1M). The absorbance (Abs_{240}) measured where no D-lactoylglutathione is present in solution is due to the absorbance of imidazole buffer.

Table 2.24: Changes in absorbance (240 nm) with respect to D- lactoylglutathione concentration (0-0.8 mM) at pH 7.1 at 37 °C (I = 0.1, KCl).

[D-lactoyl glutathione][a] (mM)	[Imidazole][b] (mM)	[KCl][c] (mM)	Absorbance[d] (Abs $_{240}$)	ε (mM^{-1} cm^{-1})
0	40	100	0.070	
0.02	40	100	0.134	
0.05	40	100	0.276	
0.10	40	100	0.519	3.73
0.20	40	100	0.859	
0.40	40	100	1.592	
0.60	40	100	2.535	
0.80	40	100	2.936	

(a) 0, 2, 5, 10, 20, 40, 60 and 80 μL of a D-lactoylglutathione stock solution (10 mM) were added to give the corresponding concentrations of 0, 0.02, 0.05, 0.1, 0.2, 0.4, 0.6 and 0.8 mM in a final volume of 1 mL. (b) 400 μL of imidazole buffer (100 mM, I = 0.1 (KCl)) were added to each reaction. (c) The volume of KCl (100 mM) added to each reaction varied relative to the volume of D-lactoylglutathione. The volume added brought the total assay volume to 1mL. (d) The absorbance of each solution was monitored at 240 nm. The pH of each assay solution was in the range of 7.07-7.09.

Figure 2.64: Experimentally determined extinction coefficient, ε for D- lactoylglutathione (0-0.8 mM) in imidazole buffer (100mM), at 37 °C (I = 0.1 , KCl).

The experimentally determined ε of 3.73 mM^{-1}cm^{-1} is in fair agreement with the literature value of 3.4 mM^{-1} cm^{-1}.

For method **2)**, a series of dilutions were made of a MG stock solution. The absorbance of a solution containing MG, imidazole, KCl and reduced glutathione was measured and the assay was initiated by the addition of glyoxalase I to the solution. Each solution (total volume 1mL) contained MG (0-0.8 mM), imidazole buffer (40 mM), reduced glutathione (1.4 mM) and KCl (0.1M). The assays were initiated on addition of glyoxalase I (4.4 µg/mL). The absorbance (Abs$_{240}$) measured where no methylglyoxal is present in solution is due to the absorbance of imidazole buffer and reduced glutathione.

A value of ΔAbs $_{240}$ was obtained from the observed difference in absorbance of the solution containing glyoxalase I and that without the glyoxalase I. Both measurements were obtained ten minutes after mixing all the assay components.

Scheme 2.24: Reaction of methylglyoxal with reduced glutathione and *glyoxalase I* to form D-lactoylglutathione.

λ$_{max}$ **240 nm**

The extinction coefficient was taken as the slope of the plot of Δ Abs $_{240}$ nm (Equation 2.25).

$$\Delta \text{ Abs }_{240} = A_{240+\text{Glx I}} - A_{240-\text{Glx I}} \qquad \textbf{Equation 2.25}$$

Shown below in Table 2.25 are ΔAbs$_{240}$ values obtained at different concentrations of methylglyoxal.
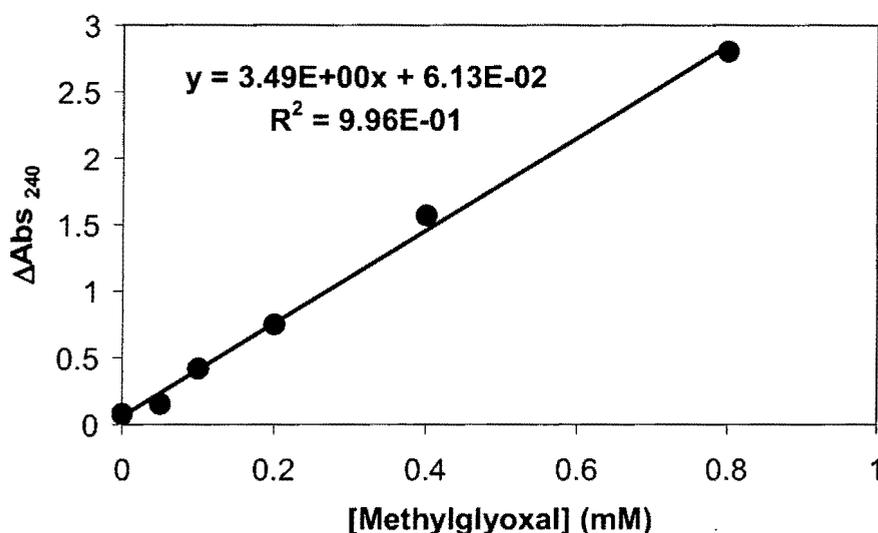
Table 2.25: Changes in absorbance (240 nm) with respect to methylglyoxal concentration (0-0.8 mM) at pH 7.1, at 37 °C (I = 0.1, KCl).

$[MG]^a$ (mM)	$[Imidazole]^b$ (mM)	$[GSH]^c$ (mM)	$[KCl]^d$ (mM)	Glyoxalase I^e (µg/mL)	Absorbance^f (Δ240nm)	ε (mM^{-1} cm^{-1})
0	40	1.4	100	4.4	0.081	
0.05	40	1.4	100	4.4	0.155	
0.10	40	1.4	100	4.4	0.419	
0.20	40	1.4	100	4.4	0.749	3.55
0.40	40	1.4	100	4.4	1.568	
0.80	40	1.4	100	4.4	2.803	

(a) 0, 2.5, 5, 10, 20 and 40 µL of a MG stock solution (20 mM) were added to give the corresponding final concentrations of 0, 0.05, 0.1, 0.2, 0.4 and 0.8 mM in a total volume of 1 mL. (b) 400 µL of imidazole buffer (100 mM) were added to each reaction giving a final concentration of 40 mM. (c) 70 µL of reduced glutathione (GSH, 20 mM) were added to each reaction giving a final concentration of 1.4 mM. (d) The volume of KCl (100 mM) added to each reaction varied relative to the volume of DHAP. The volume added brought the total assay volume to 1mL. (e) 2µL of glyoxalase I (2.2 mg/mL) was added after the absorbance of the solution containing all other reagents was measured giving a final concentration of 4.4 µg/mL. (f) Absorbance changes were monitored at 240 nm. The pH of each assay solution was in the range of 7.12-7.13.

Figure 2.65: Determination of an extinction coefficient, ε for D- lactoylglutathione from the reaction of methylglyoxal (0-0.8 mM), reduced glutathione (1.4 mM) and glyoxalase I (4.4 µg/mL).

$y = 3.49E+00x + 6.13E-02$
$R^2 = 9.96E-01$

The experimentally determined extinction coefficient, ε, of 3.49 mM^{-1} cm^{-1} is in good agreement with the literature value of 3.4 mM^{-1} cm^{-1}.

For method **(3)**, a series of dilutions of a DHAP **(1)** stock solution were made. Each solution (total volume 1mL) contained DHAP (0.1-0.8 mM), imidazole (40mM), KCl (0.1 M) and reduced glutathione (1.4mM). The assay was initiated by the addition of glyoxalase I (4.4 µg/mL) to the background solution and the subsequent increase in absorbance was quantified after waiting for 10 minutes (Scheme 2.25). This was repeated for separate assay solutions over several time points until the absorbance change recorded levelled off, consistent with complete conversion of DHAP **(1)** to MG **(8)** in the buffered solution.

235

Scheme 2.25: Reaction of DHAP with reduced glutathione and *glyoxalase I* to form D-lactoylglutathione.

λ_{max} 240 nm

The extinction coefficient was recorded as the slope of the plot of Δ Abs 240 nm (Equation 2.26).

$$\Delta \text{ Abs }_{240} = A_{240+\text{Glx I}} - A_{240-\text{Glx I}}$$ **Equation 2.26**

All of the above assays were run at a fixed ionic strength of 0.1 (KCl) and at 37 °C.

Shown below in Figure 2.66 are the absorbance changes relative to concentration of DHAP (1).

Figure 2.66: Plot of Δ Abs against time for DHAP (0.1-0.8 mM) elimination in imidazole buffer (● 0.1 mM, ◊ 0.2 mM, ● 0.4mM, ● 0.5 mM, ▲ 0.8 mM).

The data from Figure 2.66 was combined by plotting ΔAbs against concentration of DHAP (Figure 2.67). It was found that over long reaction times the ΔAbs values decreased. This was presumed likely due to methylglyoxal decomposition in solution. Thus the values for ΔAbs were taken at approximately 30000 seconds. The extinction coefficient, $\varepsilon = 3.09$ mM^{-1}cm^{-1}, is once again in fair agreement with the literature value of 3.4 mM^{-1} cm^{-1}.

Figure 2.67: Experimentally determined extinction coefficient for D- lactoylglutathione from the reaction of DHAP (1).

$y = 3.09E+00x + 1.03E-01$
$R^2 = 9.81E-01$

2.4.1.2 Elimination assays of 'mutant' substrates.

To test the viability of the 'adapted' assay procedures described above, it was decided to monitor the elimination reactions of the mutant substrates, hydroxyacetone (HA), **(49)**, dihydroxyacetone (DHA) **(26)**, DHAS **(27)**, DHATS **(25)** and BHA **(23)** by this UV-Vis assay method. From this assay we envisaged obtaining the pseudo first order rate constant, k_{obs} (s^{-1}), for the elimination reactions in various basic buffers such as quinuclidinone and quinuclidine. The UV-Vis spectrophotometric elimination assays for HA **(49)** and DHA **(26)** were carried out in quinuclidine buffers, 50 % f_B (pH 11), at 37 °C (I = 0.1, KCl). Each experiment consisted of mixing a solution of DHA or HA (15mM, I = 1.0 (KCl), total substrate concentration) with a solution of buffer (0.5M, I = 1.0 (KCl), total buffer concentration) in a 1: 10 ratio of substrate to

buffer respectively. The reaction solution was then incubated at 37 °C. At certain time-intervals aliquots of 250 µL of the reaction solution were withdrawn and quenched to pH 7 and added to a 1mL cuvette containing imidzole (40 mM), reduced glutathione (1.4mM) and KCl (0.1M). The solution was mixed gently and the absorbance at 240 nm was obtained over a period of ten minutes. Following this measurement, Glyoxalase I (2.2 µg/mL) was added to the solution in the 1mL cuvette and the absorbance was measured. The increase in absorbance, due to the formation of D-lactoylglutathione (9), would quantify the elimination of either substrate to form methylglyoxal (8), the precursor to D-lactoylglutathione.

For initial studies on the elimination assay, reactions were monitored directly i.e. solutions contained all reagents and the increase in absorbance was monitored over time as the concentration of MG and thus D-lactoylglutathione increased. However this method was not viable as an increase in ΔAbs_{240} was also observed over longer periods of time for solutions containing only buffer, reduced glutathione and KCl. This was possibly due to the oxidation of the reduced glutathione. Furthermore it was presumed that glyoxalase I would be quite unstable in solution over long periods of time.

For the substrates DHA (26) and HA (49) elimination was not expected to occur given the nature of the leaving groups, OH⁻ and H⁻ of the respective molecules (Scheme 2.26).

Scheme 2.26: 'Elimination' reactions of DHA (26) and HA (49).

The reaction of DHA was monitored in quinuclidine buffer (22.5 mM, 50% f_B) at 37 °C (I = 0.1, KCl) at pH 12. The observed change in absorbance, ΔAbs was calculated according to Equation 2.27 below.

$$\Delta_{Abs} = Abs_{240+Glx\ I} - Abs_{240-Glx\ I} \qquad \textbf{Equation 2.27}$$

Table 2.26: ΔAbs for the reaction of DHA (26) (0.75 mM) in in quinuclidine buffer (22.5 mM, 50 % f_B) at 37 °C (I = 1.0, KCl) and at pH 12.

Time(sec)	Abs_{240}[a]	$Abs_{240+GlxI}$	Δ Abs
0	0.622	0.631	0.009
1200	0.653	0.663	0.010
2400	0.645	0.658	0.013

240

4800	0.643	0.655	0.012
154800	0.624	0.639	0.015

a) Stock solutions of DHA (15 mM, I = 1.0 (KCl)) and buffer (0.25 M, I = 1.0 (KCl) were prepared and diluted 1:2 and 1:10 respectively in H$_2$O. The diluted DHA solution (500 µL) was added to 4.5 mL of the diluted buffer solution. The 5 mL solution was mixed and incubated at 37 °C. Aliquots of 250µL were withdrawn, quenched to pH 7and assayed at the specific times indicated above. Along with substrate and buffer each assay solution contained imidazole buffer (from a stock solution of 100 mM, 490µL were added giving a final assay concentration of 49 mM), reduced glutathione (70 µL of a 20 mM stock were added giving a final assay concentration of 1.4 mM), H$_2$O (500 µL) and glyoxalase I (1 µL of a 2.2mg/mL sample were added giving a final assay concentration of 2.2µg/mL). The final concentration of HA in each 1 mL cuvette was 0.187 mM while the final concentration of quinuclidine buffer was 6.2 mM.

It can be seen from the data shown that over an extensive time period Δ Abs remains constant. This indicates that essentially no elimination is occurring.

Shown below in Table 2.27 is the data obtained for the 'elimination' reaction of HA.

The reaction of HA was also monitored in quinuclidine buffer solution (22.5 mM, 50 % f$_B$), at pH 12.

Table 2.27: ΔAbs for the reaction of HA (49) (0.75 mM) in in quinuclidine buffer (22.5 mM, 50 % f_B) at 37 °C (I = 1.0, KCl) and at pH 12.

Time(sec)	Abs$_{240}$	Abs$_{240+GlxI}$	Δ Abs
0	0.621	0.635	0.014
300	0.613	0.625	0.012
1920	0.619	0.637	0.018
3300	0.622	0.633	0.011
4620	0.624	0.637	0.013

a) Stock solutions of HA (15 mM, I = 1.0 (KCl)) and buffer (0.25 M, I = 1.0 (KCl) were prepared and diluted 1:2 and 1:10 respectively in H_2O. The diluted HA solution (500 μL) was added to 4.5 mL of the diluted buffer solution. The 5 mL solution was mixed and incubated at 37 °C. Aliquots of 250μL were withdrawn, quenched to pH 7and assayed at the specific times indicated above. Along with substrate and buffer each assay solution contained imidazole buffer (from a stock solution of 100 mM, 490μL were added giving a final assay concentration of 49 mM), reduced glutathione (70 μL of a 20 mM stock were added giving a final assay concentration of 1.4 mM), H_2O (500 μL) and glyoxalase I (1 μL of a 2.2mg/mL sample were added giving a final assay concentration of 2.2μg/mL). The final concentration of HA in each 1 mL cuvette was 0.187 mM while the final concentration of quinuclidine buffer was 6.2 mM.

Similarly this reaction proceeded with little or no change in absorbance over time suggesting that no elimination occurs.

Based on the elimination reactions of DHAP (1) monitored by the above assay method, it was expected that the mutant substrates DHAS (27) and DHATS (25) and BHA (22) could eliminate given that sulfate, thiosulfate and bromide groups are reasonably good leaving groups (Scheme 2.27).

Scheme 2.27: Elimination mechanism for DHAS (27), DHATS (25) and BHA (22).

X = OSO$_3^-$, SSO^{3-}, Br

Assay analyses of the monoanionic substrates DHAS (27) and DHATS (25) and neutral substrate BHA (22) were carried out by Erasmus student Enrique Riveiros-Santiago (whom I supervised when doing the assays). The assays were carried out in the same manner as the previously described assays for HA (49) and DHA (26). The assays for DHAS (27) were carried out at three different final concentrations of substrate, 0.2, 0.4 and 0.6 mM. Shown below in Table 2.28 is the data for the imidazole (50 % f$_B$, I =0.1 (KCl)) catalyzed elimination reaction of DHAS (0.2, 0.4 and 0.6 mM) at 37 °C.

Table 2.28: Reaction of DHAS (0.2, 0.4 and 0.6 mM), imidazole buffer (20 mM, 50 % f$_B$), at

37 °C (I = 1.0, KCl) and at pH 7.

[DHAS] (mM)[a]	Time(sec)	Abs $_{240}$	Abs $_{240+GlxI}$	ΔAbs
	0	0	0	0
	3580	0.366	0.399	0.033
0.200	70,330	0.404	0.425	0.021
	86,640	0.411	0.435	0.024
	156,900	0.403	0.431	0.028
	0	0	0	0
	5460	0.355	0.451	0.096
0.400	72,900	0.391	0.485	0.094
	89,040	0.365	0.455	0.090
	159,300	0.359	0.455	0.096
	0	0	0	0
	7140	0.376	0.537	0.161
0.600	74,520	0.376	0.536	0.160
	90,240	0.356	0.520	0.164
	160,560	0.388	0.549	0.161

a) Stock solutions of DHAS (50 mM, I = 1.0 (KCl)) and buffer (100 mM, I = 0.1 (KCl)) were prepared and diluted 1:250 and 1:5 respectively in H_2O giving final DHAS concentrations of 0.2-0.6 mM and final buffer concentrations of 20mM. All other reagents were added as described for the previous assays of DHA and HA.

From Table 2.28 it can be seen that over extensive periods of time there was little change in the absorbance at 240nm. This implied that under these assay conditions dihydroxyacetone sulfate (27) appears not to eliminate.

Similarly for the reaction of BHA (22) in imidazole buffer (50 % f_B, pH 7.1) no absorbance was observed over long time frames (70,000 seconds). Due to the presence of glutathione it was presumed that rapid cleavage of the bromo substituent by the thiol of this peptide would occur thus leading to no observed absorbance change.

The elimination reactions of DHATS (25) were monitored in the same manner as for DHAS (27). However for this substrate a significant increase in absorbance was observed almost instantaneously after mixing. In this case it appeared that 'elimination' occured so fast that the most of the reaction had gone to completion after only a few hundred seconds. However as mentioned in Section 2.2.2, the reaction of DHATS (25) at pH 7 monitored by NMR spectroscopy did not lead to quantitative conversion to elimination product. Thus the rapid change in absorbance observed in the assay at 240 nm cannot be due to the formation of D-lactoylglutathione.

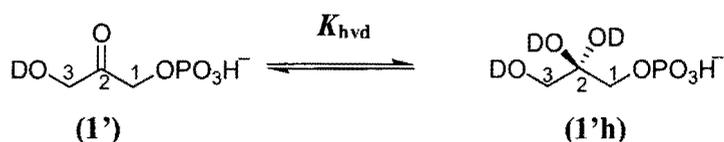## 2.4.2 ^{1}H NMR studies of the reactions of DHAP (1), DHA (26) and DHAS (27) in the presence of MGS.

High resolution ^{1}H NMR studies of the reaction of MGS in the presence of DHAP (1), DHA (26) and DHAS (27) were performed in a similar manner to the background reactions of the substrates discussed in Section 2.1. For each reaction, fixed amounts of substrate (5 mM) and methanol internal standard (2.5-10 mM) were used.

Prior to commencing the NMR experiments the MGS was dialysed in imidazole buffer (83 mM, I =0.1, KCl, pD = 7.9) at 4 °C. The buffer was initially left for 24 hours after which it was changed every 10 hours for a further 72 hours. This ensured complete deuterium exchange of all exchangeable MGS protein sites had occurred. Immediately prior to use the enzyme was gently syringed out of the cassette and stored in the fridge. After dialysis the volume of the enzyme was approximately 1.8 mL thus resulting in a final concentration of 1.96 mg/mL. To ensure complete accuracy in the kinetic results the activity of MGS was tested immediately prior to each NMR experiment.

2.4.2.1 The reaction of DHAP (1) in the presence of MGS

The elimination of DHAP (1) in the presence of MGS occurs rapidly to yield methylglyoxal and inorganic phosphate. As with the other substrates mentioned in this chapter, in solution the carbonyl group of DHAP (1) is hydrated (Scheme 2.28).

Scheme 2.28

$$K_{hyd} = [1h']/[1']$$ **Equation 2.28**

A representative partial ^{1}H NMR spectrum of DHAP (10 mM) (1) is shown below in Figure 2.68. At the pD of the zero timepoint shown below DHAP will be protonated and thus will be present as a monoanion. The equilibrium constant for the equilibrium between the free ketone and hydrate form of monomeric DHAP is represented by Equation 2.28.

The relative areas of peaks corresponding to DHAP (1') were integrated relative to the CH$_3$ hydrogens of acetic acid. The extent of carbonyl hydration of the molecule in acetic acid buffer (10% f_B) was found to be approximately 48 % ($K_{hyd} = 0.92$) from the relative areas of the signals due to the hydrate and keto forms of the molecule.

Figure 2.68 Representative ^{1}H NMR spectrum at 500 MHz of DHAP (1') (5 mM, pD 3.81), obtained at zero reaction time in acetic acid buffer (10 % f$_B$) at 25 °C (I = 1.0, KCl).

The doublets **A** (which is slightly obscured by the HOD peak) and **C** at 4.6ppm and 3.9 ppm respectively correspond to the C1 methylene hydrogens ($CH_2OPO_3^{2-}$) of the free keto and hydrate forms of the molecule respectively. The singlets **B** (4.59 ppm) and **D** (3.85 ppm) correspond respectively to the C3 methylene hydrogens of the free keto and hydrate forms of DHAP **(1)**. The singlet at 3.3 ppm is due to the CH_3 protons of acetic acid buffer.

For the reactions of DHAP **(1)** in the presence of MGS each NMR spectrum was recorded over a time period of 5 minutes (16 transients). The reaction time t was calculated from the mid-point of the times analyzed. Back to back spectra were obtained over time as the NMR tube was in the probe throughout the reaction.

248

Shown in Figure 2.69 are the representative partial ^{1}H NMR spectra for the reaction of DHAP (5 mM) in the presence of MGS (0.06 µg/mL), imidazole buffer (83 mM) at I = 0.1 (KCl) and 25 °C. The final concentration of MGS in the NMR tube represented a 1/30,000 dilution of concentrated MGS (1.96 mg/mL).

Figure 2.69: Representative partial ^{1}H NMR spectra for the elimination of DHAP (5 mM) catalyzed by MGS (0.06 µg/mL) in the presence of imidazole buffer (83 mM, 70% f_B, pD 7.9), I = 0.1 (KCl) at 25 °C. Methanol is present as internal standard (10mM). The reaction time is indicated above each spectrum.

The singlet E (5.13 ppm) corresponds to the C1 hydrogen of methglyoxal monohydrate. The singlet corresponding to the C1-hydrogen of the bis-hydrate is not visible in this spectrum. Given that the singlet due to the monohydrate has been shifted upfield by 0.12 ppm (relative to the corresponding singlet seen in buffers used to monitor elimination of DHAS (27) and BHA (22) it

249

is probable that the singlet due to the bis-hydrate of methylglyoxal has also been shifted upfield and has been masked by the HOD peak at 4.65 ppm. A similar occurance was observed for commercial methylglyoxal (40 wt %) in the presence of imidazole buffer. Over the timecourse of the reaction no other products other than the MG were observed. Also it was noted that MGS does not catalyze deuterium exchange of the α-carbonyl protons at the $CH_2OPO_3^{2-}$ side of the molecule. Furthermore it was observed that in buffers of higher pD values, a positional switch occurs of the peaks **A** and **B** due to the CH_2OD and $CH_2OPO_3^{2-}$ methylene hydrogens of the keto form of DHAP respectively when compared to the zero reaction time spectrum shown in Figure 2.64.

This is presumed to be due to a change in the phosphate protonation state of the molecule in going from reactions in lower pD buffers such as acetic acid to higher pD buffers where the substrate will be predominantly in the dianionic form.

As phosphate allosterically inhibits the enzyme, for a reaction of DHAP (5 mM), it should be expected that elimination would be retarded as time progresses in particular as high DHAP concentrations are required for analysis by ^{1}H NMR. Indeed it can be seen from the NMR spectra that the formation of MG reaches a limiting point after 25 minutes. This can be attributed to the inhibitory nature of the phosphate elimination product which accumulates over the time periods indicated above each spectrum. The progress of the elimination reaction of DHAP **(1)** was monitored by determining the integrated area of the singlet **E** (due to the monohydrate proton of methylglyoxal) over time relative to the integrated areas of singlets **B** and **C**, due to the $CH_2OPO_3^{2-}$ keto and hydrate protons of DHAP **(1)** at zero reaction time. The fraction of product formed, $f(p)$, was determined from Equation 2.29.

$$f(p) = \frac{(2(A_{MG}/0.6))}{(A_{CH2OP}\text{-keto} + A_{CH2OP}\text{-hydrate})_0} \qquad \textbf{Equation 2.29}$$

The percentage of methylglyoxal present as the monohydrate is 60 % and thus Equation 2.22 is derived from the fact that only the singlet due to the C1-H of methylglyoxal is visible.

Alternatively, the progress of the elimination reaction of DHAP **(1)** in the presence of MGS could be monitored by determining the sum of the integrated peak areas of the singlets **A** and **D** at time t over time zero. The fraction of substrate remaining, $f(s)$, was determined from Equation 2.30.

$$f(s) = \frac{(A_{CH2OD\text{-Keto}} + A_{CH2OD\text{-hydrate}})_t}{(A_{CH2OD\text{-Keto}} + A_{CH2OD\text{-hydrate}})_0} \qquad \textbf{Equation 2.30}$$

Reaction data for the formation of the methylglyoxal due to the elimination reaction of DHAP **(1)** in the presence of MGS are shown below in Table 2.29.

Table 2.29: Reaction data for the elimination reaction of DHAP (1) in imidazole buffer 70% f$_B$, 83 mM (pD 7.9) in D$_2$O at 25 °C (I=0.1, KCl) in the presence of MGS (0.06 µg/mL).

pD[a]	[MGS] (µg/mL)	Time (s)	f(p)[b]	f(s)[c]	f(p) + f(s)
		0	0	0	0
		150	0.1	0.867	0.967
		360	0.246	0.754	1.000
7.9	0.06	540	0.294	0.625	0.919
		720	0.311	0.613	0.924
		900	0.293	0.627	0.920
		1230	0.314	0.604	0.918
		1590	0.311	0.592	0.903

(a) Measurements were made in imidazole buffer, 70 % f$_B$ (83 mM, total buffer concentration) at pD 7.9 with MGS (0.06µg/mL). (b) The fraction of product formed, f(p), was calculated according to Equation 2.29. c) The fraction of substrate remaining, f(s) was calculated according to Equation 2.30 Measurements were made at an initial substrate concentration of 5 mM.
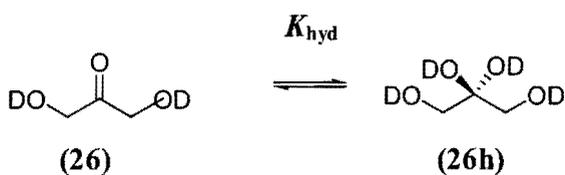
Thus it can be seen that the f(s) and f(p) values sum at all timepoints to approximately unity within experimental error indicating that only an elimination reaction is occurring.

The background solution reactions of DHAP (1) in the absence of MGS were not carried out in this work. However previous work by Dr. AnnMarie O'Donoghue have shown that formation of methylglyoxal in imidazole buffer (83mM, 70% f_B) at pD 7.9 at 25 °C occurs much more slowly. Over a timeframe of 15 hours under these conditions only 14% of methylglyoxal forms from reactant DHAP (1).

2.4.2.2 The reaction of DHA (26) in the presence of MGS

The reactions of dihydroxyacetone (DHA) (26) in the presence of MGS were monitored by 400 and 500 MHz ^{1}H NMR spectroscopy.

Scheme 2.29

(26)   (26h)

The equilibrium constant, K_{hyd}, can be represented by Equation 2.31

$$K_{hyd} = [26h]/[26] \qquad \textbf{Equation 2.31}$$

In buffered D_2O solutions the carbonyl group of DHA (26) is approximately 19 % hydrated (K_{Hyd} = 0.23) (Scheme 2.29). A representative partial ^{1}H NMR spectrum of DHA (10 mM) (26)

is shown below in Figure 2.70. The zero reaction time spectrum of DHA **(26)** was recorded in

DCl (1M) and 25 °C (I=1.0). Also present is imidazole (5 mM) as an internal standard.

Figure 2.70: Representative ^{1}H NMR spectra at 500 MHz of DHA (26) (5 mM), obtained at

zero reaction time in DCl at 25 °C (I = 1.0). Methanol (10mM) is present as the

internal standard.

The singlet **A** (4.26 ppm) corresponds to the methylene protons of the free keto form of DHA

(26). The corresponding hydrate form is represented by singlet **B** (3.41 ppm). The peak areas

were integrated relative to the CH_3 protons of methanol internal standard (3.19 ppm).

254

Prior to following the reaction of DHA (26) in the presence of MGS a background reaction in the absence of enzyme was carried out. Each NMR spectra was recorded over a time period of 40 minutes (128 transients). The reaction time t was calculated from the mid-point of the times analyzed. Shown below in Figure 2.71 are the partial ^{1}H NMR spectra for the reaction of DHA (26) in imidazole buffer (83 mM, 70 % f_B , pD 7.9), at 25 °C (I = 0.1, KCl).

Figure 2.71: Representative partial ^{1}H NMR spectrum for the reaction of DHA (5 mM) in imidazole buffer (83 mM, 70% f_B, pD 7.9), I = 0.1 (KCl) at 25 °C. Methanol IS (2.5mM). The reaction time is indicated above each spectrum (in minutes).

In the above spectra it can be seen that the peak areas of singlets A (4.26 ppm) and B (3.42 ppm) remain constant relative to methanol internal standard (peak C) over the time period investigated. No background exchange, elimination or isomerisation reactions were observed under these conditions. Shown in Figure 2.72 are the representative partial ^{1}H NMR spectra for the reaction of DHA in the presence of concentrated MGS (78.4 μg/mL).

Figure 2.72: Representative partial ^{1}H NMR spectrum for the reaction of DHA (5 mM) catalyzed by MGS (78.4 µg/mL) in the presence of imidazole buffer (83 mM, 70% f_B, pD 7.9), at 25 °C (I = 0.1, KCl). Methanol IS (2.5mM). The reaction time is indicated above each spectrum (in minutes).

In the above spectra it can be seen that over the time period investigated the peak areas **A** and **B** relative to internal standard **C** did not change despite the addition of a relatively high concentration of MGS.

The activity of MGS was monitored prior to, during and after each NMR experiment to ensure accurate kinetic results. Shown below in Table 2.29 are the absorbances obtained at 240 nm and 25 °C for a 1mL assay solution containing no MGS (fully dialyzed) and the same solution

containing MGS (0.071 µg/mL). The change in absorbance indicates the activity of the enzyme

and can be compared to the data in Table 2.30 and Equation 2.32 shown below.

$$\Delta Abs = Abs_{+MGS} - Abs_{-MGS} \qquad \textbf{Equation 2.32}$$

Table 2.30: Determination of MGS activity prior to, during and after ^{1}H NMR kinetic experiments. Absorbance measurements were made over ten minute time frames.

Time (sec)	Abs $_{-MGS}$	Abs$_{+MGS}$	ΔAbs
0	1.670	2.727	1.057
90	1.599	2.724	1.125
43200	1.604	2.814	1.210

In order to compare the activity of the MGS used in these experiments to V_{max} (Abs/min)

obtained from the Michaelis-Menten plots presented in the previous section (Table 2.23 and

Figure 2.63), a dilution of the MGS dialyzed sample (1.96 mg/mL) was made to have a

concentration comparable to the concentration of enzyme used in the former experiments (0.071

µg/mL). Therefore prior to each experiment a 1/900 dilution in imidazole buffer of the dialyzed

enzyme was made. From this solution 10 µL were added to the assay described in Table 2.23

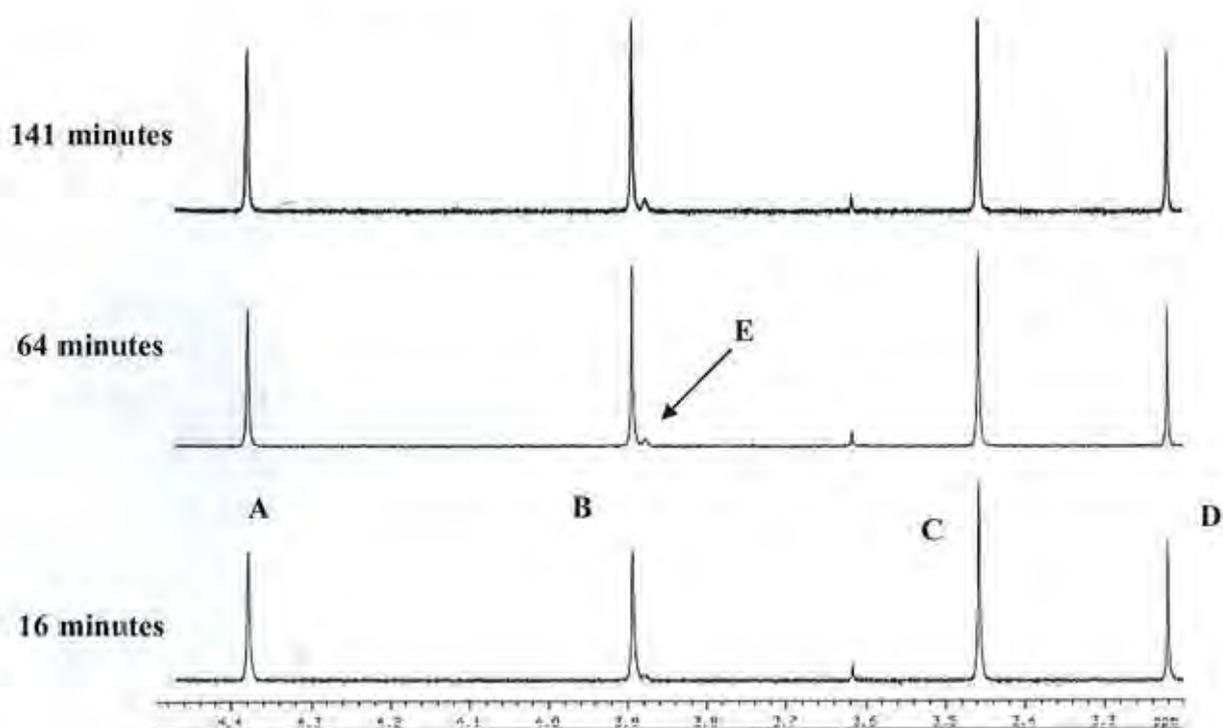giving a final concentration of 0.071 µg/mL of dialyzed enzyme. From Table 2.30 it can be seen

that at time zero an absorbance change of 1.057 occurs after a period of ten minutes. This refers to a ΔAbs of 0.106 per minute. During the reaction of the substrate the enzymes activity could also be monitored. For each ^{1}H NMR experiment a 1 mL sample was generally prepared which contained MGS (78.4 µg/mL). Each NMR tube contained 750 µL of solution thus the remaining 250 µL could be used for the assay. Of this remaining 250 µL a 1/110 dilution was made in imidazole buffer giving a concentration of 0.71 µg/mL. Of this solution, 10 µL was used for the assay giving a final MGS concentration of 0.071 µg/mL, the same concentration used in the assay described in Table 2.23. From Table 2.30 it can be seen that after 90 seconds of the NMR reaction a corresponding ΔAbs of 1.225 was observed in the assay. This corresponds to a ΔAbs of 0.123 per minute. Finally, it can be seen that after 43200 seconds of the NMR reaction a corresponding ΔAbs of 1.210 was observed in the assay. This corresponds to a ΔAbs of 0.121 per minute. As can be seen by the observed ΔAbs it can be seen that these values are very close to the value of $V_{max} = 0.11$ abs/min obtained from the Michaelis-menten assay plot in Figure 2.63.

2.4.2.3 The reaction of DHAS (27) in the presence of MGS

The reactions of DHAS (27) in the presence of MGS were monitored by 400 and 500 MHz ^{1}H NMR spectroscopy. As mentioned in section 2.1.1 the equilibrium constant for the hydration, $K_{Hyd} \sim 1.2$ for DHAS (27). Initially, reactions were carried out in the absence of MGS to obtain a background rate for exchange and elimination in the same buffer. The background reaction of DHAS (27) was monitored in imidazole buffer. The fraction of substrate remaining over time, f(s) was determined as described in Equation 2.2. The overall rate acceleration could thus be

obtained by repeating the reaction in the presence of MGS. The representative partial ^{1}H NMR spectra for the background non-enzymatic reaction of DHAS in imidazole buffer are shown below in Figure 2.73.

Figure 2.73: Representative partial ^{1}H NMR spectrum for the reaction of DHAS (5 mM) in imidazole buffer (83 mM, 70% f_B, pD 7.9), I = 0.1 (KCl) at 25 °C. Methanol is present as an internal standard (2.5mM). The reaction time is indicated above each spectrum (in minutes).

Each NMR spectrum for the background reaction was recorded over a period of 5 minutes (16 transients) with the reaction time t, calculated from the time at the midpoint of these analyses. No elimination was detectable for the non-enzymatic reaction of DHAS (27) under these conditions. Thus the singlets A (4.38 ppm) and C (3.44 ppm) corresponding to the methylene hydrogens of the CH_2OD group of DHAS (27) remained constant over the reaction time investigated relative

259

to methanol internal standard (singlet **D**). However deuterium incorporation at the C1 position of the molecule is observed. The singlet due to the methylene hydrogens, $CH_2OSO_3^-$ of the keto form of substrate has been omited from these spectra as for this experiment this peak was masked by the HOD solvent peak. However a small broad singlet **E** slightly upfield of singlet **B** at 3.99 ppm occurs which confirms deuterium exchange at this position. For this reason the fraction of substrate remaining, $f(s)$ was calculated according to Equation 2.33

$$f(s) = \frac{(A_{C1\text{-}CH2(Hyd)})_t}{(A_{C1\text{-}CH2(Hyd)})_0}$$

Equation 2.33

The observed pseudo first order rate constants for the disappearance of substrate could be determined as the slope of the semi-logarithmic plot of $f(s)$ against time (Equation 2.34)

$$\ln f(s) = -k_{obs}t$$

Equation 2.34

Shown below in Table 2.31 is the data for the disappearance of the C1-H singlet **B** (3.99 ppm). The values of k_{obs} (s^{-1}) shown in Table 2.31 were obtained as the slope of the semi logarithmic plot (Figure 2.75) of the fraction of substrate remaining, $f(s)$, against time.

Table 2.31: First order rate constants for disappearance of the C1 hydrogens of DHAS (27) in imidazole buffer 70% f_B, 83 mM (pD 7.9) in D_2O at 25 °C I=0.1 (KCl).

[MGS] (μg/mL)[a]	Time (s)	$f(s)$[b]	Ln $f(s)$	k_{obs} (s^{-1})
	0	1	0	
	960	0.947	-0.053	
	2430	0.911	-0.092	
0	3840	0.886	-0.120	2.79 x 10^{-5}
	6750	0.826	-0.190	
	8460	0.804	-0.217	
	11760	0.695	-0.363	

(a) Measurements were made in imidazole buffer, 70 % f_B (83 mM, total buffer concentration) at pD 7.9 with no added MGS. (b) The fraction of substrate remaining $f(s)$, was calculated according to Equation 2.33. Measurements were made at an initial substrate concentration of 10 mM. (c) The value of the first-order rate constant (k_{obs}^T) was obtained from the slope of the plot of ln $f(s)$ against time.

The representative partial ^{1}H NMR spectra for the reaction of DHAS in the presence of MGS (78.4 μg/mL) in imidazole buffer (70 % f_B) are shown below in Figure 2.74.

Figure 2.74: Representative partial ^1H NMR spectrum for the reaction of DHAS (5 mM) in the presence of MGS (78.4 µg/mL) and imidazole buffer (83 mM, 70% f_B, pD 7.9), at 25 °C (I = 0.1, KCl). Methanol is present as internal standard (2.5mM). The reaction time is indicated above each spectrum (in minutes).

Each NMR spectrum for the reaction of DHAS (27) in the presence of MGS was recorded over a period of 5 minutes (16 transients) with the reaction time t, calculated from the time at the midpoint of these analyses. Elimination was observed for the enzymatic reaction of DHAS (27) as seen by the singlet **E** in the spectra shown above. This singlet corresponds to the C1 proton of the monohydrate of elimination product methylglyoxal. The bishydrate singlet, along with the singlet corresponding to the $CH_2OSO_3^-$ protons of the keto form of DHAS have been obscured by the HOD peak in the spectra shown. The singlets **A** (4.38 ppm) and **C** (3.44 ppm) correspond to the methylene hydrogens of the CH_2OD group of DHAS (27). Deuterium incorporation at the C1 position of the molecule is observed. A small broad singlet **F** slightly upfield of singlet **B**

262

occurs which confirms deuterium exchange at this position. The peak at 3.2 ppm, **D**, corresponds to the CH_3 hydrogens of methanol internal standard.

The reactions of DHAS **(27)** were carried out in the presence of MGS at two different concentrations (19.6 µg/mL and 78.4 µg/mL), utilising 10 µL and 40 µL of the dialyzed MGS stock (1.96 mg/mL). The progress of the reaction at the C-1 side of substrate due to both exchange and elimination was monitored by determining the integrated peak area of the singlet **B** (due to the $CH_2OSO_3^-$ group of the hydrate form of DHAS) over time, t, relative to the sum of the same peak areas at zero reaction time. The fraction of substrate remaining, $f(s)$, was determined from Equation 2.33.

The pseudo first order rate constant k_{obs}^T (s^{-1}) is for the total disappearance of substrate due to both C1-H/D exchange and elimination. Shown below in Table 2.32 is the data for the disappearance of the C1-H singlet **B** (3.90 ppm) of DHAS **(27)** in the presence of MGS due to both exchange and elimination. The observed pseudo first order rate constant, k_{obs}^T (s^{-1}) due to the both C1-H/D exchange and elimination could be determined as the slope of the semi-logarithmic plot of $f(s)$ against time (Equation 2.33).

Table 2.32: First order rate constants for disappearance of the C1 hydrogens of DHAS (27) in the presence of MGS (19.6 µg/mL and 78.4 µg/mL), imidazole buffer 70% f_B, 83 mM (pD 7.9) in D_2O at 25 °C(I=0.1 KCl).

[MGS] (µg/mL)	Time (s)	$f(s)^b$	Ln $f(s)$	k_{obs}^T (s^{-1})
	0	1	0	
	2730	0.896	-0.109	
	3360	0.853	-0.157	
19.6	3990	0.814	-0.204	5.21×10^{-5}
	4650	0.791	-0.234	
	5310	0.756	-0.279	
	5970	0.744	-0.295	
	0	1	0	
	2520	0.784	-0.243	
	5250	0.587	-0.532	
78.4	7710	0.525	-0.644	8.61×10^{-5}
	32500	**0.136**	**-1.995***	

(a) Measurements were made in imidazole buffer, 70 % f_B (83 mM, total buffer concentration) at pD 7.9 with MGS (19.6 and 78.4 µg/mL). (b) The fraction of substrate remaining $f(s)$, was calculated according to Equation 2.32. Measurements were made at an initial substrate concentration of 5 mM. (c) The value of the first-order rate constants (k_{obs}^T (s^{-1})) were obtained from the slope of the plot of ln $f(s)$ against time.

The combined data for the non-enzymatic and enzymatic reactions of the C1-hydrogens of DHAS **(27)** are shown below in Figure 2.75. * Omited from spectrum due to error.

Figure 2.75: Semi-logarithmic plot of the fraction of remaining C1 hydrogens against time for the reaction of DHAS (27) in imidazole 70% f_B, I = 1.0 (KCl) at 25 °C, MGS (19.6 µg/mL) and MGS (78.4 µg/mL). (• 0 µg/mL, ■ 19.6 µg/mL, ▲ 78.4 µg/mL).

* The value for 0 µg/mL MGS is taken from Table 2.31

Whereas no elimination was detectable for the background reaction of DHAS **(27)**, this was observed for the reaction of the molecule in the presence of MGS (19.6 and 78.4 µg/mL). The pseudo first order rate constants, $k_{obs}^{Elim}(s^{-1})$ for the disappearance of the C3 hydrogens of DHAS due to elimination were calculated according to Equation 2.3 below. Reaction data and the

experimental first order rate constants for the elimination (k_{obs}, s^{-1}) for the disappearance of the C3 hydrogens of DHAS due to elimination are shown below in Table 2.33.

The observed pseudo first order rate constant, k_{obs} (s^{-1}) due to the C-3 elimination only could be determined as the slope of the semi-logarithmic plot of $f(s)$ (Equation 2.35) against time (Equation 2.36).

$$f(s) = \frac{(A_{C3-CH2(Hyd)})_t + (A_{C3-CH2(Keto)})_t}{(A_{C3-CH2(Hyd)})_0 + (A_{C3-CH2(Keto)})_0}$$
Equation 2.35

$$\ln f(s) = -k_{obs}t$$
Equation 2.36

Table 2.33: First order rate constants for disappearance of the C3 hydrogens of DHAS (27) in the presence of MGS (19.6 μg/mL and 78.4 μg/mL) imidazole buffer 70% f_B, 83 mM (pD 7.9) in D_2O at 25 °C I=0.1 (KCl).

[MGS] (μg/mL)	Time (s)	$f(s)^b$	Ln $f(s)$	k_{obs}^{Elim} (s^{-1})
	0	1	0	
	2730	0.954	-0.046	
	3360	0.943	-0.057	
19.6	3990	0.932	-0.070	1.53×10^{-5}
	4650	0.931	-0.073	
	5310	0.921	-0.081	
	5970	0.911	-0.092	
	0	1	0	
	2520	0.766	-0.048	
78.4	5250	0.694	-0.139	2.63×10^{-5}
	7710	0.527	-0.196	

(a) Measurements were made in imidazole buffer, 70 % f_B (83 mM, total buffer concentration) at pD 7.9 with MGS (19.6 and 78.4 μg/mL). (b) The fraction of substrate remaining $f(s)$, was calculated according to Equation 2.35. Measurements were made at an initial substrate concentration of 5 mM. (c) The value of the first-order rate constants (k_{obs}^{Elim}) were obtained from the slope of the plot of ln $f(s)$ against time.

The combined data for the enzymatic reactions of the C3-hydrogens of DHAS (27) obtained from the slopes of the semi-logarithmic plots of the fraction of substrate remaining, $f(s)$ against time are shown below in Figure 2.76.

Figure 2.76: **Semi-logarithmic plot of the fraction of remaining C3 hydrogens against time for the reaction of DHAS (27) in imidazole 70% f_B, I = 1.0 (KCl) at 25 °C, MGS (19.6 µg/mL) and MGS (78.4 µg/mL). (■ 19.6 µg/mL, ▲ 78.4 µg/mL).**

As discussed previously for the reaction of DHA (26), the activity of MGS was measured before, during and after the kinetic experiment (Equation 2.32). The ΔAbs values obtained are shown below in Table 2.34.

Table 2.34: Determination of MGS activity prior to, during and after ^{1}H NMR kinetic experiments. Absorbance measurements were made over ten minute time frames.

Time (sec)	Abs $_{-MGS}$	Abs $_{+MGS}$	ΔAbs
0	1.636	2.167	0.531
5250	1.509	2.038	0.529
7710	1.503	2.022	0.519

As described for monitoring the activity of diazlyzed MGS in the DHA (**26**) reactions, a dilution of the MGS dialyzed sample (1.96 mg/mL) was made to have a concentration comparable to the concentration of enzyme used in the former experiments (0.035 µg/mL in this case). Therefore prior to each experiment a 1/900 dilution in imidazole buffer of the dialyzed enzyme was made. From this solution 5 µL were added to the assay described in Table 2.22 giving a final concentration of 0.035 µg/mL of dialyzed enzyme. From Table 2.34 it can be seen that at time zero an absorbance change of 0.531 occurs after a period of ten minutes. This refers to a ΔAbs of 0.053 per minute. During the reaction of the substrate the enzymes activity could also be monitored. For each ^{1}H NMR experiment a 1 mL sample of was generally prepared which contained MGS (78.4 µg/mL). Each NMR tube contained 750 µL of solution thus the remaining 250 µL could be used for the assay. Of this remaining 250 µL a 1/110 dilution was made in imidazole buffer giving a concentration of 0.71 µg/mL. Of this solution, 10 µL was used for the assay giving a final MGS concentration of 0.071µg/mL, the same concentration used in the assay described in Table 2.22 and Figure 2.63. From Table 2.33 it can be seen that after 5250 seconds of the NMR reaction a corresponding ΔAbs of 0.529 abs/min was observed in the assay. This corresponds to a ΔAbs of 0.053 per minute. Finally, it can be seen that after 7710 seconds of the

NMR reaction a corresponding ΔAbs of 0.519 was observed in the assay. This corresponds to a ΔAbs of 0.052 per minute. As can be seen by the observed ΔAbs it can be seen that these values are very close to the value of V_{max} = 0.05 abs/min obtained from the Michaelis-Menten assay plots in Figure 2.63.

k_{cat} and K_M values for the reactions of MGS at the C1 and C3 positions of DHAS (27) were determined assuming that $K_M \gg$ concentration of DHAS (27), [S]. This leads to the form of the Michaelis-Menten equation shown in Equation 2.37 and Equation 2.38 below.

$$v_{obs} = k_{cat}/K_M[E][S] = k_{obs}[S] \qquad \textbf{Equation 2.37}$$

Thus the $k_{obs}(s^{-1})$ value, the slope of the semi-logarithmic plots for the reactions at the C1 and C3 positions of DHAS catalyzed by MGS can be equated to Equation 2.23.

Thus the separate values of k_{cat}/K_M for the MGS catalyzed reactions due to exchange and elimination at the C1 and elimination C3 positions of DHAS can be calculated.

Shown below in Table 2.35 and Table 2.36 are the combined results of kinetic studies of the reactions of DHAS (27) in the presence and absences of MGS.

Table 2.35: First order rate constants for the reaction of the C-1 and C-3 protons of DHAS in imidazole buffer (70% f_B, 83 mM) only and in the presence of imidazole buffer (70% f_B, 83 mM) and MGS (1.93 x 10^{-7} M (19.6 μg/mL) and 7.72 x 10^{-7} M (78.4 μg/mL)).

pD	[DHAS] (mM)	[MGS] (M)	k_{obs}^{Total} (s^{-1})	k_{obs}^{Elim} (s^{-1})	k_{obs}^{ex} (s^{-1})
7.9	5	0	2.79 x 10^{-5}	n/d*	2.79 x 10^{-5}
7.9	5	1.93 x 10^{-7}	5.21 x 10^{-5}	1.53 x 10^{-5}	3.68 x 10^{-5}
7.9	5	7.72 x 10^{-7}	8.61 x 10^{-5}	2.63 x 10^{-5}	5.98 x 10^{-5}

* Not detectable

Table 2.36: k_{cat}/K_M values for the reaction of DHAS in the presence of MGS (1.93 x 10^{-7} M and 7.72 x 10^{-7} M).

pD	[DHAS] (mM)	[MGS] (M)	k_{cat}/K_M^{Total} ($M^{-1}s^{-1}$)[a]	k_{cat}/K_M^{elim} ($M^{-1}s^{-1}$)	k_{cat}/K_M^{ex} ($M^{-1}s^{-1}$)
7.9	5	1.93 x 10^{-7}	125	79	46
7.9	5	7.72 x 10^{-7}	75	34	41

a) The final values of k_{cat}/K_M were calculated using a k_{obs} obtained by subtracting k_{obs}^{Total}, k_{obs}^{Elim} and k_{obs}^{Ex} (s^{-1}) for the background reaction of DHAS in imidazole from the corresponding values for the enzyme catalyzed reactions.

Chapter 3

Discussion

3.0 Foreword

This chapter will be divided into three sections. In Section 3.1 any difficulties encountered in synthesising the mutant substrates will be discussed. Also, any attempted alternative synthetic routes to each substrate will be presented. The discussion of the results obtained from the background kinetic studies of each mutant substrate will be presented in Section 3.2. In this section, comparisons of the rate constants obtained for the elimination and exchange of the mutant substrates will be made with existing kinetic data for compounds of similar structure and function. Finally in Section 3.3 the results obtained from the enzyme kinetic experiments carried out on the substrates DHAS **(27)**, DHAP **(1)** and DHA **(26)** will be discussed and compared to existing literature kinetic data for the reactions of TIM and MGS of these substrates.

3.1 Synthetic procedures and alternative routes investigated

Despite following literature procedures for the synthesis of the mutant substrates, the isolation and purification of the majority of the compounds investigated was not trivial. The ionic nature of the majority of these compounds and synthetic routes often leading to low yields ensured that the total synthesis of each compound was time-consuming. Furthermore, problematic issues such as decomposition and dimer formation meant that sound, reproducible kinetic experiments involving these substrates took some time to establish.

3.1.1 Bromohydroxyacetone (BHA)

This molecule was of vital importance in this project as it provided the synthetic basis for the formation of two other mutant substrates. Initial attempts to synthesise this molecule were made following a literature procedure of Druekhammer *et al* [91]. Formation of crude BHA **(22)** (which contained some NBS starting material) was achieved as discussed in Chapter 4. The fact that the synthesis of crude product was carried out in water ensured that direct flash column chromatography could not be achieved. Initial purification methods such as recrystallisation and size-exclusion chromatography proved unsuccessful in isolating purified BHA **(22)**. From later purification attempts it was discovered that the product could be isolated by flash column chromatography where the aqueous reaction mixture was concentrated to approximately 10 mL and 'dry-loaded' onto silica directly. This mixture was then dried under high vaccum for 5 hours (care had to be taken at this stage as over-drying led to decomposition, as judged by the formation of bromine vapours). Once dried, the silica mixture was slurried with the solvent system used for the column purification and loaded directly onto the top of the column. This dry-loading technique was not described in the literature procedure. Following successful isolation of the product BHA **(22)** further problems were encountered primarily due to the subsequent decomposition of the product compound. Evaporation of solvent led to a yellow oil which almost immediately decomposed to a black viscous oil. Analysis of the yellow oil by ^{1}H NMR indicated that the desired product had indeed been successfully isolated however subsequent analysis of the black 'oil' revealed an NMR spectrum with a large number of unassignable peaks. It is possible that decomposition occurred as a result of a side reaction with one of the species in Scheme3.1.
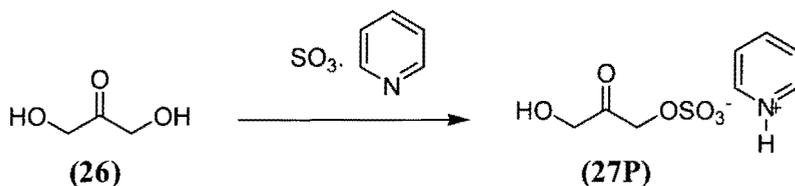
Scheme 3.1.

(50)

One potential route to the formation of elemental bromine from NBS is via a radical mechanism where two molecules of NBS homolytically cleave to form bromine and a bi-imide **(50)** product. Decomposition may have occurred as a result of the photolytic degradation of this molecule. The TLC of the fractions for bromohydroxyacetone indicated one large baseline spot however it is possible that this dimeric species had the same R_f as BHA **(22)** thus leading to decomposition on isolation. Druekhammer *et al* have suggested that recrystallisation of monomeric BHA from DCM results in the formation of a dimeric species **(23)**. Therefore all further concentration of relevant fractions after flash column chromatography involved evaporation of the solvent to approximately 10 mL (once the BHA spot had been identified from oxidative TLC) followed by the dropwise addition of approximately 10 mL of DCM and storage in the freezer. Storage for 3 days led to formation of crystalline dimer/monomer mixture which was subsequently stored at -4 °C. The formation of monomer from this dimeric species for the purposes of accurate kinetic studies has been discussed in Chapter 2.

3.1.2 Dihydroxyacetone sulfate (DHAS)

The synthesis and purification of this molecule was achieved by the method described in Chapter 2. However prior to using this synthetic route, a potentially 'simpler' route was investigated. Whereas the former synthetic method relied heavily on ion-exchange purification methods the latter method 'theoretically' involved purification based on 'simple' acid base properties of the molecules involved (Scheme 3.2).

Scheme 3.2

Following treatment of DHA (26) with sulfur trioxide-complex in DMF, which presumably would lead to the formation of the pyridyl salt (27P) product shown above, the reaction pH was brought to approximately 8 with potassium hydroxide. This would ensure complete deprotonation of the pyridyl salt (27P) to form pyridine and DHAS-potassium salt. Following a procedure of Whitesides *et al* [99] this method was attempted. Crude ^{1}H NMR spectra taken over regular time periods indicated that DHAS (27P) was indeed forming. After 24 hours (the time suggested in the literature) the DMF was evaporated and the pH brought to 8 with 2M KOH. Following this, distillation of pyridine was achieved resulting in a white-brown solid which was presumed to be the potassium salt of DHAS (27). However analysis of the product by ^{1}HNMR showed that the solid did not correspond to the desired sulfate product. Despite the presence of DHAS being apparent from ^{1}H NMR prior to concentration of DMF, following concentration of

solvent the peaks due to DHAS seemed to disappear. For each subsequent attempted synthesis of DHAS (27) using this method the outcome was the same despite attempted recrystallisation and size exclusion purification methods. To ensure that no solvent impurities were present fresh, anhydrous DMF was used for further reactions however the outcome was the same. Thus the alternative procedure presented in Chapters 2 [92] was ultimately used.

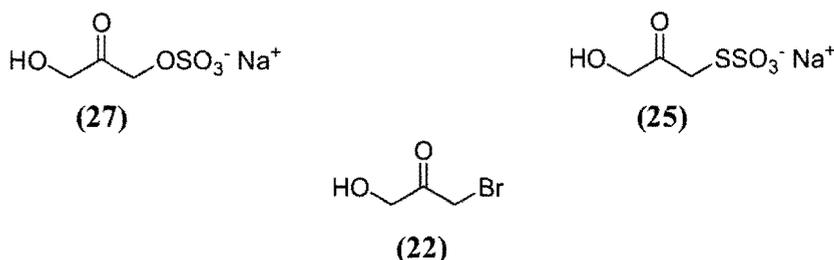## 3.2 Background, non-enzymatic ^{1}H NMR kinetic studies of mutant substrates

While being a fundamental chemical reaction, enolization forms the basis of a multitude of complex biological reactions. Deprotonation at the α-carbon position results in a "delocalised" carbanion where the bulk of the negative charge generally lies predominantly at the enolate oxygen [100, 101]. Enhancement of the acidity of the α-carbonyl protons and thus the overall rate of enolization can be achieved in a number of ways. Coordination of a Lewis acid or metal ion to this negatively charged oxygen is a favoured method of catalysis employed by a number of enzymes [102]. The fact that so many enzymes have evolved to electrophilically catalyze their respective reactions in this manner may suggest that the benefits of a high positive charge density outweigh the use of Brønsted acids for catalysis. However this is not always the case. Brønsted acid catalysis of enolization is equally important particularly when there is a thermodynamic driving force for proton transfer to the enolate of substrate [41, 103]. The fact that both MGS and TIM (among many enzymes) catalyze their respective reactions at rates close to the diffusion limit based purely on H-bonded interactions supports the latter case. In the case of the solution enolization background reactions of carbon acids such as those investigated in this work, lack of a tight binding active site pocket and electrostatic or electrophilic catalysts results

in a slower rate of enolization, and where permitted, elimination. In solution, non-enzyme catalyzed enolization is generally assumed to be rate-limiting for a variety of reactions involving key proton transfer steps. In these cases, rates of enolization and elimination can be affected due to substituent effects of the substrates in question.

3.2.1 Reactivities of DHAS (27), DHATS (25) and BHA (22) towards deprotonation at α-carbon.

Prior to carrying out non-enzymatic, solution ^{1}H NMR analysis of each of our 'mutant' substrates, (27), (25) and (22) predictions as to the extent of enolization or elimination for each compound were made based on their individual structures (Figure 3.1)

Figure 3.1

$$HO\diagdown\overset{\overset{O}{\|}}{C}\diagdown OSO_3^-\ Na^+$$
(27)

$$HO\diagdown\overset{\overset{O}{\|}}{C}\diagdown SSO_3^-\ Na^+$$
(25)

$$HO\diagdown\overset{\overset{O}{\|}}{C}\diagdown Br$$
(22)

It was expected that the susceptibility of the α-carbonyl protons of DHAS (27) and DHATS (25) to deprotonation and thus the rates for enolization and overall elimination should be similar. For BHA (22), a similar kinetic acidity of the α-carbonyl protons, certainly on the CH_2OD side and thus enolization was expected with perhaps a greater rate for elimination. This is based on the lower basicity of the bromide leaving group relative to thiosulfate and sulfate.

For similar substrates such as hydroxyacetone, proton transfer at carbon has been found to be rate-limiting for deuterium exchange in D_2O, and not any physical transport step. Thus in this case general base catalysis of exchange could be observed. As mentioned in Chapter 1, general base catalysis of elimination was observed for DHAP (1) at a range of pH values from pH 7.5-12. On this basis for the analogous reactions of substrates (27), (25) and (22) it was predicted that an increase in the buffer concentration would lead to an increase in the rate of enolization or elimination and this was found to be the case. Also, when comparing the reactivities of the C1 or C3 protons of each substrate towards deprotonation, significant differences in the overall rate constants were observed.

To quantify the significance of the rate constants obtained for the reactions of each substrate it is important to make comparisons with existing literature rates for enolization and elimination of substrates of similar structure. To date, there has been relatively little data confirming the rates of enolization and/or elimination on similar carbon acids with anionic substituents such as those presented in this work. However a wealth of information exists for the reactivity and enolization of molecules which are similar in size and structure although lack a charged functional group. These substituent effects on the rates will be presented prior to discussing the results obtained for the background enolization and elimination reactions of our own mutant substrates.
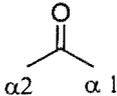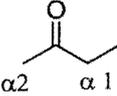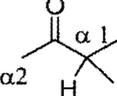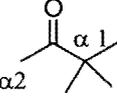
3.2.2 Enolization of acetone and alkyl substituted derivatives

Acetone is widely regarded as the prototypical carbonyl compound and therefore is a good starting point for comparing the rates of enolization with carbonyl compounds which are similar in structure. While a wide variety of methods have been used to determine rates of enolization,

279

most notably the classic halogen trapping methods discussed in Chapter 1, the majority of the literature rates discussed here were obtained by monitoring deuterium incorporation at the relevant α-carbon of the molecule in question. This provides a better comparison with the rates of enolization of the mutant substrates investigated in this work.

It is well established that for the H-D exchange reactions of simple ketones such as acetone, enolization is the rate-limiting step. Mechanistically, acid catalyzed enolization leads to a transition state where there is a net zero or positive charge buildup. For this reason the presence of alkyl groups can stabilise this transition state and thus enhance reactivities of the molecule in question. On the other hand, in basic media, mechanisms prevail which lead to an enolate like transition state where a buildup of negative charge occurs. In this case the reactivity of the species will be hampered by inductively electron donating alkyl groups. Thus depending on the media of reaction, rates of enolization are either increased or decreased relative to the corresponding rates for unsubstituted acetone. The second order rate constants, k_{OH} ($M^{-1}s^{-1}$) for the hydroxide catalyzed H-D exchange of acetone and several alkyl substituted derivatives obtained by Warkentin et al [104] are shown in Table 3.1.

Table 3.1: Second order rate constants for hydroxide catalyzed deprotonation of Cα1 and Cα2 protons of acetone and derivatives in aqueous solution.

Entry	Substrate	Base[a]	$k_{C\alpha\text{-}1}$ $(M^{-1}s^{-1})$	$k_{C\alpha\text{-}2}$ $(M^{-1}s^{-1})$	$k_{C\alpha\text{-}1}/k_{C\alpha\text{-}2}$ $(k_{rel})^{[b]}$
1		OH⁻	2.5×10^{-1}	2.5×10^{-1}	1.00
2		OH⁻	1.1×10^{-1}	1.3×10^{-1}	0.84
3		OH⁻	6.73×10^{-3}	8.36×10^{-2}	0.08
4		OH⁻	-	4.17×10^{-2}	-

a) Rates were measured at 32 °C and in 2:1 dioxane-D_2O solution (90-95 parts), ketone (5-10 parts). b) k_{rel} is determined as the ratio of the second order rate constant for deprotonation at the Cα-1 position to the Cα-2 position.

It is clear from the above second order rate data that substitution at the α-carbonyl carbon retards the rate of enolization at the substituted Cα-1 end of the molecule and also to a smaller extent at the Cα-2 site. For entry **2**, 2-butanone, the rate of enolization at the Cα-2 methyl position is approximately half of the observed rate for enolization of the corresponding methyl hydrogens of acetone. This could be accounted for by the statistically 2-fold smaller number of methyl hydrogens. The rate constant for enolization of the Cα1 protons of 2-butanone is approximately 15 % smaller than enolization at the Cα2 position. This indicates that the substitution effect is slightly greater at the Cα1 position. Further alkyl group addition (leading to entry **3**, methylisopropyl ketone, and entry **4**, methyl tertbutyl ketone) results in even greater retardation of the rate of deprotonation at both Cα positions relative to acetone. This is likely due to a combination of steric and electronic effects on kinetic acidities.

Further first order rate constants for deuteroxide catalyzed enolization at the Cα-1 and Cα-2 positions of 2-butanone are shown below in Table 3.2 as a function of base, concentration and temperature [105]. These data show again that the rates of deprotonation at the Cα-1 and Cα-2 positions are very similar (k_{rel} ~1) within error and that this similarity is maintained as temperature is changed. It could be argued that as there are statistically more Cα-2 protons, and that the true kinetic acidity of the Cα-1 protons is slightly greater than the Cα-2 protons. However the differences are small and likely within experimental error.

Table 3.2: Pseudo first order rate constants for deprotonation of 2-butanone with varying concentration of deuteroxide.
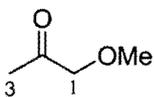
α2 α1 (M)	Temp (°C)	[DO⁻] (M)	$k_{obs\ C\alpha-1}$ (s^{-1})	$k_{obs\ C\alpha-2}$ (s^{-1})	k_{rel} ($k_{obs\ C\alpha-1}/k_{obsC\alpha-2}$)
1.67	35	0.040	2.4×10^{-3}	2.2×10^{-3}	1.06
1.67	35	0.009	5.3×10^{-4}	5.3×10^{-4}	1.03
1.40	35	0.020	1.3×10^{-4}	1.3×10^{-4}	1.00
2.20	0	0.039	1.7×10^{-4}	1.82×10^{-4}	0.95
2.20	0	0.039	1.9×10^{-4}	1.71×10^{-4}	1.04
2.10	0	0.039	2.5×10^{-4}	2.09×10^{-4}	1.03

3.2.3 Enolization of acetone and heteroatomic-substituted derivatives

Investigating alkyl substituent effects on the rates of enolization of acetone is important in understanding how polar inductive and steric effects increase or decrease the kinetic acidities of the α-protons. However, the rates of enolization of substituted ketones containing heteroatoms or charged functional groups are perhaps more important when making comparisons to the rates obtained for our 'mutant' substrates. Shown below in Table 3.3 are the second order rate constants, obtained for the deprotonation of the C1 and C3 α-protons of acetone [17], entry **1**, methoxyacetone [106], entry **2**, hydroxyacetone [100], entry **3** and dihydroxyacetone, entry **4**

with a range of different bases. By comparison with the previous section the rates obtained correspond to the deprotonation of the Cα-1 and Cα-2 hydrogens of the molecules.

Table 3.3: Second order rate constants for the deprotonation of the C1 and C3 α-protons of acetone and heteroatomically substituted derivatives in aqueous solution.

Entry	Substrate	T (°C)	Base	k_{C1} ($M^{-1}s^{-1}$)	k_{C3} ($M^{-1}s^{-1}$)	k_{C1}/k_{C3} (k_{rel})
1		35	AcO⁻	1.10×10^{-7}	1.10×10^{-7}	1.00
		35	HO⁻	2.54×10^{-1}	2.54×10^{-1}	1.00
2		35	HO⁻	1.70×10^{-2}	1.20×10^{-2}	1.42
		35	Et₃N	1.30×10^{-3}	3.70×10^{-3}	0.35
		35	PhO⁻	7.00×10^{-4}	1.00×10^{-3}	0.70

| 3 | | 25 | AcO⁻ | 1.05×10^{-4} | 8.36×10^{-4} | 0.12 |
| 4 | | 25 | DO⁻[a] | 1.70×10^{-1} | 1.70×10^{-1} | 1.00 |

a) This value was calculated by dividing the first order rate constant for H-D exchange, k_{ex} (s⁻¹) = 1.7×10^{-3} s⁻¹, by the concentration of deuteroxide, 0.01M.

For the hydroxide-catalyzed deprotonation of acetone, it is likely that the large desolvation energy of this base results in a rate which is slower than expected. Indeed the rate of deprotonation at the α-position occurs only ~ 10^6 fold faster in the presence of hydroxide than acetate buffer despite the wide differences in basicities. The data presented also shows that deprotonation of the C-3 methyl protons of methoxyacetone by amine and phenoxide bases occurs up to 2.8 fold quicker than the corresponding C-1 deprotonation reaction. The deprotonation at both positions is approximately 10^4 fold faster than for acetate catalyzed deprotonation of acetone. By contrast, the rate of hydroxide catalyzed deprotonation of methoxyacetone occurs 1.2 fold quicker at the C-1 position than at the C-3 position. Furthermore, the absolute rate constant for deprotonation at the C-1 and C-3 positions by hydroxide are approximately 15 fold slower than for the analogous deprotonation reactions of acetone. This indicates a net deactivating effect of the methoxy substituent. The introduction of inductively electron withdrawing groups such as a methoxy would be expected to enhance the acidity of the C-1 protons of the molecule to a greater extent than the C-3 protons. The fact that this is not observed (except for hydroxide catalysis) suggests that factors other than polar inductive effects govern the rates of deprotonation of these positions. A similar effect is observed

for the acetate catalyzed deprotonation of hydroxyacetone, in work which was carried out by Richard *et al*. The rate of acetate catalyzed deprotonation at the C3 position occurs 8 fold faster than at the C1 position The deprotonation of the C1 protons of hydroxyacetone occurs approximately 1000 fold faster than the corresponding reaction for acetone (it should be noted that these experiments were carried out at 25 °C instead of 35 °C as reported for the previous data. Thus a rate acceleration of 2000-3000 fold is more likely which would account for ~ 10 fold of this rate acceleration).

Clearly the effect of placing a polar substituent such as a hydroxyl or methoxy group inductively exerts, to a certain extent, an electron withdrawing effect on the molecule and thus increases the overall acidity of all the protons in question. However deprotonation at the C1 position of hydroxyacetone, dihydroxyacetone or methoxyacetone by hydroxide ion could have been predicted to be quicker than that of acetone in that the presence of a directly attached polar electron withdrawing group should dramatically increase the acidity of the methylene C1 protons. While inductively withdrawing electron density from the developing charge of the carbanion formed following initial deprotonation of hydroxyacetone, formation of the carbon-carbon double bond of the enolate will be destabilised by the presence of such a group (relative to the carbon-carbon single bond of the reactant molecule). Furthermore, the electron lone pair of the hydroxyl or methoxy oxygen will form repulsive interactions with the delocalised electron of the enolate oxygen (Figure 3.2). This may partly explain the relatively small differences in the observed rate constants in the case of deprotonation by hydroxide.
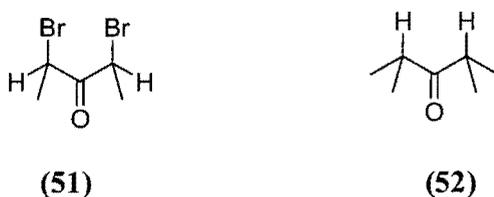
Figure 3.2

3.2.4 The effect of α-halo substitution on the rate of enolization

The effect of introducing a halide substituent (such as bromide or chloride) at the α-position of acetone is predicted to considerably increase the kinetic acidity of not only the α-methylene protons, but also the α-methyl protons of the same molecule. Thus in general, under basic conditions the rate of enolization is increased dramatically. Exceptions to this are found in systems where the α-methylene protons are sterically hindered, for example 2-bromo-2,4-dimethyl-3-pentanone **(51)** is less reactive to hydroxide catalyzed deprotonation than 2,4 dimethylpentanone **(52)** [107] (Figure 3.3)

Figure 3.3

(51)   (52)

Shown in Table 3.4 are the second order rate constants for the acetate catalyzed enolization of the Cα-1 hydrogens of a range of bromosubstituted acetone derivatives determined by halogen trapping experiments.

Table 3.4: Second order rate constants for the acetate, k_{AcO} ($M^{-1}s^{-1}$), catalyzed deprotonation of the C-1 α protons of bromosubstituted α-carbonyl derivatives in aqueous solution.

Entry	Compound	Temperature (°C)	k_{AcO} ($M^{-1}s^{-1}$)
1		30	9.4×10^{-8}
2		30	8.0×10^{-5}
3		30	6.7×10^{-3}
4		30	6.3×10^{-8}
5		30	5.8×10^{-5}
6		30	2.7×10^{-3}

7		30	6.3×10^{-8}
8		30	7.0×10^{-5}
9		30	7.6×10^{-5}
10		30	1.9×10^{-4}

In considering the substitution of a bromo by a methyl group, and vice-versa, steric effects should be similar due to the similar atomic radii of Br and CH_3. Thus polar and steric effects of substitution could be distinguished and any consequence of changing the two substituents could be explained primarily as a result of differences in their inductive effects. As well as enhancing the acidity of the adjacent α-methylene protons, halide substituents also lead to an increase in the acidity of the more remote α-methyl protons. This 'long-range' acid enhancing effect was originally presumed not to affect the remote α-methyl protons due to the presence of an 'insulating' carbonyl.

For the first three entries it can be seen that addition of a single bromine group at the C-1 position leads to an 850 fold increase in the rate of deprotonation at C-1 whereas a second remote bromo substituent leads to a rate increase of just over 70, 000 fold at C-1. For entries **4-6**,

the introduction of a bromo substituent at the C-1 position (entry **4** vs **5**, leads to a 920 fold

increase on the rate of C-1 deprotonation. The addition of a second bromo-substiutent, at the C-3

position of the molecule results in a 40,000 fold increase in the rate of deprotonation relative to

entry **4**. The lower observed increase for successive substitution of this set of molecules may be

explained by the additional steric restrictions presented by the methyl groups. Finally for entries

7-10 rate increases of ~ 1100, 1200 and 3000 fold for deprotonation at C-1 are observed for the

respective substitution of one, two and three bromine atoms at the C-3 position of the molecule.

3.3 The effect of sulfur on carbon acidities

The effect of divalent sulfur on enhancing the acidity of protons attached to an adjacent carbon

atom has been extensively studied where it has been noted that the availability of low-lying

unoccupied orbitals in divalent sulfur compounds means that sulfur can provide extra

stabilisation to α-carbanions [108, 109]. Numerous studies on the rates of ionization of sulfinyl

and sulfonyl carbon acids involving base catalyzed hydrogen/deuterium exchange have been

carried out in the first half of the 20th century [110]. The interest of early investigations was

primarily concerned with the stereochemical aspects of the processes as the hydrogens of a CH_2

group α to SOR or SO_2R are diastereotopic and thus this character shows itself in different rates

of ionization. Relatively little kinetic analysis has been carried on the effects of α-substituted

sulfate groups on the rates of deprotonation of the neighbouring α-protons. The role of sulfur

containing electron withdrawing groups has been a source of considerable controversy for a

number of years [111]. In the case of sulfones stabilization by electrostatic interactions is

important as it has been shown that here a sulfur atom has a charge of essentially +2 (Figure 3.4)

Figure 3.4

However resonance forms such as for an enolate cannot be written due to poor overlap between the p-orbital of the anion and the S-O double bond. In the early 1960's and 1970's the stabilization provided by sulfur was believed to occur due to conjugative interactions by p-dπ orbital bonding. Today it has been suggested that such a stabilization effect may be neglected . In fact is now generally assumed that the d-orbitals of sulfur do not participate or contribute to an energetic stabilization of the corresponding anion. The stabilization is a result of an overlap between the n-orbital of the carbon atom and the σ^* orbital of the C-S bond (Figure 3.5)

Figure 3.5

The results obtained by Oae *et al* [112] for the tert-butoxide catalyzed deuterium and tritium exchange reactions of a variety of sulfur containing carbon acids and their oxygen derivatives are shown below in Table 3.5.

Table 3.5: **First order rate constants, k_{ex} (s^{-1}) for the tert-butxoide catalyzed exchange of the highlighted hydrogens of sulfur and oxygen containing compounds (Entries 1-4).**

Entry	Compound	Base	T (°C)	k_{ex} (s^{-1})[a]
1	R $\times$ S–C$_8$H$_6$ / H ‾ S–C$_8$H$_6$ R= C$_8$H$_6$	t-BuOK	138	4.73 x 10^{-4}
2	R $\times$ O–C$_8$H$_6$ / H ‾ O–C$_8$H$_6$ R= C$_8$H$_6$	t-BuOK	120	0.41 x 10^{-4a}
3	S–C$_8$H$_6$ / H—C–S–C$_8$H$_6$ / S‾C$_8$H$_6$	t-BuOK	138	6.99 x 10^{-2}
4	O–C$_8$H$_6$ / H—C–O–C$_8$H$_6$ / O‾C$_8$H$_6$	t-BuOK	112	No observed exchange[b]

a) The first order rate constants, k_{ex} (s^{-1}) refer to the deuterium exchange reactions. Tritium exchange reactions were also monitored however this data has not been presented here. b) The reaction was monitored for 20 hours after which time no exchange was observed.

From the data presented above it can be seen that the rate of deuterium exchange for the sulfur containing compounds occur faster than for the analogous oxygen containing compounds. Between entries 1 and 2 there is an 11 fold difference in favour of the sulfur containing carbon acid. An 18 °C difference in reaction temperature would be expected to lead to a maximum of a

5-10 fold difference in rates however the fact that a greater increase is seen can be explained by the effect of sulfur on enhancing the acidity of the adjacent carbon atom. The substitution of an additional mercapto group (entry **3**) increases the reactivity of the hydrogen by more than 100 fold. This rate enhancement effect can also be attributed to the sulfur stabilising effect. The fact that no exchange of the oxygen analogue (entry **4**) was observed in the timescale of the reaction further supports the stabilising effect of sulfur.

Further sulfur stabilising effects on carbon acids have been investigated by Bell *et al* [36]. The sulfonate compounds studied are presented below in Table 3.5 in which the second order rate constants for enolisation at the C-1 position of entries **2** and **3** (C-1 or C-3) are compared with those of acetone (C-1 or C-3).

Table 3.6: Second order rate constants, k_{AcO} ($M^{-1}s^{-1}$) and k_{OH} ($M^{-1}s^{-1}$) for the reactions of acetone and sulfonate substituted derivatives in aqueous solution.

Entry	Compound	T (°C)	k_{AcO} ($M^{-1}s^{-1}$)	k_{OH} ($M^{-1}s^{-1}$)
1		25	1.1×10^{-7}	2.5×10^{-1}
2		25	5.2×10^{-4}	800×10^{-1}

| 3 | | 25 | 1.3×10^{-3} | - |

$$\text{-O-}\underset{\underset{O}{\overset{O}{\parallel}}}{\overset{\overset{O}{\parallel}}{S}}\underset{3}{\smile}\underset{1}{\smile}\overset{\overset{O}{\parallel}}{\underset{\underset{O}{\parallel}}{S}}\text{-O-}$$
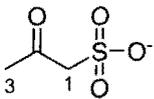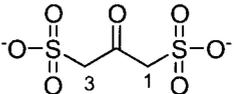
The second order rate constants for the enolization of acetone (entry **1**) presented above, were discussed in the previous sections. The addition of a sulfonate group to the molecule results in a 5000 fold increase in the rate of acetate-catalyzed enolization at the C-1 position of the molecule. In the case of hydroxide catalyzed enolization, a 320 fold increase is observed relative to the analogous reaction of acetone. Addition of a second sulfonate group further increases the rate of acetate-catalyzed enolisation at the C-1 position by 2.5 fold. From these studies of sulfur containing acetone derivatives some comparisons can be made and applied to interpreting the rates obtained for the mutant substrates DHAS (**27**) and DHATS (**25**). However the much greater electron withdrawing ability of the sulfonate group is expected to enhance adjacent carbon acidity considerably more than the sulfate and thiosulfate groups studied in this project.

3.4 The reactions of DHAP (1).

The background, non-enzymatic reactions of DHAP (**1**) have been extensively studied [17]. Shown below in Table 3.6 are the second order rate constants for the hydroxide catalyzed reactions at the C3 position of DHAP (**1**). Also shown are the second order rate constants for the hydroxide, k_{HO} ($M^{-1}s^{-1}$) catalyzed enolization of related compounds, acetone and methoxyacetone.

Table 3.7: Second order rate constants for the hydroxide, k_{HO} ($M^{-1}s^{-1}$) catalyzed deprotonation of C-3 protons DHAP (1) and the C-1 and C-3 protons of acetone and methyoxyacetone.

Entry	Substrate	T (°C)	Base	k_{C1} ($M^{-1}s^{-1}$)	k_{C3} ($M^{-1}s^{-1}$)	k_{C1}/k_{C3} (k_{rel})
1		35	HO⁻	2.54×10^{-1}	2.54×10^{-1}	1.00
2		25	HO⁻	-	1.80×10^{-1}	-
3		35	HO⁻	1.70×10^{-2}	1.20×10^{-2}	1.42
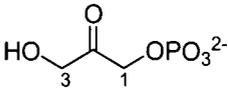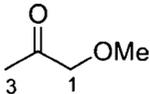
As previously mentioned, reactions for DHAP (1) were only monitored at the C-3 position. In solution, for DHAP, enolization is the rate-limiting step therefore the rates for enolization at the C-3 position correspond to the rate of elimination at the same position. Comparisons can be made with the hydroxide catalyzed reaction at the C-3 position of acetone and DHAP. It can be seen that the hydroxide catalyzed deprotonation of acetone occurs over 1.4 fold quicker than the corresponding DHAP deprotonation at the C-3 position. However, as the reaction of DHAP (1) was monitored at a 10 °C lower temperature, the C-3 deprotonation of DHAP (1) is in fact similar to acetone as a 2 fold change in rate is expected for a 10 °C change in temperature. In comparing the rates of the hydroxide catalyzed C-3 deprotonation of methoxyacetone with DHAP (1), it can be seen that the C-3 protons of DHAP are removed 15 fold faster than those of methoxyacetone. This occurs in spite of the former reaction being carried out at a temperature 10 °C lower than the corresponding reaction of methoxyacetone. Deuterium exchange for deprotonation at the C-1 position of DHAP (1) has not been reported.

3.5 The background rates of enolization and elimination of DHAS (27), DHATS (25) and BHA (22).

The remainder of this section will focus solely on the enolization and elimination reactions of our 'mutant' substrates (27), (25) and (22). Based on the polar inductive and steric effects discussed above for acetone and derivatives it was expected that similar effects would be important in the reactions of each mutant substrate particularly in the cases where sulfate and

thiosulfate substituents were present. The larger size of these substituents was predicted to have an effect on reactivity although to an unknown extent.

.

3.5.1 Dihydroxyacetone sulfate (27).

The values obtained for k_B ($M^{-1}s^{-1}$), the second order buffer catalyzed rate constant and k_{int} (s^{-1}), the pseudo first order rate constant for the buffer independent, deprotonation of the C-1 and C-3 hydrogens of DHAS (27) are shown below in Table 3.8

Table 3.8: First order rate consants, k_{int} (s^{-1}), k_{av} (s^{-1}) and second order rate

for deprotonation at C-1 or C-3. This is indicative of a general base catalyzed mechanism, although the increase in most cases was found to be relatively small (a 2.5 fold increase in buffer concentration often led to a maximum 50 % increase in the rate of either C-1 or C-3 deprotonation).

The majority of reactions above were carried out in basic buffers of pK_a values generally higher than that of acetate, the buffer most often used in the catalysis of the enolization of acetone and its derivatives discussed previously. Thus direct comparisons of k_B ($M^{-1}s^{-1}$), the second order rate constant for the buffer base catalyzed deprotonation at the C-1 and C-3 positions cannot generally be made with values obtained for other similar carbonyl compounds. One comparison can be made with the triethylamine catalyzed deprotonation of methoxyacetone. With a pK_a of approximately 11, triethylamine (50 % f_B, pH 11) was found to catalyze the deprotonation of methoxyacetone with rates of 1.30×10^{-3} $M^{-1}s^{-1}$ and 3.70×10^{-3} M^{-1} s^{-1} at the C-1 and C-3 positions respectively. The rates of quinuclidinone (90 % f_B, pD 9.2) catalyzed C-1 and C-3 deprotonation of DHAS (27) were found respectively to be 7.40×10^{-3} $M^{-1}s^{-1}$ and 3.30×10^{-3} $M^{-1}s^{-1}$. Despite a pK_a decrease of over 2 in moving from triethylamine to quinuclidinone buffers the observed second order rate constants are quite comparable. This is possibly due to the fact that quinuclidinone is a good general base catalyst for its pK_a due to the relatively unhindered nitrogen. The greater buffer catalysis could also be assigned to an acidifying effect of the sulfate group.

For the quinuclidinone catalyzed C-3 deprotonation of DHAP (1) a second order rate constant of 1.11×10^{-3} $M^{-1}s^{-1}$ was obtained (50 % f_B, pH 7.5). This is similar to the k_B value obtained for the quinuclidinone catalyzed C-3 deprotonation of DHAS (27) (1.41×10^{-3} $M^{-1}s^{-1}$ 70 % f_B ,pD 8.5).

From Table 3.6, k_{int} (s^{-1}) represents the first order rate constant for the buffer independent reactions of DHAS (27) at the pD values described above. It can be seen that a 0.7 unit increase in the buffer pD value from 8.52 to 9.2 leads to only 67 % and 12 % changes in the overall values of k_{int} (s^{-1}) for both the reactions of the C-1 and the C-3 protons of DHAS (27). This is reflected in the relatively level pD rate profile in this region which was presented in Chapter 2 (Figure 2.19) and suggests that deprotonation is pD independent in this range. From pD 8.5 to 7.3 there is a 10 fold decrease in k_{int} (s^{-1}) for deprotonation at the C-1 position.

The pD-independent first order rate constant, k_{obs} (s^{-1}), for deprotonation of DHAP (1) at C-3 has a reported value of 1.4 x 10^{-5}s^{-1} at 37 °C. This value is smaller than the average pD independent reaction of the C-3 protons of DHAS, 9.99 x 10^{-5}(s^{-1}) at 25 °C.

While the hydroxide catalyzed C-3 deprotonation reaction of DHAP (1) and acetone occur at similar rates (0.18 M^{-1}s^{-1} for DHAP and 0.25 M^{-1}s^{-1} for acetone) the value of the water-catalyzed deprotonation of the two molecules is considerably different. The water (pH-independent) catalyzed deprotonation of acetone has been reported as 4.6 x 10^{-10} s^{-1}. This value is approximately 10^5 fold smaller than the pH-independent deprotonation reaction of DHAP (1) at the C-3 position (1.4 x 10^{-5} s^{-1}). As discussed in Chapter 1 the phosphodianion group of DHAP (1) is believed to participate in an intramolecular deprotonation of the C-3 hydrogens of substrate thus accelerating the rate considerably. A similar occurance could be also expected for DHAS (27). However the less basic monoanionic sulfate group could be predicted to be less efficient at removing the C-3 protons of substrate than the corresponding phosphodianion of DHAP (1). Based on the relative pD independent rates obtained this appears not to be the case. It is possible

that the larger size of sulfur relative to phosphorus compensates for the lower basicity of the

sulfate monoanion, permitting easier intramolecular deprotonation at the C-3 position.

The k_{rel} values for the C-1 and C-3 pD-independent reactions of DHAS (27) remain relatively

constant in moving from quinuclidinone 70 % f_B buffer to 90 % f_B buffer (average k_{rel} = 1.7).

Similarly the k_{rel} values obtained from k_{av} (s^{-1}) remain quite constant in moving through the same

buffer range (average k_{rel} = 2.1). Thus the pD independent deprotonation at the C-1 position of

DHAS (27) is approximately 2 fold faster than at the C-3 position. The fact that C-1 H-D

exchange occurrs faster than elimination suggests that the presence of a sulfate group enhances

acidity and thus deprotonation to a greater degree than a hydroxyl group. This ratio is also

observed when comparing k_B values for deprotonation at C-1 and C-3 of DHAS (27). For

hydroxyacetone and methoxyacetone deprotonation directly beside the hydroxy or methoxy

group was generally found to be slower than at the remote methyl groups. As discussed for

hydroxyacetone and acetone, the presence of lone pair electrons on the oxygen atom may lead to

steric repulsion between the oxygen atom and negatively charged enolate oxygen in the

transition state of the reaction. By contrast in the case of DHAP (20) deprotonation at the C-1 is

significantly slower than at C-3 thus at pD 8 no deuterium exchange at the C1 position is

observed in competition with reaction at the C-3 position (elimination).

3.5.2 Dihydroxyacetone thiosulfate (25)

As discussed in Chapter 2, the deprotonation of the C-1 protons of DHATS (25) was monitored

in acetic acid buffers and DCl solutions. The majority of the second order rate constants obtained

for deprotonation of the C-1 protons of acetone and its substituted derivatives were also

quantified in acetate buffers. Therefore direct comparisons with the acetate catalyzed second order rate constants for DHATS **(25)** with analagous values for acetone and its derivatives can be made more readily than for the previously discussed substrate, DHAS **(27)**.

The values obtained for k_{int} (s^{-1}), the first order DCl independent catalyzed deprotonation at the C-1 position of DHATS **(25)** are shown in Table 3.9. As discussed, in the case of the reactions in DCl no buffer catalysis can occur thus values for k_{int} (s^{-1}) can be directly equated with the first order rate constants obtained for C-1 deprotonation, k_{obs} (s^{-1}). As described in Chapter 2 the kinetic data for the C-1 deprotonation of DHATS **(25)** is summarised in Table 3.7.

Table 3.9: First order rate constants k_{int} (s^{-1}) for the C-1 deprotonation of DHATS (25), in DCl solutions and acetate buffers.

Buffer (%f_B)/DCl (M)	pD	k_{int}^{Ex} (s^{-1}) $(k_{av}$ (s^{-1}))^a	k_BC-1 (M^{-1}s^{-1})
Acetate (20 % f_B)	4.38	4.07 x 10^{-4}	4.66 x 10^{-2}
		(1.11 x 10^{-3})^a	
Acetate (10 % f_B)	4.09	1.03 x 10^{-4}	6.77 x 10^{-2}
		(5.21 x 10^{-4})^a	
Acetate (5 % f_B)	3.75	9.03 x 10^{-5}	3.58 x 10^{-2}
		(2.26 x 10^{-4})^a	

DCl (0.001)	3.32	2.43×10^{-5}	-
DCl (0.003)	2.95	1.49×10^{-5}	-
DCl (0.005)	2.75	9.61×10^{-6}	-
DCl (0.007)	2.53	2.43×10^{-5}	-
DCl (0.009)	2.46	1.49×10^{-5}	-
DCl (0.012)	2.21	9.41×10^{-6}	-

a) The value of k_{av} (s^{-1}) was taken as the average of pseudo first order rate constants, k_{obs} (s^{-1}) obtained at different buffer concentrations at a given pD

For the reactions of DHATS (25) it could be expected that similar rates as those obtained for the reaction of DHAS (27) could be observed based on similarities of sulfate and thiosulfate moieties in terms of pK_a values for ionisation at oxygen. In the presence of quinuclidinone buffer it was found that C-1 deprotonation of DHATS (25) occurred too fast to monitor by ^1H NMR. Thus in

this buffer accurate kinetic data for the C-1 H/D exchange reaction of DHATS (25) was not obtainable. Similarly in buffers of lower basicity such as phosphate the exchange reactions of these protons occured too rapidly to monitor by ^{1}H NMR. The fact that the reaction at the C-1 position of the molecule occurs so rapidly in these buffers indicates a much larger α-proton acidifying effect from a thiosulfate group than a sulfate group and the replacement of an oxygen atom with a sulfur obviously has a large net acidifying effect on the adjacent C-1 hydrogens. Although this could potentially have been predicted, the extent of rate enhancement could not have been expected. Thus to obtain kinetic data the reactions at this position of the molecule were monitored in less basic buffers such as acetic acid and in DCl solutions.

For the reactions of DHATS (106) in DCl solution it appears that the reaction is pD independent. Despite a 1.1 unit increase in pD from 2.2-3.3 there is only a two fold increase in the rate of C-1 enolization. This is also the pD range where the pK_a value for the thiosulfate group lies although it is most likely in predominantly monoanionic form at pD values greater than 2. Thus the average rate constant for exchange at the C-1 position of DHATS at pD 2.3-3.3 is 1.33×10^{-5} (s^{-1}). This can be compared with an average pD independent rate constant of 9.9×10^{-5} s^{-1} For deprotonation of DHAS at the C-1 position at pD 8.5 to 9.2. Thus the replacement of oxygen by sulfur increases the C-1 kinetic acidity by $\sim 10^4$-10^5 fold. It is possible that the presence of 2 sulfurs facilitates intramolecular deprotonation at the C-1 via a five-membered ring transition state (Figure 3.6)

Figure 3.6

304
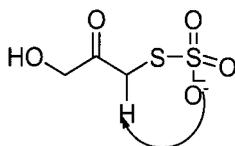
The buffer catalyzed reactions of the C-1 protons of DHATS (**25**) were monitored in acetic acid

buffers with a maximum free base content of 20 %.

For the acetate catalyzed C-1 deprotonation reactions it can be seen that moving from pD 3.75 to

4.38 leads to an overall 4.5 fold increase in the value of k_{int} (s^{-1}) for the buffer independent

deprotonation reaction of the C-1 protons of DHATS (**25**). Accordingly, in the same pD range

the values for the first order rate constants, k_{av} (s^{-1}) increase by a factor of 4.9 fold. This could

represent a hydroxide dependent reaction. An average k_B (M^{-1}s^{-1}) of 5 x 10^{-2} M^{-1}s^{-1} was obtained

for the acetate catalyzed reaction at the C-1 position of the molecule.

Represented below in Table 3.10 are the second order rate constants for the acetate catalyzed,

k_{AcO} (M^{-1}s^{-1}) deprotonation of the C-1 protons of DHATS (**25**), acetone and various substituted

derivatives which have been previously presented in this chapter.

Table 3.10: Second order rate constants for the acetate, k_{AcO} (M^{-1}s^{-1}), catalyzed

      deprotonation of the C-1 α protons of bromosubstituted α-carbonyl derivatives

      in aqueous solution.

Entry	Compound	k_{AcO} (M^{-1}s^{-1})	k_{rel}[a]
1		5.00 x 10^{-2}	1.00
2		1.10 x 10^{-7}	2.20 x 10^{-6}
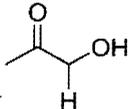
3	$CH_3C(O)CH(H)OH$	1.05×10^{-4}	2.10×10^{-3}
4	$CH_3C(O)CH(H)Br$	8.00×10^{-5}	1.45×10^{-3}
5	$BrCH_2C(O)CH(H)Br$	6.70×10^{-3}	1.22×10^{-1}
6	$CH_3C(O)CH(H)SO_3$	5.20×10^{-4}	2.70×10^{-3}
7	$^-O_3SCH_2C(O)CH(H)SO_3^-$	1.30×10^{-3}	2.36×10^{-2}

a) $k_{rel} = k_{AcO}$(substrate)$/k_{AcO}$ (DHATS). For entry 1, a $k_{rel} = k_{AcO}$ (DHATS)$/k_{AcO}$ (DHATS).

In comparing the rates of deprotonation at the C-1 position of the DHATS (25) with the corresponding rates obtained for acetone and its derivatives some interesting observations can be made. A 455,000 fold increase in the rates of C-1 deprotonation of DHATS (entry 1) occurs relative to acetone deprotonation. For hydroxyacetone, entry 3, a 476 fold decrease in the second order rate constant for C-1 deprotonation is observed. In comparing the rate of deprotonation of entry 1 with the bromosubstituted derivatives, entries 4 and 5, respective rate accelerations of 625 and 8 fold are observed in acetate buffers. Finally, comparing the rates of C-1 deprotonation of the sulfonate substituted derivatives, entries 6 and 7 with entry 1 show that rate enhancements of 105 fold and 42 fold are observed for DHATS. The k_{rel} values shown in Table 3.7 indicate

that the thiosulfate group has an acidifying effect on the adjacent C-1 protons which is far superior to the similar effects provided by other substitutents such as a bromo or sulfonate group. While the effect of a thiosulfate group was expected to enhance the acidity of the C-1 protons of the molecule, the magnitude of the effect was not expected.

As introduced in Chapter 2, it was found that the reactions at the C-3 position of DHATS (25) yielded some surprising results. Under the conditions used to monitor the deprotonation reactions at the C-1 position of DHATS (25) it was observed that the C-3 methylene protons did not react. Thus it was assumed that buffers of higher pD would be required to quantify any reaction at this C-3 position. However in the presence of buffers such as phosphate and quinuclidinone it was found that while the peaks due to the C-3 methylene protons did disappear the expected elimination product, methylglyoxal, did not correspondingly appear (a small amount was initially formed which then remained constant for the rest of the reaction). There are several mechanistic possibilities which may explain the fate of DHATS (25) under these conditions and the occurance of the peaks of the mass spectra presented in Chapter 2. Some potential reaction products are shown below in Scheme 3.4.

Scheme 3.4: Potential mechanistic pathways leading to the observed mass spectral product.
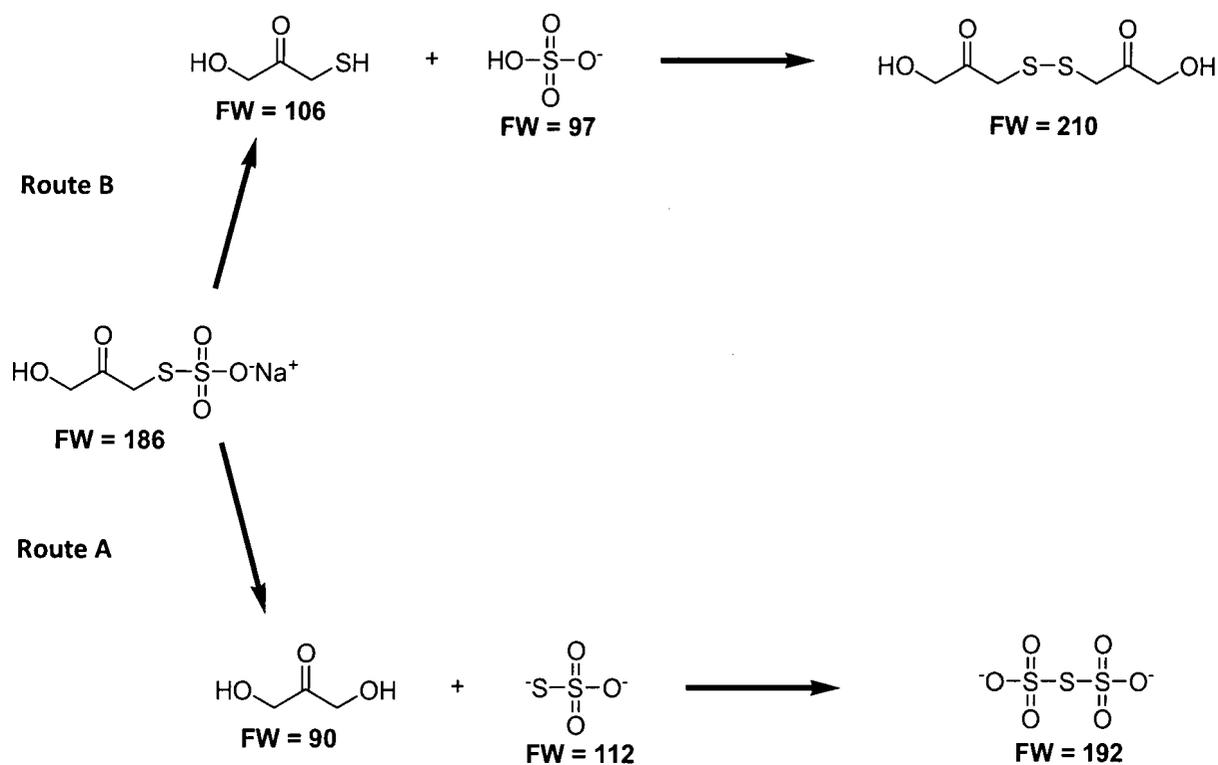
A clear molecular ion peak at 186 due to DHATS **(25)** is observed in the mass spectrum obtained at zero reaction time under negative electrospray conditions (m/z = 186). The reaction of water at the C-1 position (Route **A**) of the molecule may occur at carbon or sulfuryl sulfur. The former would result in the formation of dihydroxyacetone and thiosulfate dianion which have molecular weights of 90 and 112 respectively. However this mechanism is unlikely given that neither of these species are observed/detected under positive (Na$^+$) or negative electrospray. Alternatively, direct attack of water at the electrophillic sulfur atom of the thiosulfate moiety of parent DHATS **(25)** would lead to the formation of a hydroxyacetone thiol (FW = 106) and a sulfate molecule (FW = 97) (Route **B**). While neither of these species are visible in the mass spectra, dimerisation

308

of the thiol would yield a compound with a molecular weight of 210. Under positive electrospray conditions this compound will have a molecular weight of 233. Such a peak is clearly visible in the positive electrospray mass spectrum and is thus a mechanistic possiblity. However evidence for such a dimeric species was not observed in the ^{1}H NMR spectra presented in Chapter 2. Therefore to fully quantify the exact mechanism occurring at higher pD values more detailed analytical experiments would be required.

3.5.3 Bromohydroxyacetone (BHA)

The reactions involving the only neutral substrate investigated in this work, BHA **(22)**, were not as easily followed as the previously discussed substrates, DHAS **(27)** and DHATS **(25)**. This was mainly due to issues with dimer formation and ultimately the overall process of forming the monomeric substrate. The deprotonation reactions at the C-1 position of this molecule were followed in acetic acid buffers (70, 80 and 90 % f_B, pD 5.18- 6.09) whereas the deprotonation reaction of the C-3 protons was monitored directly in the presence of quinuclidinone buffer (90 % f_B, pD 9.2). Direct comparisons of the acetate catalyzed reactions of this substrate can be made with the majority of literature rate constants described above as well as with the previously described substrate, DHATS **(25)**. These comparisons will be dealt with before describing the reaction at the C-3 position of the molecule at which there appeared to be some competing side reactions (Chapter 2). Thus the C-3 deprotonation reactions of BHA **(22)** will be discussed separately.

The values obtained for k_B ($M^{-1}s^{-1}$), the second order acetate catalyzed rate, k_{int} (s^{-1}), the pseudo first order rate for the buffer independent deprotonation and k_{av}(s^{-1}), the average of the pseudo first order rate constants of the C-1 hydrogens of BHA (22) are shown below in Table 3.11.

Table 3.11: First order rate constants, k_{int} (s^{-1}), k_{av}(s^{-1}) and second order rate constants, k_B ($M^{-1}s^{-1}$) for the deprotonation at the C-1 position of BHA (22).

Buffer	pD	k_{int}C-1 (s^{-1}) $(k_{av}$C-1$(s^{-1}))^a$	k_BC-1 ($M^{-1}s^{-1}$)
Acetate	5.18	3.70×10^{-6}	7.86×10^{-5}
(70 % f_B)		(7.40×10^{-6})	
Acetate	5.35	4.70×10^{-6}	9.96×10^{-5}
(80 % f_B)		(1.01×10^{-5})	
Acetate	5.92	1.19×10^{-5}	9.80×10^{-5}
(90 % f_B)		(1.68×10^{-5})	

a) The value of k_{av} (s^{-1}) was taken as the average of pseudo first order rate constants, k_{obs} (s^{-1}) obtained at different buffer concentrations at a given pD

In a similar manner to the reactions of DHATS (25) it was found that monitoring the reactions of the C-1 protons of BHA (22) was only possible in buffers of relatively low pK_a values. The C-1

H/D exchange reactions in more basic buffers occurred too quickly to enable monitoring deprotonation at this side of the molecule by ^{1}H NMR.

For the C-1 deprotonation reactions it can be seen that a 0.62 change in pD leads to an overall 3.2 fold increase in the first order rate constant k_{int} (s^{-1}) for the buffer-independent reaction of the C-1 protons. In the same pD range the values of the first order rate constants, k_{av} (s^{-1}) increase by 2.2 fold. An average k_B value of 9.2 x 10^{-5} M^{-1}s^{-1} implies that acetate catalyzed deprotonation of the C-1 protons of BHA (22) occurs 543 fold slower than acetate catalyzed reaction of DHATS (25) at the same position.

Represented below in Table 3.12 are the second order rate constants for the acetate catalyzed, k_{AcO} (M^{-1}s^{-1}) deprotonation of the C-1 protons of BHA (22), acetone and various substituted derivatives which have been previously presented in this chapter.

Table 3.12: Second order rate constants for the acetate, k_{AcO} (M^{-1}s^{-1}), catalyzed
deprotonation of the C-1 α protons of bromosubstituted α-carbonyl derivatives
in aqueous solution.

Entry	Compound	k_{AcO}	k_{rel}[a]
		(M^{-1}s^{-1})	
1		9.20 x 10^{-5}	1.00
2		1.10 x 10^{-7}	1.19 x 10^{-3}

3	![structure: CH3-C(=O)-CH(OH)H]	1.05×10^{-4}	1.413
4	![structure: CH3CH2-C(=O)-CH(Br)H]	8.00×10^{-5}	0.869
5	![structure: Br-CH2-C(=O)-CH(Br)H]	6.70×10^{-3}	72.83
6	![structure: HO-CH2-C(=O)-CH(SSO3-)H]	5.00×10^{-2}	543
7	![structure: CH3-C(=O)-CH(SO3-)H]	5.20×10^{-4}	5.65
8	![structure: -O3S-CH2-C(=O)-CH(SO3-)H]	1.30×10^{-3}	14.1

a) $k_{rel} = k_{AcO}(\text{substrate})/k_{AcO} (\text{BHA})$. For entry **1**, a $k_{rel} = k_{AcO} (\text{BHA})/k_{AcO} (\text{BHA})$.

Acetate catalyzed deprotonation at the C-1 position of BHA (**25**) (entry **1**) occurs 836 fold faster than the corresponding acetate catalyzed deprotonation reaction of acetone (entry **2**).This can be somewhat expected based on the electron withdrawing capability of bromine. Comparing entry **1** and entry **3** reveals that the acetate catalyzed deprotonation of hydroxyacetone occurs 1.14 fold faster than the corresponding reaction of BHA. For entries **1** vs **4** a 1.15 fold increase in the

second order rate constant for C-1 deprotonation occurs. The similar k_{AcO} values for entires **1, 3** and **4** shows that α-bromo and α-hydroxyl substituents have similar influences on acetate catalyzed deprotonation. A 73 fold increase in the rate of C-1 deprotonation of entry **5** is observed compared to entry **1**. Clearly the addition of a second bromo substituent, despite being remote, has acidifying effect on the C-1 protons of this molecule. As discussed a 543 fold increase in the rate of C-1 deprotonation of entry **7** is observed in comparison to entry **1**. Finally, for entries **8** and **9**, 5.6 and 14.1 fold increases are observed respectively for the C-1 deprotonation reactions vs entry **1**. Based on the previous discussion, the rate increases observed here are the result of the stronger acidifying effect of an α-sulfonyl than an α-bromo substituent. However this effect is minute in comparison to the rate enhancement provided by a thiosulfate moiety.

As mentioned, the reactions at C-3 of BHA **(22)** were monitored in quinuclidinone buffers (90% f_B, pD 9.2). At this pD value it was found that elimination did occur as judged by the formation of elimination product, methylglyoxal. However it appeared that a competing side reaction also occurred, based on the formation of other small peaks in the ^1H NMR spectra over time (Figure 2.42). The nature of these side reactions is unclear although they could be predicted to be an Aldol or another condensation type reaction. Thus first order rate constants could be obtained for the total reaction of substrate at the C-3 position along with any other side reactions as well first order rates corresponding to C-3 deprotonation and therefore elimination only. Shown below in Table 3.13 are the first order rate constant, k_{int}^{elim} (s^{-1}), k_{av}^{elim} (s^{-1}) and second order rate constant k_B^E (M^{-1}s^{-1}) for the C-3 deprotonation of BHA **(22)**.

Table 3.13: First order rate constants, k_{int} (s^{-1}), k_{av}(s^{-1}) and second order rate constants, k_B (M^{-1}s^{-1}) for the deprotonation at the C-3 position of BHA (22).

Buffer	pD	$k_{int}{}^E$C-3 (s^{-1}) $(k_{av}{}^E$C-1(s^{-1}))	$k_B{}^E$C-3 (M^{-1}s^{-1})
Quinuclidinone (90 % f_B)	9.20	9.35 x 10^{-5} (2.83 x 10^{-4})	3.35 x 10^{-3}

As the C-3 deprotonation reaction of BHA (22) was monitored in quinuclidinone buffer, it is generally difficult to make any accurate comparisons with the acetone derivatives discussed above. One comparison which can be made is for triethylamine catalyzed C-1 deprotonation of methoxyacetone. While triethylamine (pKa ~11) is a stronger base than quinuclidinone, as previously described quinuclidinone is a better general base than its pK_a suggests. The second order rate constant for triethylamine catalyzed deprotonation of the C-1 protons of methoxyacetone is 1.3 x 10^{-3} M^{-1}s^{-1} (50 % f_B, pH 11). This is just under 3-fold slower than the second order rate constant, 3.35 x 10^{-3} M^{-1}s^{-1} for the quinuclidinone catalyzed deprotonation reaction at the C-3 position of BHA (22). A further comparison can be made between the k_{int} (s^{-1}) value obtained for the C-3 deprotonation reaction of DHAS (27) in quinuclidinone buffer (90% f_B, pD 9.2) and the corresponding value for BHA (22). Values of k_{int} = 9.30 x 10^{-5} s^{-1} and 9.35 x 10^{-5} s^{-1} for the respective reactions of DHAS (27) and BHA (22) indicate that the effect of a sulfate and bromo on the buffer independent rates of α-proton are similar. Furthermore the

314

second order rate constants, k_B ($M^{-1}s^{-1}$) for the quinuclidinone catalyzed deprotonation reactions of DHAS (27), $3.30 \times 10^{-3} M^{-1}s^{-1}$, and BHA (22), $3.35 \times 10^{-3} M^{-1}s^{-1}$ indicate that bromo and sulfate substitutents also have similar effects on the buffer catalyzed rate of deprotonation of the C-3 α-protons.

As mentioned in Chapter 2, it was found that BHA crystallises as a dimer. While the exact nature of this species has generally remained unclear, it is likely that the dimeric structure suggested in the literature by Druekhammer *et al* is incorrect (Figure 3.9)

Figure 3.9: The dimmer conformation of bromohydroxyacetone suggested y

Druekhammer *et al*

(23)
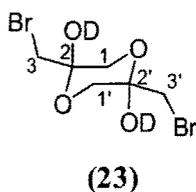
This assumption is based on the fact that H/D exchange reactions were observable by ^{1}H NMR for the reactions of the dimer in buffered D_2O solution in conditions where formation of monomer was slow. As the rate of conversion of monomer to dimer is slow (48 hours), the exchange reaction of the dimeric species cannot be explained by a rapid equilibrium favouring dimer at this pD.

This suggests that the actual dimeric species contains protons which are enolizable furthermore the formation of an upfield triplet is consistant with the formation of a CHD group. Shown below in Table 3.14 are the results obtained for the reaction of this dimeric species in phosphate buffers

(20 % f_B, pD 6.54) which includes first order rate constants, k_{int} (s^{-1}) and k_{av} (s^{-1}) and the second

order rate constant, k_B (M^{-1} s^{-1}) for the H/D exchange reaction of the dimeric species.

Table 3.14: First order rate constants, k_{int} (s^{-1}), k_{av}(s^{-1}) and second order rate constants, k_B

(M^{-1}s^{-1}) for the H/D exchange reaction of the BHA dimeric species in phosphate

buffer (20 % f_B, pD 6.54).

Buffer	pD	k_{int}^B C-3 (s^{-1})	k_{int}^D C-3 (s^{-1})	k_B^B (s^{-1})	k_B^D (s^{-1})
		$(k_{av}^B$ C-1(s^{-1}))	$(k_{av}^D$ C-1(s^{-1}))		
Phosphate	6.54	5.23 x 10^{-4}	8.80 x 10^{-4}	5.00 x 10^{-2}	2.63 x 10^{-2}
(20 % f_B)		(1.28 x 10^{-3})	(1.28 x 10^{-3})		

As described in Chapter 2, from the overlayed ^{1}H NMR spectra of the reaction of this dimeric

species, two peaks appeared to exchange over time. The identity of the exchanging singlets could

be temporarily assigned to the C-1 and C-3 methylene protons of an acyclic dimeric species

suggested dimeric species (49) shown in Figure 3.9

Figure 3.9: A potential alternative to the dimmer suggested by Druekhammer *et al*
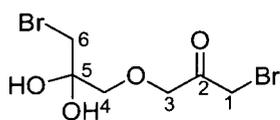
(49)

This H/D exchange reaction was confirmed by the appearance of a broad triplet slightly upfield of the main peak (peak **B**, 4.2 ppm) as well as a corresponding broad singlet (peak **K**), again slightly upfield of the corresponding singlet (peak **D**) at 3.46 ppm (Figure 2.49).

For monomeric BHA **(22)**, deprotonation and thus elimination at the C-3 position was only achieved in quinuclidinone buffers (90 % f_B, pD 9.2) whereas deprotonation of the C-1 was observed in acetate buffers (70-80 % f_B, pD 5.18-6.02). In the 'dimeric' case deprotonation at the two acidic carbons occurs at very similar rates (see k_{int} values Table 3.9) at a relatively low pD.

3.6 The background UV-Vis elimination assays of mutant substrates DHA (26) , HA (49), DHAS (27), BHA (22) and DHATS (25).

Attempts to monitor the elimination reactions of the mutant substrates, DHA **(26)**, HA **(49)**, DHAS **(27)**, BHA **(22)** and DHATS **(25)** were made using the adapted UV-Vis assay described in Chapter 2. However it was found that this method was not viable in determining overall rates of elimination for these substrates. From NMR analysis of these reactions it is possible to account for elimination or competing reactions based on the appearance of new peaks which can be integrated relative to an internal standard. For a UV-Vis assay method this is not possible and any competing side reactions which could explain the lack of observed elimination are not possible to identify. As ^{1}H NMR provided rates for both H/D exchange and elimination of the mutant substrates, it was decided not to pursue this assay method any further.

317

3.7 The reactions of DHA (26) and DHAS (27) in the presence of MGS.

MGS catalyzes the turnover of natural substrate DHAP (1) with remarkable efficiency (k_{cat}/K_M = 5.2 x 10^6 $M^{-1}s^{-1}$). The active site base Asp 71 is highly specific for the C-3, *pro*-S proton of DHAP (1). Furthermore the role of the remote phosphodianion group is believed crucial in providing extra stabilisation of the substrate at the active site of the enzyme, with X-ray crystallographic studies indicating that up to eleven H-bonded interactions occur with this group. As discussed in Chapter 1 these interactions are believed to facilitate the rapid elimination of the phosphotrianionic group. For the related enzyme TIM, DHAP (1) is also the natural substrate which is rapidly converted to isomerisation product glyceraldehyde-3-phosphate (k_{cat}/K_M = 9.25 x 10^5 $M^{-1}s^{-1}$). At the active site of TIM, X-ray crystallographic studies have indicated that there are fewer hydrogen bonded interactions with the phosphodianion group of phosphate and on this basis isomerisation is the more energetically favoured reaction relative to elimination. Therefore the origin of the product outcomes of the two enzymes is generally believed to be due to differences in the electrostatic binding of DHAP (1) at the two active site pockets.

In order to probe the role of the phosphodianion group in the MGS catalysis of DHAP (1), the reactions of the mutant substrates DHA (26) and DHAS (27) have been investigated. While the neutral substrate DHA (26) is similar in size to natural substrate DHAP (1) and contains enolizable C-3 protons, the lack of charged functionality could have ensured that the 'crucial' electrostatic interactions leading to elimination may not have been observed. For monoanionic DHAS (27), MGS turnover could perhaps have been predicted, although to a lesser extent than for DHAP (1) based on poorer electrostatic interactions with the monoanionic sulfate moiety.

318

For the reaction of DHA (26), the background reaction was carried out in imidazole buffer (70 % f_B, pD 7.9). It was found at this pD that neither H/D exchange nor elimination was observable. This is in agreement with the single $k_{obs \, (exchange)}$ value obtained for DHA (26) of 1.7×10^{-3} s^{-1} in 0.01M deuteroxide solution (Table 3.3). From this value a half-life of 94 hours can be obtained which is approximately 4 times longer than the reaction time monitored in this work. Over 94 hours it is assumed that MGS will decompose thus to quantify a reaction with DHA (26) a higher concentration of enzyme (than the 7.7×10^{-4} mM used in this experiment) would be needed.

As introduced in Chapter 1, the enzyme TIM catalyzes the downhill isomerisation reaction of GAP (8) to DHAP (1). To probe the role of the phosphodianion group to this catalyzed reaction, O'Donoghue *et al* have carried out reactions of the mutant substrate glyceraldehyde (GA) (11mM) in the presence of TIM (0.17 mM). At this concentration of enzyme it was found that the turnover of GA does occur however the value of k_{cat}/K_M for the C-2 deprotonation of the molecule, 0.34 M^{-1}s^{-1} was found to be only 50 fold greater than the second order rate constant for the quinuclidinone (50 % f_B, pH 7.5) deprotonation of the C-2 proton of GA, 6.5×10^{-3} M^{-1}s^{-1}. Clearly the presence of a higher concentration of enzyme the turnover of substrate is quantifiable as observed for the above experiments.

For the reactions of DHAP (1) in the presence of MGS (5.91×10^{-7} mM), C-1 H/D exchange was not detectable. Even at this low concentration of enzyme, occurred too rapidly to obtain an accurate rate for elimination.

For the substrate DHAS (27) in the presence of MGS elimination and exchange was observed. To quantify an enzymatic rate acceleration a comparison of the second order rate constant for the imidazole catalyzed reaction of DHAS (27) in the absence of MGS was made against the

319

reaction of DHAS (27) in the presence of MGS (1.9×10^{-4} mM and 7.7×10^{-4} mM). Shown

below in Table 3.10 are the first order rate constants, k_{obs}^{T}, k_{obs}^{Elim} and k_{obs}^{ex} for the background,

non-enzymatic reaction of DHAS in imidazole buffer (70 % f_B, 83 mM) and the first order rate

constants, k_{obs}^{T}, k_{obs}^{Elim} and k_{obs}^{ex} for the reactions of DHAS in the presence of MGS (1.9×10^{-7}

M and 7.7×10^{-4} M). Shown in Table 3.15 are the k_{cat}/K_M values for the total reaction of DHAS

in the presence of MGS (k_{cat}/K_M^{T}), the elimination of DHAS in the presence of MGS (k_{cat}/K_M^{Elim}) and the exchange of DHAS in the presence of MGS (k_{cat}/K_M^{ex}).

Table 3.15: First order rate constants for the reaction of the C-1 and C-3 protons of DHAS

in imidazole buffer (70% f_B, 83 mM) only and in the presence of imidazole

buffer (70% f_B, 83 mM) and MGS (1.93×10^{-7} M and 7.72×10^{-7} M).

pD	[DHAS]	[MGS]	k_{obs}^{Total}	k_{obs}^{Elim}	k_{obs}^{ex}
	(mM)	(M)	(s^{-1})	(s^{-1})	(s^{-1})
7.9	5	0	2.79×10^{-5}	n/d*	2.79×10^{-5}
7.9	5	1.93×10^{-7}	5.21×10^{-5}	1.53×10^{-5}	3.68×10^{-5}
7.9	5	7.72×10^{-7}	8.61×10^{-5}	2.63×10^{-5}	5.98×10^{-5}

* Not detectable

Table 3.16: k_{cat}/K_M values for the reaction of DHAS in the presence of MGS (1.93×10^{-7} M and 7.72×10^{-7} M).

pD	[DHAS]	[MGS]	k_{cat}/K_M^{Total}	k_{cat}/K_M^{elim}	k_{cat}/K_M^{ex}
	(mM)	(M)	(M⁻¹s⁻¹)	(M⁻¹s⁻¹)	(M⁻¹s⁻¹)
7.9	5	1.93×10^{-7}	125	79	46
7.9	5	7.72×10^{-7}	75	34	41

From Table 3.16 it is clear that the reaction of DHAS (**27**) in the presence of MGS leads to an acceleration of the rates of enolization and elimination compared to the background rate of the corresponding reactions. For the non-enzymatic reaction of DHAS (**27**) in the presence of imidazole buffer (70 % f_B, 83 mM) no elimination was observed in the timescale of the reaction. However in the presence of MGS, rates of elimination could be obtained, with first order rate constants, $k_{obs}^{Elim} = 1.53 \times 10^{-5}$ s⁻¹ (1.93×10^{-7} M) and 2.63×10^{-5} s⁻¹ (7.7×10^{-7} M). While H/D exchange at the C-1 position of DHAS (**27**) was observed in imidazole buffer, $k_{obs}^{ex} = 2.79 \times 10^{-5}$ s⁻¹, in the presence of MGS these rates of exchange were accelerated 1.3 fold for MGS (1.93×10^{-7} M) and 2.1 fold for MGS (7.7×10^{-7} M). From Table 3.16 the calculated average values of k_{cat}/K_M (M⁻¹s⁻¹) for total reaction, elimination and exchange are 100, 56.5 and 43.5 M⁻¹s⁻¹ respectively. From the studies by Rose *et al,* [74] for the elimination of DHAP (**1**), enolization is not rate limiting, however in the case of DHAS (**27**) it is presumed that the enolization will be the rate-determining step. This is based on the decreased average values obtained for k_{cat}/K_M which is ultimately a result of replacing the phosphodianionic group of natural substrate DHAP

321

(1) with a monoanionic sulfate group. The value of k_{cat}/K_M for elimination of DHAS (27) (56.5 $M^{-1}s^{-1}$) is approximately 90,000 fold slower than the corresponding value for DHAP (1), 5.6 x 10^6 $M^{-1}s^{-1}$. Thus the effect of replacing the phosphate group of natural substrate DHAP (1) clearly has a profound effect on the turnover of the substrate. These results partially support the QM/MM studies by Harrison *et al* that the phosphodianion group is crucial for catalysis based on electrostatic interactions at the active site of MGS however to fully experimentally quantify these theoretical studies the reactions of other mutant substrates such as dianionic DHATP (25) should be investigated. While DHAS (27) is turned over by MGS, a reduced k_{cat}/K_M values can be potentially be attributed to fewer electrostatic interactions at the active site pocket.

The effect of replacing the phosphate group of DHAP (1) with a sulfate moiety on MGS catalysis can be compared to TIM catalysis of GAP and the mutant GA (Table 3.17)

Table 3.17: Substitutent effect comparisons for TIM and MGS catalysis

Enzyme	Substrate	k_{cat}/K_M	k_B	$(k_{cat}/K_M)/(k_B)$	KOE[a]
		$(M^{-1}s^{-1})$	$(M^{-1}s^{-1})$		
TIM	GAP	2.4 x 10^8	6.5 x 10^{-3}	4 x 10^{10}	7.7 x 10^8
	GA	0.34	6.5 x 10^{-3}	52	
MGS	DHAP	5.2 x 10^6	1.1 x 10^{-3b}	4.7 x 10^9	1.2 x 10^5
	DHAS	56.5	1.4 x $10^{-3\,c}$	4 x 10^4	

a) The 'knockout effect' (KOE) observed by replacing a phosphate group with a hydroxyl group in the case of GAP-GA, or replacing a phosphate group with a sulfate group in the case of DHAP-DHAS was calculated by dividing $((k_{cat}/K_M)/k_B))/k_B$. b) The value for quinuclidinone (50 % f_B) catalyzed elimination of DHAP. c) The value for quinuclidinone, 70 % f_B catalyzed elimination of DHAS.

It can be seen that replacing the phosphate group of natural substrate with monoanionic sulfate for the MGS catalyzed reaction has a smaller KOE than for the TIM catalyzed reaction where the phosphate group of GAP has been replaced by a hydroxyl group. This is not surprising given that the sulfate moiety will still retain the ability to undergo electrostatic interactions at the active site of the enzyme whereas for GA the charge has been completely removed. To conduct more accurate experiments and make direct comparisons with the reactions catalyzed by TIM, the reactions of DHA (26) (in the presence of MGS) should be carried out at higher concentrations of enzyme.

Chapter 4

Conclusions

Prior to the commencement of this work it could was expected that any change in the structure of natural substrate DHAP, would lead to a reduced k_{cat}/K_M for the turnover of the mutant substrate in question. The fact that MGS catalyzes the elimination of DHAP with remarkable efficiency and specificity implies that the slightest change in any structural features of natural substrate DHAP may lead to a reduced rate of elimination. Furthermore the active site residue may not accommodate a 'mutant' substrate as well as a natural substrate which would lead to a reduction in the level of catalysis.

In solution, the rates for the background, non-enzymatic reactions of these substrates towards C-3 deprotonation were expected to be more similar than at the C-1 position as the former position is more remote from the site of substituent change. Differences in the rates of C-1 deprotonation were predicted given the nature of the adjacent C-1 substitutents.

For the monoanionic substrate dihydroxyacetone sulfate (DHAS) it was found that C-1 and C-3 deprotonation occurred in the same pD range. Deuterium incorporation at the C-1 position following C-1 deprotonation (indicating enolization) was found to occur at a rate of approximately twice that of C-3 deprotonation (rate-determining enolization followed by elimination) in the pD range of 7.3 to 9.2. The fact that deprotonation occurred faster at the C-1 position of this molecule suggests that the sulfate group has an acidifying effect on the adjacent α-protons greater than the effect of a hydroxyl group on its adjacent C-1 protons. For the background, non-enzymatic elimination reaction of DHAP a second order rate constant of 1.1 x 10^{-3} $M^{-1}s^{-1}$ for the quinuclidinone (50 % f_B) catalyzed deprotonation has been obtained by Richard *et al*. For the corresponding elimination reaction of DHAS, quinuclidinone (70% f_B) catalyzed C-3 deprotonation was found to occur at a rate of 1.4 x 10^{-3} $M^{-1}s^{-1}$. Despite the similar

rates for C-3 deprotonation, no C-1 deuterium incorporation was observed for the analogous reaction of DHAP in this buffer.

From the resulting pD rate profile obtained for the buffer independent reactions of DHAS it was found that the reactions from pD 8.5-9.2 are pD independent. Despite a 0.7 pD unit change, 12 % and 67 % increases in the rates of k_{int} for C-3 and C-1 deprotonation were observed respectively. This pD independent region of the pD rate profile constructed indicates that the sulfate group of DHAS may intramolecularly deprotonate the C-1 proton at the adjacent α-position.

Based on similarities of sulfate and thiosulfate moieties in terms of pK_a values for ionisation at oxygen it was expected that the rate of removal of the C-1 protons of DHAS and DHATS should be similar. However deuterium incorporation at the C-1 position of DHATS occured too fast to monitor in quinuclidinone buffers and even in phosphate buffers and thus was followed in acetic acid buffers and DCl solution. The fact that C-1 deprotonation and deuterium incorporation occurred so fast for this molecule in these buffers suggests a greater acidifying effect of the thiosulfate moiety relative to the sulfate of DHAS. In the pD range (2.2- 4.4) of these reactions the C-3 protons of the molecule did not react. For the reactions of the molecule in DCl solution it was found that a 1.1 unit pD change from pD 2.2-3.3 resulted in only a 2 fold increase in the rate of C-1 deprotonation. This suggests the reaction is pD independent also reflected in the relatively level pD rate profile in this range. Above this pD range 3.7- 4.3 the rate of C-1 deprotonation increases 4.5 fold (for the pD independent C-1 deprotonation). Accordingly the average rate for the acetate catalyzed reaction increases 4.9 fold in this range implying a hydroxide dependent reaction. An average kB for the acetate catalyzed C-3 deprotonation of DHATS of 5.2×10^{-2} M$^-$ 1s^{-1} was obtained. This rate is approximately 455,000 fold faster than the acetate catalyzed

deprotonation of acetone which emphasises the acidifying effect of the thiosulfate group of DHATS on the adjacent α-protons.

Reactions of the C-3 protons of DHATS were monitored in quinuclidinone and phosphate buffers however it was found that while a slight amount of elimination could be observed by ^{1}H NMR, the loss in peak area due to C-3 elimination was not matched by a corresponding increase in the elimination product (methylglyoxal) peak areas. Further analysis by mass spectrometry indicated formation of a dimeric species however the appearance of such a species was not observed by ^{1}H NMR. On this basis it was decided that the reactions of the C-3 protons of DHATS should be further investigated.

The only neutral substrate analogue to be investigated in these studies was bromohydroxyacetone, BHA. This molecule was found to crystallise as a dimer whose exact structure was not that suggested in the literature. Conversion of the dimer to monomeric BHA was carried out in 1M DCl solution. The reactions of the C-1 protons of BHA were obtained in acetic acid buffers. A 0.62 unit pD change results in a 3.2 fold increase in the pD independent k_{int} (s^{-1}) rate for C-1 deprotonation. In the same pD range an increase in the average rate of deprotonation k_{av} of 2.2 fold was found to occur. An average rate constant of 9.2 x 10^{-5} M^{-1}s^{-1} for the buffer catalyzed C-1 deprotonation of BHA was obtained. The C-3 deprotonation reactions of BHA were monitored in quinuclidinone buffers (90% f_B). The first order rate constants for the pD-independent reactions of the C-3 protons of BHA, 9.35 x 10^{-5} s^{-1} and DHAS, 9.30 x 10^{-5} s^{-1} are comparable indicating that perhaps the bromo and sulfate substitutents have similar long range effects on the rate of elimination at the C-3 position. Furthermore the second order rate constants for the buffer catalyzed reaction at the C-3 position for BHA, 3.30 x 10^{-3} M^{-1}s^{-1} and DHAS 3.35 x 10^{-3} M^{-1}s^{-1} are similar.

Reactions of dimeric BHA suggest that the proposed literature structure is incorrect. Reactions of this molecule were carried out in phosphate buffers (20% f_B). During the course of the reaction peaks due to the dimeric species were found to disappear with the corresponding increase in upfield triplets and singlets The appearance of such peaks is a clear indication of H/D exchange and thus protons at an enolizable position. The literature dimeric species does not contain enolizable protons thus the actual species which crystallises from solution is likely to be a dimer of an asymmetric structure such as that suggested in the discussion section. The fact that the monomer forming process occurs over 48 hours in DCl rules out a fast equilibration between dimer and monomer which could result in the H/D exchange reactions observed.

It was decided to follow the reactions of mutant substrates dihydroxyacetone, DHA and dihydroxyacetone sulfate, DHAS in the presence of MGS. The anomalous results obtained for the reactions of the C-3 protons of DHATS suggested that accurate kinetic data in the presence of MGS may not have been acquired. Similarly, the reactions of BHA were not monitored with MGS due to the presumed lability of this molecule in the presence of soft sulfur containing amino acids.

The background reactions of DHA were monitored in imidazole buffer (70 % f_B, pD 7.8). However it was found that over long reaction periods no exchange was observable. Similarly in the presence of MGS (7.7×10^{-4} mM) no exchange was observed. This could be expected based on the neutrality of the molecule and the basicity of the leaving group OH⁻.

Further ¹H NMR studies were carried out on natural substrate dihydroxyacetone phosphate, DHAP. Despite very low concentrations of MGS a rate for elimination was not possible to obtain by ¹H NMR as the reaction to form methylglyoxal occurred too quickly.

From the reactions of DHAS in the presence of MGS, average k_{cat}/K_M values for exchange and elimination of 43.5 $M^{-1}s^{-1}$ and 56.5 $M^{-1}s^{-1}$ were obtained respectively. MGS catalyzes the elimination of DHAP with a value of k_{cat}/K_M of approximately 6 x 10^6 $M^{-1}s^{-1}$. The difference in the rates of elimination of these substrates is approximately 90,000 fold. At biological pD the dianionic sulfate leaving group of DHAS has a pK_a of approximately 3 whereas the pK_a of the trianionic phosphate group of DHAP is approximately 12. Based on these values it could be expected that DHAS will eliminate faster than DHAP. An E1cB mechanism is predicted for DHAS which involves a rate-limiting deprotonation step. Elimination by this intramolecular mechanism in solution would be predicted to be faster than for DHAP as deprotonation of a monoanionic substrate would be more facile than a dianionic substrate. However in the presence of MGS this clearly was not observed. The final k_{cat}/K_M values obtained suggest that disrupting the structure of natural substrate from dianionic to monoanionic has a huge effect on the enzymatic rate for overall elimination. Clearly several enzyme-substrate interactions which favour overall elimination have been lessened as a result of this substituent change.

Chapter 5

Experimental

5.0 Foreword

This chapter is divided into four subsections. Section 5.1 describes the general instrumentation and preparation of solutions used in kinetic analysis of the substrates. The synthesis of these substrates is discussed in Section 5.2. The techniques used in the overexpression and purification of *methylglyoxal synthase* (MGS) are discussed in Section 5.3. Finally, the kinetic techniques used in analysing the non-enzymatic and enzyme catalyzed reactions of the substrates are discussed in Section 5.4.

5.1 General instrumentation

NMR samples were prepared in deuterated chloroform, deuterium oxide and d^6- dimethyl sulfoxide (DMSO). Tetramethylsilane (TMS) was used as an internal reference in deuterated chloroform. ^{1}H NMR and ^{13}C NMR spectra at 300, 400 and 500 MHz were recorded on Oxford Varian Unity Inova 300 and 500 MHz NMR spectrometers in University College Dublin. In the University of Durham NMR spectra were recorded on a Varian Unity 300, a Bruker Ultrashield 400, and an Oxford Varian Inova 500 spectrometer. ^{1}H and ^{13}C NMR chemical shifts in CDCl$_3$ are reported relative to CHCl$_3$ at 7.27 ppm and 77.0 ppm respectively. In D$_2$O ^{1}H NMR chemical shifts are reported relative to HOD at 4.67 ppm. In d^6-DMSO ^{1}H NMR and ^{13}C NMR chemical shifts are reported relative to d^5-DMSO at 2.50 ppm and 39.52 ± 0.06 ppm respectively. Elemental analyses were obtained from the Microanalytical Unit, Chemistry Department, Durham University. Melting points were measured using a Gallenkamp Melting Point Apparatus. Thin Layer Chromatography was carried out using silica-backed Merck Kieselgel 60 F254 plates.

5.1.1 Materials and preparation of solutions

Deuterium oxide (99.9 % D), deuterium chloride (35 %, 99.5 % D), potassium deuteroxide (40 wt % 98+ %D) and deuterated chloroform (99.8 % D) were purchased from Apollo Chemical company. 2-chloro-2-propen-1ol (90%), N-bromosuccinimide, sodium thiosulfate, sodium thiophosphate, sodium iodide sulphur trioxide-triethylamine complex, sulfur trioxide-pyridine complex and and mercuric oxide, were purchased from Aldrich Chemical company. The internal standard, tetramethylammonium deuteriosulfate, triisopropyl phosphite, pivaloyl chloride, chlorotrimethylsilane and triethylamine were purchased from Fluka chemical company. All other chemicals were reagent grade and were used without further purification unless otherwise stated.

5.1.1.1 Preparation of solutions for UV-Vis spectrophotometric experiments

Stock solutions of potassium hydroxide and hydrogen chloride were prepared by dilution and titration of the commercial concentrated solutions. Quinuclidine, quinuclidinone and buffers were prepared by mixing stock solutions of the respective buffer-HCl salts and stock solutions of potassium hydroxide with the addition of KCl when needed to give solutions of buffer at various acid/base ratios and I=0.1 (KCl). Imidazole buffers were prepared by mixing stock solutions of the neutral basic buffer and stock solutions of HCl with the addition of KCl when needed to give solutions of buffers at various acid/base ratios and I = 0.1 (KCl). Stock solutions of dihydroxyacetone phosphate (DHAP) and reduced glutathione were prepared with the addition of KCl to give I = 0.1 (KCl). All UV-Vis measurements were carried out on a Cary-100 UV-VIS spectrophotometer.

5.1.1.2 Preparation of solutions for ^{1}H NMR exchange experiments

For ^{1}H NMR exchange experiments stock solutions of potassium deuteroxide and potassium chloride were prepared by dilution and titration of the commercial concentrated solutions. Stock solutions of potassium salts, K_2DPO_4 and KD_2PO_4, were obtained from potassium phosphate monobasic and dibasic K_2HPO_4 and KH_2PO_4 by exchanging the hydrogen atoms for deuterium. This was achieved by dissolving the salts in D_2O, followed by removal of solvent under reduced pressure. The process was repeated five times and the salts were freeze dried. Phosphate buffers were then prepared by mixing stock solutions of K_2DPO_4 and KD_2PO_4 in D_2O with addition of KCl to give solutions of buffer at various acid/ base ratios and I=1.0 (KCl).

Quinuclidinone-DCl salts were obtained from quinucidinone-HCl salts respectively by exchanging the hydrogen atoms for deuterium in a similar method to the phosphate buffer exchange. Quinuclidinone buffers were prepared by mixing stock solutions of exchanged salt and stock solutions of potassium deuteroxide with the addition of KCl when needed to give solutions of buffer at various acid/base ratios and I=1.0 (KCl).

Stock solutions of acetate buffers were prepared by mixing stock solutions of potassium acetate and DCl with addition of KCl when needed to give buffer solutions at various acid/base ratios and I=1.0 (KCl).

5.1.1.3 Dialysis of MGS for enzyme kinetic experiments

Prior to commencing the NMR experiments the MGS was subject to dialysis in imidazole buffer (83 mM, I =0.1, KCl, pD = 7.9) at 4 °C. The buffer was initially left for 24 hours after which it was changed every 10 hours for a further 72 hours. This ensured complete deuterium exchange of all exchangeable MGS protein sites had occurred. Immediately prior to use the enzyme was gently syringed out of the cassette and stored in the fridge until ready to use.

5.1.1.4 Q TOF of MGS

Protein mass spectrometry was rnu on a waters Q-TOF premier, waters mass prep. Desalting cartridges (2.1 x 10 mm) were used with eluting gradient of acetonitrile (0.1 % formic acid). Protein mass was deconvuluted using max ent. 1 Infused from a Hamilton 20 µL syringe.

5.2 Synthesis of Substrates for Kinetic Measurements

The majority of substrates used in this project were synthesised following established literature procedures. In some cases the conditions were altered to improve the yields or purity of the compounds being synthesised.

5.2.1 Bromohydroxyacetone (22)

(20)   (22)
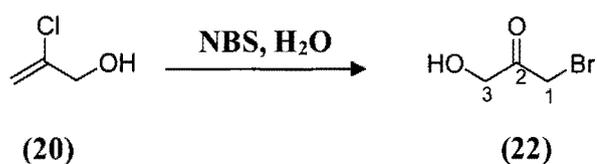
2-Chloro-2-propen-1-ol **(51)** (3.8 mL, 50 mmol) was added dropwise to a stirred solution of *N*-bromosuccinimide (8.8 g, 50 mmol) in H_2O (250 mL). After 30 minutes of stirring at room temperature the pale yellow solution was concentrated to 10 mL. Silica (10g) was added to the solution which was then dried under vacuum for 5 hours. The dry-loaded silica was slurried with hexane/ethylacetate 2:1 (20 mL) and poured directly onto a packed silica column. The fractions were combined and concentrated to approximately 5 mL. The purified bromohydroxyacetone **(22)** was recrystallised by the dropwise addition of dichloromethane to yield a white crystalline solid. R_f 0.2 (hexane/ethylacetate 2:1) (4.2g, 55%); **mp** 87-89 °C (at this temperature strong bromine fumes were given off).

Bromohydroxyacaetone **(22)** crystallises as a mixture of dimer **(23)** and monomer (Scheme 4.1) which redissociates into the monomer (over time) when dissolved in DCl. In non-hydroxylic solvents bromohydroxyacetone is present mainly in dimeric form. As discussed, based on the reactions observed, the exact structure of the dimer species is unclear. The chemical shifts of the protons in the dimer/monomer mixture are presumed to correspond to the methylene protons of the acyclic dimer previously discussed in Chapter 2.

Scheme 5.1.

2 HO⟍3↓↓1↘Br ⟶ (22)   (48)
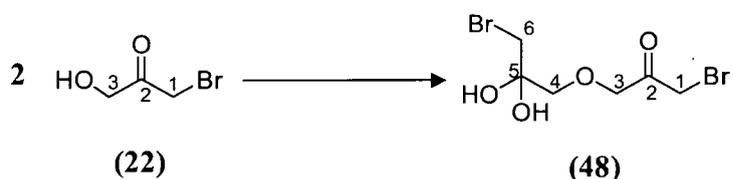
IR: Not possible to obtain due to decomposition on grinding sample; **¹H NMR**: **Dimer/monomer mixture** (D_2O); δ 3.54 ppm (Dimer C-4, s, 2H, OC*H₂*C), 3.59 ppm (Monomer C-3, s, 2H, C*H₂*OH, hydrate), 3.63 ppm (Dimer C-6, s, 2H, CC*H₂*Br), 3.65 ppm (Monomer C-1,

s, 2H, C*H₂*Br, hydrate), 4.21 (Dimer C-3, s, 2H, OC*H₂*CO), 4.43 (Monomer C-1, s, 2H, C*H₂*Br, keto), 4.47 (Monomer C-3, s, 2H, C*H₂*OH, keto), 4.51 (Dimer C-1, s, 2H, C*H₂*Br); **¹H NMR; Monomer** (D₂O); δ 3.47 ppm (C-3, s, 2H, C*H₂*OH, hydrate), 3.53 ppm (C-1, s, 2H, C*H₂*Br, hydrate), 4.31 (C-1, s, 2H, C*H₂*Br, keto), 4.35 (C-3, s, 2H, C*H₂*OH, keto); **¹³C NMR: Dimer/monomer mixture (only dimer peaks detectable)** (DMSO); δ 34.5 ppm (Dimer C-6, *C*H₂Br), 38.3 (Dimer C-1, *C*H₂Br), 77.3 (Dimer C-4, *C*H₂O), 78.1 (Dimer C-3, O*C*H₂), 201.9 (*C*OCH₂Br); **ES:m/z:**(TOF MSMS ES⁻, ES⁺) 152.9 (M⁻, 100 %), 150.9 (M⁻ 100 %), 328.8 (M⁺ (Na⁺), 100 %).

Lit: **¹H NMR** (D₂O) δ 3.48 ppm (s, 2H, C*H₂*OH, hydrate), 3.52 ppm (s, 2H, C*H₂*Br, hydrate), δ 4.31 ppm (s, 2H, C*H₂*Br, keto), 4.35 ppm (s, 2H, C*H₂*OH, keto); **¹³C NMR*Dimer** (DMSO) δ 35.9 ppm (s, *C*H₂COH), 63.9 ppm (s, *C*OHOC), 91.4 ppm (*C*H₂Br)

5.2.2 Dihydroxyacetone thiosulfate (25)

(22) → **(25)**
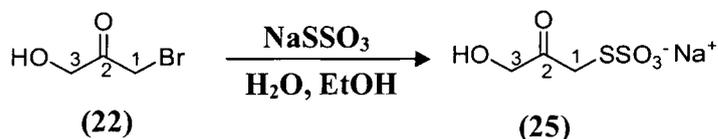
Sodium thiosulfate (320 mg, 2.0 mmol) was added to a stirred solution of bromohydroxyacetone **(22)** (110 mg, 1.0 mmol) in H₂O (1 mL) and ethanol (1.5 mL). Stirring was continued at room temperature for 3 hours after which time the solution was concentrated *in vacuo* and the residual material was dissolved in ethanol. The yellow precipitate which formed was filtered by suction

and the ethanol filtrate was concentrated to yield dihydroxyacetone thiosulfate (25) as a pale yellow powder. R_f = 0.32 (ethanol) (44 mg, 21 %); **mp** 91-93 ° C.

IR (cm^{-1}): ν 761 cm^{-1}(CSS), 1203 cm^{-1} (S=O), 1711 cm^{-1} (C=O), 2897 cm^{-1} (CH$_2$), 3428 cm^{-1} (OH); **^{1}H NMR** (D$_2$O); δ 3.41 ppm (C-1, s, 2H, CH_2-SSO$_3^-$, hydrate), 3.60 (C-3, s, 2H, CH_2OH, hydrate), 3.98 (C-1, s, 2H, CH_2-SSO$_3^-$, keto), 4.55 (s, 2H, CH_2OH, keto); **^{13}C NMR** (D$_2$O) δ 62.5 ppm (C-1, CH$_2$SSO$_3^-$, keto), 63.2 (C-1, CH$_2$SSO$_3^-$, hydrate), 70.7 (C-3, CH$_2$OH, keto), 71.1 (C-3, CH$_2$OH, hydrate), 94.8 ppm (C(OH)$_2$, hydrate), 203.2 (CO); **ES:m/z**: (ES$^-$) 184.9 (M$^-$, 100 %); **C$_3$H$_5$O$_5$S$_2$Na**: C, 17.30, H 2.40, Found C, 17.32, H 2.39.

5.2.3 Dihydroxyacetone thiophosphate (24)

(22)   (24)
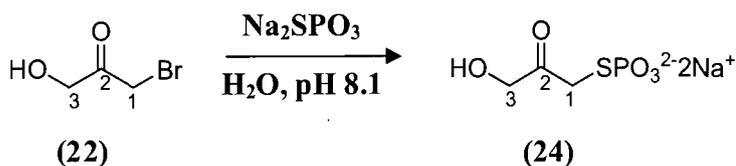
Bromohydroxyacetone (22) (75 mg, 0.50 mmol) was added to a stirred solution of sodium thiophosphate (120 mg, 0.75 mmol) in 10 mL H$_2$O. The solution was stirred at room temperature for 1 hour maintaining a pH of 8.1 with 2M KOH. The pale yellow solution was then concentrated and dissolved in methanol. The precipitate formed was suction filtered and the methanol filtrate was concentrated to form a yellow oil. 10mL THF (10 mL) was added dropwise to the oily residue and a yellow precipitate formed which was filtered through a sintered glass

funnel. Analysis of the yellow powder showed that the product thiophosphate (24) was formed. R_f =0.24 (ethanol) (20 mg, 19 %); **mp** 95-97 °C.

IR (cm^{-1}): Not possible to obtain due to decomposition. **^{1}H NMR** (D$_2$O) δ 2.88 ppm (C-1, d, 2H, CH_2-SPO$_3^{2-}$, hydrate, $^3J_{H,P}$ 13.2 Hz), 3.49 (C-3, s, 2H, CH_2OH, hydrate), 3.51 (C-1, d, 2H, CH_2-SPO$_3^{2-}$, keto, $^3J_{H,P}$10 Hz), 4.42 (C-3, s, 2H, CH_2OH, keto); **^{13}C NMR;** Not possible to obtain due to long NMR reaction time. **^{31}P NMR** (D$_2$O) δ 16.77 ppm (SPO_3^{2-}, hydrate), δ 20.12 ppm (SPO_3^{2-}, keto); **ES:m/z:** (ES$^-$) 191.2 (M$^-$, 100 %).

C$_3$H$_5$O$_5$SP2Na: Not possible to obtain due to decomposition.

Lit: **^{1}H NMR** (D$_2$O) δ 3.0 ppm (d, 2H, CH_2-SPO$_3^{2-}$, hydrate), δ 3.98 ppm (s, 2H, CH_2OH, hydrate), δ 4.01 ppm (d, 2H, CH_2-SPO$_3^{2-}$, keto), δ 4.55 ppm (s, 2H, CH_2OH, keto);

5.2.4 Dihydroxyacetone Sulfate (27)
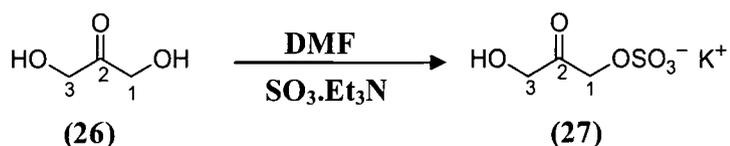
Dihydroxyacetone (26) (0.25 g, 2.5 mmol) was dissolved in N,N-Dimethylformamide (1.5 mL) under argon and the solution was cooled to 0° C in ice. Triethylamine-sulfur trioxide complex (0.84 g, 5 mmol) dissolved N,N-dimethylformamide (1.5 mL) was added slowly to the stirred solution of dihydroxyacetone. After 2 hours of stirring at 0 ° C, H$_2$O (50 mL) was added and the

solution was poured through an 11 x 1.5 cm column loaded with dowex 50Wx2 (hydrogen form) resin (8 g). (This resin was equilibrated in water for 1 hour prior to use). The effluent and washings were collected and dowex 1 x 4 50 resin (1g) was added. The mixture was swirled for 5 minutes. After this time more dowex 1 x 4 50 resin (8 g) was added to the solution and swirling was continued for a further 5 minutes. Perchloric acid (20 mL, 1.0 M) was added dropwise to the resin/mixture until a pH of 1.8 was reached. The resin was filtered through sintered glass and washed with deionised H_2O (100 mL). The eluent was brought to pH 4.1 with the addition of potassium carbonate (0.1M). The solution was then concentrated in *vaccuo* to approximately 15 mL. Acetone (12mL) and ethanol (36 mL) were added to the solution and concentrated once again to 15 mL. The solution was left at -20 ° C for 12 hours. After this the white precipitate which had formed was filtered and removed. The remaining solution was concentrated and methanol (20 mL) was added resulting in further precipitation. The remaining solution was concentrated resulting in pure dihydroxyacetone sulphate R_f = 0.2, Methanol (30 mg, 25 %); **m.p**, 87-90 ° C;

IR (cm^{-1}): ν 790 cm^{-1} (COS), 1241 cm^{-1} (S=O), 1711 cm^{-1} (C=O), 2906 cm^{-1} (CH$_2$), 3417 cm^{-1} (OH); **^{1}H NMR** (D$_2$O) δ 3.55 ppm (C-3, s, 2H, CH_2OH, hydrate), 3.99 (C-1, s, 2H, CH_2OSO$_3^-$, hydrate), 4.43 (C-3, s, 2H, CH_2OH, keto), 4.73 (C-1, s, 2H, CH_2OSO$_3^-$, keto), **^{13}C NMR** (D$_2$O) δ 61.9 ppm (HOCH$_2$, hydrate), 62.9 (HOCH$_2$, keto), 69.7 (CH$_2$OSO$_3^-$, hydrate), 70.1 (CH$_2$OSO$_3^-$, keto), 92.8 (C(OH)$_2$,hydrate), 209.3 (CO); **ES:m/z** (ES$^-$) 185.1 (M$^-$, 100 %). **C$_3$H$_6$O$_6$SK** : Requires: C 17.22 , H 2.88. Found C 17.24, H 2.94.

(C-4, s, 2H, HOCH_2CO); ^{13}C NMR (CDCl$_3$) δ 14.9 ppm (OCH$_2$CH$_3$), 38.9 (CH$_2$CH$_2$OEt), 64.4

(OCH$_2$CH$_3$), 68.5 (CH$_2$CH$_2$OEt), 72.4 (HOCH$_2$CO), 204.4 (COCH$_2$CH$_2$); ES:m/z:(ES$^+$) 155.2

(M$^+$, (Na$^+$) 100 %).

5.2.6 4'-Ethoxy-2'-Oxobutyl ester (30)

(29)   (30)

4'-Ethoxy-1-hydroxybutan-2-one (29) (10.2 g, 77 mmol) was dissolved in dry ether (200 mL)

under argon and cooled in an ice-bath to 0 °C. Triethylamine (42 mL, 300 mmol) was then

added, followed by the addition of pivaloyl chloride (25.3 g, 210 mmol) over a period of twenty

minutes. The mixture was stirred overnight at room temperature. After this time it was then

poured into ice-water. The organic layer was washed with HCl (20 mL, 1.0 M), aqueous

NaHCO$_3$ (20 mL, 5% (w/v) and H$_2$O (20 mL) and dried over MgSO$_4$. The drying agent was

removed by filtration. The desired product was purified by column chromatography (1:9 ether

/pet. Spirits) to yield a pale yellow oil. R$_f$ = 0.43 (ether/pet.spirits) (12.6 g, 75 %); bp (110-112

°C)/10 mBar.

IR (cm^{-1}): ν 1721 cm^{-1} (C=O), 2911 cm^{-1} (CH$_2$), cm^{-1}; ^{1}H NMR (CDCl$_3$) δ 1.17 ppm (t, 3H,

OCH$_2$CH_3,^{3}J 6.9 Hz), 1.34 (s, 9H, Me$_3$C), 2.66 (C-1, t, 2H, CH_2OEt, ^{3}J 6.8 Hz), 3.44 (q, 2H,

OCH_2CH$_3$, ^{3}J 7.3 Hz), 3.61 (C-2, t, 2H, CH_2CH$_2$OEt, ^{3}J 6.3 Hz), 4.67 (C-4, s, 2H, OCH_2CO);

(C-4, s, 2H, HOCH_2CO); ^{13}C NMR (CDCl$_3$) δ 14.9 ppm (OCH$_2$CH$_3$), 38.9 (CH$_2$CH$_2$OEt), 64.4

(OCH$_2$CH$_3$), 68.5 (CH$_2$CH$_2$OEt), 72.4 (HOCH$_2$CO), 204.4 (COCH$_2$CH$_2$); ES:m/z:(ES$^+$) 155.2

(M$^+$, (Na$^+$) 100 %).

5.2.6 4'-Ethoxy-2'-Oxobutyl ester (30)
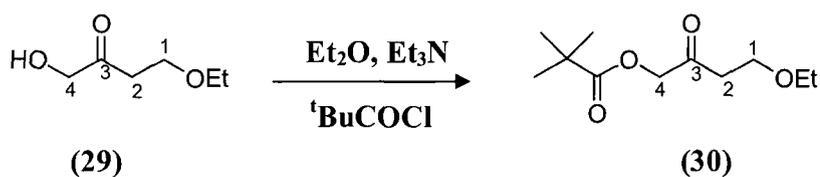

4'-Ethoxy-1-hydroxybutan-2-one (29) (10.2 g, 77 mmol) was dissolved in dry ether (200 mL)

under argon and cooled in an ice-bath to 0 °C. Triethylamine (42 mL, 300 mmol) was then

added, followed by the addition of pivaloyl chloride (25.3 g, 210 mmol) over a period of twenty

minutes. The mixture was stirred overnight at room temperature. After this time it was then

poured into ice-water. The organic layer was washed with HCl (20 mL, 1.0 M), aqueous

NaHCO$_3$ (20 mL, 5% (w/v) and H$_2$O (20 mL) and dried over MgSO$_4$. The drying agent was

removed by filtration. The desired product was purified by column chromatography (1:9 ether

/pet. Spirits) to yield a pale yellow oil. R$_f$ = 0.43 (ether/pet.spirits) (12.6 g, 75 %); bp (110-112

°C)/10 mBar.

IR (cm^{-1}): ν 1721 cm^{-1} (C=O), 2911 cm^{-1} (CH$_2$), cm^{-1}; ^{1}H NMR (CDCl$_3$) δ 1.17 ppm (t, 3H,

OCH$_2$CH_3,^3J 6.9 Hz), 1.34 (s, 9H, Me$_3$C), 2.66 (C-1, t, 2H, CH_2OEt, ^3J 6.8 Hz), 3.44 (q, 2H,

OCH_2CH$_3$, ^3J 7.3 Hz), 3.61 (C-2, t, 2H, CH_2CH$_2$OEt, ^3J 6.3 Hz), 4.67 (C-4, s, 2H, OCH_2CO);

^{13}**C NMR** (CDCl$_3$) δ 15.4 ppm (OCH$_2$*C*H$_3$), 26.8 (*Me$_3$*C), 37.9 (Me$_3$*C*), 38.4 (C-2, *C*H$_2$CH$_2$OEt), 64.1 (C-1, O*C*H$_2$CH$_3$), 66.2 (CH$_2$*C*H$_2$OEt), 179.9 (*C*OO), 205.5 (*C*OCH$_2$); **ES**:m/z:(ES$^+$) 239 (M$^+$, (Na$^+$) 100 %), **C$_{11}$H$_{20}$O$_4$**: Requires: C 61.09, H 9.32. Found C 61.15 H 9.28.

Lit: IR (cm^{-1}): ν 1733 cm^{-1}(C=O), 1135 cm^{-1} (OEt), 1162cm^{-1}(COCOCH$_2$); ^{1}**H NMR** (CDCl$_3$) δ 1.18 ppm (t, 3H, OC*H$_2$*CH$_3$, ^3J 7.1 Hz), 1.27 ppm (s, 9H, Me$_3$C), 2.67 ppm (C-1, t, 2H, C*H$_2$*OEt ^3J 6.4 Hz), 3.70 ppm (C-2, t, 2H, C*H$_2$*CH$_2$OEt, 6.4 Hz), 4.69 (s, 2H, OC*H$_2$*CO); ^{13}**C NMR** (CDCl$_3$) δ 15.1 ppm (OCH$_2$*C*H$_3$), 27.1 ppm (*Me$_3$*C), 38.7 ppm (Me$_3$*C*), 39.5 ppm (*C*H$_2$CH$_2$OEt), 64.9 ppm (O*C*H$_2$CH$_3$), 66.5 ppm (CO*C*H$_2$CH$_2$O), δ 68.4 ppm (O*C*H$_2$), δ 177.8 ppm (*C*OO), δ 202.6 ppm (*C*OCH$_2$); ES:m/z (ES$^+$) 216; **C$_{11}$H$_{20}$O$_4$** : Requires: C 61.09, H 9.32. Found C 60.82, H 9.17

5.2.7 4'-Iodo-2'-oxobutyl ester (31)

(30)   (31)
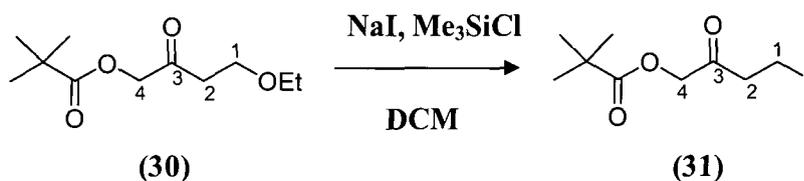
To a stirred solution of 4'-Ethoxy-2'-oxobutyl ester (15.0g, 72 mmol) and sodium iodide (12.2 g, 81 mM) in dry dichloromethane (250 mL) flushed with argon was added at 0 ° C Me$_3$SiCl (10.3 mL, 81 mM) during 15 minutes. Stirring was continued at room temperature for complete conversion. The reaction was monitored over 15 minute intervals by ^{1}H NMR spectroscopy. The brown mixture was poured into ice water and washed with 10% Na$_2$S$_2$O$_3$ (50 mL), H$_2$O (50 mL)

and dried over MgSO$_4$. The Drying agent was removed by filtration. The iodide (31) was prepared immediately prior to use without further purification due to its lability (11.3 g, 53 %).

^{1}H NMR (CDCl$_3$) δ 1.24 ppm (s, 9H, Me$_3$C), 3.08 (C-1, t, 2H, CH$_2$CH$_2$I, ^3J 7.6 Hz), δ 3.20 (C-2, t, 2H, CH$_2$CH$_2$I , ^3J 7.2 Hz), 4.59 (C-4, s, 2H, OCH$_2$CO); ^{13}C NMR (CDCl$_3$) δ -2.1 ppm (C-1, CH$_2$CH$_2$I), δ 27.3 (Me$_3$C), δ 38.8 (Me$_3$C), δ 38.6 (C-2, CH$_2$CH$_2$I), δ 66.2 (C-4, OCH$_2$CO) δ 178.9 (COO), δ 205.5 (COCH$_2$).

Lit: ^{1}H NMR (CDCl$_3$) δ 1.27 ppm (s, 9H, Me$_3$C), δ 3.10 ppm (C-1, t, 2H, CH$_2$CH$_2$I, ^3J 7.1 Hz), δ 3.30 ppm (C-2, t, 2H, CH$_2$CH$_2$OEt ^3J 6.4 Hz), δ 4.63 ppm (C-4, s, 2H, OCH$_2$CO); ^{13}C NMR (CDCl$_3$) δ -6.1 ppm (CH2CH$_2$I), δ 27.1 ppm (Me$_3$C), δ 38.6 ppm (Me$_3$C), δ 42.7 ppm (C-3'), δ 67.8 ppm (COCH$_2$CH$_2$O), δ 177.7 ppm (COO), δ 201.8 ppm (COCH$_2$)

5.2.8 3-Oxo-4-(2,2-dimethylpropionly)oxobutylphosphonic Acid Diisopropyl ester (32)
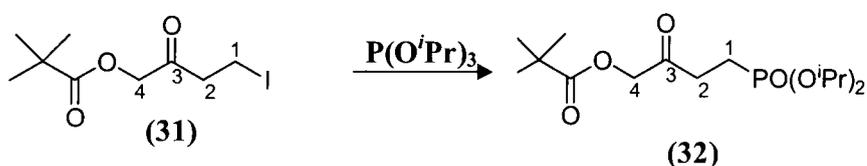
A solution of 4'-iodo-2'-oxobutylester (**31**) (21.2 g, 71 mM) in triisopropyl phosphite (175 mL, 710 mM) was heated at 120 °C under argon for four hours. The phosphite was then removed under reduced pressure and the remaining residue was purified by silica chromatography (EtOAc) to give (**32**) as a pale yellow solid. Rf = 0.4 (EtOAc) (12.5 g, 52 %).

^{1}H NMR (CDCl$_3$) δ 1.25 ppm (s, 9H *Me$_3$*C), δ 1.29 ppm (2d, 12 , OCH*Me$_2$*, ^3J 6.6 Hz), δ 1.98 ppm (C-1, m, 2H, CH$_2$C*H$_2$*PO, ^3J 6.7 Hz, ^{2}J$_{H,P}$ 11.3 Hz), δ 2.68 ppm (C-2, m, 2H, C*H$_2$*CH$_2$PO, ^3J 6.8 Hz, ^{3}J$_{H,P}$ 11.8 Hz), δ 4.67 (C-4, s, 2H, C*H$_2$*CO), δ 4.71 ppm (sep, 2H, OC*H*Me$_2$, ^2J 6.3 Hz, ^{3}J$_{H,P}$ 13 Hz); **^{13}C NMR** (CDCl$_3$) δ 19.8 ppm (C-1, d, C*H$_2$*PO, Jc,p 154.0 Hz), 24.2 (2d, OCH*Me$_2$*, Jc,p 4.9 Hz, Jc',p 4.8 Hz), 27.4 (*Me$_3$*C), 38.5 (Me$_3$*C*), 35.9 (*C*H$_2$CH$_2$PO, ^{2}J$_{C,P}$ 34.2 Hz), 70.1 (O*C*HMe$_2$), 71.4 (O*C*H$_2$CO), 177.5 (*C*OOCH$_2$), 203.1 (*C*OO); **ES:m/z:(ES$^+$)** 358.3 (M$^+$ (Na$^+$) 100 %), **C$_{15}$H$_{29}$O$_6$P** : Requires: C 53.56, H 8.69. Found C 53.57, H 8.71

Lit: **^{1}H NMR** (CDCl$_3$) δ 1.28 ppm (s, 9H, *Me$_3$*C), δ 1.33 ppm (2d, 12H, OC*H*Me$_2$, ^3J 6.1 Hz), δ 2.00 ppm (C-1, m, 2H, CH$_2$C*H$_2$*PO ^3J 6.4 Hz), δ 2.72 ppm (C-2, m, 2H, C*H$_2$*CH$_2$PO ^{3}J 6.4 Hz), 4.68 (s, 2H, OC*H$_2$*CO), δ 4.71 ppm (m, 2H, OC*H*Me$_2$, ^{2}J 6.1 Hz); **^{13}C NMR** (CDCl$_3$) δ 20.2 ppm (C-1, d, C*H$_2$*PO, Jc,p 146.4 Hz), 23.9 (2d, OCH*Me$_2$*, Jc,p 3.7 Hz, Jc',p 5.5 Hz), 27.1 (*Me$_3$*C), 38.7 (Me$_3$*C*), 32.2 (*C*H$_2$CH$_2$PO, ^{2}J$_{C,P}$ 34.2 Hz), 70.4 (O*C*HMe$_2$), 67.7 (O*C*H$_2$CO), 177.8 (*C*OOCH$_2$), 202.1 (*C*OO); **ES:m/z:(ES$^+$)** 336 (M$^+$ (Na$^+$) 100 %), **C$_{15}$H$_{29}$O$_6$P** : Requires: C 53.56, H 8.69. Found C 53.54, H 8.76

5.2.8 2-Hydroxy-3-Oxobutylphosphonic Acid (33)
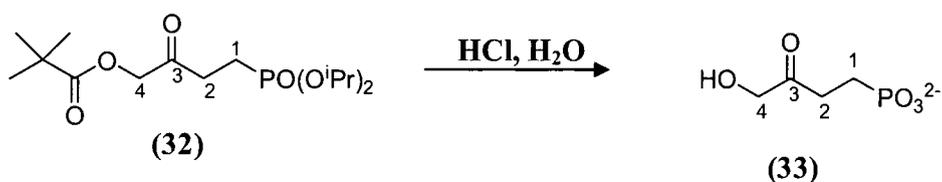
A stirred mixture of 3-oxo-4-(2,2-dimethylpropionly)oxybutylphosphonic acid (32) (20.2 g, 69 mM), H_2O (120 mL) and HCl (2 M 50 mL) was boiled under reflux for three hours. After diluting H_2O (100 mL), the solution was extracted with ether. The aqueous layer was evaporated and the remaining residue was dissolved in H_2O (120 mL). The solvent was evaporated and the remaining pale yellow oil. Analysis revealed that the desired product was not fully synthesized (as discussed in Chapter 2).

5.3 Overexpression of *methylglyoxal synthase* and general molecular biology methods

In this section the biological techniques used in the overexpression and purification of *methylglyoxal synthase* are discussed.

All procedures involving bacteria (or bacterial cultures) were carried out near a flame. All apparatus and solutions (with the exception of ampicillin stocks) were fully sterilized by autoclaving prior to use. Luria broth, bacto-agar, acrylamide, N'N'-bis-methylene-acrylamide, sodium dodecylsulfate (SDS), Tris base and β-mercaptoethanol were purchase from Fluka.

Reduced glutathione, glyoxlase I, D-lactoylglutathione, ammonium persulfate, TEMED, D-lactoylglutathione and dihydroxyacetone phosphate were purchase from Aldrich Chemical company.

E.Coli cells (BL 21) lacking endogenous MGS and pET16mgs plasmids were kindly provided by the Robert Edwards group at Durham university.

5.3.1 SDS-PAGE Gels:

SDS-PAGE was performed using a Bio-Rad 'mini-protean II' apparatus. The resolving and stacking gel solutions were made immediately prior to use

5.3.1.1 Resolving gel

10-12.5 % loading gels were prepared as follows: 30% acrylamide/bis (3.1 mL) were mixed with 1.0 M Tris-Cl (pH 8.8) (3 mL) and 20 % SDS (w/v) (38 µL). Deionised H_2O (1.3 mL) was added to the mixture. Immediately prior to pouring the buffer, Ammonium persulfate (36 µL) was added followed by TEMED (5 µL). The resolving gel buffer was poured to approximately 3cm from the top of the gel plates. The gel was covered with deionised H_2O (2.0 mL) and left to solidify for approximately 1 hour.

5.3.1.2 Stacking gel

In general the percentage of stacking gel buffer used in complete SDS PAGE preparation was less than that of the resolving gel buffer. Typically this method was found to provide better spreads in bands of higher to lower molecular weights (In this case percentage buffer used was 6 %). Preparation of the gel was carried out as follows: 30% acrylamide/bis (1.0 mL) was mixed with 1.0 M Tris-Cl (pH 6.8) (630 µL) and 20 % SDS (25 µL). Deionised H_2O (3.6 mL) were

added to the mixture. Immediately prior to pouring the buffer ammonium persulfate (36 μL) were added followed by TEMED (5 μL). The stacking buffer mix was poured gently on top of the resolving buffer gel, gel comb inserted, and left to solidify for approximately 40 minutes. After this time the gel comb was removed and the gel lanes were washed with water several times prior to addition of protein sample to each lane.

5.3.1.3 Protein sample preparation

Protein samples were prepared in a sample buffer (Protein: Buffer, 1:2). The sample buffer was prepared by the addition of Tris-Cl (pH 6.8) (2.4 mL) to 20% (w/v) SDS (3 mL) and 100% Glycerol (3.0 mL). β-mercaptoethanol (50 μL) was added followed by bromophenol blue (6.0 mg). The sample buffer had a dark brown colour which when mixed with protein samples turned to a purple colour. For each lane, 10 μL of a protein sample and 20 μL of sample buffer were mixed and heated to 95 °C for 5 minutes followed by centrifugation. Each well was then loaded with 20 μL of the solution.

5.3.1.4 Conditions for running gels

Gel running buffer (10X) was prepared by adding Tris base (30.3 g) to glycine (144 g) and SDS (10g) made up to 1L with deionised H_2O. For the Biorad apparatus 500 mL of 1X was generally needed to run a gel. Therefore 50 mL of the 10X buffer was diluted to 500 mL with deionised H_2O (450 mL). Gels were run at 200 mV for 1 hour at room temperature.

5.3.1.5 Staining and destaining gels

Once finished running, the gels were carefully removed from the cassette and washed once with deionised H_2O. Coomassie blue stain (20 mL) were added to the gel in a suitable container and

left to agitate over night. After approximately 18 hours of staining the gel was washed three times with water and dried. The gel was visualised using a Syngene gel doc.

5.3.2 Bacterial procedures

All procedures involving bacterial growth and manipulation were carried out following the procedure of Harrison *et al* [40].

5.3.2.1 Bacterial cultures

Bacterial cultures were generally incubated overnight. Cultures were prepared by adding a 10 μL pipette tip of an isolated bacterial colony to LB (Luria-Bertani) media (10 mL) supplemented with ampicillin (50 μg/mL). The resulting solutions were incubated a 37 °C with shaking at 100-180 rpm for 12-14 hours.

5.3.2.2 LB Agar bacterial plate preparation

LB-Agar plates were prepared by adding LB (6.25 g) and agar (3.75 g) to deionised H_2O (250 mL). The top of the conical flask was sealed with aluminium foil and the LB and agar were swirled to dissolve. Following autoclaving and cooling to below 50 °C, the solution was suplemented with ampicillin (150 μL, 500μg/mL). Approximately 20 mL of LB Agar was poured into each plate and allowed to set.

5.3.2.3 Compotent cell preparation and transformation procedures

LB (5mL) was inoculated with *E.Coli* BL 21 de3 and incubated overnight at 37 °C. The following morning the culture (1ml) was inoculated into freshly prepared LB (100 mL) and

incubated at 37 ° C for 4 hours (at this point the A_{600} was approximately 0.7). The cells were then centrifuged for 30 minutes at 3000 rpm and 4 ° C. The supernatant was discarded and the cells resuspended in 34 ml of RF1. The solution was then incubated on ice for 30 minutes, before being centrifuged at 3000 rpm and 4 ° C for 10 minutes. The supernatant was discarded and the cells were resuspended in 8 ml of RF2. The cells were divided into 200 µL aliquots and stored at -80 ° C until required.

RF1: KCl (100mM), $MnCl_2$ (50 mM), KAcO (30 mM), $CaCl_2$ (10 mM) and glycerol (15 %). Solution pH was then adjusted to pH 5.8 with glacial acetic acid and filtered through a 0.22 micron filter.

RF2: MOPS (10 mM), KCl (10 mM), $CaCl_2$ (75 mM), glycerol (15 %). Solution was adjusted to pH 6.8 with NaOH (100 mM) and filtered through a pre-rinsed 0.22 micron filter.

1 µL of plasmid (1ng/µL) was added to compotent cells. The cells were then incubated on ice for 30 minutes before being heat shocked at 42 ° C for exactly 90 seconds. The cells were then returned to ice for a further 2 minutes. The cells were then incubated on ice for 2 minutes and 400 µl of LB broth was added to the cells which were then incubated at 37 ° C for 1 hour. The transformation mixtures were then pipetted onto labelled plates containing ampicillin (100 µg/mL) and spread around the plates using a sterilized glass rod spreader.

5.3.3 Overexpression of MGS

5.3.3.1 Expression of wild-type MGS

1 ml of overnight culture from a single colony of *E.Coli* which had been transformed with the expression plasmid PET 16 mgs wt was added into a 1L culture and incubated at 37 ° C until the A_{600} was between 0.6-0.8. (Usually between 4 and 5 hours). Expression of the protein was induced by the addition of IPTG to a final concentration of 1mM. The culture was incubated for a further 4 hours at 30 ° C.

The bacteria were harvested by centrifugation after which the supernatant was discarded and the pellets were stored at -80 ° C until required.

5.3.3.2 Protein purification.

Protein purification was achieved using fast protein liquid chromatography (FPLC) using Capto Q^{TM} DEAE (anion exchange-weak) columns (1 mL). The bacterial cell pellet was defrosted and suspended in 40 mL of cell lysis buffer (imidazole/phosphate 50 mM/1mM, pH 7.3, I =0.1) and sonicated on ice at 30 % power for 5 cycles of 15 seconds on and 15 seconds off. The solution was then centrifuged at 20000g and 4 ° C for 30 hour to remove the cell debris from the solution.

Prior to purification by this chromatographic method the supernatant was heated to 80 ° C for 2 minutes and rapidly cooled in an ice-bath which led to the formation of a white precipitate. The suspension was then centrifuged at 2000g and 4 °C for 10 minutes and the supernatant was removed and stored in the fridge prior to use. The protein sample was adjusted to the pH of the imidazole/phosphate buffer system using a High–Trap desalting column. Before application to

the column the sample solution was centrifuged and filtered using Whatmann 0.45 µm cellulose nitrate membrane filters and degassed.

The protein was then purified by ion-exchange chromatogaphy at 4 ° C. Prior to use all solutions and buffers were filtered using Whatmann 0.45 um cellulose nitrate membrane filters and degassed before being loaded onto the column.

The pre-packed column was connected to a Pharmacia XK24 column and the system was washed with 5 column volumes of ethanol solution and 5 column volumes of water before being equilibrated with 5 column volumes of the cell lysis buffer described above at 1ml/min. The protein was loaded onto the column at 1ml/min, and washed with the two column volumes of imidazole/phosphate buffer (50 mM/1mM, pH 7.3, I = 0.1). The protein was eluted by increasing the salt concentration. This was achieved by increasing the concentration of the same buffer from 0 to 20 % in a step and holding at this concentration for 0.5 column volumes, and then increasing the concentration of buffer B 100 % steadily for 10 column volumes at flow rate of 1ml/min. 5ml fractions were collected. The UV absorbance sat 280nm was monitored on a UV-spectrophotometer and the fractions were analyzed for purity using the established literature assay for methylglyoxal synthase activity, SDS-PAGE and MALDI-TOF mass spectrometry.

5.3.3.3 Protein Concentration Detemination

MGS is a homohexameric protein with each monomer having a molecular weight of 17 kDa. Analysis by MALDI-TOFF mass spectrometry showed that the molecular weight of our purified MGS was 17,817 Da (in good agreement with the literature value of 17,000 Da). The concentration of MGS was determined using the Bradford assay method (Biorad), using bovine

serum albumin (BSA) as the protein standard. BSA standard (200 µL) were added to Coomassie brilliant dye reagent (800 µL). Prior to measuring the absorbance at 595 nm the solution was incubated at room temperature for 5 minutes.

5.4 Kinetic methods

5.4.1 Deuterium Exchange

H/D exchange reactions were generally carried out in the NMR tube and monitored directly by obtaining back to back scans on the instrument in use. In these cases the temperature of the instrument was calibrated to 25 °C prior to monitoring the reaction. For deuterium exchange of substrates which were followed out by quenching, reactions were carried out in 12.5 mL vials which were incubated at 25 ± 0.1 ° C in a thermostated water bath. All reactions were carried out in D_2O with the ionic strength maintained at I = 1.0 (with the exception of enzymatic reactions which were carried out at I =0.1) with KCl. For reactions which were monitored directly by obtaining back to back scans, 850-950 µL of buffer and 50-100 µL of internal standard solution were added directly to solid substrate. Typically (quenched) reactions were run on a 5 or 6 mL scale, and were initiated by injection of 500, or 1000 µL of substrate stock solution (50 mM) to the DCl, KOD or buffer solution, containing internal standards methanol or imidzole. In general, the final substrate and internal standard concentrations in the reaction solutions were 5 - 10 mM. The reaction progress was monitored over time by withdrawing aliquots (~850-950 µL) at timed intervals. Depending on the substrate these aliquots were quenched to pD 1-3 by addition of >1 M DCl solution. The samples were either analysed immediately or placed in a sealed plastic bag containing calcium chloride and stored in the freezer for analysis at a later time.

The pD of buffered solutions was determined at 25 °C using a MeterLab[TM] PHM 290 pH-Stat Controller equipped with a radiometer (pH 4 - 7 - 10 @ 25 °C) combination electrode, that could be standardised between pH 4 - 7 or pH 7 - 10 to encompass the pD of the buffer solution. The deuteroxide concentration was calculated from the equation $[DO^-] = (10^{pD - pK_w})/\gamma_{DO}$, where K_w = $10^{-14.87}$ M^2 is the ion product of D_2O at 25 °C and $\gamma_{DO} = 0.747$ is the apparent activity coefficient of deuterium ion under our experimental conditions. The estimated error on the observed pseudo-first-order rate constant (k_{obs}, s^{-1}) is $\pm$ 5 % based on the error of the ^1H NMR measurement. Although the measurements of k_{obs} and the calculation of pK_a are single determinations, the calculated error in similar measurements and calculations performed by Richard *et al* is $\pm$ 5 % for k_{obs} and $\pm$ 0.5 units for the pK_a.

^1H NMR spectra of all 'mutant' substrates were recorded on an Oxford Varian Unity Inova 300 spectrometer, Bruker Ultrashield 400 and Oxford Varian Inova 500 spectrometer. For spectra recorded on the Oxford Varian Inova 300 spectrometer a relaxation delay of 1 second was used between pluses for all compounds. Spectra (64 – 128 transients) were recorded with a 45.0 ° pulse angle, sweep width of 2999 Hz, and an acquisition time of 3.744 s (total acquisition time 5-10 min). Baselines were subject to first – order drift correction before integration of the peak areas. Substrate and product peak areas were compared with the peak of the internal standard that was set to an arbitrary figure of 1000.

Preliminary H/D ^1H NMR exchange experiments were generally recorded on a Bruker 400 Ultrashield spectrometer. The relaxation delay between pulses was set to 1 s on this

spectrometer. Spectra were recorded at a pulse angle of 90°, a sweep width of 8278.1 Hz, an acquisition time of 7.899 s, and 16 transients (total acquisition time 5-10 min). Baselines were subject to first–order drift correction before integration of the peak areas. The integrated peak area for the singlet due to the C2-H, and in cases where a further reaction occurred the area of other relevant peaks of was compared with the peak of the internal standard that was set to an arbitrary figure of 1000.

High resolution ^{1}H NMR spectra, in the case of the enzyme and non-enzyme catalyzed exchange and elimination reactions, were recorded on an Oxford Varian Inova 500 spectrometer with a relaxation delay of 20 s, sweep width of 7996.8 Hz, and acquisition time of between 4 - 6 s, and a 90° pulse angle. Spectra were run with 16 – 256 transients with a total acquisition time of between 5 minutes and 1 hour.

5.4.2 UV-Vis spectrophotometric measurement

UV-Vis measurements were made on Cary-100 and 300 instruments. Background elimination assays of substrates were carried out in 10 mL vials which were incubated at 37 ° C ± 0.1 ° C in a thermostated water-bath. All reactions were carried out at ionic strength 0.1 (KCl). Reactions were run on a 5 ml scale where substrate stocks (0.5 mL, 15 mM) were added to buffer (4.5 mL, 0.25 M). Aliquots (500 μL) were taken at recorded time intervlas for the assay. The assays were initiated by the addition of the above solution (500 μL) to imidzole (400 μL, 0.1 M) and reduced glutathione (15 mM, 30 μL). This comprised the background which was scanned at 240 nm for 5 minutes. After this time the assay was initiated by the addition of glyoxalase I (2.2 mg/mL, 1 μL). The reaction progress was monitored over time by observing the increase in absorbance at

240 nm on addition of glyoxalase I. For buffers of pH greater than 7 the reaction was quenched to pH 7 prior to addition of the aliquot of glyoxalase I.

References

356

1. Richard, J.P. and T.L. Amyes, *Proton transfer at carbon.* Curr Opin Chem Biol, 2001. **5**(6): p. 626-33.
2. Futer, O., et al., *Phosphoryl transfer is not rate-limiting for the ROCK I-catalyzed kinase reaction.* Biochemistry, 2006. **45**(25): p. 7913-23.
3. Richard, J.P., *Kinetic parameters for the elimination reaction catalyzed by triosephosphate isomerase and an estimation of the reaction's physiological significance.* Biochemistry, 1991. **30**(18): p. 4581-5.
4. Bruice, T.C. and A.F. Hegarty, *Biotin-bound CO2 and the mechanism of enzymatic carboxylation reactions.* Proc Natl Acad Sci U S A, 1970. **65**(4): p. 805-9.
5. Sibi, M.P. and K. Patil, *Enantioselective H-atom transfer reaction: a strategy to synthesize formaldehyde aldol products.* Org Lett, 2005. **7**(8): p. 1453-6.
6. Toth, K., et al., *Claisen-type addition of glycine to pyridoxal in water.* J Am Chem Soc, 2004. **126**(34): p. 10538-9.
7. Williams, N.H., *Models for biological phosphoryl transfer.* Biochim Biophys Acta, 2004. **1697**(1-2): p. 279-87.
8. Bronsted, *Acid and Basic Catalysis.* Chem. Reviews, 1905. **5**(3): p. 231

9. Maskill, H., *Structure and reactivity in organic chemistry.* Oxford chemistry primers 81. 1999, Oxford ; New York: Oxford University Press. 95 p.
10. Xudong, Y., Gold, M.A., Pollak, R. M, *Transition state imbalances in proton transfer from phenyl ring-substituted 2-tetralones to acetate ions.* J Am Chem Soc, 1999. **121**(26): p. 6220-6225.
11. Lee, I., Chang, K., Lee, B., Han.I, *Theoretical studies on the transition-state imbalance in malonitrile anion-forming reactions in the gas-phase an in water.* Journal of Physical organic chemistry, 1998. **10**(12): p. 908-916.
12. Bernasconi, C.F. and P.J. Wenzel, *Proton transfers from carbon acids activated by pi-acceptors. Changes in intrinsic barriers and transition state imbalances induced by a cyano group. An ab initio study.* J Org Chem, 2003. **68**(18): p. 6870-9.
13. Kresge, A.J., *What makes proton transfer fast.* Acc Chem Res, 1975. **8**(10): p. 354.
14. Bronsted, N., Pederson, K., Z. Phys Chem, 1924. **108**: p. 185

15. Robinson, J.R. and L.E. Matheson, *Linear free-energy relationship between alcohol pKa and solvolysis rates of esters where substituent variation is in the alkyl portion of the ester.* J Org Chem, 1969. **34**(11): p. 3630-3.
16. J, S., *An introduction to free energy relationships.* 1973.
17. Richard, J.P., *Acid-Base catalysis of the elimination and isomerisation reactions of triose phosphates.* J Am Chem Soc, 1984. **106**(17): p. 4926-4936.
18. Bell, R.P.e.a., Proc R. Soc. London, Ser. A, 1949. **176**(88).
19. Hupe, D.J., Wu, D, *The effect of solvation on .beta. values for nucleophilic reactions.* J Am Chem Soc, 1977. **99**(23): p. 7653.
20. Richard, J.P., Amyes, T. L, *Determination of the pKa of ethylacetate: Bronsted correlation for deprotonation of a simple oxygen ester in aqueous solution.* J Am Chem Soc, 1996. **118**(13): p. 3129-3141.
21. Bordwell, F.G., Boyle, W. J., Hautala, Jr. J. A., Yee, K. C.,, *Bronsted Coefficients Larger than 1 and Less Than 0 for Proton Transfer from Carbon Acids.* 1969. **91**(14): p. 4002-4003.

22. Bordwell, F.G., Boyle, W. J., Chun-Yee, K, *Equilibrium and kinetic acidities of nitroalkanes and their relation to transition state structure*

J Am Chem Soc, 1970. **92**(20): p. 5926-5932.

23. Agmon, N., *Is there a nitroalkane anomaly?* J Am Chem Soc, 1980. **102**(7): p. 2164-2167.

24. Albery, W.J., Bernasconi, C., Kresge, J., *Marcus-Grunwald theory and the nitroalkane anomaly.* Journal of Physical organic chemistry, 2004. **1**(1): p. 29-31.

25. Turnbull, D., Maron, D.H, *The ionization constants of Aci and Nitro forms of some Nitroparaffins.* J Am Chem Soc, 1943. **65**(2): p. 212-218.

26. Bernasconi, C.F., *Intrinsic barriers of reactions and the principle of nonperfect synchronization* Acc. Chem. Res., 1987. **20**(8): p. 301-308.

27. Bernasconi, C.F., Schuck, D. F.,, *Kinetics of reversible tholate addition to substituted B-itrostyrenes in water. Radicaloid trasition state or principle of nonperfect synchronization?* J. Org. Chem, 1992. **57**: p. 2365-2373.

28. Eigen, M.,
.   Angew Chem Int Ed Engl, 1964. **3**: p. 1.

29. Maskill, H., *Mechanisms of organic reactions.* Oxford chemistry primers 45. 1996, New York: Oxford University Press. 96 p.

30. Kresge, A.J., *The Bronsted relation-recent developments. Chem. Soc. Reviews,* 1973. **2**: p. 475-503.

31. Crugeiras, J., et al., *Glycine enolates: the effect of formation of iminium ions to simple ketones on alpha-amino carbon acidity and a comparison with pyridoxal iminium ions.* J Am Chem Soc, 2008. **130**(6): p. 2041-50.

32. Chiang, Y. and A.J. Kresge, *Enols and Other Reactive Species.* Science, 1991. **253**(5018): p. 395-400.

33. Guthrie, P.J., Kluger, R, *Electrostatic stabilization can explain the unexpected acidity of carbon acids in enzyme-catalyzed reactions.* J Am Chem Soc, 1993. **115**(24): p. 11569-11572.

34. Gerlt, J.A., Gassman, P, *Understanding enyzme-catalyzed proton abstraction frmo carbon acids: Details of stepwise mechanism for beta elimination reactions.* J Am Chem Soc, 1992. **114**(14): p. 5928-5934.

35. Kresge, A.J., Keefe, J. R, *The Chemistry of enols.* 1990.

36. Hammett, L.A., Zucker., L, *The mechanism of the acid catalyzed enolization of acetophenone derivatives.* J Am Chem Soc, 1939. **61**(10): p. 2785-2791.

37. Richard, J.P., et al., *Formation and stability of enolates of acetamide and acetate anion: an Eigen plot for proton transfer at alpha-carbonyl carbon.* J Am Chem Soc, 2002. **124**(12): p. 2957-68.

38. Amyes, T.L., A.C. O'Donoghue, and J.P. Richard, *Contribution of phosphate intrinsic binding energy to the enzymatic rate acceleration for triosephosphate isomerase.* J Am Chem Soc, 2001. **123**(45): p. 11325-6.

39. Stryer, *Biochemistry, 5th edition.*

40. Saadat, D. and D.H. Harrison, *Identification of catalytic bases in the active site of Escherichia coli methylglyoxal synthase: cloning, expression, and functional characterization of conserved aspartic acid residues.* Biochemistry, 1998. **37**(28): p. 10074-86.

41. Richard, J.P., *The enhancement of enzymatic rate accelerations by Bronsted acid-base catalysis.* Biochemistry, 1998. **37**(13): p. 4305-9.

42. Gerlt, J.A., *Electrophilic catalysis can explain the unexpected acidity of carbon acids in enzyme-catalyzed reactions.* J Am Chem Soc, 1991. **113**(25): p. 9667-9669.

43. Gerlt, J.A., Gassman, P, *Understanding enzyme-cataylzed proton abstraction from carbon acids: Details of stepwise mechanisms for beta elimination.* J Am Chem Soc, 1992. **114**(15): p. 5928-5934.

44. Taylor, E., Palmer, D.R, Gerlt, J, *The Lesser "Burden Borne" by o-succinylbenzoate synthase : An "Easy" reaction involving a carboxylate carbon acid.* J Am Chem Soc, 2001. **123**(24): p. 5824-5825.

45. O'Donoghue, A.C., T.L. Amyes, and J.P. Richard, *Hydron transfer catalyzed by triosephosphate isomerase. Products of isomerization of (R)-glyceraldehyde 3-phosphate in D2O.* Biochemistry, 2005. **44**(7): p. 2610-21.

46. Thornalley, P.J., *Glyoxalase I--structure, function and a critical role in the enzymatic defence against glycation.* Biochem Soc Trans, 2003. **31**(Pt 6): p. 1343-8.

47. Kenyon, G.L., Gerlt, J. A., Petsko, G, Kozarich J.W, *Mandelate Racemase: Structure-function studies of a pseudosymmetric enzyme.* Acc Chem Res, 1995. **28**: p. 178-186.

48. Bearne, S.L. and R. Wolfenden, *Mandelate racemase in pieces: effective concentrations of enzyme functional groups in the transition state.* Biochemistry, 1997. **36**(7): p. 1646-56.

49. Ha, N.C., et al., *Structure and enzymology of Delta5-3-ketosteroid isomerase.* Curr Opin Struct Biol, 2001. **11**(6): p. 674-8.

50. Feierberg, I. and J. Aqvist, *The catalytic power of ketosteroid isomerase investigated by computer simulation.* Biochemistry, 2002. **41**(52): p. 15728-35.

51. Zeng, B., Pollack, R., *Microscopic rate constants for the acetate ion catalyzed isomerisation of 5-Androstene-3, 17-dione to 4--Androstene-3, 17 dione: A model for steroid isomerase.* J Am Chem Soc, 1991. **113**(10): p. 3838-3842.

52. Babbitt, P.C., et al., *The enolase superfamily: a general strategy for enzyme-catalyzed abstraction of the alpha-protons of carboxylic acids.* Biochemistry, 1996. **35**(51): p. 16489-501.

53. Mitra, B., et al., *Mechanism of the reaction catalyzed by mandelate racemase: importance of electrophilic catalysis by glutamic acid 317.* Biochemistry, 1995. **34**(9): p. 2777-87.

54. Powers, V.M., et al., *Mechanism of the reaction catalyzed by mandelate racemase. 1. Chemical and kinetic evidence for a two-base mechanism.* Biochemistry, 1991. **30**(38): p. 9255-63.

55. Marsh, J.J., Lebherz, H.G, *Fructose bis-phosphate aldolases: an evolutionary history.* Trends Biochem Sci, 1992. **17**(3): p. 110-113.

56. Littlechild., J., Watson, H.C, *A data-based reaction mechanism for type I fructose bisphosphate aldolase.* Trends Biochem Sci, 1993. **18**(2): p. 36-39.

57. Lorentzen, E., et al., *Mechanism of the Schiff base forming fructose-1,6-bisphosphate aldolase: structural analysis of reaction intermediates.* Biochemistry, 2005. **44**(11): p. 4222-9.

58. Rieder, S.V. and I.A. Rose, *The mechanism of the triosephosphate isomerase reaction.* J Biol Chem, 1959. **234**(5): p. 1007-10.

59.   Iyengar, R. and I.A. Rose, *Liberation of the triosephosphate isomerase reaction intermediate and its trapping by isomerase, yeast aldolase, and methylglyoxal synthase.* Biochemistry, 1981. **20**(5): p. 1229-35.

60.   Bloom, B. and Y.J. Topper, *Absolute configuration of enantiomorphic carbanions involved in the aldolase and triose phosphate isomerase reactions.* Nature, 1958. **181**(4616): p. 1128-9.

61.   Bloom, B. and Y.J. Topper, *Mechanism of action of aldolase and phosphotriose isomerase.* Science, 1956. **124**(3229): p. 982-3.

62.   Blacklow, S.C., et al., *Triosephosphate isomerase catalysis is diffusion controlled. Appendix: Analysis of triose phosphate equilibria in aqueous solution by 31P NMR.* Biochemistry, 1988. **27**(4): p. 1158-67.

63.   Cooper, R.A., *Methylglyoxal synthase.* Methods Enzymol, 1975. **41**: p. 502-8.

64.   Hopper, D.J. and R.A. Cooper, *The regulation of Escherichia coli methylglyoxal synthase; a new control site in glycolysis?* FEBS Lett, 1971. **13**(4): p. 213-216.

65.   Hopper, D.J. and R.A. Cooper, *The purification and properties of Escherichia coli methylglyoxal synthase.* Biochem J, 1972. **128**(2): p. 321-9.

66.   Summers, M.C. and I.A. Rose, *Proton transfer reactions of methylglyoxal synthase.* J Am Chem Soc, 1977. **99**(13): p. 4475-8.

67.   Rose, I.A. and J.S. Nowick, *Methylglyoxal synthetase, enol-pyruvaldehyde, glutathione and the glyoxalase system.* J Am Chem Soc, 2002. **124**(44): p. 13047-52.

68.   Totemeyer, S., et al., *From famine to feast: the role of methylglyoxal production in Escherichia coli.* Mol Microbiol, 1998. **27**(3): p. 553-62.

69.   Saadat, D. and D.H. Harrison, *The crystal structure of methylglyoxal synthase from Escherichia coli.* Structure, 1999. **7**(3): p. 309-17.

70.   Marks, G.T., M. Susler, and D.H. Harrison, *Mutagenic studies on histidine 98 of methylglyoxal synthase: effects on mechanism and conformational change.* Biochemistry, 2004. **43**(13): p. 3802-13.

71.   Ray, S. and M. Ray, *Isolation of methylglyoxal synthase from goat liver.* J Biol Chem, 1981. **256**(12): p. 6230-3.

72.   Thornalley, P.J., *The glyoxalase system: new developments towards functional characterization of a metabolic pathway fundamental to biological life.* Biochem J, 1990. **269**(1): p. 1-11.

73.   Thornalley, P.J., *Glutathione-dependent detoxification of alpha-oxoaldehydes by the glyoxalase system: involvement in disease mechanisms and antiproliferative activity of glyoxalase I inhibitors.* Chem Biol Interact, 1998. **111-112**: p. 137-51.

74.   Rose, I., Iyenager, R., *Methylglyoxal Synthase uses the trans isomer or triose-1,2-enediol 3-phosphate.* J Am Chem Soc, 1983. **105**: p. 3301-3303.

75.   Bell, R.P., *The Proton in Chemisry.* 1973

76.   Zhang, Z., et al., *Crystal structure of recombinant chicken triosephosphate isomerase-phosphoglycolohydroxamate complex at 1.8-A resolution.* Biochemistry, 1994. **33**(10): p. 2830-7.

77.   Wierenga, R.K., et al., *The crystal structure of the "open" and the "closed" conformation of the flexible loop of trypanosomal triosephosphate isomerase.* Proteins, 1991. **10**(1): p. 33-49.

78. Berlow, R.B., T.I. Igumenova, and J.P. Loria, *Value of a hydrogen bond in triosephosphate isomerase loop motion.* Biochemistry, 2007. **46**(20): p. 6001-10.

79. Derreumaux, P. and T. Schlick, *The loop opening/closing motion of the enzyme triosephosphate isomerase.* Biophys J, 1998. **74**(1): p. 72-81.

80. Joseph, D., G.A. Petsko, and M. Karplus, *Anatomy of a conformational change: hinged "lid" motion of the triosephosphate isomerase loop.* Science, 1990. **249**(4975): p. 1425-8.

81. Williams, J.C. and A.E. McDermott, *Dynamics of the flexible loop of triosephosphate isomerase: the loop motion is not ligand gated.* Biochemistry, 1995. **34**(26): p. 8309-19.

82. Pompliano, D.L., A. Peyman, and J.R. Knowles, *Stabilization of a reaction intermediate as a catalytic device: definition of the functional role of the flexible loop in triosephosphate isomerase.* Biochemistry, 1990. **29**(13): p. 3186-94.

83. Schreuder, H.A., et al., *Formation of the active site of ribulose-1,5-bisphosphate carboxylase/oxygenase by a disorder-order transition from the unactivated to the activated form.* Proc Natl Acad Sci U S A, 1993. **90**(21): p. 9968-72.

84. Zhang, E., et al., *Mechanism of enolase: the crystal structure of asymmetric dimer enolase-2-phospho-D-glycerate/enolase-phosphoenolpyruvate at 2.0 A resolution.* Biochemistry, 1997. **36**(41): p. 12526-34.

85. Lan, Y., et al., *Evidence for a (triosephosphate isomerase-like) "catalytic loop" near the active site of glyoxalase I.* J Biol Chem, 1995. **270**(22): p. 12957-60.

86. Saadat, D. and D.H. Harrison, *Mirroring perfection: the structure of methylglyoxal synthase complexed with the competitive inhibitor 2-phosphoglycolate.* Biochemistry, 2000. **39**(11): p. 2950-60.

87. Deslongchamps, P., Atlani, P., Frehel, D., Malaval, A/, *The importnace of conformation of the tetrahedral intermediate in the hydrolysis of esters. Selective cleavage of the tetrahedral intermediate controlled by orbital orientation.* Can. Journal of chemistry, 1972. **50**: p. 3405-3408.

88. Kirby, A.J., *The anmoeric effect and related steroelectronic effects at oxygen.* 1983.

89. Nagorski, R.W., Richard, J.P., *Mechanistic imperatives for Aldose-ketose isomerisation in water: Specific, general-base and metal-ion catalyzed isomerisation of glyceraldehyde with proton and hydride transfer.* J Am Chem Soc, 2000. **123**(5): p. 794-802.

90. Nickbarg, E.B. and J.R. Knowles, *Triosephosphate isomerase: energetics of the reaction catalyzed by the yeast enzyme expressed in Escherichia coli.* Biochemistry, 1988. **27**(16): p. 5939-47.

91. Druekhammer, D., Duncan, R, *Phosporthioate and Phosphoramide Analogues of Dihydroxyacetone Phoshpate.* Tetrahedron Letters, 1993. **34**(11): p. 1733-1736.

92. Grazi, E., et al., *Complexes of fructose diphosphate aldolase with dihydroxyacetone phosphate and dihydroxyacetone sulfate.* Biochemistry, 1973. **12**(14): p. 2583-90.

93. Hennion, G.F., Kupieki, F., *Some reactions of 2-butyne-1,4-diol.* J Org Chem, 1953. **18**(11): p. 1601-1609.

94. Arth, H., Fessner. W, *Practical synthesis of 4-hydroxy-3-oxobutylphosphonic acid and its evaluation as a bio-isosteric substrate of DHAP aldolase.* Carbohydr Res, 1998. **305**: p. 313-321.

95. Amyes, T.L., Rios. A, Richard, J. P., *Fromation and stability of organic zwitterions in aqueous solution: enolates of the amino acid glycine and its derivatives.* J Am Chem Soc, 2000. **122**(39): p. 9373-9385.

96. Burkhard, R., Sellars, D., DeCou, F., Lambert, J, *The pKa's of aromatic sulfinic acids.* J Org Chem, 1959. **24**(6): p. 767-769.

97. Cohen, T., Bennet, D., Mura., A, *Nitrogen acids.1.Carboxamides and sufonamides.* J Org Chem, 1976. **41**(14): p. 2507-2508.

98. 2000, J.S.M.T.

99. Whitesides, G.M., Wong, C., *Synthesis of sugars by Aldolase-catalyzed condensation reactions.* J Org Chem, 1983. **48**(19): p. 3199-3205.

100. Crugeiras, J. and J.P. Richard, *A comparison of the electrophilic reactivities of Zn2+ and acetic acid as catalysts of enolization: imperatives for enzymatic catalysis of proton transfer at carbon.* J Am Chem Soc, 2004. **126**(16): p. 5164-73.

101. Wiberg., K., Castejon., H, *Carbanions 2. Intramolecular interactions in carbanions stabilised by carbonyl, cyano, isocyano and nitro groups.* J Org Chem, 1995. **60**(20): p. 6327-6334.

102. Suh, J., *Model studies of metalloenzymes involving metal ions as lewis acid catalysts.* Acc Chem Res, 1992. **25**(7): p. 273-279.

103. Jencks, W., *Requirements for general acid-base catalysis of complex reactions.* J Am Chem Soc, 1972. **94**(13): p. 4731-4732.

104. Warkentin, J., Barnett, C. , *Relative rates of base-catalyzed enolization of methyl alkyl ketones in aqueous dioxane.* J Am Chem Soc, 1968. **90**(17): p. 4629-4633.

105. Warkentin, D.L., Tee. O, *Relative rates of base-catalyzed enolization of 2-butanone.* J Am Chem Soc, 1966. **88**(23): p. 5540-5543.

106. Hine, J., Hampton G.,Menon, B, *Catalysis of alpha-hydrogen exchange. Deuterium exchange of methyoxyacetone.* J Am Chem Soc, 1967. **89**(11): p. 2664-2668.

107. Warkentin, J., Cox, *Effects of Bromine substituents on rates of acetate-promoted enolization of ketones.* Can. Journal of chemistry, 1971. **50**: p. 3242-3247.

108. Bordwell, F.G., Van der puy, M., Vanier, N, *The effects of divalent sulfur and divalent oxygen on carbonanion stabilities.* J Org Chem, 1976. **41**(10): p. 1885-1887.

109. Parthasarathy, R., Row., G, *Directional preferences of non-bonded atomic contacts with divalent sulfur in terms of its orbital orientations.2 S-S interactions and non-spherical shape of sulfur in crystals.* J Am Chem Soc, 1981. **103**(3): p. 477-479.

110. Oae, S., *Organic sulfur chemistry: Structure and mechanism.* p. S.

111. Bernarrdi, F., et al., *The irrelevance of d-orbital orbital conjugation.1. alpha - Thiocarbanion. comparitive quantum chemical study of the static and dynamic properties and proton affinities of carbanionis adjacent to oxygen and sulfur.* J Am Chem Soc, 1975. **97**(8): p. 2209-2218.

112. Oae, S., Tagaki, W., Ohno, A, *3d-orbital resonance in divalent sulphides-IV. Acidity of hydrogen atom adjacent to mercapto groups.* Tetrahedron, 1964. **20**(2): p. 417-425.